

https://dspace.org/

Characterisation of time-dependent deformations in structural rubberised concrete

Mushunje, Kudzai

2022
https://hdl.handle.net/10539/34938

Downloaded from a DSpace repository. https://dspace.org/

CHARACTERISATION OF TIME-DEPENDENT DEFORMATIONS IN STRUCTURAL RUBBERISED CONCRETE

KUDZAI MUSHUNJE

464396

A thesis submitted to the Faculty of Engineering and the Built Environment, University of the Witwatersrand, Johannesburg, in fulfilment of the requirements for the degree of Doctor of Philosophy.

Johannesburg, 2022

DECLARATION

I declare that this thesis is my own unaided work. It is being submitted for the Degree of Doctor of Philosophy to the University of the Witwatersrand, Johannesburg. It has not been submitted before for any degree or examination to any other University.

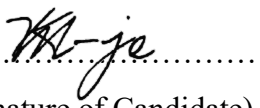

(Signature of Candidate)

14th day of June year 2022
(day) *(month)* *(year)*

ABSTRACT

The use of concrete incorporating waste tyre rubber particles (rubberised concrete or rubcrete) as aggregates has always been restricted to non-structural uses due to the pronounced reduction in the strength. Recent, strength and durability studies have shown that, optimising rubber content and pretreating tyre rubber surfaces can produce rubberised concrete that performs comparably well as conventional structural concrete. Despite these promising research outcomes, uptake of rubberised concrete into the construction industry has also been hindered by limited studies on the shrinkage and creep behaviour of the material. This study was therefore conducted to characterise time-dependent deformations, shrinkage and creep, to provide a basis for comparison with plain concrete during the planning and design stage of a building construction project.

This study was conducted on structural rubberised concrete obtained primarily by optimising crumb rubber content while avoiding the use of admixtures. Three crumb rubber tyre particle sizes (2.36 mm, 1.18 mm, 0.425 mm) were used to replace fine aggregate in concrete at a 10% replacement level to produce structural concrete with a mean strength of 30 MPa. The creep stress was 30% of the concrete compressive strength.

The results showed that the shape and texture of the tyre crumb rubber particles had a significant role in the mechanical properties of rubberised concrete as it impacted the concrete porosity. Smaller sized crumb rubber particles (<2.36 mm) which are irregularly shaped and rough textured resulted in concrete with higher porosity. The higher porosity resulted in higher autogenous, drying shrinkage, basic and total creep strains in rubberised concrete. In addition, lower tyre rubber stiffness, low water absorption and poor cement-rubber bonding were also found to have an effect of increasing shrinkage and creep. However, these increases were within reasonable range as they did not exceed 50% of the plain concrete. Furthermore, the rubberised concrete creep behaviour, as simulated by rheological modelling, remained fundamentally the same in terms of basic mechanical components used to model this behaviour. It was concluded that rubberised concrete can be safely used for structural applications, without concerns over unexpected deformations occurring, if the appropriate concrete strain multipliers are applied to account for the tyre rubber in concrete during the design process.

DEDICATION

To my dear wife, Sithandweyinkosi, and our adorable daughter Gabriella.

ACKNOWLEDGEMENTS

I would like to thank the following people for being part of my long journey:

Professor Mike Benjamin Otieno for literally holding my hand throughout the whole process;

Professor Yunus Ballim for his support and insights;

The University of the Witwatersrand School of Civil and Environmental Engineering Technical Staff for their assistance during my laboratory work;

The National University of Science and Technology Department of Civil and Water Engineering for allowing me time away to focus on this work.

TABLE OF CONTENTS

DECLARATION ..... **ii**

ABSTRACT ..... **iii**

DEDICATION ..... **iv**

ACKNOWLEDGEMENTS ..... **v**

TABLE OF CONTENTS ..... **vi**

LIST OF FIGURES ..... **ix**

LIST OF TABLES ..... **xiv**

CHAPTER ONE: INTRODUCTION **1**

1.1 BACKGROUND 1

1.2 JUSTIFICATION FOR THE STUDY 6

1.3 SCOPE AND LIMITATION 10

1.4 AIM AND OBJECTIVES 11

1.5 THESIS OUTLINE 12

CHAPTER TWO: LITERATURE REVIEW **13**

2.1 INTRODUCTION 13

2.2 PNEUMATIC RUBBER TYRE 13

2.2.1 Pneumatic tyre manufacturing 17

2.2.2 Pneumatic tyre composition 20

2.3 WASTE TYRE 21

2.3.1 Management of waste tyres 22

2.3.2 Waste tyre rubber classification, production, and properties 26

2.4 REVIEW OF RUBBERISED CONCRETE PROPERTIES 29

2.4.1 Workability 30

2.4.2 Air content 31

2.4.3 Rubberised concrete strength and static modulus 32

2.4.4 Shrinkage 37

2.4.5 Creep 40

2.4.6 Freeze-thaw resistance 43

2.4.7 Carbonation resistance 44

2.4.8 Chloride penetration resistance 46

2.4.9 Thermal conductivity 48

2.4.10 Acoustic properties 49

2.4.11 Summary of rubberised concrete properties review 50

2.5 TIME-DEPENDENT DEFORMATIONS IN CONCRETE 52

2.5.1 Shrinkage 52

2.5.2 Types of shrinkage 53

2.5.3 Creep 65

2.5.4 Effects of shrinkage and creep in concrete 85
2.5.5 Identified gaps in literature 87
CHAPTER THREE: METHODOLOGY 89
3.1 INTRODUCTION 89
3.2 MATERIALS 89
3.2.1 Cement 89
3.2.2 Aggregates 90
3.3 EXPERIMENTAL PROCEDURES 96
3.3.1 Mix proportions 96
3.3.2 Crumb rubber aggregate characterisation 98
3.3.3 Compressive strength tests: Selection of rubber replacement level 103
3.3.4 Shrinkage and creep specimen preparation 106
3.3.5 Concrete prisms for creep test 107
3.3.6 Creep set-up and measurements 108
3.3.7 Determination of elastic modulus of concrete 111
3.3.8 Micro-crack detection 113
3.3.9 Concrete porosity determination 117
CHAPTER FOUR: RESULTS AND ANALYSIS 118
4.1 INTRODUCTION 118
4.2 TYRE CRUMB RUBBER SHAPE AND TEXTURE CHARACTERISATION 119
4.2.1 Crumb rubber particle shape 119
4.2.2 Surface texture 121
4.3 FLUORESCENT MICROSCOPY RESULTS 126
4.3.1 Micro-cracking 127
4.3.2 Crumb rubber particle-matrix interaction 128
4.4 CONCRETE POROSITY 130
4.5 ELASTIC MODULUS RESULTS 132
4.6 SHRINKAGE RESULTS 133
4.6.1 Autogenous shrinkage 133
4.6.2 Drying shrinkage 140
4.7 CREEP DEFORMATION RESULTS 146
4.7.1 Basic creep deformation 148
4.7.2 Total creep deformation 153
4.7.3 Creep coefficients 159
4.8 SUMMARY OF RESULTS 161
CHAPTER FIVE: RHEOLOGICAL MODELLING THEORY 165
5.1 INTRODUCTION 165
5.2 RHEOLOGICAL MODELS 165
5.2.1 Basic rheological models 166
5.2.2 Solid rheological models 170
5.3 DEVELOPING A RHEOLOGICAL MODEL 174

CHAPTER SIX: CONCRETE CREEP RHEOLOGICAL MODELLING 176

6.1 INTRODUCTION 176

6.2 DETERMINATION OF MODEL PARAMETERS 176

6.2.1 Application of Burgers model to measured creep data 176

6.2.2 Model section governing equations 178

6.3 MODELLING CREEP BEHAVIOUR 185

6.3.1 Basic Creep Prediction Model 185

6.3.2 Total Creep Prediction Model 188

6.4 CREEP MODELLING SUMMARY 192

CHAPTER SEVEN: CONCLUSIONS & RECOMMENDATIONS 193

7.1 INTRODUCTION 193

7.2 CONCLUSIONS 194

7.2.1 Time-dependent deformation of structural rubberised concrete 194

7.2.2 Effect of properties of crumb rubber on time dependent deformation characteristics of rubberised structural concrete 198

7.2.3 Strength and stiffness characteristics of structural rubberised concrete 199

7.2.4 Significance and practical implications of the study 199

7.3 RECOMMENDATIONS 200

REFERENCES 202

APPENDIX A: EXPERIMENTAL TEST PROCEDURES 233

A.1 RELATIVE DENSITY 233

A.2 HARDENED CONCRETE POROSITY 234

APPENDIX B: COMPRESSIVE STRENGTH RESULTS 236

B.1 COMPRESSIVE STRENGTH RESULTS DISCUSSION 236

B.1.1 Effect of crumb tyre rubber size and content 236

B.1.2 Effect of crumb tyre rubber surface treatment 241

B.2 RAW COMPRESSIVE STRENGTH RESULTS 244

B.3 STATISTICAL ANALYSIS OF COMPRESSIVE STRENGTH RESULTS 246

APPENDIX C: HARDENED CONCRETE POROSITY RESULTS 249

APPENDIX D: STATISTICAL ANALYSIS OF HARDENED CONCRETE POROSITY 250

APPENDIX E: SHRINKAGE RESULTS 252

APPENDIX F: CREEP RESULTS 265

LIST OF FIGURES

Figure 2.1: Cross section showing components of typical passenger tyre (Evans and Evans, 2006) ... 14

Figure 2.2: Sections showing different components of passenger and truck tyres (Yokohama tyres, 2018) ... 15

Figure 2.3: Typical Tyre manufacturing flow chart (Maxxis Tires, 2018) ... 17

Figure 2.4: Basel convention technical guidelines tyre waste management (United Nations, 2012) ... 24

Figure 2.5: American 2015 waste tyre use proportions (Rubber Manufacturers Association, 2016) ... 26

Figure 2.6: Different tyre rubber particle sizes ... 26

Figure 2.7: Typical ambient rubber particle processing (Recycling Research Institute, 2017) ... 28

Figure 2.8: Typical cryogenic rubber particle processing (Recycling Research Institute, 2017) ... 28

Figure 2.9: Strength increase due to surface pre-treatment relative to untreated rubber ... 35

Figure 2.10: Governing mechanisms of total shrinkage in concrete (Esping, 2007) ... 52

Figure 2.11: Formation of plastic shrinkage cracks (Soroushian and Ravanbakhsh, 1998) ... 53

Figure 2.12: Typical plastic shrinkage cracking (Cement concrete and aggregates, 2005) ... 54

Figure 2.13: The chemical and autogenous shrinkage relationship (Wu et al., 2017) ... 55

Figure 2.14: Capillary tension shrinking mechanism (Mindess et al., 2003) ... 60

Figure 2.15: Disjoining shrinking mechanism (Mindess et al., 2003) ... 61

Figure 2.16: Gibbs-Bangham shrinkage mechanism (Mindess et al., 2003) ... 61

Figure 2.17: Effect of Aggregate volume on concrete shrinkage (Cement Concrete & Aggregate, 2002) ... 63

Figure 2.18: Effect of water-cement ratio on drying shrinkage of concrete (Cement Concrete & Aggregate, 2002) ... 64

Figure 2.19: Effect of relative humidity on the drying shrinakge of concrete (Bissonette,1999) ... 65

Figure 2.20: Concrete strain components under sustained stress (Gilbert and Ranzi, 2010) ... 66

Figure 2.21: Creep components in drying concreete under sustained load (Gilbert, 1988) ... 67

Figure 2.22: Effect of aggregate stiffness on concrete creep (Alexander and Beushausen, 2009) ... 74

Figure 2.23: Creep of concretes made with different aggregates (Neville et al, 1983) ... 75

Figure 2.24: Effect of w/c on creep of cement paste (Alexander and Beushausen, 2009)..... 76
Figure 2.25: Effect of previous drying on basic creep of cement paste (Wittmann, 1973) 77
Figure 2.26: Effect of size on crreep of concrete (Neville et al, 1983)..... 80
Figure 2.27: Effect of relative humidity on concrete creep (Troxell et al., 1958) 81
Figure 2.28: Effects of temperature on creep of concrete (Vidal et al, 2013)..... 82
Figure 2.29: Relationship of creep and stress:strength ratio (Neville et al. 1983)..... 83
Figure 2.30: Influence of age at application of load on creep as a fraction of creep for concrete loaded at 7 days (L'Hermite, 1959) 84
Figure 3.1: Cement particle size distribution..... 89
Figure 3.2: Particle size distribution of fine and coarse mineral aggregates..... 91
Figure 3.3: Crumb tyre rubber particle distribution..... 92
Figure 3.4: Crumb tyre rubber general appearance..... 93
Figure 3.5: Tyre crumb rubber particles being washed with tap water..... 95
Figure 3.6: Tyre crumb rubber air drying after washing..... 95
Figure 3.7: Carl Zeiss Sigma Field Emission Scanning Electron with Energy-Dispersive X-ray spectroscope..... 98
Figure 3.8: Coated crumb rubber particles on stage 99
Figure 3.9: X-ray spectrum for untreated crumb rubber..... 101
Figure 3.10: X-ray spectrum for NaOH treated crumb rubber..... 101
Figure 3.11: X-ray spectrum for water-soaked crumb rubber..... 102
Figure 3.12: Effect of crumb rubber content and size on concrete compressive strength 105
Figure 3.13: Effect of crumb rubber pretreatment on concrete compressive strength..... 105
Figure 3.14: Shrinkage and creep Specimens..... 107
Figure 3.15: Schematic arrangement of the hydraulic creep loading rig..... 108
Figure 3.16: Shrinkage specimens on racks..... 110
Figure 3.17: 100 mm Demec gauge..... 110
Figure 3.18: Elastic modulus specimen placed centrally in loading machine 111
Figure 3.19: Demec gauge held in place on one face of the test specimen..... 112

Figure 3.20: 80 mm concrete specimen sustained loading rig 114
Figure 3.21: Measuring the distance between the base plate and the bottom loading plate 115
Figure 3.22: Concrete specimens immersed in ethanol with fluorescent dye 115
Figure 3.23: Fluorescence microscopy specimens 116
Figure 4.1: SEM micrograph of a 2.36 mm particle (magnification 100×) 119
Figure 4.2: SEM micrograph of a 1.18 mm particle (magnification 100×) 120
Figure 4.3: SEM micrograph of 0.425 mm crumb rubber particles (magnification 100×) 120
Figure 4.4: Reference concrete flourescent micrographs (blue and green light) 127
Figure 4.5: Rubberised concrete flourescent micrographs (blue and green light) 127
Figure 4.6: M8 concrete flourescent micrographs (red light) 128
Figure 4.7: M16 concrete flourescent micrographs (red and green light) 129
Figure 4.8: M40 concrete flourescent micrographs (red and green light) 129
Figure 4.9: Effect of crumb rubber size on hardened concrete percent voids 130
Figure 4.10: Effect of pretreatment on hardened percent voids 131
Figure 4.11: Effect of crumb rubber size and surface treatment on concrete elastic modulus 132
Figure 4.12: Effect of crumb rubber size on autogenous shrinkage 134
Figure 4.13: Autogenous shrinkage equality graph 135
Figure 4.14: Ratio of rubberised concrete to reference concrete autogenous shrinkage 137
Figure 4.15: Effect of surface treatment of 2.36 mm crumb rubber on autogenous shrinkage 138
Figure 4.16: Effect of surface treatment of 1.18 mm crumb rubber on autogenous shrinkage 139
Figure 4.17: Effect of surface treatment of 0.425 mm crumb rubber on autogenous shrinkage 139
Figure 4.18: Effect of crumb rubber size on drying shrinkage 141
Figure 4.19: Drying shrinkage equality graph 142
Figure 4.20: Ratio of rubberised concrete to reference concrete drying shrinkage 143
Figure 4.21: Effect of surface treatment of 2.36 mm crumb rubber on drying shrinkage 144
Figure 4.22: Effect of surface treatment of 1.18 mm crumb rubber on drying shrinkage 145
Figure 4.23: Effect of surface treatment of 0.425 mm crumb rubber on drying shrinkage 145
Figure 4.24: Effect of crumb rubber size on basic creep 148

Figure 4.25: Specific basic creep equality graph 149
Figure 4.26: Ratio of rubberised concrete to reference concrete specific basic creep 150
Figure 4.27: Effect of surface treatment of 2.36 mm crumb rubber on basic creep..... 151
Figure 4.28: Effect of surface treatment of 1.18 mm crumb rubber on basic creep..... 151
Figure 4.29: Effect of surface treatment of 0.425 mm crumb rubber on basic creep..... 152
Figure 4.30: Effect of crumb rubber size on total creep 153
Figure 4.31: Spefic total creep equality graph 154
Figure 4.32: Ratio of rubberised concrete to reference concrete specific total creep 156
Figure 4.33: Effect of surface treatment of 2.36 mm crumb rubber on total creep..... 157
Figure 4.34: Effect of surface treatment of 1.18 mm crumb rubber on total creep..... 157
Figure 4.35: Effect of surface treatment of 0.425 mm crumb rubber on total creep..... 158
Figure 4.36: Effect of crumb rubber on basic creep coefficient 159
Figure 4.37: Effect of crumb rubber on total creep coefficient 160
Figure 5.1: Linear elastic spring element..... 166
Figure 5.2: Linear dash-pot element 166
Figure 5.3: Two-element Maxwell and Kelvin models 167
Figure 5.4: Maxwell model creep-recovery response..... 168
Figure 5.5: Kelvin model creep-recovery response 169
Figure 5.6: Standard solid (Zener) models..... 170
Figure 5.7: Typical standard solid model response..... 171
Figure 5.8: Burgers model 171
Figure 5.9: Typical Burgers model response (Neville et al, 1983) 172
Figure 5.10: Generalised rheological models 173
Figure 6.1: Division of Burgers model 177
Figure 6.2: Assigning deformation response to curve sections..... 177
Figure 6.3: Spring compliance variation with crumb rubber size..... 181
Figure 6.4: Maxwell model coefficient of viscocity variation with crumb rubber size 181
Figure 6.5: Kelvin model coefficient of viscocity variation with crumb rubber size 182

Figure 6.6: Spring compliance variation with crumb rubber size 183
Figure 6.7: Maxwell model coefficient of viscocity variation with crumb rubber size 184
Figure 6.8: Kelvin model coefficient of viscocity variation with crumb rubber size 184
Figure 6.9: Predicted and measured basic strain for reference concrete 186
Figure 6.10: Predicted and measured basic creep strain for M8 concrete 187
Figure 6.11: Predicted and measured basic creep strain for M16 concrete 187
Figure 6.12: Predicted and measured basic creep strain for M40 concrete 188
Figure 6.13: Line of equality for control and rubberised basic creep strain 188
Figure 6.14: Predicted and measured total creep strain for reference concrete 189
Figure 6.15: Predicted and measured total creep strain for M8 concrete 190
Figure 6.16: Predicted and measured total creep strain for M16 concrete 190
Figure 6.17: Predicted and measured total creep strain for M40 concrete 191
Figure 6.18: Line of equality for control and rubberised total creep 191

LIST OF TABLES

Table 2.1: Pneumatic tyre production raw materials 18

Table 2.2: Typical material composition of major tyre categories 21

Table 2.3: Waste tyre re-use applications 23

Table 2.4: Recycling applications 23

Table 2.5: Tyre rubber elemental composition 23

Table 2.6: Rubberised concrete creep studies 43

Table 3.1: Cement mineral composition 90

Table 3.2: Concrete mix proportions 97

Table 3.3: Elements identified in the untreated and treated crumb rubber 100

Table 4.1: Micrographs showing the surfaces texture of the different crumber rubber sizes (magnification 500×) 122

Table 4.2: 2.36 mm tyre rubber micrographs with different pretreatment methods 123

Table 4.3: 1.18 mm tyre rubber micrographs with different pretreatment methods 124

Table 4.4: 0.425 mm tyre rubber micrographs with different pretreatment methods 125

Table 6.1: Application of creep governing equations 179

Table 6.2: Burgers model parameters for basic creep 180

Table 6.3: Burgers model parameters for total creep 182

CHAPTER ONE: INTRODUCTION

1.1 BACKGROUND

Concrete is one of the most commonly used materials globally after water (Watts, 2019). Global concrete production is estimated to be about 33 billion tonnes per annum, which is about 4.7 tonnes per person worldwide annually (ISO Technical Committee, 2016). The history of concrete dates back to ancient Egypt and its demand continues to grow because of its durable and versatile nature (Crow, 2008; Mead, 2019). The versatility of concrete can largely be attributed to its ability to evolve with changing times through the use of different types of admixtures to make concrete that is suited for different kinds of construction demands.

The use of different ingredients in concrete is driven by the need to produce a material that adequately satisfies the desired performance criteria, mainly for structural applications. In construction, concrete can be classified as either non-structural or structural. Structural concrete is concrete that has sufficient compressive strength (>25 MPa) to be used for load-bearing applications (The Concrete Society, 2021). Compressive strength can be used as a measure of other concrete properties because of the relative ease with which it can be measured, thus strength is used to classify concrete types. It can be used to estimate properties such as the Young's modulus and tensile strength (Neville, 2011). Structural concrete makes up a good proportion of the total concrete usage. The suitability of a type of concrete to be used for structural applications is evaluated in terms of its compressive strength, durability, sustainability, and deformation characteristics. Therefore, most modifications made to concrete are meant to produce a variety of

concrete that is suited for structural applications in terms of strength, deformation, durability, cost, ease of handling and sustainability.

One of the important characteristics of structural concrete is its delayed deformation behaviour. Delayed deformations, also known as time-dependent deformations, encompass such deformations as shrinkage and creep (Torrenti and Le Roy, 2018). Shrinkage is the volume reduction of concrete due to moisture loss, while creep is an increase in strain due to a sustained load (Bompa and Elghazouli, 2019; Sellin et al., 2015). Time-dependent deformations are a vital consideration when choosing concrete materials as they affect the long-term functionality of a structure (Li et al., 2020b; Sellin et al., 2015). This is because time-dependent deformations, if not properly catered for in design, might lead to excessive cracking which may result in durability problems or excessive deformation which may cause loss of prestress. In some cases, these deformations have led to structural collapse (Li et al., 2020b; Sellin et al., 2015; Yang et al., 2020). In cases where collapse has not happened, the deformation leads to high maintenance costs, rendering such a project, uneconomical and unsustainable, even if serviceability is preserved.

Economic, social and environmental sustainability in the construction industry has come to the fore in recent years. The sustainability approach has influenced the need for environmentally friendly technologies and a reduction in the use of non-renewable resources. The drive has contributed to the increased usage of alternative materials in concrete. In this regard, the use of waste materials in concrete has become common practice. This practice has seen the development of high strength

and more durable concrete without the need to further exploit natural resources. The continued use of these materials is a result of the way they have been observed to enhance engineering properties of concrete. Examples of such waste materials include ground granulated blast-furnace slag, fly ash and silica fume.

In the past, focus has been on reducing the amount of cement used in concrete to reduce the carbon footprint resulting from cement production, but in recent years, there has been a broadening of scope to also reduce the amount of virgin aggregates used in concrete. This is because natural mineral aggregates are a finite resource and according to Alexander and Mindess (2015), it is a resource that is fast running out. To increase the longevity of mineral aggregate resources, a broader resource supply base has been established. Instead of using one type of mineral aggregate, other unconventional, locally occurring rock types have been evaluated for use in concrete in many countries. Alexander and Davis (1992) assessed 13 natural mineral aggregate types from across South Africa that can be used in concrete. Although this has reduced the risk of exhausting one mineral aggregate type, it has not stopped the depletion of the finite natural mineral resources. To reduce the use of virgin mineral aggregates, recycling aggregates and other building materials has been suggested (Bjegovic et al., 2013; Ezema, 2019; Janotka et al., 2021; Khalaf, 2004; McNeil and Kang, 2013; Safiuddin et al., 2013). This has indeed contributed, to an extent, to the limiting the use of virgin aggregates in building projects where strict material specifications are not applicable. These alternative materials are slowly being accepted in the construction industry through research. The attraction

of these materials is their dual purpose. They allow for the disposal of waste while being an almost infinite source of concrete constituent.

In the recent past, the use of waste tyre rubber aggregate in concrete to make rubberised concrete has been suggested (Naik, and Singh, 1991; Polydorou et al., 2020; Sun et al., 2020). This is because of the abundance of waste tyres and the problem that comes with their disposal. With an estimation of over 1.2 billion new tyres being produced annually worldwide, their disposal at the end of their life has become a serious problem (Alsaif et al., 2018; Jain, 2014; Li et al., 2020a; Strukar et al., 2019). Annually, Europe and the United States generate 245 million and 270 million waste tyres respectively (Bjegovic et al., 2013; Pilkington, 2021; Siddique and Naik, 2004; Strukar et al., 2019). The disposal of waste tyres in landfills is a challenge because the tyres tend to rise to the surface during compaction. When stockpiled, the tyres are a health risk as they provide breeding ground for rodents and mosquitoes, which may carry diseases (Naik, and Singh, 1991; Ruwona et al., 2019). In a bid to curb the risks associated with waste tyre disposal, some countries have passed legislation that governs the disposal of waste tyres in landfills. The European Union directive 1999/31/EC, for example, prohibits the disposal of waste tyres in landfills starting from 2006 (Bjegovic et al., 2013; Mavroulidou and Figueiredo, 2010; Nkosi et al., 2021; Strukar et al., 2019). The awareness of the hazards associated with waste tyre disposal has resulted in the development of several alternatives to disposing of waste tyres in landfills such as using them as kiln fuel in industrial furnaces, stock feed for making carbon black, artificial reefs, playground mats, erosion control, guard rail posts, noise barriers, highway crash

barriers and asphalt pavements (Jain, 2014; Ruwona et al., 2019; Sebola et al., 2018; Siddique and Naik, 2004). The challenge of waste tyre disposal is a global issue that is negatively affecting both developed and developing countries like Zimbabwe, Botswana and Ghana, including South Africa (Arreguia, 2017; Arthur et al., 2020; Mmereki et al., 2019; Sebola et al., 2018).

In 2011, South Africa had over 60 million stockpiled waste tyres and was set to increase by about 10 million every year but in 2019, this annual figure increased to 14 million (Nkosi et al., 2021, 2013). Mahlangu (2009), Banzibaganye (2014) and Muzenda (2014) reported that only 6% of the waste tyres generated in South Africa were being recycled in 2011. To improve these numbers, the Recycling and Economic Development Initiative of South Africa (REDISA) waste management plan was put in place (Muzenda, 2014; Nkosi et al., 2021). The waste management plan encourages the useful application of waste tyre instead of landfilling. These applications include, the shredding of waste tyre to make playground mats, turfs and asphalt concrete. The REDISA initiative has resulted in a little under 20% of waste tyre being recycled, which was higher than previous years but was still not enough to solve the waste tyre challenge (Sebola et al., 2018). Banzibaganye (2014) suggested that the construction industry has the potential to make use of a large portion of the waste tyres generated in South Africa. The use of waste tyre rubber within the construction industry together with the already existing uses for waste tyres may be able to make use of all the waste tyre generated within developing countries and eliminate the issues associated with its disposal.

1.2 JUSTIFICATION FOR THE STUDY

The presence of tyre rubber aggregates in concrete alters its performance. Some researchers report improved sound absorption and thermal insulation due to the inclusion of rubber in concrete (Elchalakani, 2015; Li et al., 2019; Nehdi and Khan, 2001; Siddique and Naik, 2004). Fiore et al. (2014) found that the inclusion of 10% by volume, of fine rubber aggregate results in a 23% improvement of thermal insulation. Ghedan and Hamza (2011) also found an improvement in thermal insulation of 26.7% for 15% by volume crumb rubber replacement of natural fine aggregates. Holmes et al. (2014) reported that the sound absorption coefficient of concrete increases by 107% when 15% by volume of crumb rubber is used to replace fine aggregate in concrete. Bjevgovic et al. (2013) also reported that incorporating rubber in concrete noise barriers increases the sound absorption capabilities of the barriers by 6 dB.

Initially, the use of rubberised concrete was considered unsuitable for structural applications because of the marked reduction in its mechanical performance compared to conventional concrete. Researchers reported notable reductions in both the compressive and tensile strength and the elastic modulus of the rubberised concrete (Naik & Singh, 1991; Eldin & Senouci, 1993; Malladi 2004; Zheng et al., 2008; Panda et al., 2012; Jain, 2014; Elchalakani, 2015; Polydorou et al., 2020). The reduction in mechanical performance has been attributed to the significantly lower stiffness (<5 MPa) of tyre rubber, the uneven distribution of the rubber aggregates due to its light weight and the poor bonding between the rubber aggregate and the cement paste (Eldin and Senouci, 1993; Malladi, 2004; Naik, and

Singh, 1991; Panda et al., 2012; Pham et al., 2018). Efforts have been made to limit the reduction in the mechanical performance of rubberised concrete by pretreating the rubber aggregate and making use of different binder types like magnesium oxychloride cement and cements with supplementary cementitious materials (SCMs) such as fly ash and silica fume (Eldin and Senouci, 1993; Fiore et al., 2014; Li et al., 2019; Rostami et al., 1993; Segre and Joekes, 2000; Youssf et al., 2020). Rostami et al. (1993) found that when crumb tyre rubber is pretreated with carbon tetrachloride, the compressive strength improved by 57% when compared to rubberized concrete with untreated crumb rubber. Segre and Joekes (2000) reported an improvement of 17% in compressive strength when crumb rubber pretreated with 0.1M Sodium Hydroxide (NaOH) is used compared to untreated crumb rubber. Changing the binder type has also resulted in rubberised concrete with sufficient strength (>25 MPa) for structural applications. Pelliser et al. (2010) made a 48 MPa strength rubberised concrete, with 10% crumb rubber to fine mineral aggregate replacement by volume and a 15% silica fume-cement replacement at a water-to-binder ratio of 0.4 concrete mix. Other researchers (Elchalamani, 2015; Thomas et al. 2015) also reported similar results for a similar mix and an improvement in the permeability, chloride and sulphuric acid attack resistance of the rubberised concrete.

The reduction in strength reported for rubberised concrete had restricted the use of the material to non-structural applications (Siddique and Naik, 2004). The prospects of producing a rubberised concrete with improved strength comparable to conventional concrete has brought about the possibility of the material being used

for structural applications (Elchalakani, 2015; Li et al., 2020a; Pelisser et al., 2010; Strukar et al., 2019; Thomas et al., 2015). The bulk of the studies on rubberised structural concrete (>25 MPa) have focused on the mechanical strength and durability aspects of the material. Prior to 2016, there was limited research (Fiore et al., 2014; Zhang et al., 2015; Zaoiai et al., 2015; Mohammadi & Khabbaz, 2015) on the shrinkage behaviour of the material and no published studies on creep deformation when compared to conventional concrete. The lack of publications in this area was the motivation in the formulation of this study. In general, these studies reported that drying shrinkage is higher in rubberized concrete. However, during the progression of this study several shrinkage and creep studies were published (Alsaif et al., 2018; Bompa and Elghazouli, 2019; Li et al., 2020b; Sun et al., 2020) with some of the studies (Sun et al., 2020; Youssf et al., 2020) reporting findings contrary to previously published work where shrinkage had been reported to increase with the inclusion of tyre rubber particles. The recent studies also found that, in general, creep deformation is higher in rubberised concrete. Regarding shrinkage deformation, these recent studies show a need for more research to develop a basic understanding of what drives shrinkage in rubberised concrete due to these contradicting findings. In addition, the creep deformation studies that have been carried out are all on concretes that have been modified already, for example, using blended cements (Bompa and Elghazouli, 2019; Youssf et al., 2020) or super plasticisers and water-reducing agents (Li et al., 2020; Youssf et al., 2020). The use of concrete modified in this manner makes it difficult to use these results to gain a basic understanding of the raw effects of tyre rubber particles in concrete because the effects of these modifications on rubberised concrete time-dependent

deformations are unknown. The effect of tyre rubber size on creep is also not investigated. In all the currently available literature a blend of crumb rubber sizes is used to replace mineral aggregates, which makes it difficult to assess the effect of a particular crumb rubber size on time-dependent behaviour.

The full utilisation of rubberised concrete as a structural material in construction is only possible when its basic time-dependent deformation properties are understood. Time-dependent deformations are normally much larger than elastic deformations in concrete structures (Bažant and Panula, 1984; Neville et al., 1983). These deformations often result in excessive cracking and deflections or possible failure with an inherent loss in serviceability, durability and long-term safety of concrete structures (Bažant and Panula, 1984; Li et al., 2020b; Neville et al., 1983; Torrenti and Le Roy, 2018). Considerable amount of research has been done to understand the time-dependent behaviour of conventional concrete because of the importance of this knowledge in ensuring safe, serviceable and durable structures. Aggregates have a significant influence on the time-dependent deformation of concrete. Therefore, as the aggregate type changes, the time-dependent behaviour is also expected to change relative to the stiffness of the aggregate. The stiffness of the crumb rubber particles is less than 5 MPa (Edeskär, 2004) therefore, it is expected that the restraint that the aggregates should offer during shrinkage and creep deformation will be much less than that offered by mineral aggregates. It is therefore important, to quantify the extent of the change in the magnitude of the deformation and resulting internal microstructural changes. Quantifying these deformations will allow for decisions on the use of rubberised concrete to be made

without the need for extensive work to be done at planning and design stage. Rheological modelling of these deformations allows for the understanding of the underlying physical properties governing the deformations. It is also important that the time-dependent deformations are quantified on unmodified concrete except for the inclusion of rubber particles. This allows for a basic understanding of the effects of tyre rubber in plain concrete thus making it easy to quantify other modifications when they are effected later. It is also important to understand if crumb rubber size has the same effect on time-dependent deformations as it has on other mechanical properties.

1.3 SCOPE AND LIMITATION

The study focused on developing a basic understanding of the time-dependant behaviour of rubberised concrete; therefore, three waste tyre rubber sizes were used. This allowed the assessment of the effect of crumb rubber size on the time-dependent behaviour of the concrete. The crumb rubber size replacement was for fine aggregate in the range 0.150 mm - 2.36 mm, this was mainly due to availability. The shrinkage and creep strains were measured for only one set of representative conditions, that is, single constant relative humidity, one loading age, one constant loading stress and one unloading age. Water to cement ratio was kept constant at 0.6 and one binder type was used, plain Portland Cement CEM I 52.5R. The water to cement ratio was guided by the desired compressive strength without having to use an admixture as the effects of such an admixture are not known. The 0.6 water to cement ratio compared to other trial mixes allowed for the desired

target reference concrete strength to be attained without the use of admixtures and also made handling much easier.

1.4 AIM AND OBJECTIVES

The aim of the study was to characterise time-dependent deformations in structural rubberised concrete in order to provide insight into its shrinkage and creep behaviour. The shrinkage was characterised with respect to autogenous and drying shrinkage strains and microcrack properties while creep was characterised with respect to basic and total specific creep, creep coefficient and microcrack properties.

In order to achieve this aim the following objectives were adopted:

a) To characterise the crumb tyre rubber with respect to its shape, size, texture and density.
b) Evaluate the effect of different crumb rubber size (2.36 mm, 1.18 mm, 0.425 mm) on basic creep, total creep and drying shrinkage behaviour of the structural concrete.
c) Evaluate the effect of crumb rubber surface modification by various crumb tyre rubber surface treatments on basic creep, total creep and drying shrinkage behaviour of structural rubberised concrete.
d) Assess the interaction of the crumb rubber particles with the concrete matrix undergoing shrinkage and creep deformations.
e) Model rubberised concrete creep behaviour using an existing rheological model.

1.5 THESIS OUTLINE

The rest of the thesis is divided into six chapters. The chapters are arranged as follows:

- Chapter 2 - Literature review, presents a review of literature on the manufacture, properties, and disposal of tyres. The chapter also discusses advances made in the use of waste tyre rubber in concrete, and lastly discusses time-dependent deformations in concrete and gaps in research.
- Chapter 3 - Materials and methodology, presents material and test methods employed in the study. In some instances, test results are presented and discussed to give background to the chosen methodology.
- Chapter 4 – Results and discussion, presents the study's main experimental results and discussions. The crumb rubber characterization, microcrack, shrinkage and creep results are presented and compared with published works and any difference in observations are discussed.
- Chapter 5 – Rheological models review, provide a theoretical background to rheological modelling to lay foundation for the modelling chapter.
- Chapter 6 - Rheological modeling, lays out the procedure followed in the development of the model parameters. The model parameters are also presented and discussed in relation to published studies and prediction accuracy.
- Chapter 7 – Conclusions and recommendations, gives a summary of the research findings and offers recommendation for future research.

CHAPTER TWO: LITERATURE REVIEW

2.1 INTRODUCTION

This chapter provides details on pneumatic tyres, waste tyre generation, a review of the use of waste tyre rubber in concrete and the theory of time dependent behaviour of concrete. The review follows the development of rubberised concrete starting with a discussion on the background of tyre rubber and then followed by different research that has been done to incorporate tyre rubber into concrete. In conclusion a discussion on the shrinkage and creep behaviour of concrete is presented.

2.2 PNEUMATIC RUBBER TYRE

Rubber tyres can either be pneumatic or non-pneumatic. Pneumatic tyre are air inflated tyres while non-pneumatic tyres are not supported by air pressure. However, this section focuses on pneumatic tyres because they are the most widely used compared to non-pneumatic tyres (Rangdale et al., 2018). A tyre is defined as "*continuous pneumatic covering made of natural or synthetic rubber (elastomer) or a combination of natural and synthetic rubber encircling a wheel, whether new, used or retreaded*" (South African Tyre Recycling Process Company, 2013). It can be described as a combination of intricate elastomer compounds, textile fibres, steel strands and steel cords (Siddique and Naik, 2004). An elastomer is defined as "*a high molar mass material which when deformed at room temperature reverts quickly to nearly original size and form when the load causing deformation has been removed*" (ISO 1382, 2012).

A tyre allows a vehicle to move by transmitting motor forces required for motion. It serves as a vessel to carry pressured air. Figure 2.1 shows the anatomy of a typical pneumatic tyre.

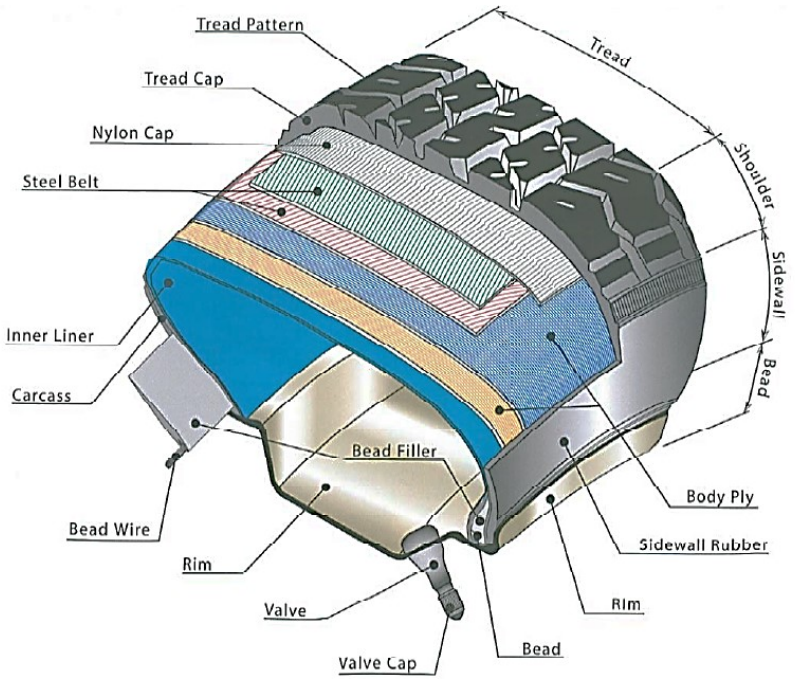

Figure 2.1: Cross section showing components of typical passenger tyre (Evans and Evans, 2006)

The anatomy of a pneumatic tyre differs slightly depending on the category of the tyre. Tyres are categorised based on their use or application. The South African Department of Environmental Affairs (2012) suggests the use of nine categories for ease of management. The categories are:

i) passenger car tyres,

ii) light commercial tyres,

iii) heavy commercial tyres,

iv) agricultural tyres,

v) motorcycle tyres,

vi) industrial tyres,

vii) aircraft tyres,

viii) earth moving tyres and

ix) other pneumatic tyres.

The Basel convention technical guidelines (United Nations, 2012) identify passenger vehicles tyres and truck tyres as the two major categories of tyres. They report that passenger and truck tyres represent 85% of the total tyres produced. The difference in the anatomy of these two major tyre categories is shown in Figure 2.2.

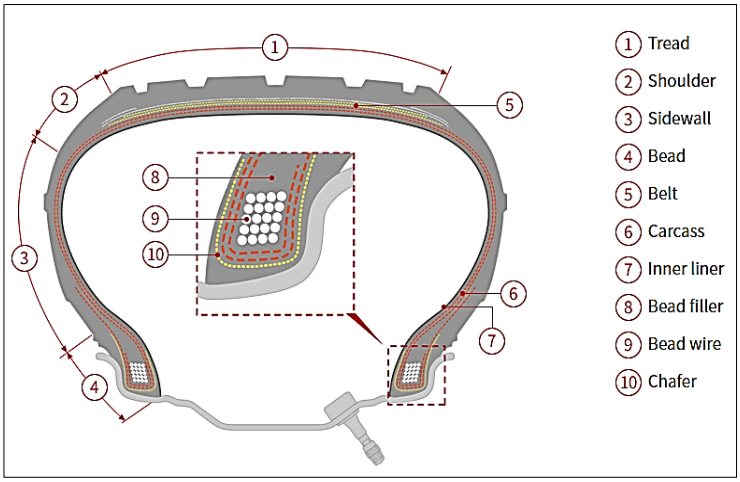

a) Typical pneumatic passenger tyre

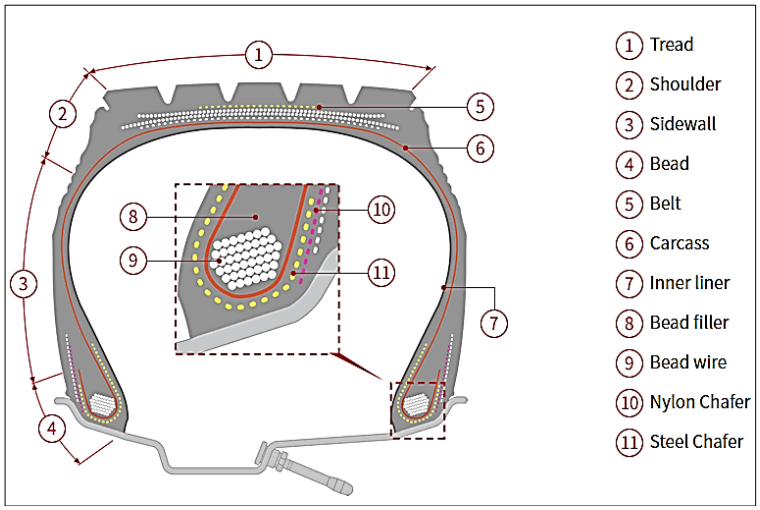

b) Typical pneumatic truck tyre

Figure 2.2: Sections showing different components of passenger and truck tyres (Yokohama tyres, 2018)

Both tyres have relatively the same components but configured differently. The tyre components and their uses are listed below:

(1) *The tread* is the portion of the tyre that contacts the tarmac or the actual road. It is made up of a layer of compounded rubber to cater for its application purposes. The belt and carcass are protected by the tread though its thickness.

(2) *The shoulder* serves to dispel heat created during operation to the environment and protects the carcass and the belt from damage.

(3) *The sidewall* is the part between the shoulder and the bead. It stretches the most during operation.

(4) *The bead area* provides support to the carcass peripheries on each side of the tyre. It also has the purpose of anchoring the tyre to the wheel. It fits to the rim and holds the tyre on to it

(5) *The belt* is a reinforced layer that goes around the outer periphery of the carcass which is beneath the tread. It is meant to stiffen the tread section.

(6) *The carcass* is the load-carrying skeletal structure that gives the form of the tyre. It consists of a rubber fabric overlaid with rubber laying in a radial direction. It contains the compressed air assisting in carrying the weight and diffusing the effect of impact loads.

(7) *The inner liner* is a special type of rubber layer with high air leakage resistance.

(8) *The bead filler* is the bead stiffening rubber with a triangular cross section.

(10) *The bead wire* comprises of numerous steel wires bundled up together to form a circular reinforcement material.

(11) *The Nylon and steel chafer* is nylon or steel cords wound around the bead area in order provide protection to the carcass from damage due to action of the wheel rim like chafing and abrasion.

2.2.1 Pneumatic tyre manufacturing

The manufacturing process of a pneumatic tyre shown in Figure 2.3 involves 4 major stages; materials preparation, tyre component fabrication, tyre building and finally inspection.

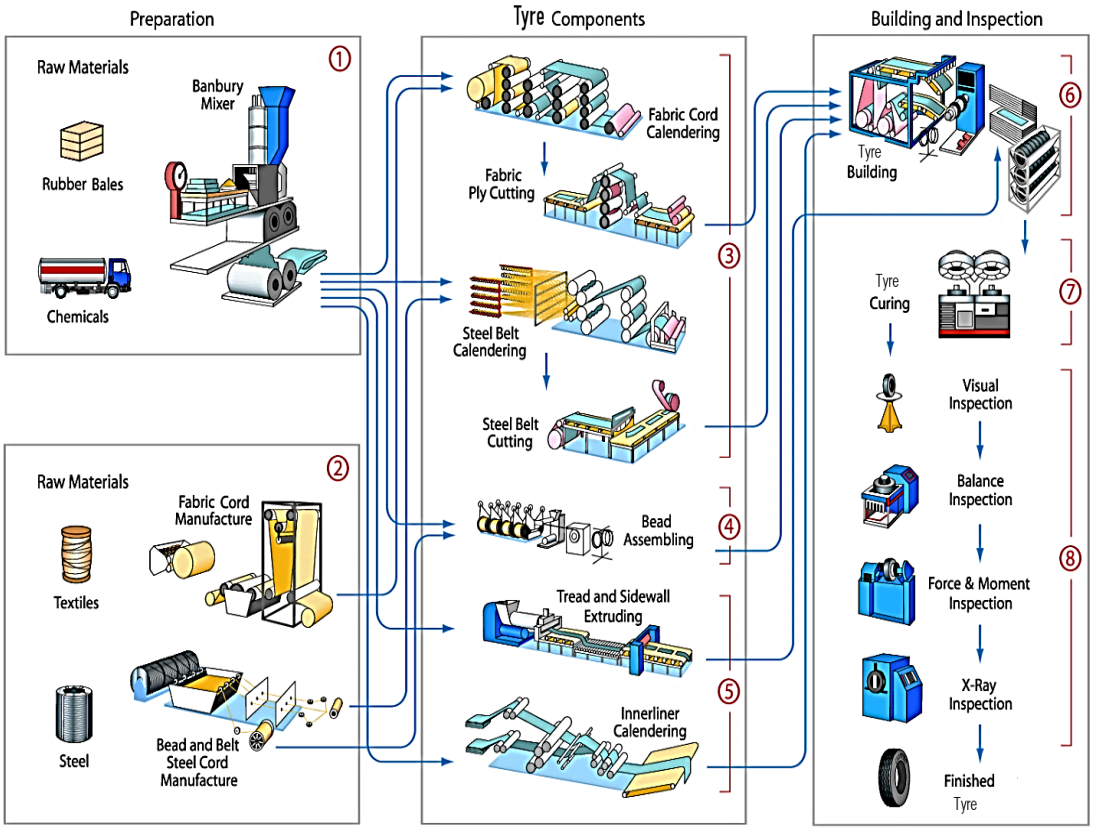

Figure 2.3: Typical tyre manufacturing flow chart (Maxxis Tires, 2018)

Raw materials: The production process makes use of four main classes of raw materials rubber, chemicals, textiles and steel wire. The variation in each of the major classes depends on the type of tyre being manufactured. Table 2.1 shows the detailed list of raw materials used in pneumatic tyre production.

Table 2.1: Pneumatic tyre production raw materials (United Nations, 2012)

Raw material	**Specific type**
Rubber	Natural Synthetic
Chemicals	Sulphur Sulphur compounds
Phenolic resin	Novolak Resole
Oil	Aromatic Naphthenic Paraffinic
Textile	Nylon Polyester
Petroleum waxes	Paraffin wax Microcrystalline wax
Pigments	Zinc oxide Titanium dioxide
Carbon black	Super abrasion furnace Intermediate super abrasion furnace High abrasion furnace General purpose furnace Fast extrusion furnace Semi- reinforcing surface
Fatty acids	Lauric Palmitic Stearic
Inert materials	Silica Barytes

Four major rubber types are used in the production of tyres; natural rubber, polybutadiene rubber (BR), styrene-butadiene rubber (SBR) and butyl rubber. The natural rubber, the SBR and the BR are used to make tyre treads and sidewalls. Buytl rubber together with haloganated butyl rubber are used to make the inside part of the tyre that keeps the compressed air. The two most common fillers are silica and carbon black (Maxxis Tires, 2018). Carbon black is a fine, soft black powder produced when hydrocarbons (oil or natural gas) are not fully combusted. The selection criteria on which to use between silica and carbon black depends on the performance criteria for the tyre component being made. Other contributing

ingredients include antioxidants, antiozonants, anti-aging and curing agents. The determination of the appropriate compound for a particular tyre type is important to produce a strong and durable tyre. In a production plant, the batching process is automated, and the determination is made by computer controlled systems that have a database with different tyre formulations.

Rubber Compound Mixing The mixing of the chosen compound (rubber and chemical) is done by huge mixers (Banbury mixers) in batches of up to 450 kg. The mixers have the capacity to mix more than 200 kg of rubber compound in less than five minutes. The mixing can be done in up to three stages; however, the mixing is typically completed in two stages. In all the stages of mixing, the mix is heated at about 100 – 110ºC under friction to soften the rubber and even spread the chemicals. The chemical composition of the different batches depends on the component of the tyre for which the mix will be used to make.

Body, beads and Tread On completion of the mixing, the batch is taken through a series of rolling mills and squeezed into thick blanket sheet known as a slap. This is then passed to other sections of the process such as bead wire assembly preparation, inner liner calendering, fibre and steel cord calendering, tyre side wall extrusion and tyre tread extrusion.

Tyre building The various tyre components formed from the different machines are all delivered to a tyre-building machine. The tyre building process starts by wrapping the machine with the rubber-layered fibre body plies. Before adding the beads, the body plies ends are stuck together by glue. The ply edges are carefully shaped before extruded side walls and tread are stuck in place by glue and the complete tyre (green tyre) is moved to curing stage.

Curing The green tyre now undergoes a series of chemical reactions at high temperatures of up to 208ºC in a mould. The mould is clam shaped and has a big inflatable bladder. The "*green tyre*" is put over the bladder, as the mould closes the bladder is inflated using steam which shapes the tyre and presses the plain tread rubber on the inside of the mould. The desired tyre properties determine the amount of time spent by the tyre in the mould. Thereafter the tyre is removed from the mould to be tested.

Inspection The tyre is inspected in four stages; visual inspection, x-ray inspection, balance inspection finally force and movement inspection. The visual inspection is for spotting obvious defects. The x-ray examination inspection checks for internal structural defects. The balance and movement inspection ensures that the tyre operates in motion as required. (Maxxis Tires, 2018)

2.2.2 Pneumatic tyre composition

Rubber is the main constituent of pneumatic tyres making up to about 75 - 80% of truck and passenger car tyre weight respectively (United Nations, 2012). The rubber content in each of the tyre classes is fairly comparable but the rubber in truck tyres have a higher natural rubber content. Truck tyre rubber is comprised 65% natural and 35% synthetic rubber; the opposite is true for other tyres (Kocak, 2016).

Table 2.2 gives a simplified representation of tyre material composition, but a typical all-weather tyre can consist of 30 different varieties of synthetic rubber, 8 types of natural rubber and carbon black, 40 kinds of chemicals, waxes, oils,

pigments, silicas and clays (Evans and Evans, 2006). This variance in tyre rubber makes it difficult to recycle waste tyres in making new ones. This means no two tyres from different manufacturers are the same. This results in tyre disposal by means of recycling difficult. The Basel convention technical guidelines (United Nations, 2012) state that tyres have about 1.5% by weight of what can be termed hazardous waste which is considered to be negligible.

Table 2.2: Typical material composition of major tyre categories (Evans and Evans, 2006)

Material	**Percentage composition (%)**		
	Passenger tyre	**Truck tyre**	**Off-the-road**
Rubber	47	45	47
Carbon black	21.5	22	22
Metallic components	16.5	25	12
Textile	5.5	-	10
Zinc oxide	1	2	2
Sulphur	1	1	1
Additives	7.5	5	6

2.3 WASTE TYRE

Tyres have an expected service life of about five years. At the end of their life they need to be disposed of in an environmentally friendly manner. It is estimated that over 1 billion waste tyres are generated annually globally (Forrest, 2017). Tyres are considered waste when they are no longer mountable on vehicles and due to wear and tear, can no longer perform as originally intended by the manufacturer. According to the South African department of environmental affairs (2012) a waste tyre is *"a new, used, retreaded or unroadworthy tyre, not suitable to be retreaded, repaired or sold as a part- worn tyre and not fit for its original intended use "*. Waste tyre generation is unavoidable for as long as there are no alternatives to tyres for use on motor vehicles. However, it is possible to limit the effects of the tyre

waste on the environment by the implementation of sound waste management systems.

2.3.1 Management of waste tyres

Waste tyre stockpiling is minimised by the application of waste hierarchy; reduce, reuse, recycle. The first stage of tyre management is waste avoidance and reduction. In order to reduce the amount of waste tyre produced efforts have been made to educate tyre users on the maintenance of tyres in order to increase the service life of the tyres. Retreading of tyres is also identified as another way of increasing the service life of tyres. A passenger tyre can be retreaded at least once before disposal while treading for a heavy commercial tyre a can be done more than three times dependant of the tyre tread cap. The re-use of a waste tyre is defined as "*the utilisation of waste tyres, in whole or in part, without changing the composition or properties of the waste tyres*" (United Nations, 2012). Table 2.3 gives possible applications for waste tyres. The applications require the tyres to be used whole (WT), shredded (ST) or chipped (CT). The process of producing the chipped and shredded tyre is either through ambient, mechanical or cryogenic process (Naik, and Singh, 1991, Li et al, 2019). These processes are described in Section 2.2.2. Table 2.3 shows that there are a lot of applications for which the tyre does not have to be modified before it is used. Once a tyre has reached its end of life and is beyond retreading, there are a number of applications it can be used for without even needing to cut the tyre up. The bulk of these applications are civil engineering applications.

Table 2.3: Waste tyre re-use applications (United Nations, 2012)

Application	Tyre type	Tyre particle size	Tyre particle production process (see Section 2.3.2)
Embankments	Passenger or Truck	WT/ST/CT	Manual/Ambient
Erosion control	Passenger or Truck	WT/ST/CT	Manual/Ambient
Landfill engineering	Passenger or Truck	WT/ST/CT	Manual/Ambient
Slope stabilisation	Passenger or Truck	WT/ST/CT	Manual/Ambient
Temporary roads	Passenger or Truck	WT/ST/CT	Manual/Ambient
Thermal insulation	Passenger or Truck	WT/ST/CT	Manual/Ambient
Collision barriers	Passenger or Truck	WT/ST/CT	Manual/Ambient
Light weight fill	Passenger or Truck	WT/ST/CT	Ambient
Noise barriers	Passenger or Truck	WT/ST/CT	Manual/Ambient
Train and tram rail beds	Passenger or Truck	CT	Manual/Ambient/Cryogenic
WT – whole tyre; ST – Shredded tyre; CT – crumb tyre			

Waste tyre recycling is the extraction and modification of waste tyre materials to make completely new products or resources. Waste tyre recycling does not include processing of tyres for use as fuels or for backfilling purposes. Table 2.4 shows waste tyre recycling applications. One of the recycling process, pyrolysis, involves the decomposition of tyre rubber using heat in two stages in the absence of oxygen.

The process breaks the rubber down into separate components like carbon black, oils and steel. The carbon black is the one that has been sometimes used in concrete construction as an additive (Ali et al., 2020).

Table 2.4: Recycling applications (United Nations, 2012)

Application	**Waste rubber material used**
Concrete construction additives	Granulates, powder, pyrolytics
Asphalt additives	Granulates, Devulcanisates, pyrolytics
Asphalt rubber	Granulates, powder
Road furniture	Granulates, powder, reclaim, devulcanisates

When the waste management hierarchy of the three Rs (Reduce, Reuse, Recycle) has not exhausted all the waste tyres the other two options left are energy recovery and disposal in landfill or stockpiling. The disposal option is normally the last in the Basel convention technical guidelines (United Nations, 2012) for waste tyre management hierarchy shown on Figure 2.4.

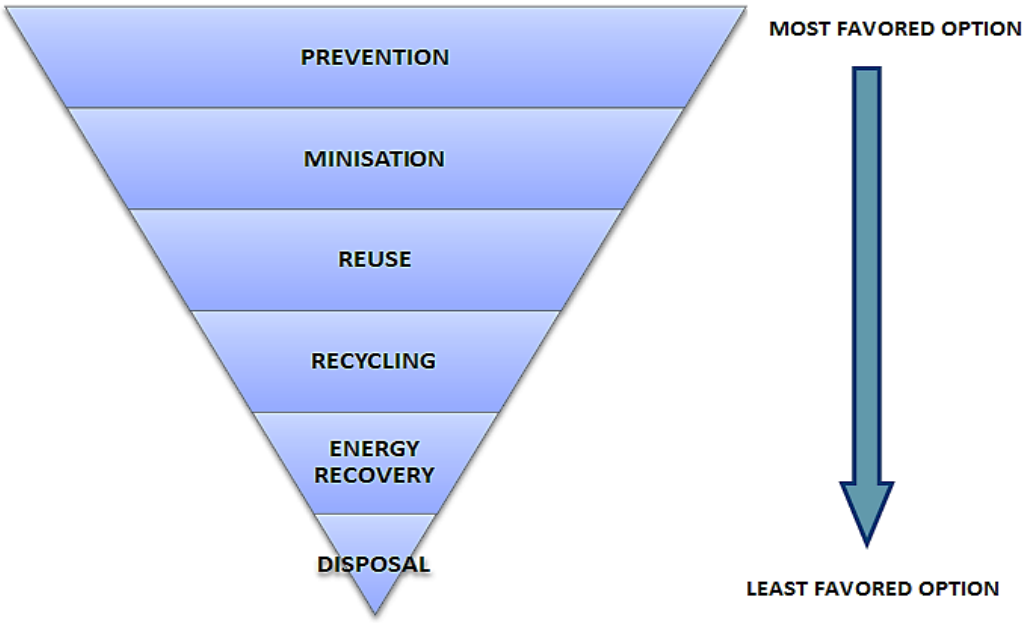

Figure 2.4: Basel convention technical guidelines tyre waste management (United Nations, 2012)

Energy recovery produced by waste tyre crumb rubber has a 20% less carbon footprint compared to coal. When waste tyres are used as a fuel source the products are called tyre derived fuel (TDF). The waste tyres can be used as a fuel in cement kilns, power station, steel and paper industry. According to the Basel convention technical guidelines (United Nations, 2012) TDF does not have any detrimental effects over and above that of traditional fuel sources provided the additional sulphur and nitrogen oxides produced are filtered out of the emissions before releasing into the environment. This is a plausible approach when adequate research and financial backup is available to implement and maintain it for the long haul. The challenge in Africa is lack of financial backing required to install air scrubbers with the capacity to clean the air adequately. The private sector is not willing to invest in a technology they do not need for the sake of the environment without any financial benefit to them. In South Africa the government has offered companies that make use of the TDF financial backing to upgrade their facilities to allow them to use TDF. The money is raised through a tariff charged on each tyre purchased by the consumers (Muzenda, 2014; Nkosi et al., 2013; van Staden, 2012). The money pays for legal collection and disposal of all waste tyres in South Africa. In more developed countries like the US where this technology has been fully developed, manuals on how to use waste tyre energy recovery have been published (Rubber manufacturers Association, 2016). The Figure 2.5 shows that when this technology is fully utilised, TDF can take a huge chunk of the waste tyres.

Although several alternatives to landfilling and stockpiling exist, waste tyres always find their way to landfills. In South Africa it is reported that under 20% of

waste tyres are recycled and a large proportion is dumped illegally. This has left the country with an excess of over 10 million waste tyres to contend with annually (Muzenda, 2014, Sebola et al., 2018; Nkosi et al., 2020). Basel convention guidelines recommend (United Nations, 2012) that when landfilling and stockpiling are the only option left, it should be done in a manner that does not impact negatively on the environment.

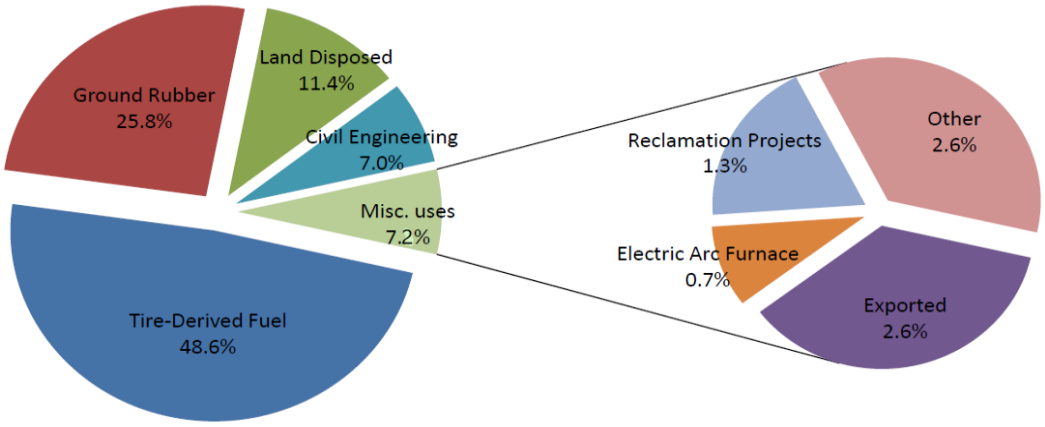

Figure 2.5: American 2015 waste tyre use proportions (Rubber Manufacturers Association, 2016)

2.3.2 Waste tyre rubber classification, production, and properties

Waste tyres which have to be used for different applications are rarely used as whole tyres. They must be reduced to small sizes for easier handling. Waste tyre is then classified according to the size of these particles that is, whole, slit, shredded or chipped, crumb and ground tyre rubber (Figure 2.6).



a) Chipped b) Crumbed c) Ground

Figure 2.6: Different tyre rubber particle sizes (Genever et al., 2017)

Though the cut-off sizes for each group differ, authors generally agree on three classes of waste tyre rubber particles (Li et al., 2019; Strukar et al., 2019; Eldin and Senouci, 1993; Naik, and Singh, 1991). The three main classes are:

i) Shredded / chipped rubber (13 – 73 mm)

ii) Crumb rubber (0.425 – 4.75 mm)

iii) Ground rubber (0.075 – 0.425 mm)

The whole tyres are reduced to these different sizes by one of two tyre processing methods, the ambient process or the cryogenic process. The most commonly used method is the ambient method. The ambient process of making waste tyre rubber particles for use in concrete involves the cutting of the whole scrap tyre diametrically into two halves with the side walls being separated from the threads of the tyre using tyre cutting machines. The slit tyres then undergo primary and secondary shredding to produce tyre shreds or chips. The tyre chips then go through a two-stage magnetic separation and screening process, which removes the steel and fibres present in the tyre. The fibre and steel free rubber is then subjected to further grinding using special mills that produce the crumb and powder tyre rubber (Shulman, 2019; Siddique and Naik, 2004). The process is shown in Figure 2.7.

The cryogenic process makes use of liquid nitrogen to embrittle the tyre rubber particles. The particles are first shredded in ambient process to between 2.54 mm – 7.62 mm. The shredded particles are then chilled using liquid nitrogen. The rubber particles achieve a glass-like brittleness at a temperature below -80°C. These embrittled particles are then ground further before being sorted according to size.

This process mostly yields particles that are less than 2 mm (70% – 80%) (Blumenthal, 1996).

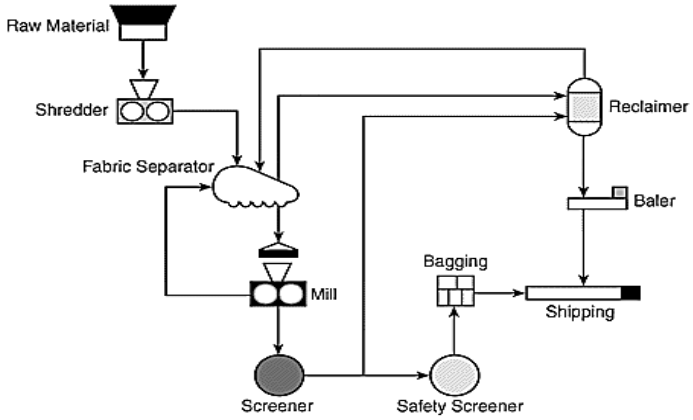

Figure 2.7: Typical ambient rubber particle processing (Recycling Research Institute, 2017)

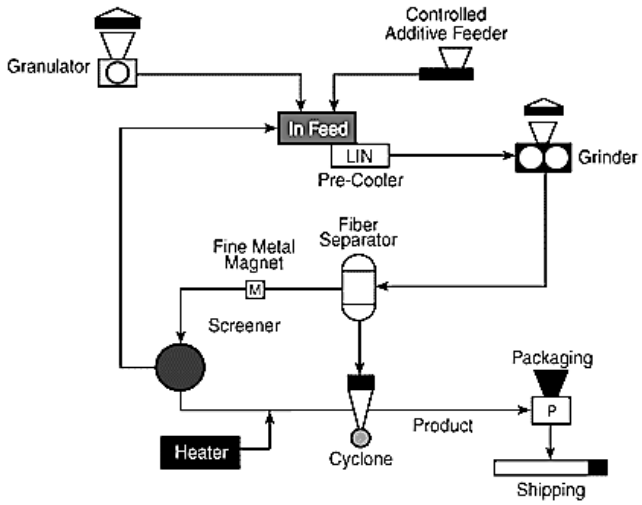

Figure 2.8: Typical cryogenic rubber particle processing (Recycling Research Institute, 2017)

Tyre chips have a loose density of about 320 - 490 kg/m^3 and a compacted density of about 570 - 730 kg/m^3 (Bosscher et al., 1992). The specific gravity of crumb rubber is 1.05 -1.15 (Bompa and Elghazouli, 2019; Heitzman, 1992). The unit weight of rubber particles is much less than that of mineral aggregates thus resulting in a 2 - 2.5 times more tyre rubber aggregate volume for the same mass of mineral aggregate. The elastic modulus and Poisson's ratio of tyre rubber particles

is <5 MPa and 0.5, respectively (Edeskär, 2004). The crumb tyre rubber water absorption is reported to be between 1 – 7% (Bhatt, 2017; Bompa and Elghazouli, 2019; Su et al., 2015a). Crumb tyre rubber produced by ambient mechanical method is generally characterised as being rough-edged, with the finer crumb rubber particles having a rougher surface than larger ones (Kara De Maeijer et al., 2021; Shulman, 2019; Su et al., 2015b). The typical chemical composition of tyre rubber particles as found by different researchers using Energy-dispersive spectrometry is given in Table 2.5. The elemental composition may vary widely among tyres depending on manufacturers, but most tyres will have Carbon, Silicon, Oxygen, Sulphur and a metal in varying percentages though.

Table 2.5: Tyre rubber chemical composition

Element		**Percentage composition (%)**		
Name	**Symbol**	Richardson et al. (2016)	Polydorou et al. (2020)	Sun et al. (2020)
Carbon	C	75.32	91.2	83.18
Oxygen	O	6.95	5.9	14.15
Magnesium	Mg	0.097	-	-
Aluminium	Al	0.085	0.2	-
Silicon	Si	22.17	0.2	1.71
Phosphorus	P	0.25	-	-
Sulfur	S	1.00	1.2	0.96
Potassium	K	0.015	-	-
Calcium	Ca	0.074	-	-
Iron	Fe	0.25	-	-
Cobalt	Co	0.002	-	-
Zinc	Zn	0.64	0.4	-
Sodium	Na	-	0.8	-

2.4 REVIEW OF RUBBERISED CONCRETE PROPERTIES

Waste tyre particles used as aggregates in concrete are also referred to as tyre derived aggregates (TDA). When TDA are used in concrete, rubberised concrete is produced also known as rubberised concrete. The shredded / chipped rubber is

commonly used in concrete to replace the coarse aggregates, while crumb rubber replaces fine aggregates and ground rubber or carbon black is used as filler (Siddique and Naik, 2004, Li et al., 2019). Concrete made with partial or full replacement of mineral aggregates with TDA is used for various applications ranging from crash barriers, railway slippers and road pavements. The applications of rubberised concrete have been assisted by a number of researches that have suggested an improvement in concrete with the inclusion TDA. The following is a discussion on the fresh and hardened rubberised concrete properties.

2.4.1 Workability

Workability is a vital property of fresh concrete which affects the strength and durability of hardened concrete. The American Concrete Institute (2000) defines workability as, "*that property of freshly mixed concrete or mortar which determines the ease and homogeneity with which it can be mixed, placed, consolidated, and finished".* Workability is also thought of as the *"amount of useful internal work needed to adequately compact concrete without bleeding or segregation in hardened concrete"* (Glanville et al., 1947). There are contradicting research findings on the effect of tyre rubber particles as aggregates on the workability of concrete. Some researchers report a decrease in the workability with the addition of rubber in concrete (Albano et al., 2005; Elchalakani, 2015; Yasin, 2012) while others report an opposite trend (Aiello and Leuzzi, 2010; Kotresh and Belachew, 2014). The increase in workability is attributed to the lower water absorption of the rubber aggregates, yet other researchers who reported a decrease in workability attributed it to the high-water absorption of rubber particles.

Khatib and Bayomy (1999) noted that crumb rubber particles result in more workable mixes than chipped rubber particles. Khaloo *et al*. (2008) found that, for crumb rubber mixes, workability increased with tyre aggregate concentrations of up to 15% and thereafter decreased. They observed an opposite trend for chipped tyre. They, however, noted that all the rubberised concrete mixes had acceptable levels of workability in terms of ease handling. Gupta *et al*. (2014) measured workability in terms of compaction factor and slump values. They found that workability was not significantly affected by the crumb rubber particles.

Nehdi and Khan (2001) suggested the use of methods other than the slump test to assess the workability of the mix like the taking of rheological measurements. They argue that the slump test does not provide enough information to ascertain the probable causes of the workability changes observed, and that the knowledge of the rheology of rubberised concrete would give more information. The main divergence on the workability results reported by researchers seems to come from the varying water absorption capacity of the rubber particles. It is however most unlikely that rubber could have such high water absorption to effect significant changes in the workability of the concrete as reported by some researchers due to the non-porous nature of the material (Rashad, 2016).

2.4.2 Air content

Several researchers (Pierce and Blackwell, 2003; Richardson et al., 2011; Sherwood, 1995) found that rubberised concrete has higher air content than conventional concrete. They suggested that tyre rubber aggregates can be used in

place to air entraining admixtures. Richardson et al. (2011) noted that the use of rubber aggregates to increase air content when required should not exceed 0.5% by volume of the aggregates in order not to affect the strength performance of the concrete. However, Topcu and Demir (2007) recommended a much higher replacement value of 10% by volume. Siddique and Naik (2004) attributed the higher air content to the tyre not being partially charged, thus repelling water and tending to trap air on their rough surfaces. Boudaoud and Beddar (2012) reported no change in air content when they replaced 15% by volume of coarse mineral aggregates. The discrepancy between the Boudaoud and Beddar (2012) results, Richardson et al. (2011) and others can be explained by the fact that the former made use of chipped rubber while the latter made use of crumb rubber. Fine rubber aggregates tend to have more rugged edges and rough spots that allow air to be entrapped as compared to coarser or larger tyre rubber aggregates. During mixing these smaller particles also entrap and generate more air bubbles due to their greater specific surface (Zimmermann et al., 2016a).

2.4.3 Rubberised concrete strength and static modulus

It is generally agreed that the incorporation of rubber in concrete reduces the strength of the concrete. Zheng et al. (2008), Jain (2014) and many other researchers (Elchalakani, 2015; Jain, 2014; Malladi, 2004; Naik, and Singh, 1991; Zheng et al., 2008; Polydorou et al., 2020) agree that as the amount of rubber content is increased in the concrete both its flexural and compressive strengths decrease. This behaviour is true for both coarse and fine aggregate replacements. Researchers report strength losses of up to 85% for coarse mineral aggregates and

65% for fine mineral aggregates at 100% replacement level with rubber aggregates (Naik, and Singh, 1991; Malladi, 2004; Zheng et al., 2008; Jain, 2014; Elchalakani, 2015). The elastic modulus decreases by 35% at only 10% fine aggregate replacement. Rubberised concrete properties are influenced by the size, shape, texture and the content of the rubber particles (Sherwood, 1995; Pierce and Blackwell, 2003; Jain, 2014). The reduction in the mechanical performance has been attributed to the significantly lower stiffness (<5 MPa) of the tyre rubber, the uneven distribution of the rubber aggregate in concrete due to its light weight and the poor bonding between the rubber aggregate and the cement paste (Elchalakani, 2015; Jain, 2014; Malladi, 2004; Naik, and Singh, 1991; Nkosi et al., 2013; Zheng et al., 2008). Efforts to limit the reduction in the mechanical performance of rubberised concrete include the optimizing tyre rubber size and content, pretreating the rubber aggregate and using different binder types, such as, magnesium oxychloride cement and cements with supplementary cementitious materials (SCMs) (Eldin and Senouci, 1993; Fiore et al., 2014; Rostami et al., 1993; Segre and Joekes, 2000).

Several authors (Eldin and Senouci, 1993; Khatib and Bayomy, 1999; Topçu and Avcular, 1997) reported that chipped tyre rubber resulted in higher strength losses compared to crumb tyre rubber. Huang et al. (2013) attributes the reduced strength loss for smaller tyre rubber particles to the reduction of stress and strain concentrations in the concrete. The effect of tyre rubber content and rubber aggregate size on the mechanical performance of concrete was assessed by Li et al. (2014). They found that high rubber content and smaller tyre rubber aggregate size

reduced the concrete compressive strength and elastic modulus but increased the ultimate strain. In addition to that, crack length, width and occurrence decreased as well. Their findings concurred with other studies (Atahan and Sevim, 2008; Hernández-Olivares and Barluenga, 2004; Wang, 1984). Thus, with regards to rubber content and size, most researchers have suggested a maximum rubber content of less than 20% total aggregate volume and a tyre rubber size no bigger than crumb rubber (Thomas and Gupta, 2016).

To enhance the bonding between tyre rubber aggregate and cement paste, surface pretreatment of the tyre rubber has been suggested (Lee et al., 1998; Li et al., 2014; Segre and Joekes, 2000; Su et al., 2015, Polydorou et al., 2020; Li et al., 2019). Chou et al. (2010) in his investigation, pretreated crumb tyres with waste organic sulfur compounds from a petroleum refining factory. They found that there was a notable increase in the compressive, tensile, and flexural strengths of concrete specimens containing treated rubber particles. Segre and Joekes (2000) reported an improvement of 17% in compressive strength when crumb rubber (maximum size 35 mesh) was pretreated with 0.1M Sodium Hydroxide (NaOH). Huang et al. (2013) performed a two-stage surface treatment to improve properties of rubber modified rubber cement composites. They used silane coupling agent to modify rubber particle surface and then used cement to coat the treated rubber particles. This method was said to result in up to 30% strength gain. Rostami et al. (1993) found that when crumb tyre rubber is pretreated with carbon tetrachloride, the rubberised strength improved by 57%. Haibo et al. (2014) reported a 25.4% strength improvement in compressive strength at 10% rubber particle content when

the rubber particles were treated with analytically pure anhydrous ethanol solvent (AE), acrylic acid (ACA) and polyethylene glycol (PEG) to reduce the hydrophobic behaviour of their surfaces. Eldin and Senouci (1993) soaked and washed off the surface of the rubber powder with water. Albano et al. (2005) reports an increase in the compressive and splitting tensile strengths of rubberised concrete made from crumb rubber pretreated with NaOH and silane. Balaha et al. (2007) found that when crumb rubber was pretreated with polyvinyl alcohol (PVA) and sodium hydroxide, strength performance of rubberised concrete improved significantly. He et al. (2016) proposed a pretreatment method to generate strong chemical bonds between the rubber and the cement paste. The crumb rubber particles were polarized by first oxidizing them with potassium permanganate solution ($KMnO_4$) and then sulphonated with sodium bisulphite solution ($NaHSO_3$). The results showed a 48.7% strength improvement. Figure 2.9 shows the effect of the pretreat methods discussed on concrete strength.

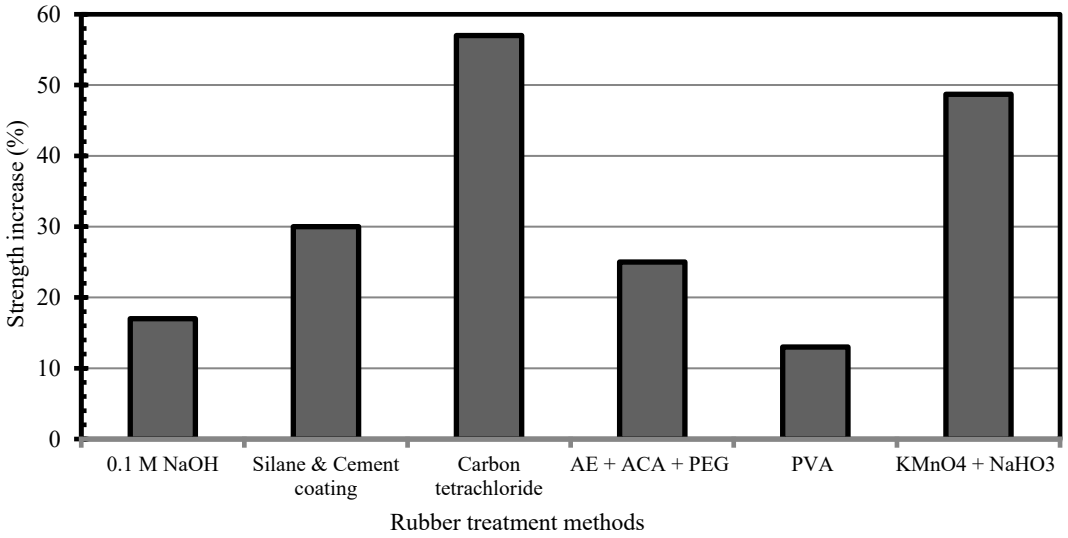

Figure 2.9: Strength increase due to surface pre-treatment relative to untreated rubber (Mushunje et al., 2018a)

Another method that has been utilised to limit strength reduction is the use of different binder types. Some of the suggested binder types include magnesium

oxychloride cement (MOC), Portland cement blended with SCMs. Biel and Lee (1996) noted that the binder type had a significant influence on the compressive strength of rubberised concrete. They made rubberised concrete from two cement types, Portland cement (PC) and MOC. They found that MOC concrete showed about 250% the PC strength. They suggested a limit of 17% fine aggregate replacement with crumb rubber if MOC was to be used to make high strength concrete for structural applications.

When silica fume was used, it was found that a 40% increase in compressive strength was possible for high w/c concretes containing 15% or 25% crumb rubber aggregates by volume (Gesoğlu and Güneyisi, 2007; Güneyisi et al., 2004; Sohrabi and Karbalaie, 2011). Pelliser et al. (2010) produced a 48 MPa structural rubberised concrete, with 10% crumb rubber to fine mineral aggregate replacement by volume and a 15% silica fume-cement replacement at a water-to-binder ratio of 0.40 concrete mix. They reported a synergy between the combinations of sodium hydroxide pretreatment and use of 15% silica fume, with an improvement in the strength performance. A similar synergetic relationship is reported to exist between fly ash and metakaolin with regards to the reduction of strength loss attributed to the presence of waste rubbers (Azevedo et al., 2012). Youssf et al. (2016) evaluated the effect of combining silica fume and varied NaOH pretreatment times on compressive strength. They found that pretreatment greater than 30 min was not beneficial and that a 0% silica fume content gave better results than mixes with silica fume. Despite all these efforts to improve the affected mechanical performance of rubberised concrete, the most viable options would be the

optimization of rubber size and content, followed by using SCMs, because these methods are easier to apply, and their effects are not disputed. This is mainly because most viable pretreatment methods still require further work to be done on them to establish solid standpoint with regards their effect on rubberised concrete performance. Li et al. (2019) having reviewed several published works on tyre rubber pretreatment and precoating methods concluded that these methods could be effective if they were applied in different combinations. However, this makes the whole exercise expensive and not viable. Further research is therefore required to find cheaper and easy to apply tyre rubber surface improvement methods.

2.4.4 Shrinkage

Shrinkage is an important property of concrete because it affects the volume stability of concrete and hence the serviceability functions of the material in structural design (Alexander and Beushausen, 2009). Shrinkage may also influence the strength and durability performance of concrete due to shrinkage-induced microcracks (Li et al., 2020). The microcracks may become crack propagation sites when a mechanical load is applied and may also provide pathways for deleterious substances to get into the concrete (Moonen et al., 2008; Neubauer et al., 1997). Boudaoud and Beddar (2012) found that when coarse mineral aggregate is replaced with tyre rubber aggregate the 28-day drying shrinkage is reduced. They report a 30% reduction in drying shrinkage with 30% replacement. Zaoiai et al. (2016), also reported a 15% decrease in drying shrinkage of self-compacting concrete when 2.5% of fine mineral aggregate is replaced with crumb rubber (0 - 8 mm). Li et al. (2013) investigated effects of crumb rubber on the drying shrinkage and plastic

shrinkage cracking of alkali-activated slag mortar (AASM). They replaced sand with water quenched raw slag to make AASM. They used crumb rubber aggregate size between 1 - 1.5 mm and a partial fine aggregate replacement of 3% - 15%. They found that AASM with crumb rubber had comparatively lower drying shrinkage strains and higher resistance to drying shrinkage cracking. Drying shrinkage reduced by 28.5% at 3% fine aggregate replacement. Other researchers found similar shrinkage behaviour for different types of rubberised concrete (Youssf et al., 2020; Sun et al., 2020). Youssf et al. (2020) found that structural rubberised concrete, for use in ordinary concrete works, had lower shrinkage than conventional concrete. Sun et al., (2020) evaluated the shrinkage performance of macadam with fine rubber particles (40-mesh, 60-mesh and 80-mesh). They found that the crumb rubber enhanced the shrinkage behaviour of the macadam and the improvement increased with crumb rubber size. The reduction in drying shrinkage reported by the researchers agrees with findings that report a reduction in workability due to high water absorption of the rubber. In drying shrinkage, the less water there is to lose the less the concrete deforms. This argument requires further interrogation, there is no explanation as to how the rubber actually absorbs water because rubber would be expected to have less pores compared to mineral aggregates which would make rubber have a lower absorption capability. This would result in higher drying shrinkage strain values for rubberised concrete.

However, other researchers have reported an opposite trend; Sukontasukkul and Tiamlon (2012) found that the inclusion of crumb rubber aggregate in concrete resulted in an increase in drying shrinkage. They also found that smaller crumb

rubber aggregate size (0.707 mm) resulted in 83% more shrinkage than bigger crumb rubber aggregates (3.36 mm) at the same fine aggregate percentage replacement level. This suggests that the rubberised concrete deformations can be more than twice the deformation of the conventional concrete. Rana & Rughooputh (2014) investigated the effects of crumb rubber (0.3 – 4.75 mm) on the properties of fresh and hardened properties of high strength concrete (50 MPa). They found that 20 - 25% replacement improves plastic shrinkage cracking potential of the rubberised concrete. However, they found that a 40% replacement resulted in a 5 to 15% drying shrinkage increase. Bravo and Brito (2012) having investigated the effect of the use of coarse and fine rubber particles, produced by ambient and cryogenic processes on drying shrinkage, concluded that the increase in shrinkage was due to the water-to-binder ratio required when rubber is used and the lower restraint offered by the rubber particles. They also found that the size of the crumb rubber played a greater role than crumb rubber particle production method or shape. Li et al. (2020) found that treating crumb tyre rubber with 0.1M NaOH resulted in a lower increase in shrinkage, 15% less, when compared to rubberised concrete with untreated crumb rubber. Separate studies by other researchers have confirmed this trend, that the inclusion of crumb rubber aggregate in concrete results in an increase in the drying shrinkage of concrete (Elchalakani, 2015; Mohammadi and Khabbaz, 2015; Zhang et al., 2013, Alsaif et al., 2018). There is also consensus that, the increase in shrinkage is mainly due reduced restraint offered by the rubber to the deformation of the concrete due to its lower stiffness. Other reasons that have been suggested include the high porosity and diffusivity of the rubberised concrete due to increased air content which elevates the moisture loss and ultimately shrinkage

(Alsaif et al., 2018). While some have suggested a possibility of the occurrence of stress concentrations which induce microcracks that lead to higher shrinkage (Li et al., 2020). Like other rubberised fresh concrete properties discussed previously, there is little consensus on the effect of rubber on drying shrinkage. It is clear that in-depth studies needed to understand the fundamental changes that affect drying shrinkage mechanisms when rubber aggregate is used. In drying shrinkage, aggregates have the role of restraining the shrinkage movement of the paste; this implies that a stiffer aggregate offers more restraint. In the case of rubber aggregates, it could be assumed that they offer much less restraint than that offered by mineral aggregates thus allowing the concrete to deform more during drying shrinkage.

2.4.5 Creep

Concrete creep is an important aspect of concrete that has received significant attention, particularly with regards to conventional concrete. Creep can have devastating implications to concrete structures in the long-term if not catered for properly (Yang et al., 2020). In recent years, several studies have been done to assess the effects of incorporating tyre rubber into structural concrete on creep (Adamu et al., 2018; Bompa and Elghazouli, 2019; Li et al., 2020b; Mushunje et al., 2018b; Youssf et al., 2020). Most of these researchers found that rubber particles result in an increase in concrete creep. Bompa and Elghazouli (2019) investigated the effect of high rubber content (60% by volume) on the creep performance of high strength (80 MPa) confined fibre reinforced polymer (FRP) concrete. They found that at a loading stress of 20%, rubberised concrete creep is

53% and 20% higher than conventional concrete for confined and unconfined concrete, respectively. Youssf et al. (2020), as part of formulating a concrete mix that could be used for everyday structural works in Australia, subjected his chosen mix to creep tests. The design mix had a strength of 32 MPa and fine aggregate replacement level of 20% by volume and was loaded at 40% of the strength. They noted that with these conditions rubberised concrete creep was 24% higher than conventional concrete. The higher rubberised concrete creep is attributed to the low compressive strength of the rubberised concrete and the low stiffness of the crumb rubber particles which makes the concrete more deformable. Adamu et al. (2018) incorporated 10% crumb rubber particles in roller compacted concrete and observed in increase in creep. They also noted the same increase when the cement was blended with fly ash but found that nano-silica resulted in a decrease in creep. They attribute the decrease observed when nano-silica was used to improved strength and greater concrete stiffness.

Some research have shown a comparable-to-superior creep response of rubberised concrete when compared to conventional concrete. Li et al. (2020) assessed the effect of crumb rubber pretreatment (0.1M NaOH) on creep behaviour of structural concrete (40 – 50 MPa). They discovered that, with 18% replacement by volume of fine aggregates and at a 40% stress level, rubberised concrete creep was lower for both the treated and the untreated concretes. They also noted that the NaOH pretreatment did not have a significant effect on the creep behaviour when compared to the untreated crumb rubber. The deviation of the creep behaviour from what is reported by others in the literature in this case is attributed to the

replacement of the mineral aggregates with rubber particles that were coarser than the mineral aggregate. This is suspected to have changed the void distribution on the concrete and thus affecting the creep behaviour. Although the general trend shows that rubberised concrete creep is higher than conventional concrete, between 20 - 25%, it does not rule it out as a potential candidate for structural application as these could be considered insignificant depending on application. The challenge with comparing these results is that, although they give an indication of the expected creep behaviour of rubberised concrete, their results are generally specific to a certain type of concrete.

Table 2.6 shows a summary of the different concrete types, strength classes investigated, and the tyre rubber particle sizes used by other researchers. All investigations involved the blending of different crumb rubber sizes and none investigated the effect of size on creep deformation. As a recent area of study, the establishment of baseline information is important to better understand the behaviour of the material under constant stress. Baseline information would require the use of concrete with as little modifications as possible. Youssf et al., (2020) note that their incorporation of a water reducing agent resulted in an increase in air content which could have contributed to the observed creep response. Adamu et al. (2018) reported that the nano-silica resulted in reduced creep, while Bompa and Elghazouli (2020) used micro-silica and observed an increase in creep, it can therefore not be ruled out that the presence of silica influenced creep behaviour of the rubberised concrete.

Table 2.6: Rubberised concrete creep studies

Reference	Concrete type	Rubber size and replacement	Applied Stress (strength%)	Creep response
Adamu et al. (2018)	Roller Compacted Concrete (RCC) (Fly Ash, Nano-silica)	40%, mesh 30 40%, 1 – 3 mm 20%, 3 – 5 mm Blended 10% by volume	40%	Increased but Decreased (with nano-silica)
Bompa and Elghazouli (2019)	High Strength Structural (80 MPa)	0 – 20 mm 60% by volume	20%	Increased
Li et al. (2020)	Normal Strength Structural (45 – 50 MPa)	50%, 1.18 mm 50%, 2.36 mm Blended 18% by volume	40%	Comparable and lower
Youssf et al. (2020)	Normal Strength Structural (32 MPa)	2 – 5 mm 20% by volume	40%	Increased

2.4.6 Freeze-thaw resistance

Freeze-thaw durability was one of the first aspects to be investigated in rubberised concrete because of its obvious link to concrete air content. Deterioration in concrete due to freeze-thaw, is a result of freezing and thawing cycles in concrete. Cracks form in the concrete as capillary pore water in the hardened cement paste freezes and expands thus inducing stresses. As the frozen pore water thaws and re-freezes again the induced stresses increase and further expansion occurs and cracking continues. According to Savas et al. (1997), entrained air is used to protect against the adverse effects of freeze-thaw attack. The entrained air results in the formation of small evenly spread-out bubbles that can accommodate the expansion of water inside them during the freezing process. Topçu & Demir (2007) conducted a study to optimize crumb tyre rubber aggregate percentage content by volume in concrete for effective freeze/thaw protection. Their specimens were subjected to 30 freeze-thaw cycles in accordance to ASTM C666 before their compressive strength was determined. In their study they replaced fine aggregate with 10%, 20% and

30% crumb rubber (1 – 4 mm). They found that 10% crumb rubber content allowed for the beneficial freeze-thaw protection effects to take effect without significant strength reduction due to the incorporation of rubber. Richardson et al. (2011) also investigated the feasibility of using crumb rubber to protect against freeze-thaw attack on concrete. They found that 0.5% by volume of crumb rubber was the optimum content that could be used without loss in concrete strength. Kardos & Durham (2015) exposed beams with crumb aggregates to 324 freeze-thaw cycles also in accordance to ASTM C 666 with exception that they tested their specimens after 28 days. They found that the 10% by volume replacement specimens gave the best durability factors, which they define as "*the ratio of the number of cycles at test termination to the number of cycles when the test was terminated*" (324), of all the other specimens. They also noted that the durability factors began to decrease significantly after 20% crumb rubber content. Zhu et al. (2012) found that freeze-thaw resistance increase with an increase in rubber particle fineness. Research on the beneficial effects of rubber aggregate with respect to freeze-thaw durability has shown that the inclusion of tyre rubber improves the free-thaw resistance of concrete. The positive effect is attributed to the increase in air content with the inclusion of rubber aggregate (Bravo and de Brito, 2012; Panda et al., 2012; Sherwood, 1995; Thomas et al., 2014). Researchers agree that tyre rubber is beneficial when it comes to freeze-thaw durability due to the increased air content.

2.4.7 Carbonation resistance

The carbonation resistance of concrete with waste tyre rubber aggregates has been investigated. Carbonation involves the reaction of atmospheric carbon dioxide with

calcium hydroxide in hardened cement paste pores to form calcium carbonate. The reaction results in the reduction of the concrete pH which when it reaches the reinforcing steel destabilises the iron layer on the steel and depassivates the steel. This depassivation makes the steel more susceptible to corrosion. Carbonation rate is related to the permeability of the concrete, that is, the ease with which the carbon dioxide can penetrate the concrete. This is a function of the structure and interconnectedness of the pores in the concrete. The carbonation resistance of rubberised concrete is reported to increase by some authors while others reported an opposite trend. Bravo and Brito (2012) investigated the effect of crumb and chipped tyre rubber aggregates produced by ambient and cryogenic processes on carbonation resistance of the concrete. They found that the carbonation depth increased with increase in tyre rubber aggregate volume. They also found that the tyre production method did not influence the carbonation durability performance of the concrete. They reported lower carbonation resistance for chipped rubber when compared to crumb rubber aggregates. They attributed the general higher carbonation depth to the increased void volume between tyre rubber particles and the binder. Gupta et al. (2014) assessed the carbonation resistance of concrete with tyre rubber particles (0.15-1.9 mm) at different replacement levels (0 - 25%) and 3 w/c ratios (0.35, 0.45 & 0.55). Their findings concurred with those of Bravo and Brito (2012).

Thomas et al (2014) reported an opposite trend. They reported a decrease in carbonation depth for rubberised concrete with crumb rubber aggregate up to 12.5% replacement. They however report a gradual increase in carbonation depth from

10% up to 20% crumb rubber substitution. The assertion that rubberised concrete has higher air content than plain concrete is a more accepted proposition than the contrary. The effect of this increase in air content on penetrability is dependent on the distribution of the pores in the concrete. The distribution of the rubber particles is strongly influenced by the mixing and compaction method used. An analysis on the pore and rubber distribution in the matrix would likely explain the difference in the reported durability performances. Nonetheless, in general, rubberised concrete has reduced carbonation resistance save for very low w/c ratios (0.3) and low replacement levels (<10%).

2.4.8 Chloride penetration resistance

Chloride penetration resistance of rubberised concrete has been investigated with little agreement amongst researchers. Chloride ingress is the penetration of chloride ions into the concrete through its pores, which mainly thought to be by diffusion and migration (Nissen, 2016). This means the more porous a concrete is the less resistant to chloride ingress it is. The prevention of chloride ingress in concrete is important since upon penetration to the reinforcement steel, the chlorine ions destroy the passive layer around the steel and leave the steel more susceptible to corrosion (Roy et al., 1993). Some researchers report an increase in chloride penetration resistance with an increase in rubber content, and some researchers report a decrease. According to Oikonomou and Mavridou (2009) the introduction of crumb rubber in concrete mortar improved the chloride ion penetration resistance of the mortar. They found that the lowest rubber content produced a significant reduction in chloride ion penetration when compared to the control mix. The 2.5 %

and 15% rubber content mixes gave a 14.22% and 35.85% decrease respectively. Several other researchers (Ghedan and Hamza, 2011; Mohammed et al., 2012; Thomas et al., 2014) had similar findings to those of Oikonomou and Mavridou (2009).

Gupta et al. (2016, 2014) reported a decrease in the chloride diffusion coefficient with an increase in rubber content for all water-cement ratios compared to the reference mix. Onuaguluchi and Panesar (2014) replaced 5 - 10% by volume of fine aggregate with crumb. They report a reduced charge transmission for all the replacement levels. Li et al. (2016) conducted rapid chloride permeability tests for concrete made with treated and untreated rubber aggregates. The rubber aggregates were pretreated with silane coupling agent and carboxylated strene-butadiene rubber latex. They found that for both treated and untreated rubber aggregate mixes there was a decrease in chloride penetration up to a limiting replacement level, 5% and 15% for untreated and treated rubber mixes respectively. They report that higher replacement levels result in poor durability performance. Bravo and Brito (2012) reported a contrary behaviour. Their chloride migration test showed an increase in chloride diffusion coefficients for the 5% to 15% replacement levels of tyre rubber aggregates. They found that the replacement of coarse aggregates with chipped rubber particles resulted in a much higher decrease in chloride penetration resistance as compared to crumb rubber. They also found that aggregate produced by the ambient process had better durability performance than those produced by cryogenic process. Similarly, Gesoglu and Guneyisi (2007) reported a continuous decrease in the chloride penetration resistance with increasing crumb rubber content

in self-compacting rubberised concrete. Thomas et al. (2015) found that rubberised concrete with up to 10 % crumb rubber by volume replacement level had lower or similar chloride penetration depth and mixes with 12.5% - 20% crumb rubber had high chloride penetration compared to the control mix. As highlighted in the carbonation section the distribution of rubber particles in the matrix might have a great influence on the penetrability of a concrete.

2.4.9 Thermal conductivity

The thermal conductivity of concrete measures the ability of concrete to conduct heat (Sinha, 2012; Taylor, 1991; Vengatesan et al., 2018). Thermal conductivity of concrete is an important factor in construction as it relates to the total of heat loss through walls and roofs which directly influences the energy consumption of buildings (Asadi et al., 2018). It is dependent on the concrete moisture content, the aggregate type, the concrete density, and the porosity of the concrete (Sinha, 2012; Taylor, 1991; Vengatesan et al., 2018). The higher the porosity the lower the thermal conductivity. Ghedan and Hamza (2011) used treated and untreated chipped rubber particles to replace coarse aggregates in concrete. They found a reduction in thermal conductivity of 26.7% for 15% untreated rubber content and an increase of 17.8% for treated rubber when compared to the control mix. The treated rubber was treated with silane and it also exhibited an increase in thermal conductivity when compared with untreated rubberised concrete with same rubber aggregate replacement level. Mohammed et al. (2012) replaced cement with a combination of 10% silica fume and fly ash and found that it resulted in a reduction of the thermal conductivity of rubberized concrete. This was attributed to the

thermal conductivity of the materials, which are lower than that of Portland cement. Fiore et al. (2014) found that the inclusion of 10% by volume, of fine rubber aggregate resulted in a 23% improvement of thermal insulation. These studies have shown that rubberised concrete containing either chipped or crumb rubber particles exhibit a lower thermal conductivity when compared to plain concrete. Ocholi et al. (2014) in their study of the thermal performance of rubberised concrete, found that the thermal conductivity of concrete had reduced by 29% at rubber replacement level of 25%. The concrete specific heat capacity also dropped by 30% for the same rubber replacement level. The research on the thermal conductivity of rubberised concrete suggests that the material is a thermal insulator because of its lower conductivity when compared to plain concrete.

2.4.10 Acoustic properties

Acoustic properties of a material covers two aspects; its sound absorption and its sound insulator or transmission capabilities. Holmes et al. (2014) defines acoustic properties of concrete as its capability to transmit or absorb of sound waves. Porous concrete is a good sound absorber but is a poor sound insulator (Kim and Lee, 2010; Park et al., 2005). Rubberized concrete is effective in absorbing sound, impact and vibrations energy compared to plain concrete (Pacheco-Torgal et al., 2012). The sound absorption properties of crumb rubber concrete are better compared to plain concrete. Jedidi et al. (2014) found that the sound absorption and noise reduction coefficient increased with an increase in crumb rubber percentage replacement levels. They suggested that the higher sound absorption of rubberised concrete was due to the increase in air voids in the concrete. Holmes et al. (2014)

investigated the sound absorbance and insulation properties of rubberized concrete at low (63, 125, 250 & 500 Hz) and high (1000, 2000, 4000, 5000 Hz) frequencies. They found that the sound insulation performance of rubberised concrete was comparable to plain concrete for all the replacement levels. They noted that the absorption coefficient, however, increased for all replacement levels and for all rubber particle sizes. The crumb rubber concrete was a more effective sound absorbent than plain concrete in different temperature conditions. It was also found that crumb rubber particles produced concrete with better high frequency sound absorption performance because of its higher surface area. Bjevgovic et al. (2013) also reported that incorporating rubber in concrete noise barriers increases the sound absorption capabilities of the barriers by 6 dB. Generally, research supports the assertion that rubberised concrete is a better sound absorbent compared to plain concrete. This observation is attributed to the increased voids in the concrete and the existence of cracks between the matrix and the rubber particles due to lack of bond.

2.4.11 Summary of rubberised concrete properties review

There is still much disagreement in literature with regards to most of the rubberised concrete properties. However, there is general agreement on the great potential for the application of rubberised concrete in structural construction and its ability to help tackle the waste tyre disposal problem. The following are conclusions drawn from the literature review on rubberised concrete.

a) There are contradicting findings on the effects of waste tyre rubber on the fresh properties of concrete, particularly, its workability in terms of slump. There is

a need for other tests besides the slump test to study the rheology of fresh rubberised concrete in order to understand how rubber actually interacts with other concrete constituents in this state.

b) The inclusion of waste tyre rubber in concrete results in reduced strength but with optimisation of rubber aggregate size and content, pretreatment of the rubber aggregate and use of supplementary cementitious materials (SCMs) it is possible to produce concrete fit for structural use.

c) The durability of rubberised concrete with regards to chloride attack and carbonation is still questionable.

d) There is an improvement in the freeze-thaw durability of concrete with the introduction of tyre rubber aggregate in the concrete. This is attributed to the increase in air content of the concrete.

e) The shrinkage deformation behaviour of rubberised concrete is also not fully understood. It is agreed, though, that the micro cracking resulting from shrinkage is significantly reduced by the presence of rubber.

f) Majority of the limited literature show that rubberised concrete creep is higher than that of conventional concrete. This is attributed to the low stiffness of the rubber particles that offer little restraint during deformation.

g) Rubberised concrete exhibits superior qualities in terms of thermal conductivity, sound absorption and impact resistance.

h) There exists gaps in the rheological studies of fresh rubberised concrete. Also, in time-dependent studies of structural rubberised concrete, particularly creep, using concrete that has not been modified (by extenders or admixtures) to

eliminate the known effect of rubber in concrete. The effect of crumb rubber size on time-dependent deformations has also not been fully investigated.

2.5 TIME-DEPENDENT DEFORMATIONS IN CONCRETE

2.5.1 Shrinkage

Throughout its life, concrete undergoes volumetric changes both in its fresh and hardened state (Alexander and Beushausen, 2009). In unloaded concrete, the volumetric changes can be due the movement of water in concrete. Depending on the nature of the movement of water, the concrete will either shrink or swell. Swelling occurs when water is absorbed by the cement gel and the gel particles are forced apart by the water molecules acting against the binding forces. When there is removal of water from the concrete system by any means the concrete will undergo shrinkage. The various means by which water is removed from concrete includes processes such as evaporation, hydration and carbonation. According to Esping (2007) shrinkage is a time dependent phenomenon that can be divided into early age shrinkage and long term shrinkage. Early age shrinkage of concrete occurs within the first 24 hours of mixing and long-term shrinkage occurs beyond the 24 hours. Figure 2.10 shows various types of shrinkage and the mechanisms thereof.

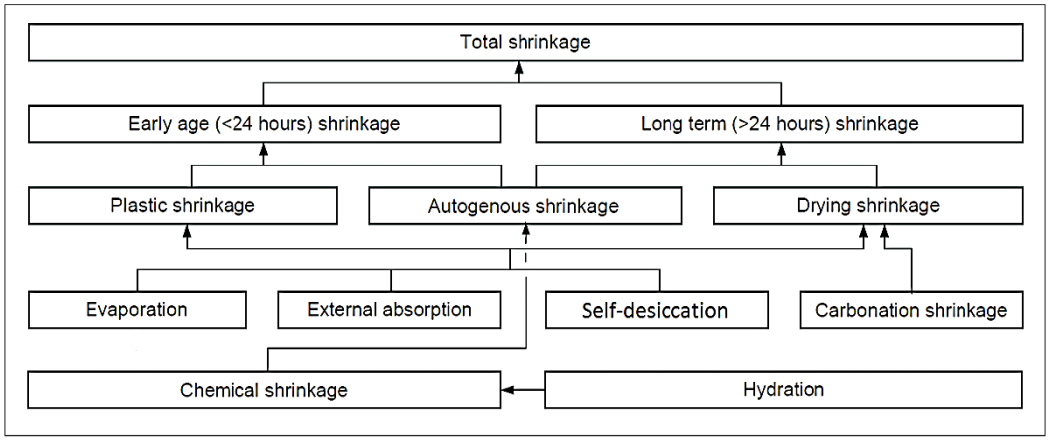

Figure 2.10: Governing mechanisms of total shrinkage in concrete (Esping, 2007)

2.5.2 Types of shrinkage

Plastic shrinkage

Early age volume reduction of concrete due to a high rate of water loss in compacted fresh concrete is referred to as plastic shrinkage (Owens, 2013). The concrete reduces by the same amount of water. The volume reduction is due to the fast drop in the pore water level resulting in an increase in pore water pressure causing neighboring solid particles to get closer together (Sadiqul Islam and Gupta, 2016). Water can be removed from the fresh concrete through evaporation or by suction by underlying dry surfaces like old concrete and in-situ soil. The rate and magnitude of the water loss from the concrete surface through evaporation is affected by several factors. These factors include, the concrete temperature, the ambient temperature, the relative humidity, and the wind speed. If the evaporation rate exceeds the movement of water to the upper surface of the concrete through bleeding and the concrete movement is restrained by non-shrinking concrete, the mould or reinforcement, tensile stresses are set up at the concrete surface. When these tensile stresses are more than the tensile strength of the concrete surface, cracking occurs (Figure 2.11) (Neville, 2011; Sayahi, 2016).

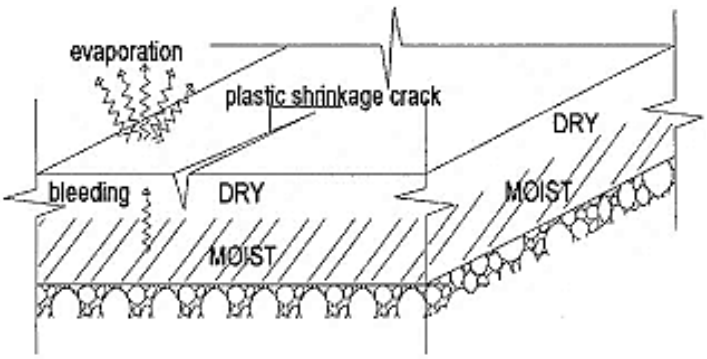

Figure 2.11: Formation of plastic shrinkage cracks (Soroushian and Ravanbakhsh, 1998)

The cracking is referred to as plastic shrinkage cracking. Plastic shrinkage cracks typically form parallel to each other (Figure 2.12a) or in a random manner (Figure 2.12b). The crack lengths range between 25 – 2 000 mm and are often near straight, spaced between 300 – 1000 mm next to each other (Cement Concrete and Aggregates, 2005). They rarely extend to the concrete surface perimeter because unrestrained movement is possible there.

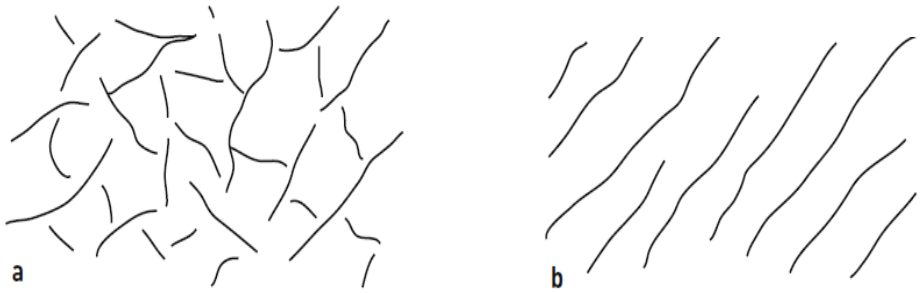

Figure 2.12: Typical plastic shrinkage cracking (Cement concrete and aggregates, 2005)

According to the National Ready Mixed Concrete Association (2014) concrete mixes with a lower bleeding rate or amount are most prone to plastic shrinkage cracking even when ambient conditions are not adverse. On the other hand, Neville, (2011) noted that the relationship between bleeding and plastic shrinkage is not straightforward. He, however, notes that the lower the water-to-cement ratio and higher cement content the greater plastic shrinkage. Generally, any factor that reduces bleeding such as high binder content, more fines content, low water content, entrained air and elevated concrete temperatures increase the susceptibility of concrete to plastic shrinkage cracking. Plastic shrinkage cracks rarely result in impaired concrete but the hairline cracks can act as entry points for deleterious agents that will affect the durability of the concrete (Combrinck and Boshoff, 2009).

Autogenous shrinkage

Autogenous shrinkage also referred to as basic shrinkage, is the reduction in volume through a phenomenon called self-desiccation, which is the removal of capillary pore water during hydration of hitherto unhydrated cement and the formation of hydration products which occupy lesser volume than the original reagents. Autogenous shrinkage is the reason concrete contracts even in sealed conditions where there is no moisture loss to the environment (Alexander and Beushausen, 2009; Neville, 2011). In normal strength concrete, with normal range w/c ratios (>0.4), autogenous shrinkage is considered negligible when considering total shrinkage. Autogenous shrinkage micro strain values can go up to about 40 in one month to only about 100 after five years (Davis, 1940). Autogenous shrinkage in high performance concrete, with w/c ratios lower than 0.4, has a significantly higher proportion in total shrinkage. In fact, at very low water/cement ratios, autogenous shrinkage microstrain can go as high as 700 (Tazawa and Miyazawa, 1995a).

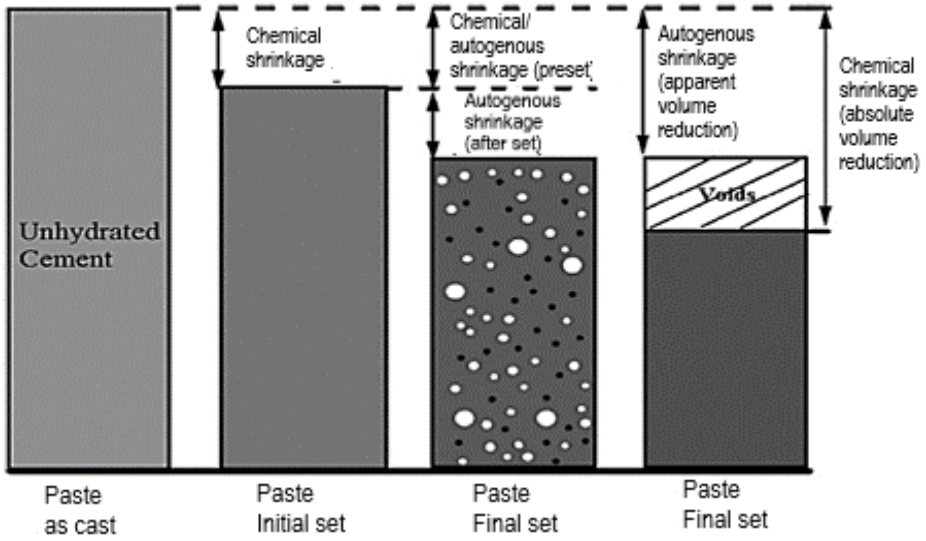

Figure 2.13: The chemical and autogenous shrinkage relationship (Wu et al., 2017)

A close relationship exists between autogenous shrinkage and chemical shrinkage. Chemical shrinkage, is viewed as the microscopic volumetric change that drives autogenous shrinkage which represents the macroscopic volume change of concrete as illustrated in Figure 2.13 (Wu et al., 2017). Tazawa (1999) presents chemical shrinkage as the complete volume reduction of reactants during the hydration process described by the Equation 2.1.

$$S_{hy} = \frac{(V_c + V_w) - V_{hy}}{V_{ci} + V_{wi}} \times 100 \quad \text{..... Eqn. 2.1}$$

where:

S_{hy} *is chemical shrinkage ratio (%)*

V_{ci} *is volume of cement before mixing*

V_c *is volume of hydrated cement*

V_{wi} *is volume of water before mixing*

V_w *is volume of reacted water*

V_{hy} *is volume hydration products*

The autogenous shrinkage mechanism involves a reduction in the volume of fresh cement during the hydration process and a decrease in the internal relative humidity of the system in the long run (Mors, 2011). The mechanism occurs over 3 stages, namely; the liquid stage, the skeleton formation stage and the hardened stage (Holt, 2001; Rajayogan, 2009). In the liquid phase of the concrete chemical shrinkage is well known to be the primary driver of basic shrinkage (Lura et al., 2003; Wu et al., 2017). As the concrete sets and hardens chemical shrinkage becomes greater than autogenous shrinkage as the hardening cement paste frame restricts of further volume reduction. This restriction of volume reduction due to chemical shrinkage causes voids to be formed, further to this, the continued hydration results in the drawdown and emptying of water particles from the pores. This has the effect of decreasing the relative humidity and increasing the curvature of water-air menisci,

which in turn increases the surface tension (Rajayogan, 2009). The increased surface tension induces compression forces on the capillary pore walls causing the hardened cement paste to contract, in this process of self-desiccation. In this process an increase in the menisci due smaller pore diameter can increase the surface tension as well, resulting in increased basic shrinkage (Fang et al., 2018; Nawa and Horita, 2005).

Given that autogenous shrinkage originates from the hydration process of cement it is expected that factors affecting the hydration process like cement composition and fineness, would have an effect on the shrinkage of concrete as well. According to work done by Tazawa and Miyazawa (1995b) the mineral composition of cement, with regards to tricalcium silicate (C_3S), dicalcium silicate (C_2S), tricalcium aluminate (C_3A) and tetra calcium aluminate ferrite (C_4AF), has an effect on the autogenous shrinkage because of the way these mineral compounds hydrate. They found that when comparing experimental autogenous shrinkage measurements and with values obtained from an equation (Equation 2.2) used to predict autogenous shrinkage, there was close correspondence. The equation is obtained by multiple regression of mineral composition of cement as given by the Bogue method with the autogenous shrinkage measured for the respective cements at corresponding ages.

$$\varepsilon_{as}(t) = -0.012\alpha C_3S(t)(\%C_3S) - 0.070\alpha C_2S(t)(\%C_2S) + 2.256\alpha C_3A(t)(\%C_3A) + 0.859\alpha C_4AF(t)(\%C_4AF) \quad \text{Eqn. 2.2}$$

where $\varepsilon_{as}(t)$ *= autogenous shrinkage at age t*

$\alpha(t)$ *= degree of hydration of mineral at age t*

$(\%C_3S)$ *=* C_3S *content,e.t.c*

Neville (2011) reports that basic shrinkage is higher for cements with an increased C_3A and C_4AF content. In terms of impact, C_3A has the most influence followed by C_3S, C_4AF and lastly C_2S (van Breugel and van Tuan, 2014). With regards to fineness, research shows that finer cement results in higher autogenous shrinkage. This is attributed to the increased specific surface area of cement which elevates the hydration rate and accelerates the reduction of the internal relative humidity (Bentz and Jensen, 2004). Autogenous shrinkage is also reported to decrease with the use of fly ash in cement because it inhibits the reduction of the internal relative humidity of the concrete (Alexander and Beushausen, 2009). However, slag and silica fume have an opposite effect on autogenous shrinkage. Their presence results in more refined pores which causes an increase of the capillary tension which in terms increases autogenous shrinkage (Khairallah, 2009). Elevated temperatures and decrease in the water to binder ratio resulted in increased autogenous shrinkage. Autogenous shrinkage initiates and reaches a limiting at about 10 weeks, with 40% occurring within the first 24 hours (Alexander and Beushausen, 2009).

Carbonation shrinkage

Carbonation shrinkage occurs when atmospheric carbon dioxide and the constituents of hardened cement paste react to form calcium carbonate with other cement compounds disintegrated shown in Equation 2.3 and Equation 2.4 (Wu et al., 2017). Atmospheric carbon dioxide (CO_2) dissolved in water is thought to react with cement hydration products like calcium silicate hydrate (C-S-H) resulting in a reduction of the calcium/silicate ratio and an accompanying loss of water (Mindess

et al., 2003) or reacts with calcium hydroxide to form calcium carbonate and water (Šahinagić-Isović et al., 2012).

$$CaO\text{-}SiO_2\text{-}H_2O + CO_2 \rightarrow CaCO_3 + SiO_2 + H_2O \quad \text{Eqn. 2.3}$$

$$Ca(OH)_2 + CO_2 \rightarrow CaCO_3 + H_2O \quad \text{Eqn. 2.4}$$

The level of shrinkage due to carbonation that takes place is normally at its peak at a relative humidity of about 50% but negligible at lower (20%) and higher (100%) relative humidities (Clarke, 2009). Carbonation cannot occur at high humidities because the penetration of carbon dioxide into the cement paste is hindered by the saturation of pores with water, while at very low humidities carbonation cannot occur due to lack of moisture (Swenson and Sereda, 1968). Carbonation shrinkage takes place over a long period of time and may even be more than drying shrinkage in magnitude (Alexander and Beushausen, 2009).

Drying shrinkage

Drying shrinkage is a process that involves the reduction in hardened concrete volume when exposed to a drying environment due to the withdrawal of water from the concrete. A significant amount of drying shrinkage occurs when adsorbed water is lost as compared to free water (Neville, 2011). This means that the removal of bond water that is held in the gel pores during the drying of the concrete is the main reason behind volume change. Drying shrinkage is a time dependent deformation as it happens over a period of time. According to Neubauer et al. (1997) there are four generally accepted drying shrinkage mechanisms; capillary stress (P_{cap}), disjoining pressure (P_{dis}), Gibbs-Bangham (surface free energy- P_{sfe}) shrinkage and the

removal of interlayer water. The capillary stress and the disjoining pressure mechanisms are said to operate at relative humidity greater than 40%. The Gibbs-Bangham and the removal of interlayer water operate at relative humidities of less than 30% and 11% respectively.

Capillary stress. When capillary pore water is lost in a drying environment a meniscus is formed in the capillaries. The menisci formed in the partially filled capillary pores are under hydrostatic tension which it transfers to the pore walls placing the paste under compression. This action causes contraction and shrinkage of the overall volume of the paste (Figure 2.14) (Neubauer et al., 1997; Mindess et al., 2003).

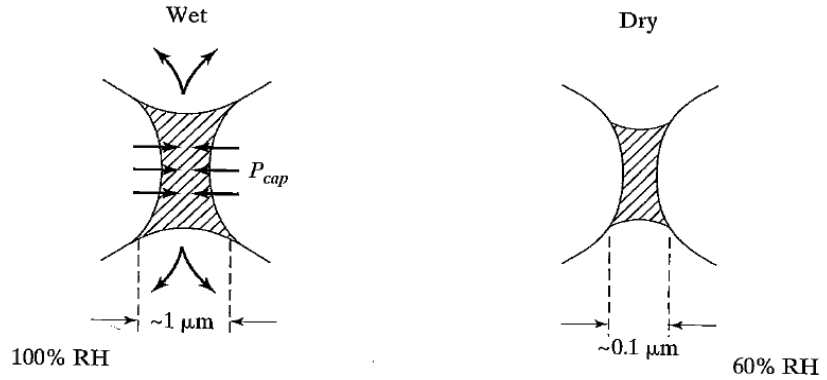

Figure 2.14: Capillary tension shrinking mechanism (Mindess et al., 2003)

Disjoining pressure (P_{dis}). It is also known as swelling pressure is due to the evaporation of adsorbed water from surfaces of linked Calcium-Silicate-Hydrate particles. The removal of water results in a volume reduction of the paste as the layer of water is also reduced (Figure 2.15) (Neubauer et al., 1997; Mindess et al., 2003).

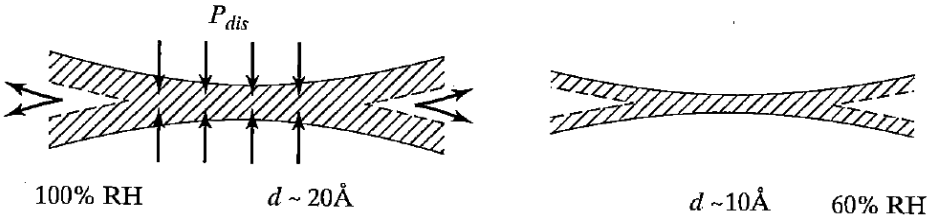

Figure 2.15: Disjoining shrinking mechanism (Mindess et al., 2003)

Gibbs-Bangham shrinkage. Is also referred to as the surface free energy. It is due to removal of adsorbed surface water which causes an increase in the Calcium-Silcate-Hydrate specific surface free energy. Shrinkage occurs as the paste reduces its surface area to reduce the surface tension (Figure 2.16) (Neubauer et al., 1997; Mindess et al., 2003).

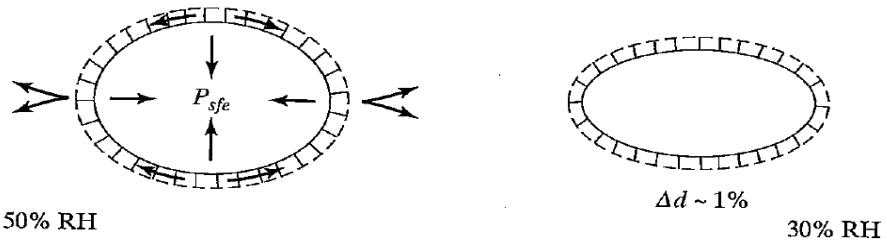

Figure 2.16: Gibbs-Bangham shrinkage mechanism (Mindess et al., 2003)

Loss of the final interlayer. Loss of final monolayer of interlayer water occurs within individual calcium-Silcate-hydrate particles. This is the removal of adsorbed water from in-beetween layers of C-S-H particles at very low humidity (<11%) resulting in somee volume reduction of the paste (Neubauer et al., 1997).

All shrinkage in concrete normally originates from the cement paste and in order to limit the amount of volume change, aggregates are added to dilute and restrain the movement. This means that when the volume of aggregate is increased shrinkage is expected to decrease and that when the aggregate is stiffer, shrinkage will also be reduced. Hobbs and Parrot (1979) suggest that this assertion of the effect of

aggregate stiffness is only valid for low-density aggregates or weathered materials. Alexander and Beushausen (2009) report that there is considerable disagreement on the work reported by Hobbs and Parrot (1979) with regards to aggregate stiffness, citing work done by the National Building Research Institute in Pretoria which found a good correlation between shrinkage and specific surface of the aggregate. Work carried out by Troxell et al. (1958) and Alexander (1993) revealed an obvious dependence of concrete shrinkage on the properties of the aggregates. Neville (2011) also concurs with the proposition that aggregate stiffness plays a major role in restraining concrete shrinkage. To this effect, Pickett (1956) proposed a model that predicts the ratio of shrinkage of concrete to shrinkage of cement paste based on the volume fraction of the aggregate and a complex function of the elastic modulus and Poisson's ratio (Equation 2.5).

$$S_c/S_p = (1 - V_a)^n \quad \text{.....Eqn. 2.5}$$

where S_c and S_p are the shrinkage of the concrete and paste respectively, V_a is the volume fraction of the aggregate, and n is a function of the elastic moduli (E) and Poisson's ratios(μ) of the concrete and aggregate and varies between 1.2 and 1.7 given as (Equation 2.5a):

$$n = \frac{3(1-\mu)}{1+\mu+2(1-2\mu_g)E/E_g} \quad \text{.....Eqn. 2.5a}$$

Using equation Eq. 2.5, concrete with 70% aggregate volume will show shrinkage of about 10 – 15% of the corresponding paste shrinkage. Similarly, a 1% increase in paste content will result in a 6% increase in concrete shrinkage. The equation shows a great dependancy of shrinkage on aggregate content, thus minor changes in aggregate volumes will result in large effects on shrinkage as shown on Figure 2.17.

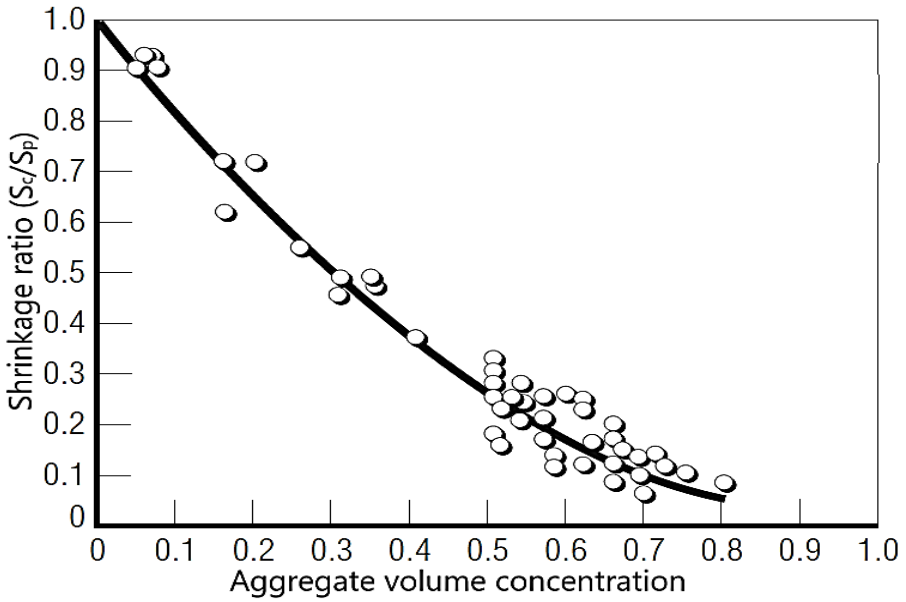

Figure 2.17: Effect of aggregate volume on concrete shrinkage (Cement Concrete & Aggregates, 2002)

When concrete shrinks and the volume change is restrained by aggregates, high stresses are induced at the interface. The shear stresses induced result in the formation of radial and circumferential microcracking around the aggregate (Bisschop and van Mier, 2002; Moonen et al., 2008). The intensity of the stress depends on the stiffness of the aggregate or rather the deformation compatibility of the paste and the aggregate. Stiffer aggregates induce higher stresses and hence more microcracking.

One of the particularly important factors that affect drying shrinkage is the water-to-cement (w/c) ratio. It is generally accepted that an increase in the w/c ratio results in an increase in drying shrinkage (Figure 2.18) this is because it increases the amount of evapoble water in the cement matrix and the porosity of the hardened cement matrix (Neville, 2011).

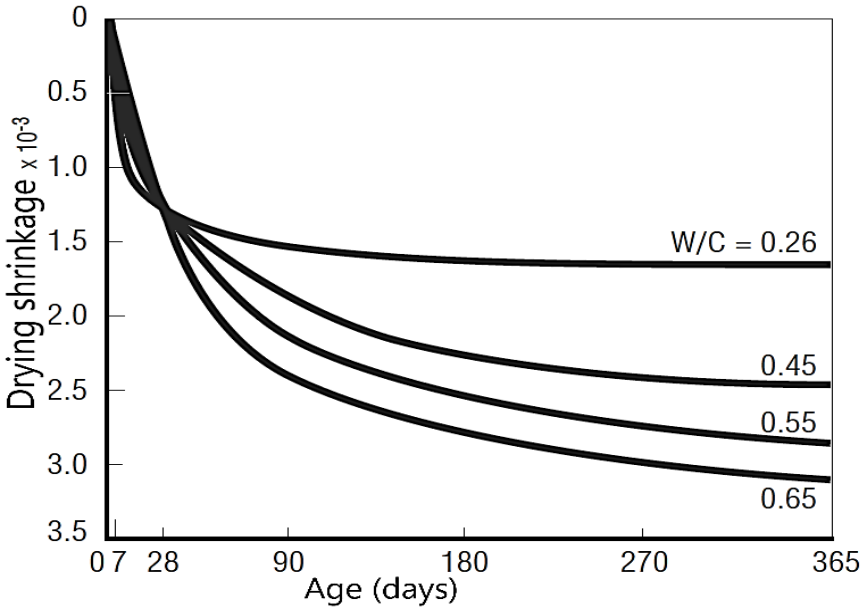

Figure 2.18: Effect of water-cement ratio on drying shrinkage of concrete (Cement Concrete & Aggregates, 2002)

The use of SCMs has differing effects on drying shrinkage depending on the whether its slag, fly ash or silica fume. There is however similarility in the effect GGBS and fly ash on drying shrinkage of concrete. Generally, researchers have found that both these SCMs have no notable effect on the drying shrinkage of concrete for the same water-to-binder ratio as the ordinary concrete (Alexander, 1994; Hooton et al., 2014; Lopez, 2005). It is worth noting though that because GGBS and fly ash concrete mixes require less water for the same workability there is a reduction in the water-to-binder ratio thus resulting in reduction in the drying shrinkage. Silica fume however has the opposite effect on drying shrinkage. It produces a slight decrease as the silica fume proportion is increased (Alexander, 1994; Hooton et al., 2014). The decrease is attributed to the refined pores that increase autogenous shrinkage while reducing drying shrinkage by restricting movement of water from the cement matrix.

External factors like environmental conditions are the main parameters that set how severe the drying shrinkage process will be. The most severe being when there is an occurance of low ambient relative humidity, high ambient temperatures and high wind speed at the same time. According to Bissonnete (1999) low ambient relative humidity results in high drying gradients close to the exposed surface, thereby increasing the drying rate (Figure 2.19). Although causing more detrimental effects together with relative ambient humidity, wind and temperature are not as influential in drying shrinakge of hardened concrete.

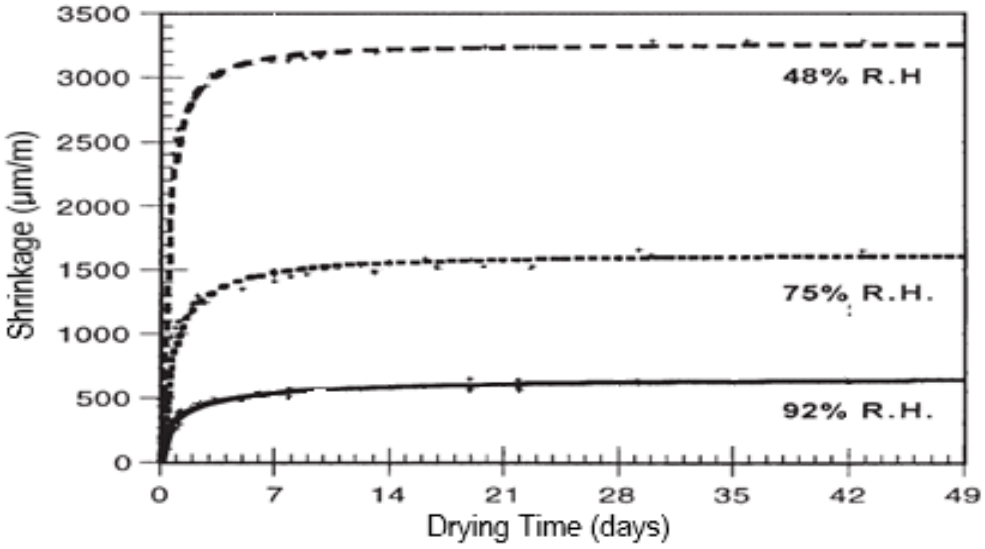

Figure 2.19: Effect of relative humidity on the drying shrinakge of concrete (Bissonette,1999)

2.5.3 Creep

Creep is the phenomenon in which concrete under a sustained stress gradually increases in strain with time. Creep is also an important concrete property due to its implications on the serviceability of concrete (Torrenti and Le Roy, 2018). Creep occurs at all stress levels in concrete and simultaneously with elastic strain and sometimes shrinkage (Owens, 2013). However in order to analyse the different

components of deformation, they are assumed to be independent and their effects superimposed. Such an assumption though, is not an accurate representation of what happens in the concrete. According to Maney (1941) shrinkage actually has the effect of increasing the magnitude of the creep strain. Creep strain for a drying specimen under a load is higher than the summation of basic creep (creep without drying), elastic and free shrinkage strain. However it is common not to separate basic creep from drying creep (additional creep due to drying) and simply consider creep to be the deformation experienced by concrete when subject to a sustained in addition of the sum of elastic and unrestrained drying shrinkage (Figure 2.20). The creep strain at any time, $\varepsilon_c(t)$, is determined as given in Equation 2.6.

$$\varepsilon_c(t) = \varepsilon(t) - \varepsilon_e - \varepsilon_{sh}(t) \quad \text{.....Eqn. 2.6}$$

where,

$\varepsilon(t)$ – *total measured strain at any time t;*

ε_e – *average instantaneous elastic strain recorded immediately after loading;*

$\varepsilon_{sh}(t)$ – *drying shrinkage strain at any time t (determined on unloaded specimen)*

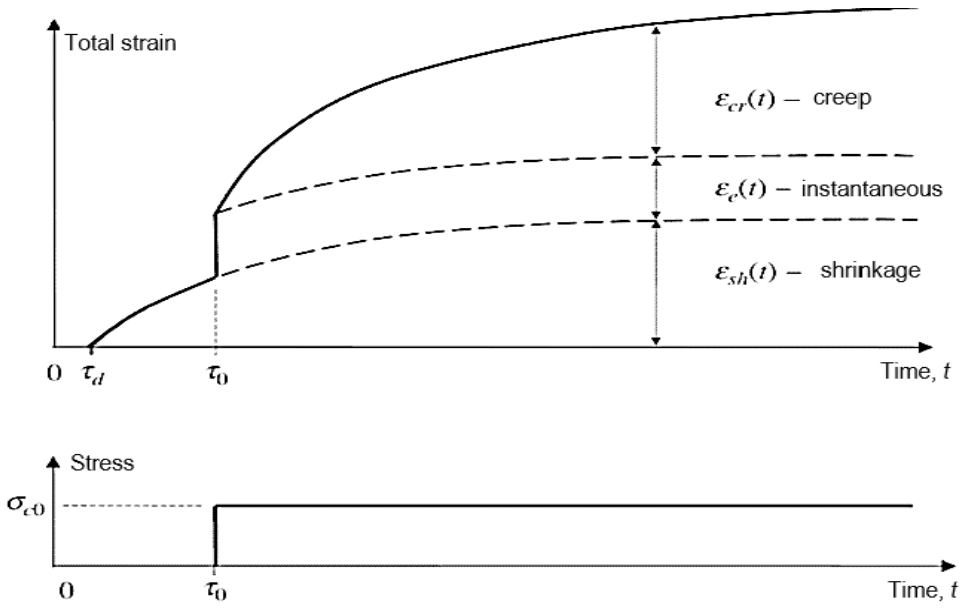

Figure 2.20: Concrete strain components under sustained stress (Gilbert and Ranzi, 2010)

The total creep strain, $\varepsilon_c(t)$, at any given time can considered to comprise of 2 components, drying creep and basic creep. These are better explained by considering the 4 sub-divisions of total creep:

a) delayed elastic strain (reversable), $\varepsilon_d(t)$;

b) rapid initial flow which occurs within 24 hours and is dependent on the age at first loading $\varepsilon_{fi}(t)$;

c) basic flow, dependent on the consitution of the concrete mix $\varepsilon_{fb}(t)$;

d) drying flow, dependent on specimen size, shape, moisture content and gradient, $\varepsilon_{fd}(t)$.

These components are graphically represented in Figure 2.21 (after Gilbert, 1988)

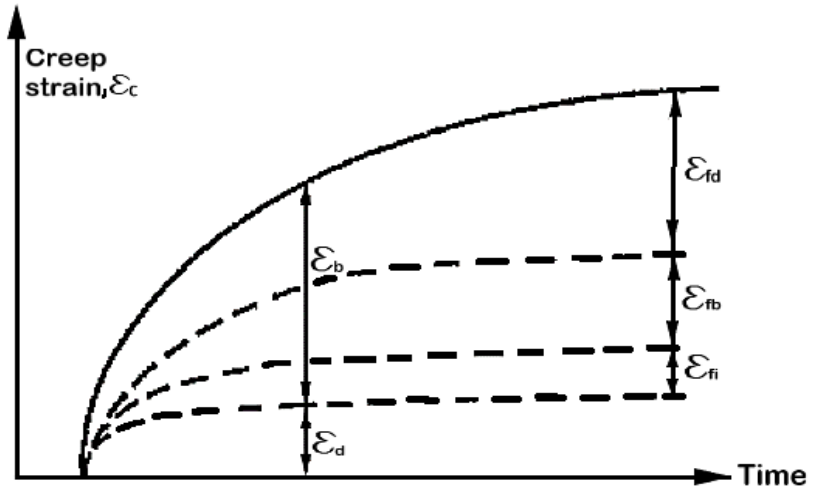

Figure 2.21: Creep components in drying concreete under sustained load (Gilbert, 1988)

The first three sub-components of the four make up the basic creeep component. While the fourth component, drying flow creep component is commonly referred to as drying creep. Drying creep is when a concrete under sustained load in a drying

environment hence moisture is lost from thee concreete to the environment. Basic creep takes place when concrete is under a sustained load but is sealed such that there is not net exchange of moisture between the environment and the concrete. It is worth noting that although creep occurs at all stress levels as noted by the Owens (2013) the creep mechanisms for stress levels higher than 40% short strength are diffeerent from those below this stress level (Alexander and Beushausen, 2009).

Creep mechanisms

There are a number of mechanisms that have been proposed for creep but none fully account for what happens in concrete. Some of the most prominent are discussed below:

- *Plastic flow theory* states that concrete creep is a result of crystalline flow similar to what happens to metals beyond their elastic range (Neville, 1964). Although the theory has possible application to the creep of stressed concrete subject to near ultimate strength loads, the theory does not seem to hold for creep of concrete subjected to normal stress (Neville et al., 1983). The inapplicability of this theory for normal load cases stems from the fact that creep is detected in concrete and neat cement paste, in particular, at as little stress as a single percent of their ultimate strengths (Jensen and Richart, 1938). Kesler and Ali (1964) note that unlike in creep deformation, plastic deformation is not proportional to the applied stress. They also noted that there was no relation between plastic deformation and moisture changes as is the case for creep deformation in concrete. These observations make it unlikely that plastic theory is the mechanism behind creep at normal stress levels. Neville (1964) reports that other studies have also drawn the same

conclusions as inter-crystalline slip has not been proven to occur during creep.

- *Viscous flow theory* states that cement paste is a viscous material which is highly fluid and flows under load (Thomas, 1937). The load is transferred to the aggregate which slows the flow since it does not flow. This theory explains why creep happens at all levels (Neville et al, 1983). According to Kesler and Ali (1964) the theory also explains the non-occurrence of a stress threshold in creep and well represents its stress dependency. Neville (1955) suggested that the viscous theory could not possibly capture fully all the creep undergone by concrete because volumetric consistency required in viscous flow is not present in concrete. Despite its shortcomings, the theory by Thomas (1937) still remains an import creep mechanism.

- *Seepage theory* states that creep is due to the movement of water from actual adsorbed layers to capillary pores (Lynam, 1934). Stressing the concrete causes a rise in vapour pressure in the adsorbed layers, then in order to maintain equilibrium with surrounding environment, moisture is removed from the surface of the Calcium-Silica-Hydrate to capillary pores (Neville et al., 1983). According to Xi and Jennings (1992), the theory explains the large creep observed in drying concrete compared to wet or dry concrete. Han (1996) highlighted that although seepage theory explained the relation between creep and water during loading, this was not the case for recovery during unloading. Han (1996) notes that if the theory was to be

applied to creep recovery because vapour pressure in the calcium-Silica-Hydrate surface must decline upon unloading. This should result in the restoration of adsorbed water and hence total recovery but this is not the case upon unloading concrete. Neville (1955) suggests that the reason for incomplete creep recovery as expected in the seepage theory can be explained by the possibility of the creation of new bonds in calcium-silica-hydrate that hinder complete restoration.

- *Delayed elasticity theory* is also known as the viscoelasticity theory. It premised on the microstructure of the cement paste being modelled as a two-phase structure. The one phase, compromising of crystalline hydrates, is an elastic structure. The second phase, comprising of non-crystalline elements with adsorbed water, is viscous (Lopez, 2005). So in this theory when the microstructure in under stress, elastic phase and the viscous phase absorb the stress relative to the individual stiffness of the phases. The load absorbed by the viscous phase is transfered to the elastic skeleton component as it gradually deforms. Upon receiving the progressive load from the viscous phase the elastic phase reaches a point where it deforms elastically. This elastic deformation which comes to a while after the paste microstructure is what is termed the delayed elastic behaviour. Kesler and Ali (1964) concluded that the theory does not satisfactorily explain the relation between moisture exchange and creep. Furthermore, the theory does not account for the irrecoverable creep when the concrete is unloaded.

- *Microcracking effect theory* was first proposed by Hsu (1965), to explain the nonlinear stress-strain relationship of concrete due to the inter-transitional zone (ITZ) around the aggregate. Concrete can be considered to be a 3 phase material, consisting of aggregates, cement matrix and the ITZ. The ITZ is considered to be the weakest of the three phases. As a result, the ITZ has high porosity and a greater density of microcracks than in the other phases. Neville and Dilger (1970) suggested that creep microcracks propagate from already existing microcracks in the ITZ formed during initial loading, drying or thermal shrinkage. Bazant et al. (1997) proposed that microcracking, initiated by drying, might be the reason for an increase in creep in a drying environment. The theory through the preexisting microcracks makes it possible to account for the residual strain when the concrete is no longer loaded (Lopez, 2005). Besides the permanent strain in cracks, residual strain can be a result of the formation of new bonds in Calcium-Silica-Hydrate similar to what happens on the seepage theory (Neville et al.,1983). Creep occurs at all stress levels but the creep mechanism for concrete loaded at less than 40% of the concrete's short strength is different from that of concrete loaded at higher stresses. This is because of the significant role microcracks play in the higher stress creep mechanism. According to Meyers (1967), microcracks contributed 10-25% of the total creep.

- *Mechanical deformation theory* proposed by Freyssinet (1936) suggests that the load applied on the concrete sets up stresses in it that causes that

capillary structure to change and water to be displaced from the stressed pores. This internal movement reduces the induced compressive stress in the concrete while partly counter-balancing the externally applied stress. In addition, the internal moisture balance is disrupted and water will evaporate from the capillary pores to a point where the vapour pressure is in equilibrium with the ambient value. Tensile stresses in the capillary water rise and in order to keep equilibrium there is an increase in the solid phase compression. This macro-deformation resulting from these changes is a creep (Neville et al, 1983). According to this theory, moisture loss by drying is greater in loaded concrete than in unloaded concrete and concrete subjected to shear stress would not creep. However, this is not the case in practice. Regardless of the loading status of concrete, the water loss and humidity distribution inside the concrete are the same (Coutinho, 1977).

The American Concrete Institute (2005) identifies four main mechanisms which describe creep namely; viscous flow of cement paste, consolidation due to seepage, delayed elasticity (as a result of the cement paste restraining gel pores elastic deformation) and permanent deformation (as a result of confined cracking, recrystallisation and creation of fresh physical links). The mechanisms that are generally accepted as being in creep deformation are the seepage and viscous flow. Although there is some level of concensus around these two theories, the role of water in each of these is not clear. Ye (2015) notes that despite the extensive research that has been conducted into creep mechanism over decades, there is no universal agreement to accept one creep mechanism as the only one responsible. He

further notes that this is because different investigational approaches leads to varied observations which result in an array of creep mechanisms to explain their experimental data which would not necessarily concur with other researchers.

Factors affecting creep

Creep is affected by both internal and external factors. The internal factors are w/c ratio, moisture content, cement and extender type and aggregate properties and content. In terms of creep, *aggregate volume and stiffness* play a significant role in the creep behaviour of concrete (Alexander and Beushausen, 2009). Aggregates play a role of diluting the effects of hardened cement paste by its stiffness and volume fraction. According to Hobbs (1971) the relationship that exists between the volume fraction of concrete and the creep of concrete can be expressed as shown in Equation 2.7:

$$\varepsilon_c = [(1 - V_a)/(1 + V_a)] \cdot \varepsilon_{\mathrm{p}} \quad \text{.....Eqn. 2.7}$$

where ε_c and ε_p , are the creep of the concrete and the paste respectively, and V_a is the volume fraction of the aggregate.

Alexander and Mindess (2015) report that for concrete with 25 – 35% by volume of cement paste, a 1% increase of the paste results in a 5% increase in creep. They further state that a stiffer aggregate offers more restraint of the paste than a less stiffer aggregate (Figure 2.22).

The importance of the elastic modulus of the aggregate in restraining creep is illustrated by work done by Evans and Kong (1966). They found that for aggregates with elastic modulus ranging between 10 GPa and 115 GPa, creep may vary as much as four times in magnitude. These findings suggest that since the elastic

modulus of tyre rubber is much lower (<5 MPa), its ability to restrain the paste will also be low. As mentioned before, stiffer aggregates though offering more restraint, cause more microcracking due to greater shear stresses being induced as a result of incompatible deformation characteristics. In other words, the more compatible the deformations of the paste and the aggregate, the lower the stress concentrations and the lower the risk of microcracking.

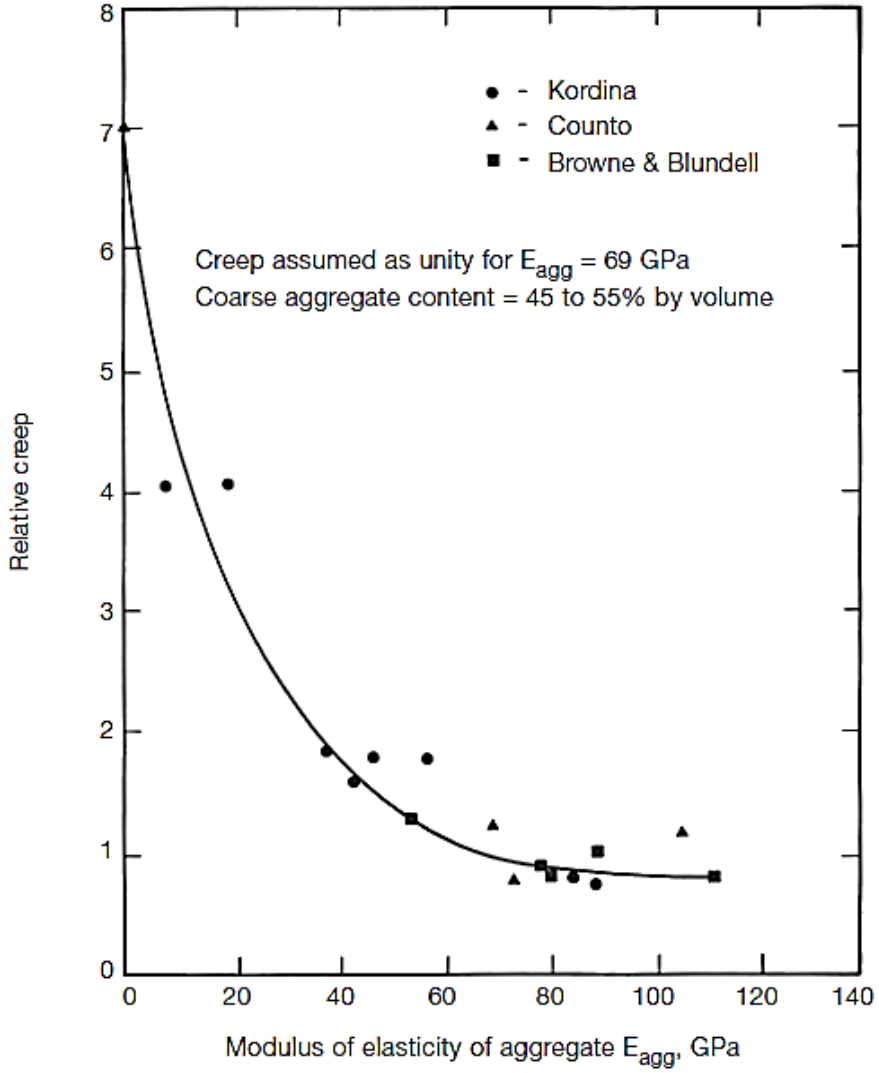

Figure 2.22: Effect of aggregate stiffness on concrete creep (Alexander and Beushausen, 2009)

The microcracks also have an effect on the creep deformation of concrete (Bazant and Xi, 1994). Rubber aggregates are likely to result in reduced microcracks and

thus reducing the microcrack effects on the rubberised concrete creep behaviour. Figure 2.23 shows the creep of concrete made from different aggregates. Concrete with the same aggregate proportions exhibits different creep behaviour depending on the aggregate characteristics. Fanourakis and Ballim (2006) note that other aggregate characteristics besides stiffness may have a significant role in the creep behaviour of concrete.

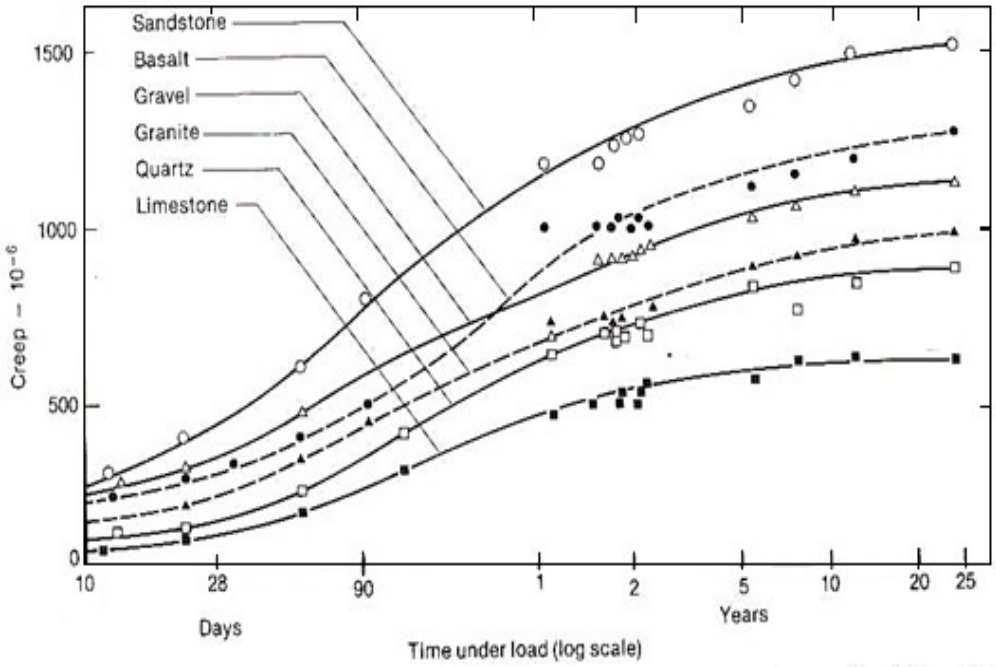

Figure 2.23: Creep of concretes made with different aggregates (Neville et al, 1983)

The *water-to-cement ratio* of concrete is perhaps one of the crucial factors affecting concrete creep. The w/c ratio determines the workability, strength, and porosity, therefore it indirectly influences the creep behaviour of concrete (Alexander and Beushausen, 2009; Lopez, 2005). According to Neville (1959) "for constant mix proportions and the same type of aggregate, creep is proportional to the applied stress and inversely proportional to the strength at the time of application of load". If this is the case then by inference since the strength is inversely proportional to w/c ratio it implies that to an extent the creep is also proportional to w/c ratio

(Figure 2.24). Neville and Meyers (1964) were able to show that in order to compare creep for concrete made with different w/c ratios it is necessary to adjust the specific creep values obtained to those that would be obtained if the concrete had contained the same volume of cement.

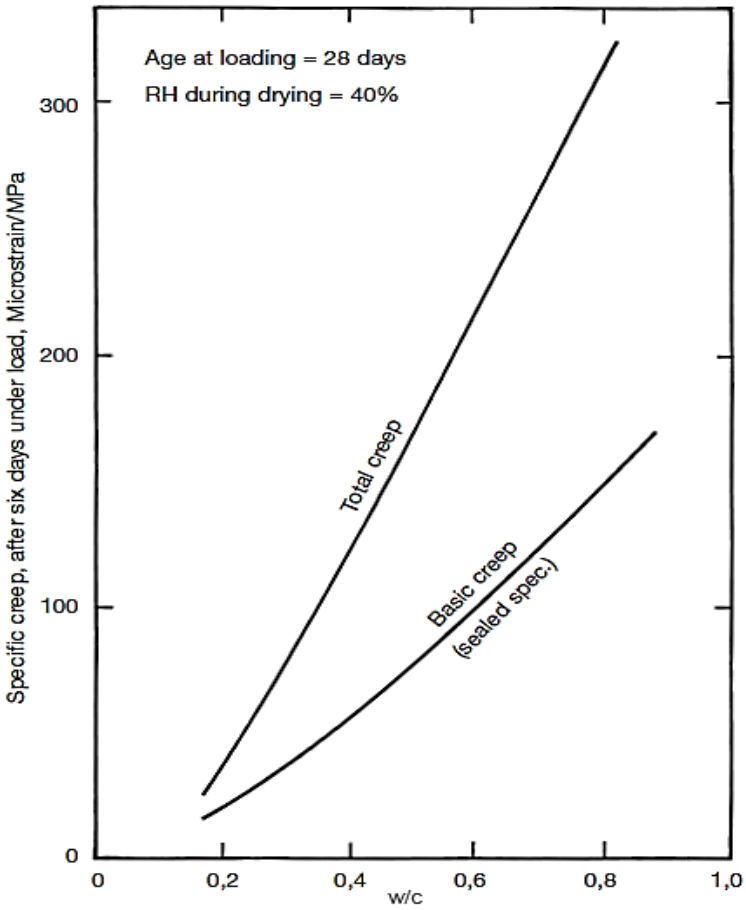

Figure 2.24: Effect of w/c on creep of cement paste (Alexander and Beushausen, 2009)

This adjustment is necessary because according to Neville (2011) it is not possible to change the w/c ratio without altering the cement content. Alexander and Beushausen (2009) report that the decrease in creep when w/c ratio is reduced is due to the low w/c ratio resulting in a stiffer and less permeable paste.

Creep also involves the movement of mobile water from the hardened cement paste. The *moisture content* of the hardened cement paste is a measure of mobile

water present in the cement that has an effect on the creep behaviour of the material. According to Fanourakis (2011) the greater the moisture content of the hardened cement paste at the time of loading and during the time under constant sustained loading the greater the creep. Alexander and Beushausen (2009) emphasise the existence of the effects due to the moisture content of the hardened cement paste. They note that concrete that is permitted to dry and lose moisture before being placed under the constant sustained loading will experience less creep because less mobile water is available during the time under loading (Figure 2.25). They also note that, concrete that is only permitted to dry for the first time while under load will experience more creep than concrete kept saturated. They attribute the increase to an additional creep component, drying creep. The figure shows that the concrete that is allowed to dry in a higher drying environment (0% relative humidity) and loses the most water thus reducing the amount of drying creep.

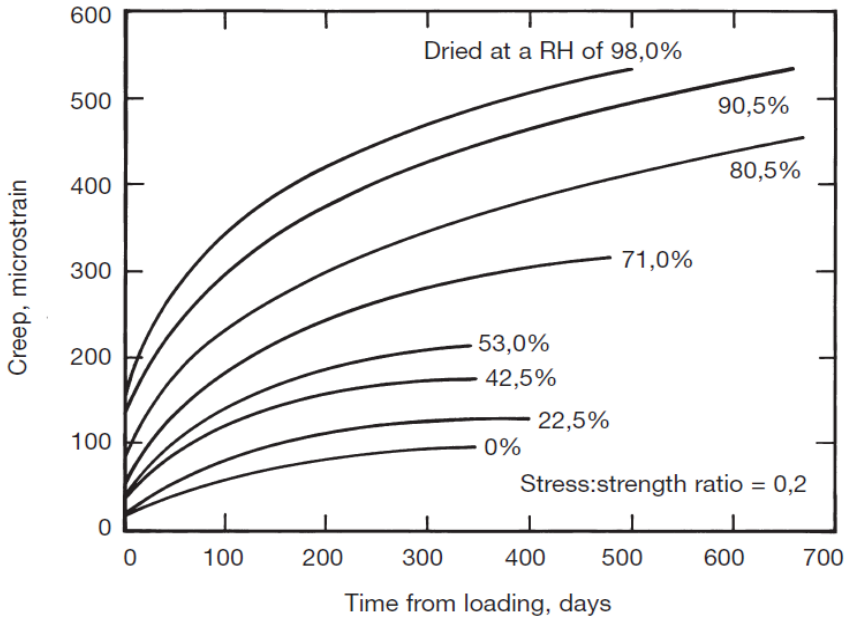

Figure 2.25: Effect of previous drying on basic creep of cement paste (Wittmann, 1973)

Cement requires important consideration when it comes to concrete creep because it is a key ingredient in the hydration process to make the paste which forms part of the concrete matrix. Neville et al. (1983) describe cement as having a dual influence on concrete creep, firstly due to its physicochemical properties and secondly due to the degree of inconsistency in the amount of the hydrated paste. The second effect is curtailed by the presence of aggregates which restrain the shrinking of the hardened paste. Mindess et al. (2003) note that increasing C_3A content or lowering C_3S in cement has the effect of increasing concrete creep. According to Alexander (1994), the variation of concrete creep amongst several different cements can be explained in part by the varying rates of the development of strength which in itself is dependent on the cement fineness and composition. He also notes that cement fineness seems to affect concrete creep in as far as it affects the strength development of the cement paste at early ages. It has also been observed that ordinary Portland cement tends to creep more than rapid-hardening but less than low-heat cement (Neville, 2011).

The use of *supplementary cementitious materials (SCMs)* in cement and concrete production is now a norm in the construction industry. The effects of SCMs on creep have been investigated and reported on by a number of researchers (Neville et al, 1983; Lopez, 2005; Alexander, 1994). According to Lopez the influence of SCMs on creep is directly related to its impact on the microstructure of the cement paste at the time of loading. Alexander and Beushausen (2009) note that although the use of GGBS in concrete might be thought to result in an increase in creep this was not a universal trend as this is dependent on a number of factors such as the

cement and GGBS characteristics, GGBS proportion, ages of loading and conditions of drying. They note that in addition to the age of loading as highlighted by Lopez (2005), the fact of whether or not the specimens are sealed is also key. Alexander (1994) found that slag resulted in a possible increase in creep at early ages but this effect was reversed at later ages. He noted a marked reduction in creep for sealed specimens. These results are confirmed in ACI 233 (2017). They report conflicting creep results with regards to total creep but report a consistent reduction of basic creep.

Fly ash concretes are reported to have reduced drying and basic creep when compared to ordinary Portland cement concrete when loaded at similar strengths (American Concrete Institute, 2017; Grieve, 1991). There was also no consistency in total creep results fly ash as well. Lopez (2005) notes that, in general, concretes containing Class C and Class F fly ash had higher and lower creep compared to plain Portland cement concrete respectively. In their work with Class C fly ash, Yuan and Cook (1983) confirmed the increase in creep compared to plain portland cement concrete. Unlike slag and fly ash, silica fume has the effect of early age strength of concrete. Therefore, at the same stress level, concretes with silica fume exhibit lower creep that plain Portland cement concrete (Lopez, 2005).

The extrinsic factors that affect creep deformation include specimen size, shape and drying conditions. The rate and magnitude of creep of concrete are affected by the shape and size of the concrete member (Alexander and Beushausen, 2009). The

bigger the size of the member assessed the lower creep as shown in Figure 2.26 (Neville et al. 1983).

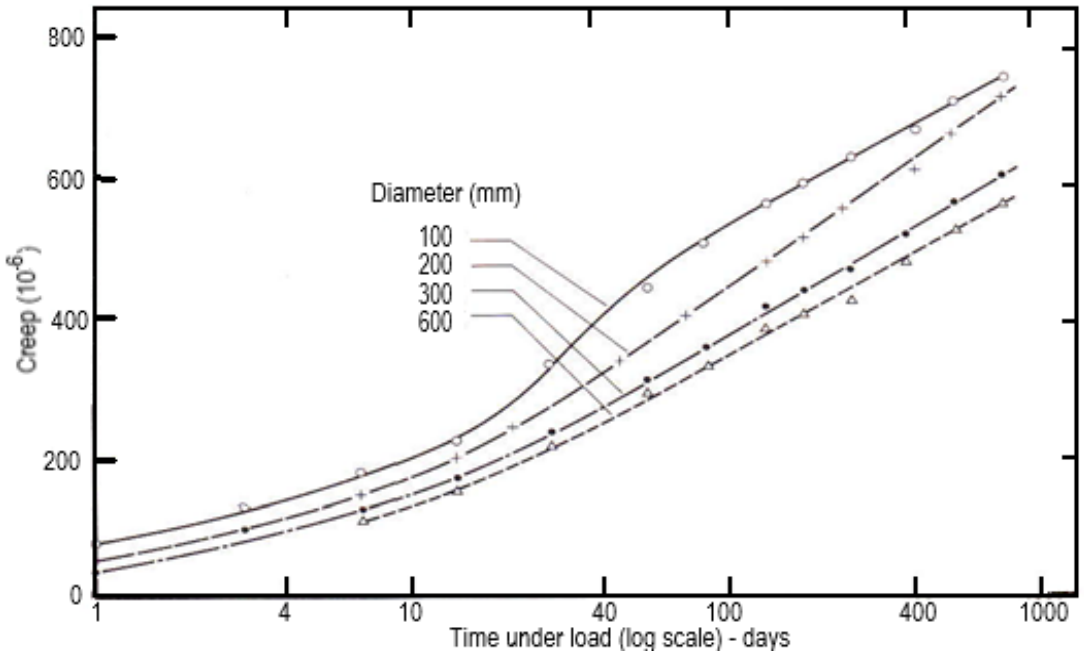

Figure 2.26: Effect of size on creep of concrete (Neville et al, 1983)

Nemati (2015) made use of what he terms a theoretical thickness, $h = 2A/P$, where A is the cross-sectional area and P is the cross-sectional perimeter. He states that as the theoretical thickness increases the creep reduces. Similarly, Hansen and Mattock (1966) related creep to shape and size by making use of a volume: surface ratio. The greater the ratio the longer the diffusion path for moisture loss and subsequently the lower the creep measured. However, Neville et al. (1983) note that this relationship reaches a limiting value at a thickness of 900 mm. They also note that this effect of size is also mainly prominent in the early ages of the concrete. This assertion is corroborated by Howells et al. (2005) who stated that an increase in member size resulted in an increase to the volume/surface ratio which had an effect of decreasing short-term creep.

The *drying conditions, ambient humidity and temperature*, have a major role in the rate and magnitude of concrete creep (Neville, 2011; Alexander and Beushausen, 2009). Neville (2011) noted that the total creep measured is higher at lower relative ambient humidity and at higher ambient temperature. The effect of the low ambient relative humidity and high temperature lessen if the concrete is allowed to dry in these conditions prior to being loaded. The higher creep at low relative humidity and high temperature is attributed to the accelerated loss of moisture from the concrete this increases the creep rate at early ages (Chowdhary and Sharma, 2013). Figure 2.27 shows the effect of relative humidity on concrete creep as discussed.

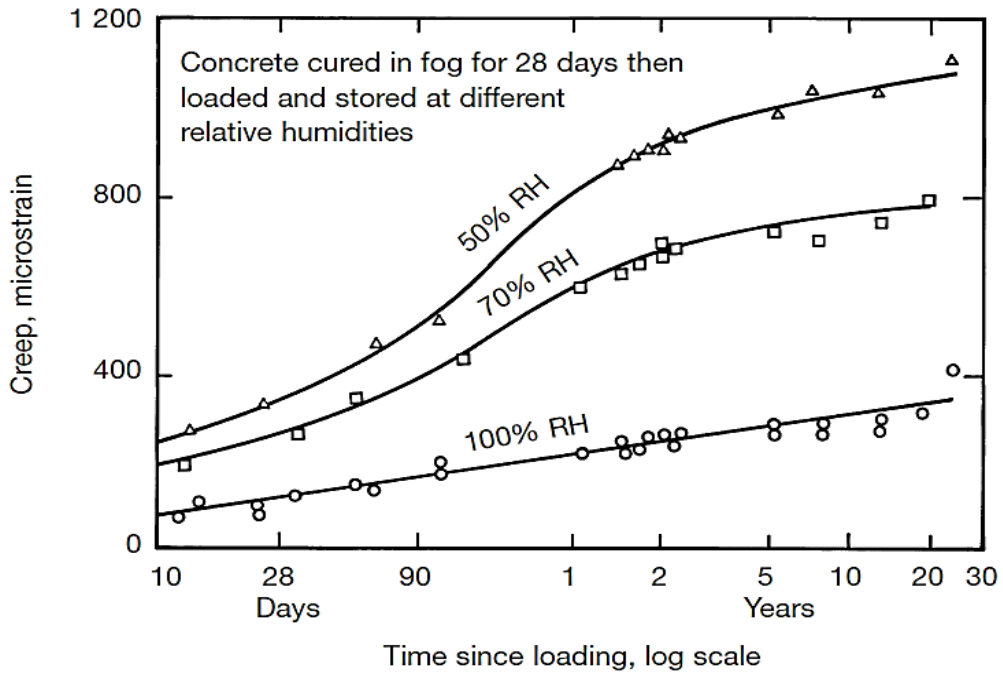

Figure 2.27: Effect of relative humidity on concrete creep (Troxell et al., 1958)

Bazant et al. (2004) suggest that high temperatures have a dual effect on creep. Firstly, they speed up the bond breakages and restorations responsible for creep, therefore increasing the rate of creep. Secondly, they increase cement hydration reaction casing the concrete to mature faster, thus reducing the rate of creep. They

suggest that although both these effects take place, the first effect normally prevails thus there is an overall increase in creep. They however, also note that if the temperature is elevated too high for very young concrete the rapid progression of hydration might result in a completely opposite effect. Vidal et al., (2013) in their work to evaluate the temperature effects on basic creep, subjected concrete under sustained loading to temperatures of 20ºC, 50ºC and 80ºC. They found at higher temperatures yields more creep strains as shown in Figure 2.28.

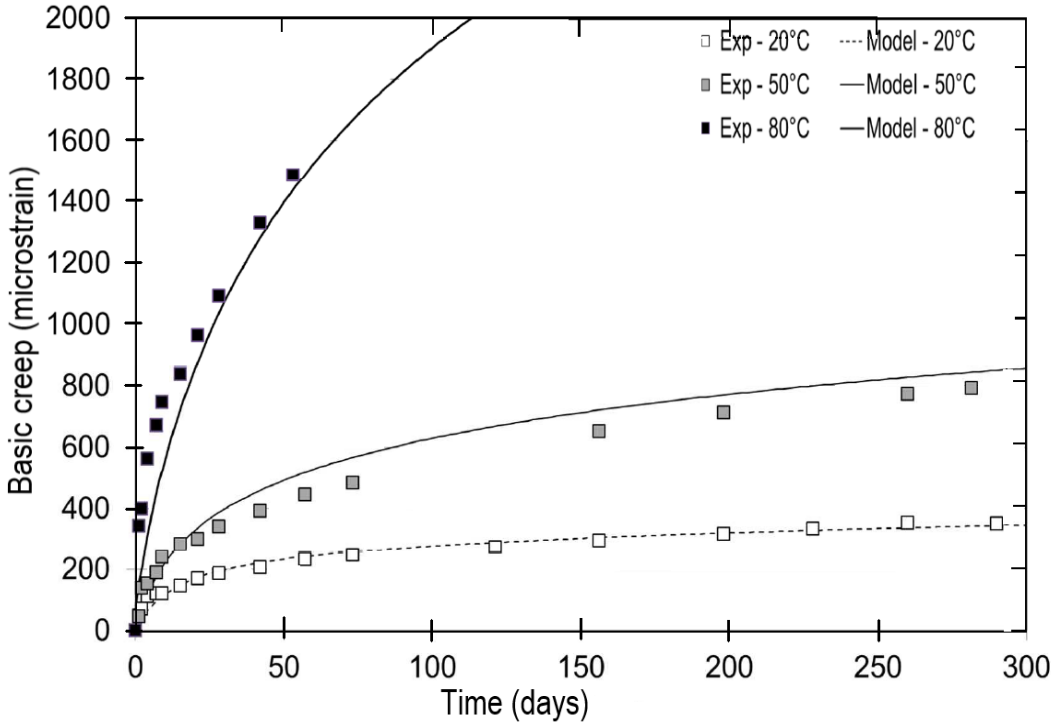

Figure 2.28: Effects of temperature on creep of concrete (Vidal et al, 2013)

According to Alexander and Beushausen (2009) the *stress/strength ratio* encapsulates the influence of numerous other concrete creep factors such as, the magnitude of stress, the duration and type of curing, age at loading and water-to-cement ratio. Alexander (1994) noted that creep is directly proportional to the applied stress but is inversely proportional to the strength of the concrete at the

instance of loading. At a loading stress 40% of short-term strength of concrete, the stress/strength ratio and creep relationship is assumed to be linear (Neville et al., 1983). Figure 2.29 shows the relationship between creep and the stress/strength ratio (Neville et al, 1983).

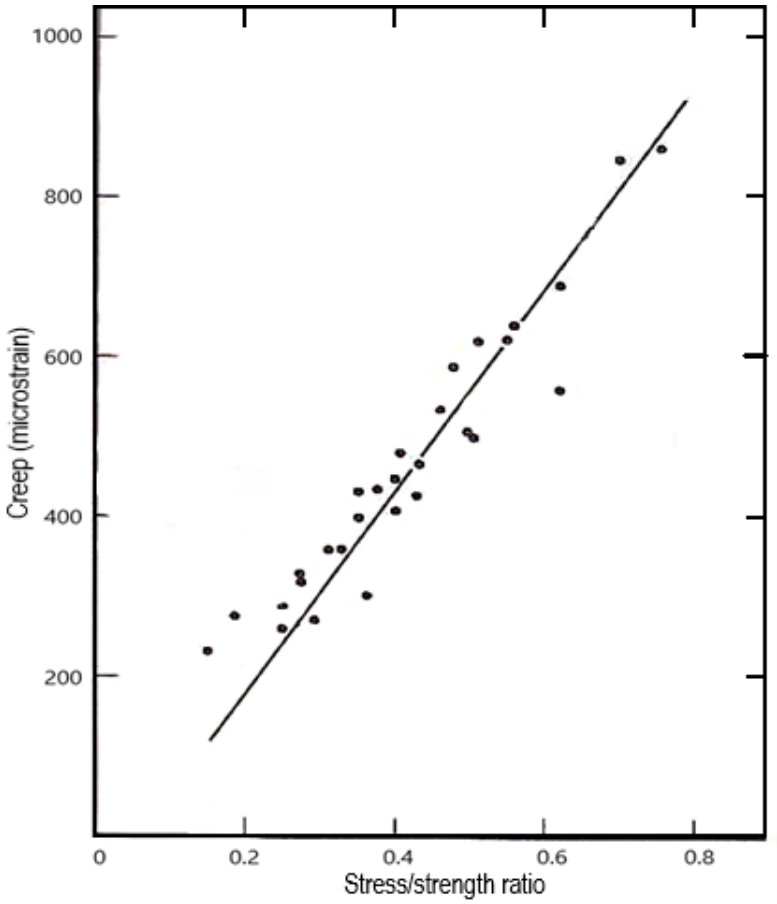

Figure 2.29: Relationship of creep and stress/strength ratio (Neville et al. 1983)

Davis et al. (1934) compared creep measurements on *concretes loaded* at three different ages, 7 days, 28 days and 3 months yet subject to the same stress. They found that after 80 months under load their creep ratios averaged 3:2:1 respectively. They noted 10% - 20% difference between the specimen loaded at 28 days and 3 months, which they report as insignificant. Yang et al. (2016) also found that this ascertion was true for light weight aggregate concrete. According to Neville

(1983), creep is inversely proportional to the strength of the concrete at the instance of load application. The general influence of age of loading is shown in Figure 2.30.

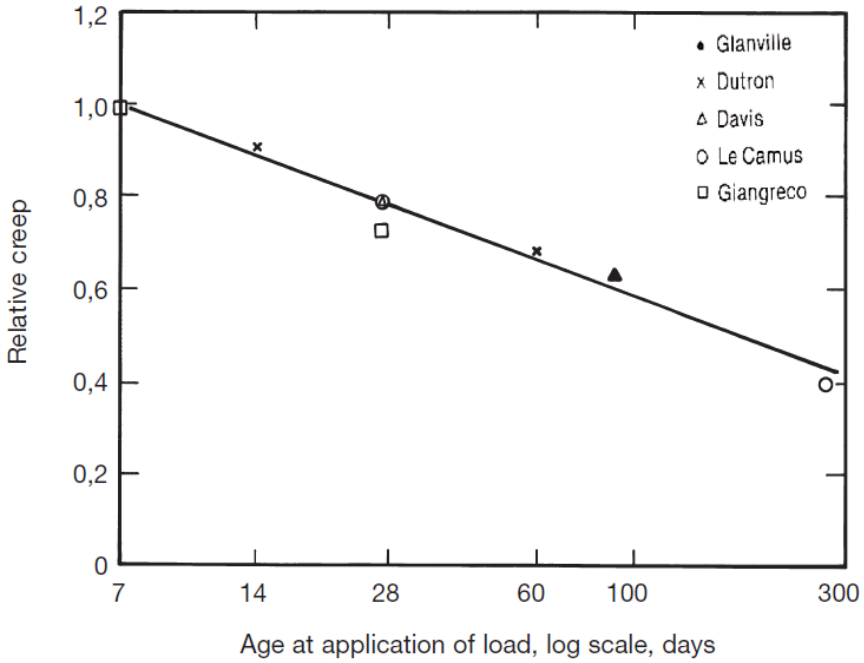

Figure 2.30: Influence of age at application of load on creep as a fraction of creep for concrete loaded at 7 days (L'Hermite, 1959)

Time under load. Creep of concrete occurs as long as it is subjected to an external load, if not indefinitely. It is evident from Figure 2.27 that measurable creep still occurs at an age of approximately 25 years after loading. In general, approximately 50% of the 20 year creep occurs within a period of two to six months after loading, while 80% occurs after about one or two years (Alexander and Beushausen, 2009).

Creep is normally specified in terms of creep coefficient; which is a comparsion of elastic strain (ε_0) with the creep strain (ε_c), expressed as given in Equation 2.8.

$$\text{Creep coefficient; } \psi = \varepsilon_c / \varepsilon_0 \quad \text{.....Eqn. 2.8}$$

Though the creep-stress relationship is non-linear, for practicality purposes a linear proportionality is often used. The linear relationship gives rise to the concept of specific creep (C_c), which allows for the comparison of creep for different concrete specimens experincing varied stress levels to be done. It is computed as shown in Equation 2.9:

$$\text{Specific creep; } C_c = \varepsilon_c/\sigma \quad \text{.....Eqn. 2.9}$$

2.5.4 Effects of shrinkage and creep in concrete

Shrinkage is an important property of concrete because it affects the volume stability of concrete and hence the serviceability functions of the material in structural design (Alexander and Beushausen, 2009). Shrinkage may have an adverse effect on the strength and durability performance of concrete due to shrinkage-induced microcracks. The microcracks may become crack propagation sites when a mechanical load is applied and may also provide pathways for deleterious substances to get into the concrete (Moonen et al., 2008; Neubauer et al., 1997). In reinforced flexural members shrinkage can lead to excessive deflections reducing the serviceability of the structure. In eccentrically loaded columns the effect of magnifying the deflection might lead to much lower buckling stress for the column (Neville et al., 1983).

Creep deformation effects are largely beneficial, although they can also be detrimental in some instances. Creep effects are generally beneficial in that it tends to relieve induced stresses in concrete. When a reinforced concrete column is under a sustained concentric compressive load, creep causes a slow transmission of the

applied load from the concrete part of the column to the rebar in the column. The transfer allows for the full strength of the rebar steel and of the concrete to be fully mobilised before the column fails (Troxell et al., 1968).. In structures undergoing restrained deformation due to shrinkage, temperature fluctuations or differential movements of supports, creep redistributes the induced stress, it reduces stress in highly stressed portion and increases stresses in the adjacent parts thus uniformly distributing the load throughout the structure. This redistribution of stresses reduces the risk of the concrete to crack. However, like shrinkage, creep can cause undesirable deflection of thin, long span slabs and buckling in long columns resulting in reducing the serviceability and safety of structures (Troxell et al., 1968; Alexander and Beushausen, 2009). Loss of prestress leading to collapse of prestressed structures has also be reported to occur due to creep deformation. Bazant et al. (2015) emphasise the point that creep plays a significant role in the super-tall buildings and prestressed concrete structures due to their higher flexibility and slenderness. They also pointed out that for structures exposed to high temperatures creep can be significantly high enough to cause concern. Importance of creep behaviour for all structures and materials was highlighted in the collapse of several historic masonry towers, whose collapse was partially or wholly attributed to creep deformations (Verstrynge and Van Gemert, 2018). These occurrences brought to the fore the importance of understanding the creep behaviour of all materials intended for structural applications. Since the effects of creep can be both beneficial and detrimental to concrete structures it important to be understand how a particular concrete material behaves under creep. This understanding assists in the

design of structures where this knowledge can be incorporated in design when long-term deflections are assessed.

2.5.5 Identified gaps in literature

The literature survey above makes it evident that the addition of tyre rubber particles in concrete as aggregates has both desirable and undesirable effects on its properties. It showed that the mechanical behaviour of concrete, in terms of strength and elastic modulus is adversely affected. While some properties like thermal insulation, sound absorption, dynamic and impact load resistance are enhanced with rubber particles as aggregates in concrete. The effect of the rubber is believed to be linked to the low elastic modulus of the tyre rubber particles; the increased air content in concrete due air pockets around the tyre rubber particles and finally the lack of adequate bond between tyre rubber particle and the cement matrix. The literature review has revealed that these effects can be minimised and the mechanical performance of the concrete can be improved to the extent that rubberised concrete can be used for structural purposes.

The use of rubberised concrete for structural purposes has been hindered firstly, by the lack of sufficient body of knowledge to support its durability performance. Durability is an important aspect in structural concrete particularly because of the use of rebar. The second most crucial aspect is the behaviour of the material under long term sustained loading. This is important because it informs on the time-dependent behaviour of the material under actual anticipated working conditions. It is also crucial because these deformations can be as high as three times the

instantaneous deformations. The effect and the quantification of the use of tyre rubber particles in concrete on time-dependent deformations is not well documented. The few studies that have been published on creep, have studied creep in concrete that has been modified in some way. The use of extenders and admixtures to enhance concrete performance of concrete have an unknown effect on the time-dependent deformations. This is precisely because other studies have shown that certain synergies exist when some extenders and reagents interact, thus these studies should aim to quantify these separately. To facilitate a basic and fundamental understanding of the raw effects of tyre rubber in concrete it is important of assess these deformations on concrete with as little-to-no modifications as possible. This approach allows for measured modifications to be done in the future using this information as the baseline. There is therefore a need to investigate and quantify this effect, to ascertain the suitability of the material for use in normal strength structural concrete (without admixtures or extenders) with respect to time-dependent deformations. Together with this assessment, is the need to understand the effect of crumb rubber size so as to better relate the behaviour to particular crumb rubber characteristics. The blending of tyre rubber of different sizes in concrete while investigating time-dependent deformations may present a challenge when trying to identify specific tyre rubber characteristics that may be affecting performance. This is precisely because it is known that different size tyre rubber particles influence concrete behaviour differently.

CHAPTER THREE: METHODOLOGY

3.1 INTRODUCTION

This chapter provides details of materials, apparatus and experimental methods employed in this research to characterise the time-dependent behaviour of structural rubberised concrete. The material details include the cement and aggregate types and their sources as well as their mix proportions. The experimental details include descriptions of the specimen preparation and the tests conducted on the aggregates, fresh and hardened concrete.

3.2 MATERIALS

3.2.1 Cement

A single batch of CEM I 52.5R plain Portland Cement (PC), conforming to SANS 50197 Part 1 (2013) & Part 2 (2017) standards was used. The particle size distribution is shown in Figure 3.1. The mineralogy was determined using x-ray fluorescence and is shown in Table 3.1. The cement was used for all the tests carried out in the research investigation because it was not blended and was more readily available.

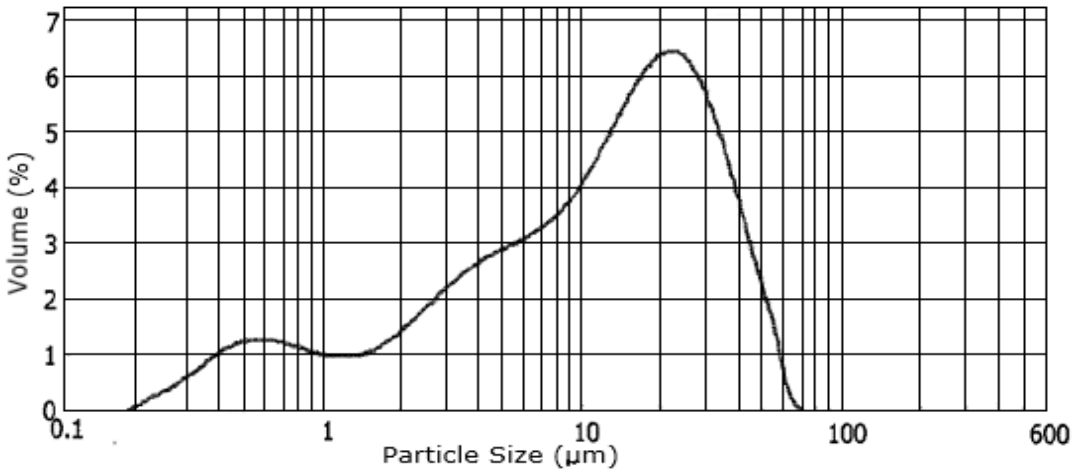

Figure 3.1: Cement particle size distribution

Table 3.1: Cement mineral composition

Mineral oxide	**Percentage weight (%)**
SiO_2	21.15
Al_2O_3	5.37
Fe_2O_3	2.78
MnO	0.47
MgO	2.5
CaO	61.41
Na_2O	0.05
K_2O	0.25
TiO_2	0.34
P_2O_5	0.07
Cr_2O_3	0.06
NiO	0.01
Loss on Ignition	3.57
Total	98.02

3.2.2 Aggregates

Mineral aggregates

Crushed andesite, obtained from Afrisam, Eikenhof quarry in South Africa, was used as both fine and coarse mineral aggregate. The maximum coarse aggregate size was 22 mm for concrete used for all tests except for the micro-cracking tests where 6 mm stones were used. The fine aggregates had a finess modulus of 3.52. The particle size distribution of the coarse and fine aggregates is shown in Figure 3.2. The choice of mineral aggregates was mainly due to availability.

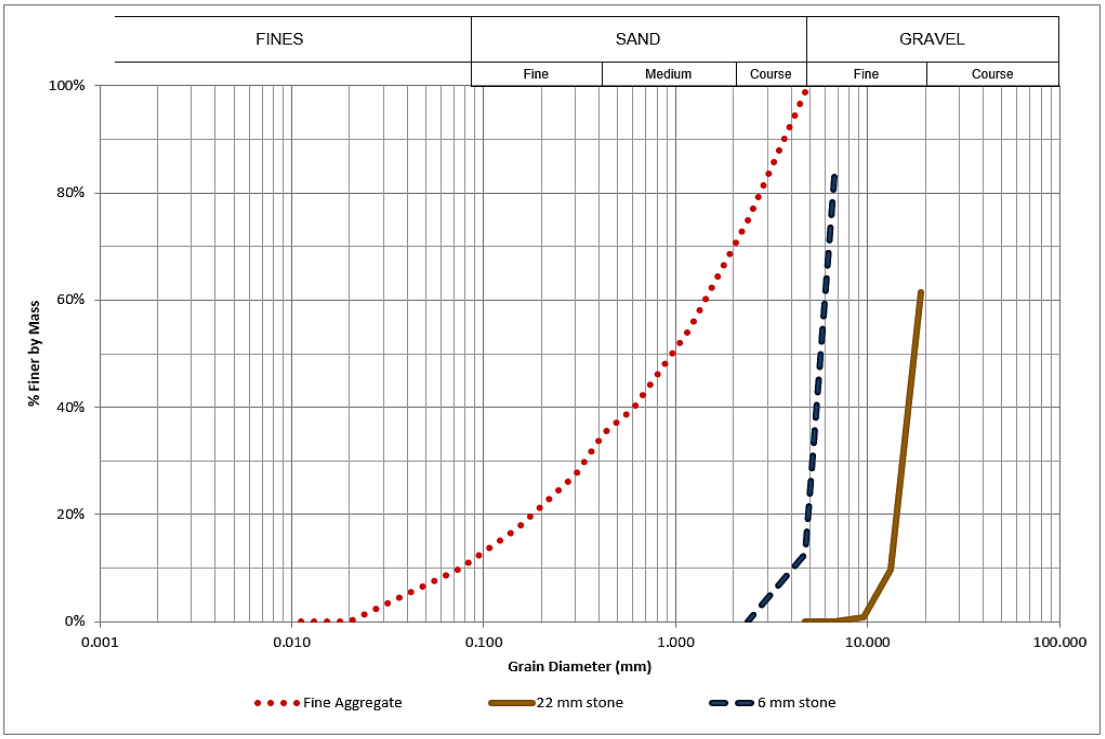

Figure 3.2: Particle size distribution of fine and coarse mineral aggregates

Crumb tyre rubber particles

Procurement

Crumb tyre rubber particles were used to replace fine aggregates in the concrete because research has shown that crumb rubber results in lower strength reduction compared to chipped rubber particles as discussed in chapter 2 (Naik, and Singh, 1991; Siddique and Naik, 2004). The crumb tyre rubber aggregates were procured from a local South African truck tyre recycling company. The recycling company produces crumb tyre rubber particles from ambient shredding and grinding of whole end-of-life truck tyres from various tyre manufacturers. The use of crumb rubber particles made from tyres made by different manufacturers meant that the specific chemical composition of tyre particles could not be determined with certainty thus an indicative chemical analysis of the rubber particles was carried out as detailed in Section 3.3.2.

Particle Sizes

Three crumb tyre rubber sizes were obtained from the recycling company. The crumb tyre rubber sizes were given as a mesh number. A mesh number is the number of openings across a linear inch of a sieve. The three crumb rubber sizes obtained, in mesh number designation, were 8-mesh (2.36 mm), 10-mesh (2.0 mm) and 40-mesh (0.425 mm). The upper limit of the fine aggregate size that could be replaced was 2.36 mm as this was the biggest size that could be supplied. The particle size distribution of the crumb rubber particles as received from the supplier is shown in Figure 3.3.

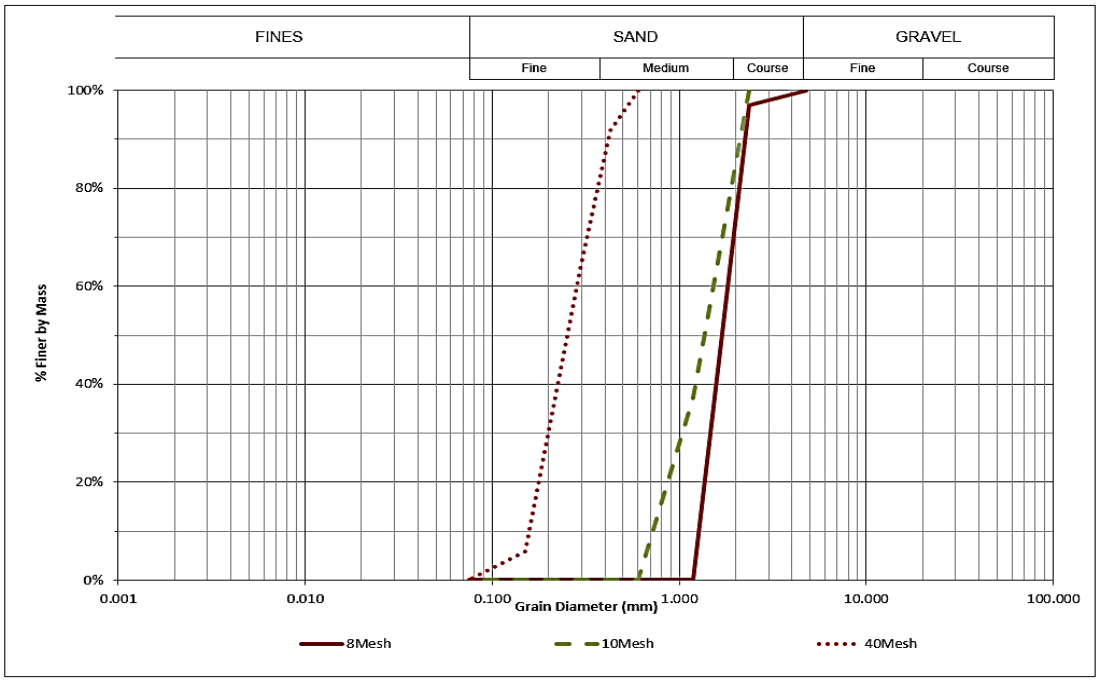

Figure 3.3: Crumb tyre rubber particle distribution

For the purposes of this study, the crumb rubber was further sifted in the laboratory using standard British standard (BS) sieves. This was done to reduce the size variation in a particular size classification. The re-sifting resulted in three size ranges that were used in the experiments. The three size ranges were 0.150 - 0.425 mm, 0.60 - 1.18 mm and 1.18 - 2.36 mm. In these size ranges, the smaller size is

the sieve which retained the crumb rubber, and the bigger size is the size of sieve allowing particles to pass. For ease of referencing the 0.150 – 0.425 mm, 0.60 – 1.18 mm and the 1.18 – 2.36 mm crumb rubber were designated identifiers M8 (for mesh-8), M16 (for mesh-16) and M40 (for mesh-40) respectively. The general appearance of the three crumb rubber particles is shown in Figures 3.4. The crumb rubber particles were further characterized as detailed in Section 3.3.2.

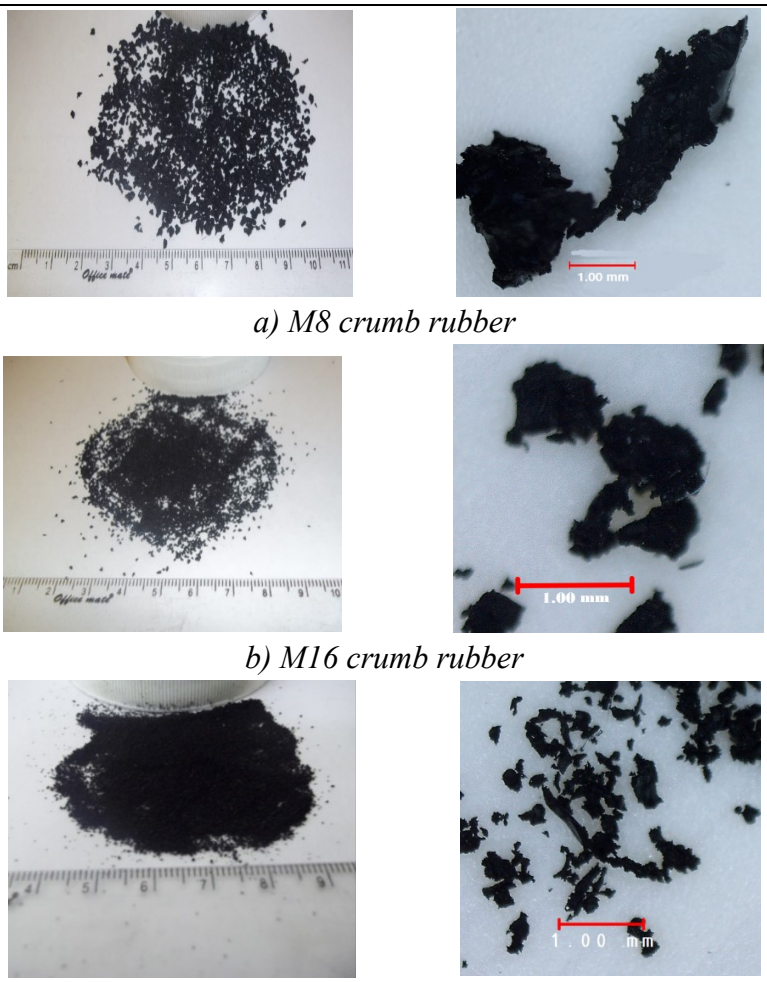

a) M8 crumb rubber

b) M16 crumb rubber

c) M40 crumb rubber

Figure 3.4: Crumb tyre rubber general appearance

Crumb tyre rubber surface pretreatment

For making the concrete, some of the crumb rubber particles were pretreated by two methods. The first method involved soaking the crumb tyre rubber in sodium hydroxide (NaOH). The second method involved soaking the tyre crumb rubber

particles in tap water. These two methods were selected for a number of reasons that include, their availability, the low cost of the pretreatment materials, the ease of application (with respect to pretreatment procedures) and their non-hazardous nature when compared to other methods that are reported to give similar results. Altogether, there were 3 crumb rubber types for use to make concrete namely; untreated crumb tyre rubber, NaOH treated crumb tyre rubber and tap-water treated crumb tyre rubber. The details of each of the treatment processes are presented below:

- *NaOH pretreatment* involved the immersion of crumb rubber particles for 24 hours in a 0.1M NaOH solution based on work that has been done by other researchers (Ma and Yue, 2013; Segre et al., 2002). Thereafter the particles were washed with tap water to remove the NaOH (Figure 3.5) and allowed to air dry for 24 hours (Figure 3.6). The NaOH is reported to enhance the cement paste-rubber particle bonding by reacting with zinc-stearate which makes the rubber particles more hydrophobic (Segre et al., 2002; Li et al., 2019).

- *Water pretreatment* method involved the washing of the crumb rubber under running tap water. After the washing, the crumb rubber was then immersed and allowed to soak in tap water for 24 hours. At the lapsing of the 24 hours the rubber was allowed to air dry for 24 hours before use. The water pretreatment is reported to assist with the reduction of the formation of air bubbles around the particles by pre-exposing the particles to water and also

removing impurities on the particles that make it hydrophobic (Mohammadi and Khabbaz, 2015).



Figure 3.5: Tyre crumb rubber particles being washed with tap water



Figure 3.6: Tyre crumb rubber air drying after washing

3.3 EXPERIMENTAL PROCEDURES

3.3.1 Mix proportions

The mixes were designed according to the Building Research Establishment (Teychenné et al., 1997) mix design method. The method is mainly focused on the design of mixes making use of Portland cement, water and normal-density aggregates only. It is used to determine concrete mixes with characteristic cube strengths of not more than 70 MPa. It considers the use of both crushed and uncrushed coarse aggregate.

The reference concrete mix design was aimed at achieving target mean compressive strength of 40 MPa. The mean target strength was obtained by applying a standard deviation of 6 MPa, representing average degree of control, to the chosen characteristic strength of 30 MPa (McDonald, 2009; Owens, 2011). The characteristic strength of 30 MPa was chosen because it is reported to be the minimum strength class required for pavements and sidewalks which are considered the most appropriate use for rubberised concrete (Mavroulidou and Figueiredo, 2010; Siddique and Naik, 2004, Base Concrete, 2020). It was also selected for its suitability for all domestic structural applications and most of the basic commercial structural applications (Owens, 2013). The mix proportions for all the concrete mixes used for compressive strength, elastic modulus, shrinkage and creep are given in Table 3.2 rounded off to the nearest kilogram. Crumb rubber particles replaced fine mineral aggregates by volume. There was a total of 10 concrete mixes. One plain PC concrete mix (which was taken as a reference mix), three untreated crumb rubber mixes and six treated crumb tyre rubber mixes. The mixes with crumb rubber pretreated with NaOH and tap water were suffixed with

the letter S and W respectively, for example, M8S and M8W. The rubberised concrete mixes were designed to achieve at least 30 MPa target compressive strength concrete for all sizes and rubber surface treatments. The 30 MPa strength rubberised concrete was achieved by selecting for each rubberised concrete mix, the mix which had the highest crumb rubber content within the required compressive strength range. For all the 10 mixes the w/c ratio was kept constant at 0.6.

Table 3.2: Concrete mix proportions (kg/m^3)

Mix Designation	**Description**	**Cement CEM I 52,5 R**	**Potable water**	**Coarse mineral aggregates (22mm andesite)**	**Fine mineral aggregates (Crushed andesite)**	**Crumb tyre rubber**
CM	Control Mix	350	210	1050	790	0
M8/S/W	5% Replacement level by volume for all rubber mixes	350	210	1050	751	18
M16/S/W		350	210	1050	751	18
M40/S/W		350	210	1050	751	18
M8/S/W	10% Replacement level by volume for all rubber mixes	350	210	1050	711	35
M16/S/W		350	210	1050	711	35
M40/S/W		350	210	1050	711	35
M8/S/W	15% Replacement level by volume for all rubber mixes	350	210	1050	672	53
M16/S/W		350	210	1050	672	53
M40/S/W		350	210	1050	672	53

The selection of 40 MPa and 30 MPa compressive strength for plain concrete and rubberised concrete respectively was to have a basis of comparison of the concretes given they both have the same w/c ratio and lie within the normal curve distribution for a 30 MPa characteristic strength class concrete with a standard deviation of 6. This means that the only variation in the strength is due to an anticipated effect of crumb rubber on the reference concrete of a reduction in strength and in this case the reduction has been restricted to achieve compressive strength of at least 30 MPa for rubberised concrete. According to Alexander and Beushausen (2009) typically

the time dependent behaviour of concrete lying in the same strength class are affected by similar factors. Thus, having kept the other parameters constant, the only factors that could possibly influence the observed time dependent deformation in the concrete will be the crumb rubber.

3.3.2 Crumb rubber aggregate characterisation

The crumb tyre rubber was characterised by its shape, texture, relative density and chemical composition.

Shape and texture

A Carl Zeiss Sigma Field Emission Scanning Electron microscope (FESEM) with Energy-Dispersive X-ray spectroscope (EDS) (Figure 3.7), was used to study the shape and texture of crumb tyre rubber. Both the treated and the untreated crumb tyre rubber particles were assessed.

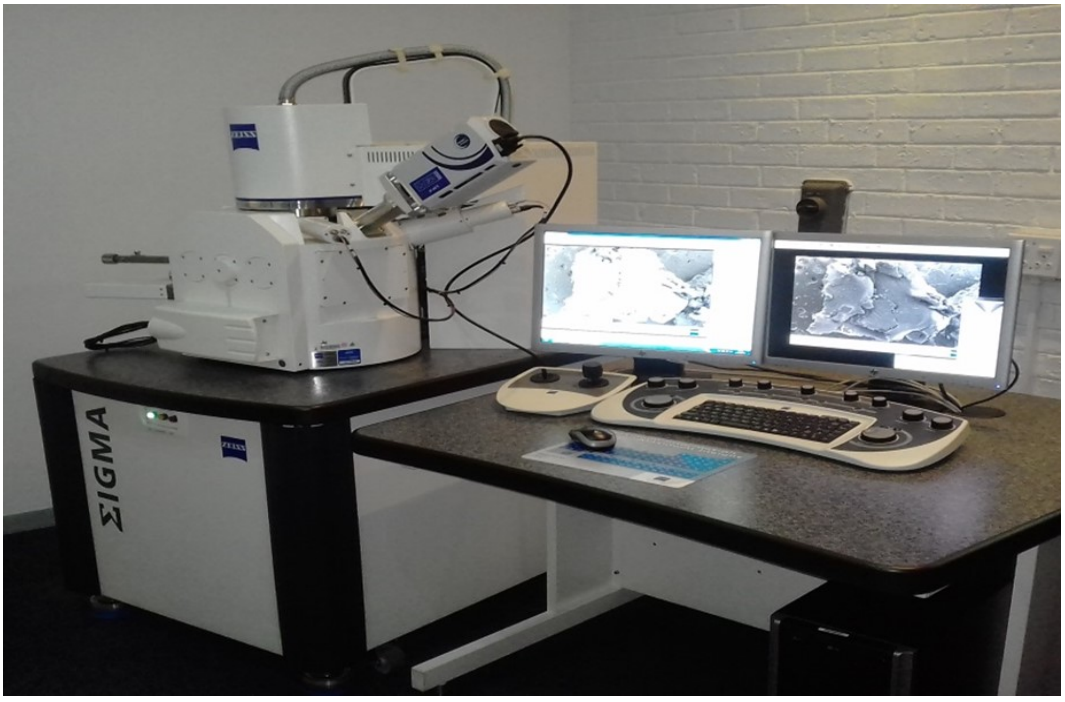

Figure 3.7: Carl Zeiss sigma field emission scanning electron with energy-dispersive x-ray spectroscope

The FESEM can produce high resolution micrographs at high magnifications exceeding 100 000 for a wide range of specimens. The EDS allows for elemental analysis. In preparation for analysis, the crumb rubber particle specimens were first spray-coated with a thin layer of carbon then followed by two very thin (2-3 nm) layers of palladium-gold. The coating is meant to reduce charging effects during the scanning, as this might result in a distorted image if the specimen becomes negatively charged. The rubber particles are placed on a stage with a double-sided carbon tape to hold them in place during preparation and viewing as shown in Figure 3.8**.**

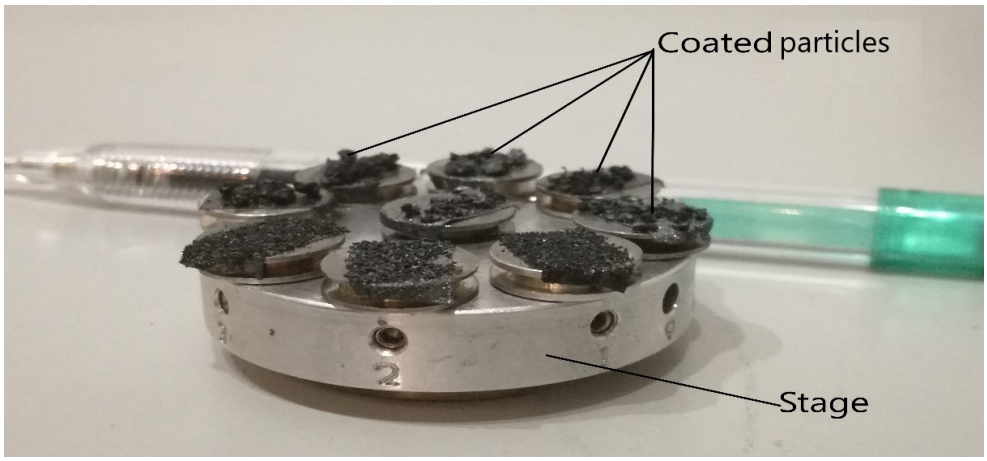

Figure 3.8: Coated crumb rubber particles mounted on stage

Relative density

The relative density of the crumb rubber was determined by the pycnometer method in accordance with SANS 5844:2014 using 100 ml volumetric flasks. The detailed test procedure is presented in Appendix A. The relative density of the aggregates was calculated using the formula given in SANS 5844:2014. The relative density of the crumb tyre rubber particles was found to be 1.1, which is less than half that of the mineral aggregate. This falls within the range of what is reported in literature (Alsaif et al., 2018; Bompa and Elghazouli, 2019). The implication of this lower

relative density is that crumb rubber particles would occupy more volume for the same mass as andesite aggregates.

Crumb tyre rubber elemental composition

The elemental composition of the crumb tyre rubber was determined using EDS. The analysis was carried out primarily to have a basic picture of the elemental composition of the tyres being used. The secondary purpose of the analysis was to check changes to the elemental composition of the tyre rubber associated with the pretreatment processes. The elemental analysis was carried out on the same specimens used in the surface morphology, thus, the specimen preparation was the same. However, because the specimens had been coated with palladium-gold, the element peaks for palladium and gold were supressed in the graph. Table 3.3 is a summary of the elements identified in the crumb tyre rubber particles. Figures 3.9 – 11 show the elements identified in each of the three crumb rubber elements (untreated, water soaked and NaOH soaked).

Table 3.3: Elements identified in the untreated and treated crumb rubber

Element	**Compound Presence**		
	Untreated	NaOH soaked	Water Soaked
C	✓ .	✓ .	✓ .
O	✓ .	✓ .	✓ .
Al	✓ .	Not present	Not present
Si	✓ .	✓	✓ .
S	✓ .	✓ .	✓ .
Cl	✓ .	Not present	Not present
Ca	✓ .	✓ .	Not present
Fe	✓ .	Not present	Not present
Zn	✓ .	✓ .	✓ .
Total	**9**	**6**	**5**

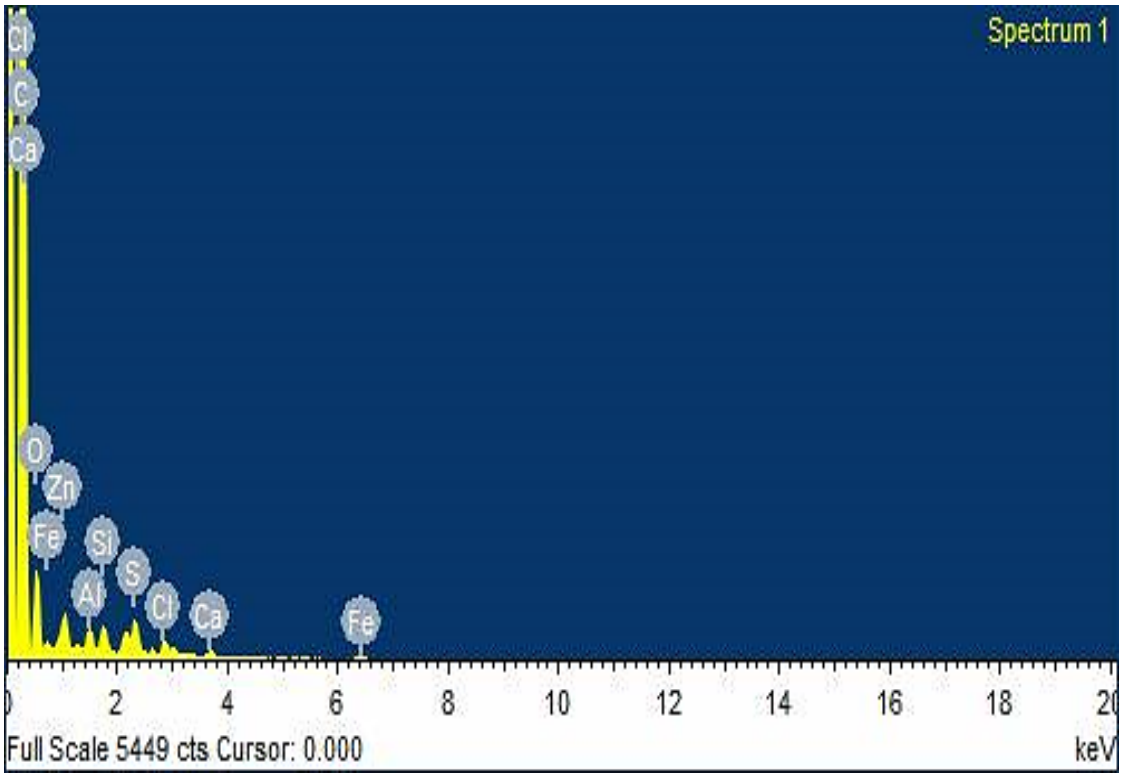

Figure 3.9: X-ray spectrum for untreated crumb rubber

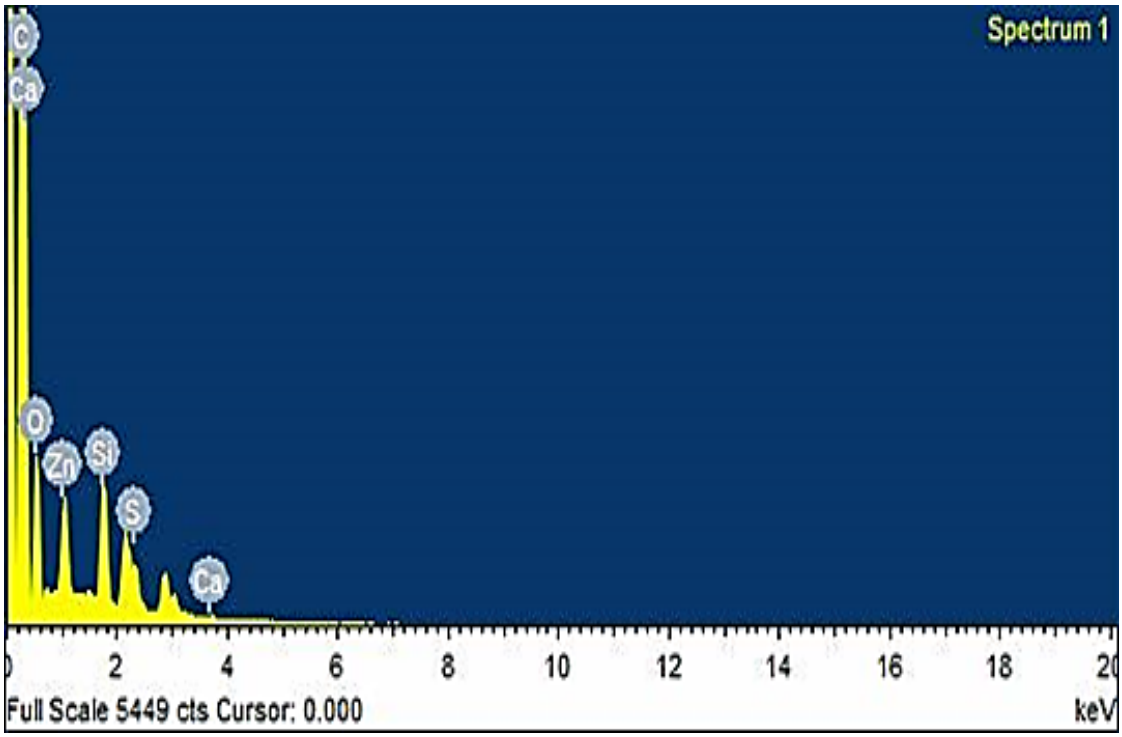

Figure 3.10: X-ray spectrum for NaOH treated crumb rubber

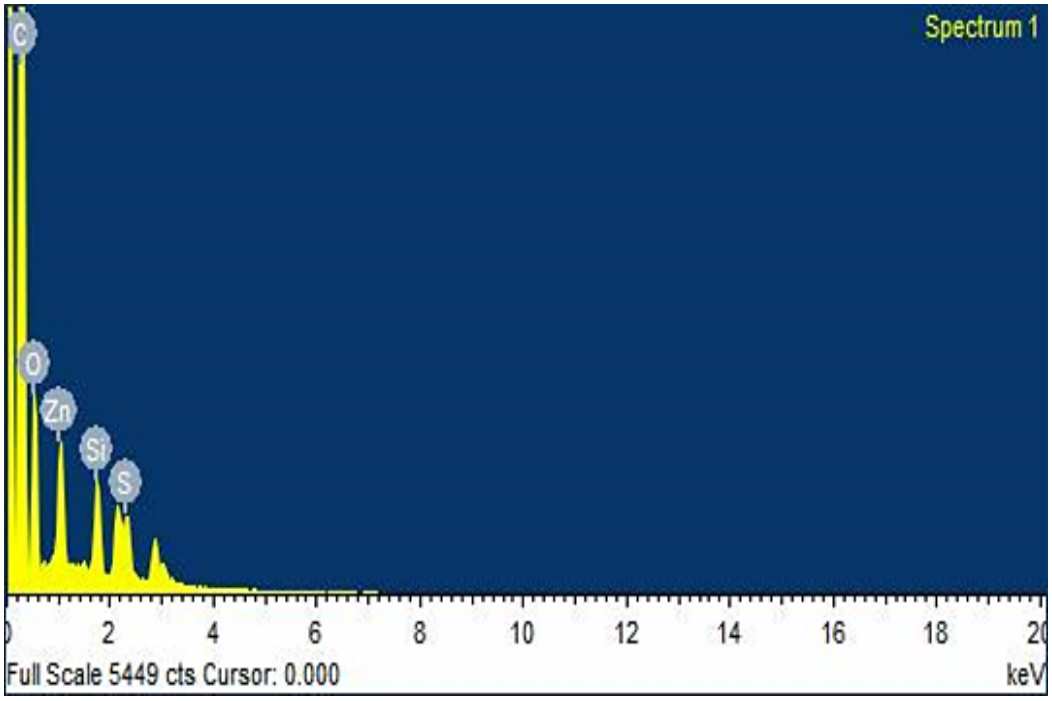

Figure 3.11: X-ray spectrum for water-soaked crumb rubber

The elemental composition analysis revealed that the NaOH treatment resulted in rubber with three elements less than untreated tyre rubber and water soaking resulted in tyre rubber with four elements less than untreated tyre rubber. In both pretreatments, Aluminum, Chlorine and Iron were not detected, in addition to these for the water-soaked tyre rubber, Calcium was also not detected. The explanation for the presence of certain elements in the untreated rubber and not present in the treated rubber might be that these elements are only on the surface of the rubber thus during the treatment these elements are removed from the surface of the rubber. This is confirmed by elemental composition given by Sun et al. (2020) and Polydorou et al. (2020), which shows an elemental composition similar to the pretreated rubber particles. It is unlikely that the removal of the metal elements was due to chemical reactions since similar elements were removed by either method and there is no known chemical reaction that water may have with any of the metals in 24 hours. The absence of these elements suggests that the two pretreatment

methods have an effect on the surface elemental composition of the tyre rubber, which might influence its behaviour in concrete. It is worth noting that all three elemental compositions can be typical compositions for an untreated crumb rubber as evidenced by elemental compositions reported by other researchers. (Polydorou et al., 2020; Sun et al., 2020; Richardson et al., 2016).

3.3.3 Compressive strength tests: Selection of rubber replacement level

Compressive strength specimen preparation

In order to find the optimum crumb rubber replacement level, the concrete mixes containing different percentages (0%, 5%, 10%, 15%) of crumb rubber by volume of fine aggregates were cast using the mix proportions given in Table 3.2. Three 100 mm cube specimens per mix were cast for compressive strength tests at 28 days for the trial mix and creep testing stage. The material batches were measured on a laboratory digital scale to the nearest 100 g. The materials were initially mixed, using a 30 kg pan mixer, without any water until the cement had been evenly mixed with the mineral and rubber aggregates, shown by an even grey colouring of the dry mix. To prevent the uneven distribution of crumb rubber particles, the crumb rubber particles were added last by sprinkling them slowly over the mineral aggregate and cement dry mix as it was being mixed before water was poured in. Tap water was then slowly poured in over a one minute-period.. The wet mix was mixed further to the minute of adding water until a homogeneous mix was achieved before placing the fresh concrete in the moulds. The concrete in the moulds was compacted by placing them on a vibrating table and vibrating them for between half a minute to a minute, until the concrete surface was smooth and it was no longer releasing any

bubbles. The slumps of each of the mixes was measured before casting to check adhesion to mix design specification. The cast concrete in the moulds was immediately covered with polyethene sheets at room temperature and left for 24 hours. After the 24 hours the hardened concrete cubes were removed from the moulds and immersed in water for curing at 23 ± 2°C.

Compressive strength testing procedure

The compressive strength test was carried out in accordance with South African standard SANS 5863. The test was conducted on an Amsler, which is a hydraulic compression-testing machine able to apply loads of upto 2000 kN. The load was applied at a rate of approximately 15 MPa per minute until failure at which point the maximum load was recorded as the "failure load" to the nearest of 0.1 kN. The concrete mix with the highest fine mineral aggregate replacement percentage at the desired strength for each size was the mix which was then used in the time dependent tests. The concrete mix with the lowest untreated crumb rubber content that fell below the desire target strength (30 MPa) was cast afresh, now using pretreated crumb rubber particles at the same replacement level and retested to check if the pretreatment would improve the compressive strength.

Compressive strength results

After testing the concrete, the results showed that the 10% replacement level was the optimum replacement level for untreated crumb rubber particles as shown in Figure 3.12. The results also revealed that the use of pretreated crumb rubber particles does not improve the compressive strength of the rubberised concrete as

shown in Figure 3.13. Therefore, the 10% replacement level was also adopted for rubberised concrete mixes using pretreated crumb rubber particles. To that end, all the concrete mixes for the main tests were conducted at a replaced level of 10%. A full discussion of the compressive strength results is presented in Appendix B.

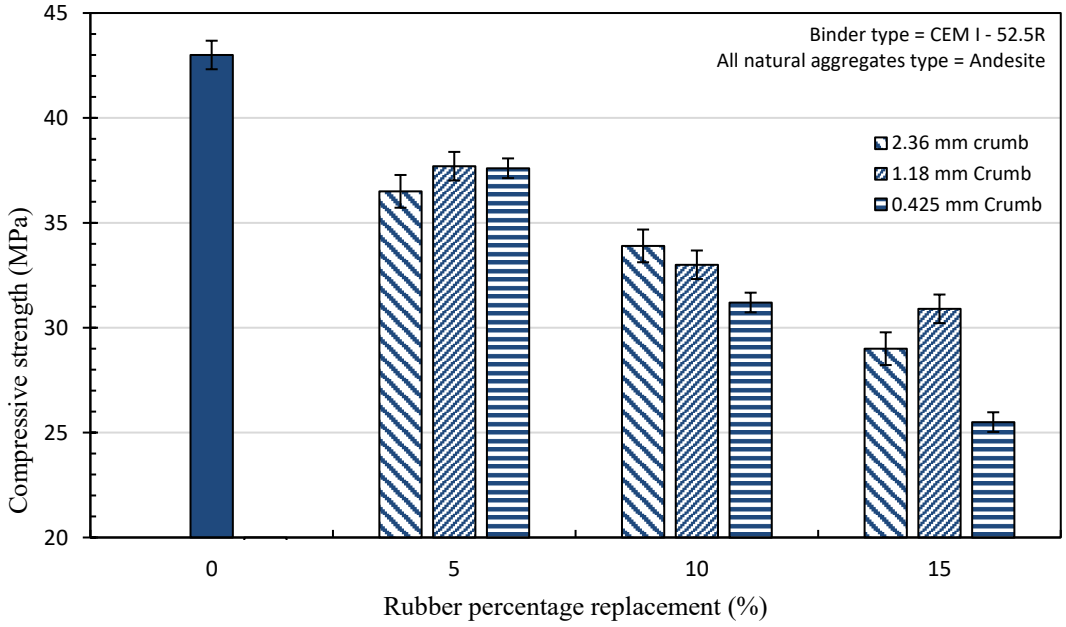

Figure 3.12: Effect of crumb rubber content and size on concrete compresive strength (Untreated)

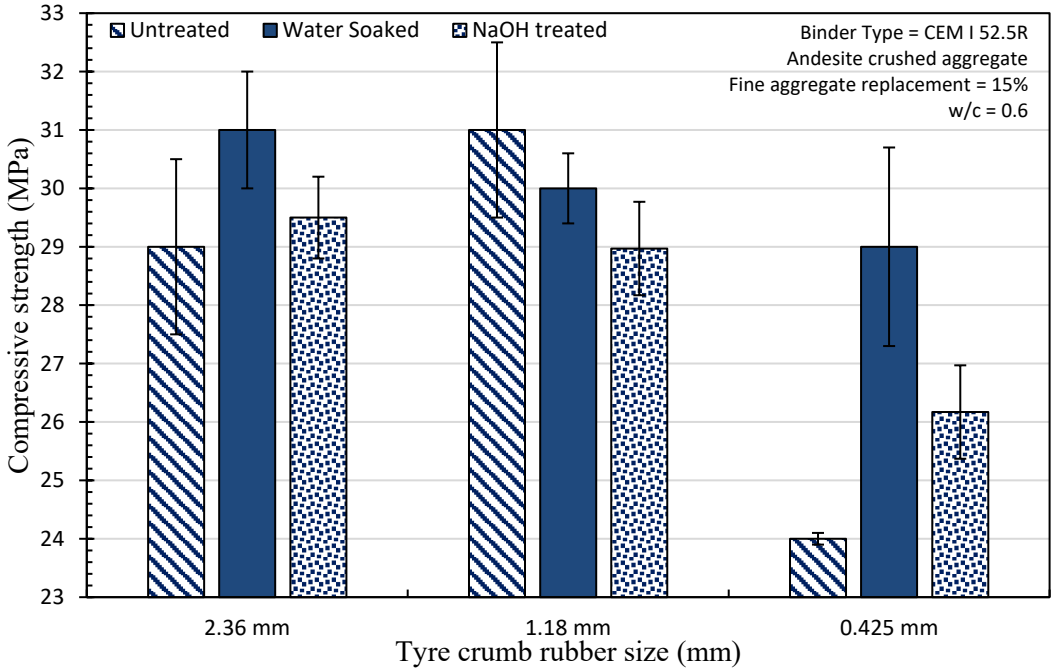

Figure 3.13: Effect of crumb rubber pretreatment on concrete compresive strength (15% repacement level)

3.3.4 Shrinkage and creep specimen preparation

Concrete prisms used for shrinkage and creep tests were made from concrete beams cast using 710 × 100 × 100 mm moulds. The same procedure used for preparing fresh concrete for compressive tests was used in preparing fresh concrete for time dependent deformation tests, the concrete beams were also compacted on a vibrating table until the concrete was no longer releasing any large bubbles and its surface was smooth.

Immediately after casting the concrete beams, the moulds were covered using polythene sheet at room temperature. After 24 hours the beams were demoulded and placed in a water bath for curing at 23 ± 2°C. After 20 days of water curing, three 100 mm × 200 mm prisms (Figure 3.14) were made from each beam by cutting the concrete beams using a diamond saw. The concrete prism end faces were ground flat and parallel to each other using a high-speed facing machine. Two demountable mechanical gauge (Demec) targets made of stainless steel, to allow for the reading of strains using a 100 mm Demec gauge, were placed on two opposite sides (100 mm × 200 mm) of the specimens using quick setting glue (schnellklebstoff X 60 epoxy glue). The glue was allowed to set before the prisms were put back in the water bath to continue curing. The total time the specimens spent out of the water bath was less than 6 hours. This process was done before 28 days to ensure that the specimens would be tested as soon as they left the water-bath at 28 days. For each mix, three prisms were used for creep test and another three for shrinkage test.

3.3.5 Concrete prisms for creep test

At the end of the 28 days of curing the prisms were taken to a climate-controlled room (creep room) to be set up. The climate-controlled room temperature was kept at 20 ± 3ºC with the humidity set at 60 ± 5%. In some instances, the temperature and humidity would fluctuate due to power-cuts and equipment failure, these deviations were not allowed to persist for periods longer than 12 hours, in most cases, these were corrected within 6 – 8 hours. However, on the day of taking readings, the conditions prevailing at the time would be recorded regardless of duration or the correction having been done. The temperature and humidity of the climate-controlled room were monitored daily and corrected appropriately. This was done to ensure that these fluctuations would not impact of the results. Twelve prisms for each mix were prepared, half of which were sealed. The prisms were sealed by coating them with a thick coat of a water-based bituminous waterproofer and wrapped with aluminum foil after the waterproofer had dried. The unsealed concrete prisms meant to be used as drying shrinkage specimens were coated with transparent silicone glue on both end faces (Figure 3.14). This was meant to resemble what happens when creep specimens are set up one on top of the other and moisture is not lost.

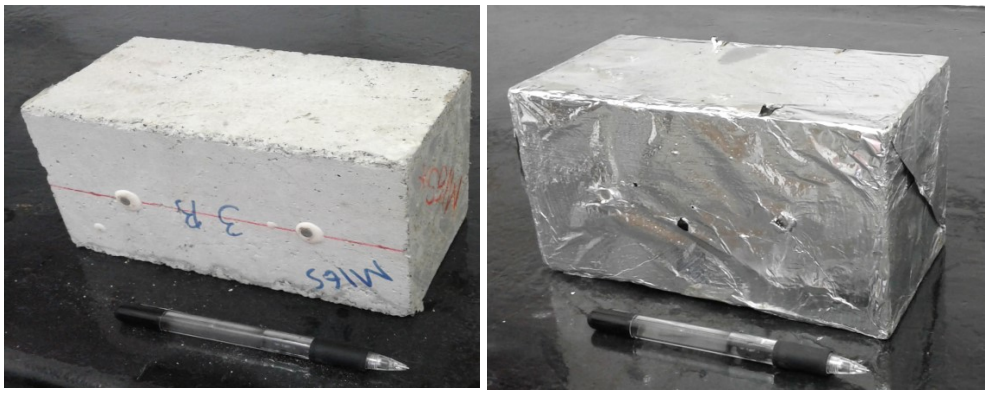

a) Unsealed specimen b) Sealed specimen

Figure 3.14: Shrinkage and creep specimens

3.3.6 Creep set-up and measurements

Three of the six unsealed specimens and three of the six sealed specimens were subjected to the creep test with the remaining being left unloaded and placed in the creep room to monitor shrinkage. Figure 3.15 shows a schematic diagram of concrete specimens arranged in a creep loading rig based on ASTM C-512 (2015) and modified by Ballim (1983) with a hydraulic flat jack. The specimens were centered using a plumline and were arranged to ensure the Demec targets were all on one side and running down along a vertical line. Dummy concrete specimens were placed in each creep frame at the top and the bottom of the specimen stake to reduce the loading plates end-restraint effect on the test specimens.

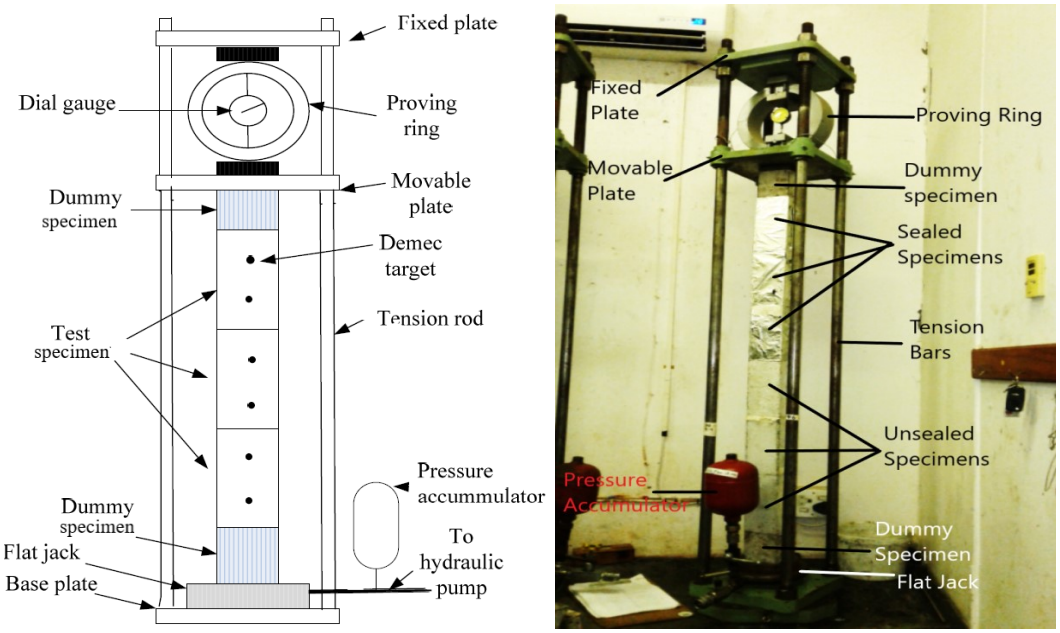

Figure 3.15: Schematic arrangement of the hydraulic creep loading rig

The following details the procedure followed in loading and measuring deformation of the specimens:

- The concrete specimens were arranged in the creep rig as already described and their straightness was checked to ensure concentric loading;

- The valve between the accumulator and the flat jack that controls the flow of hydraulic oil in and out of the flat jack that loads the specimens kept was closed
- The specimens were loaded with 30% of the 28-day compressive concrete strength (σ_a), at a rate of 15 MPa per minute, this load was sustained for a minute mainly to eliminate creep and achieve seating of the gauge (Neville, 2011). The 30% stress level was selected for all specimens in all mixes to ensure that the test was done within the elastic range and to also have all the specimens at the same stress:strength ratio for ease of analysis.
- The valve was opened and nitrogen gas, from the gas cylinder connected to the accumulator, was applied to keep the load at the desired level if there was any reduction, the valve was then closed and maintained for 1 minute.
- The specimens were unloaded at the same rate as loading, to minimise distortions in strains recorded, using a pump to a pre-load of σ_b = 1 MPa and maintained for half a minute;
- "Zero" load strain measurements were recorded for all specimens at σ_b;
- The valve was opened and specimens were reloaded using an oil pump at the same loading rate to (σ_a) and;
- The elastic strain readings were taken while the load was sustained,
- A set of "zero shrinkage" strain measurements were also recorded on accompanying the free shrinkage specimens.

Once the specimens had been placed and loaded as outlined above, creep strain measurements were recorded every day for a week, then every week for a month and thereafter once every month for the duration the experiment. For the duration of

the test, the load was maintained at an accuracy of ±2% and was monitored by means of a dial gauge incorporated into the proving ring shown in Figure 3.15.

The free shrinkage specimens were placed on steel racks, with thin edged supporting members to allow free air flow around the specimens, in the same environment-controlled room as the creep specimens. (Figure 3.16). All shrinkage strain readings were taken off these specimens. These free shrinkage strain measurements were taken at the same time as the ones for creep.



Figure 3.16: Shrinkage specimens on racks

The readings were taken using 100 mm Demec gauge with and accuracy of 16 microstrains (Figure 3.17).

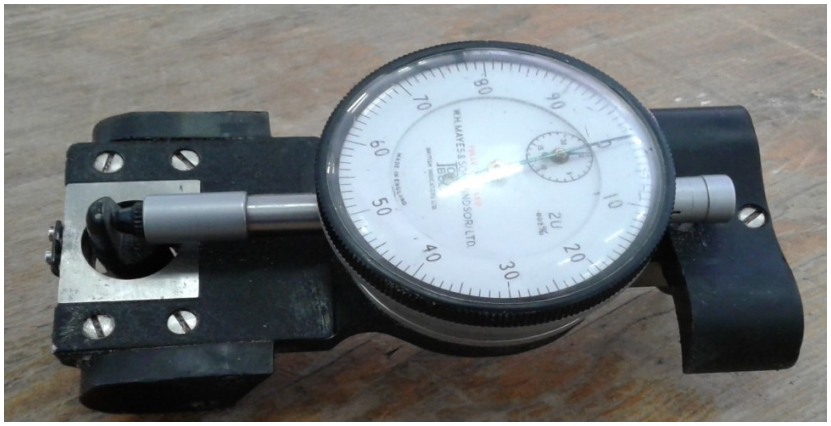

Figure 3.17: 100 mm Demec gauge (accuracy ± 16με)

3.3.7 Determination of elastic modulus of concrete

The elastic modulus of the rubberized concrete was also determined in order to compare the effect of rubber on the elastic deformation and the time-dependent deformation. Three 100 mm × 100 mm × 200 mm concrete prisms of each of the mixes in Table 3.2 were prepared to measure the elastic moduli of the concretes in accordance to BS 1881-121(1983). The test specimen was placed centrally in the compression testing machine (Figure 3.18). A basic stress (σ_b), the minimum stress specified in the British Standard (BS 1881-121:1983) that is necessary to keep the specimen from moving in the testing machine, of 0.5 N/mm^2 and the strain was measured on each face of the specimen using two 100 mm Demec gauges held in place by hand (Figure 3.19).



Figure 3.18: Elastic modulus specimen placed centrally in loading machine



Figure 3.19: Demec gauge held in place on one face of the test specimen

The load was steadily increased at a rate of 0.6 ± 0.4 N/(mm^2·s) until the stress reached the chosen upper limit to keep the concrete within the elastic region, which is a third of the concrete compressive strength ($\sigma_a = f_c/3$). The stress was maintained for 60 s and the strain readings were recorded simultaneously from each face. The individual strain readings were checked to see if they were within a range of ±10% of their mean value at σ_a. The specimen was centered to ensure that the strains obtained were within the specified range. After ensuring that the specimen had been well centred and that the readings were within range, the test proceeded. The load was reduced to the basic stress at the same rate as during loading. Two preloading

cycles were done, at the same rate for both the loading and unloading cycle, maintaining the stress (σ_a and σ_b) constant for a period of 60 s each time. Preloading cycles are required to eliminate creep during the test. After completing the last preloading cycle and waiting a period of 60 s under the basic stress, the strain readings on each face were during the succeeding 30 s. The specimen was then reloaded to a stress a third of the concrete compressive strength at specified rate. During this loading exercise readings were taken at 1.5 N/mm^2 intervals in order to have enough points to plot a stress-strain graph. The strain readings were then plotted against the corresponding stress to find the secant elastic modulus for each specimen.

3.3.8 Micro-crack detection

Specimen preparation

The micro-cracking potential of rubberized concrete due to time-dependent deformation is investigated in order to ascertain the extent to which rubber affects micro-cracking in cementitious materials. The micro-cracking potential of concrete under sustained loading was assessed on 40 × 40 × 80 mm concrete prisms. To distinguish the effect of creep deformation from shrinkage deformation, other unloaded specimens were kept under the same humidity conditions. The loading rig shown in Figure 3.20 was used to load the prisms. For each mix one sealed specimen and one unsealed specimen was loaded. Similarly, one sealed specimen and one unsealed specimen was prepared for free shrinkage tests. Sixteen specimens were prepared for each concrete mix. Two creep specimens and two shrinkage specimens were tested at each testing stage.

Sustained loading rig

The rig was fabricated in the lab from mild steel flat bars and bright mild steel rods (Figure 3.20). The load was applied by turning the eye bolt which was then pushed down on the loading plate that is in contact with the specimen. The desired stress ($f_c/3$) was reached when the prescribed distance between the bottom loading plate and the base plated was achieved. This distance was measured by a Vernier calipers (Figure 3.21). The distance corresponding to a particular load is specified by the disc spring manufacturer, this was also verified by calibration. Each disc spring has a load (F) that is able to achieve a full deflection (h) of the disc spring. The load was sustained by disc springs that were located underneath the bottom moving plate as shown in Figure 3.20.

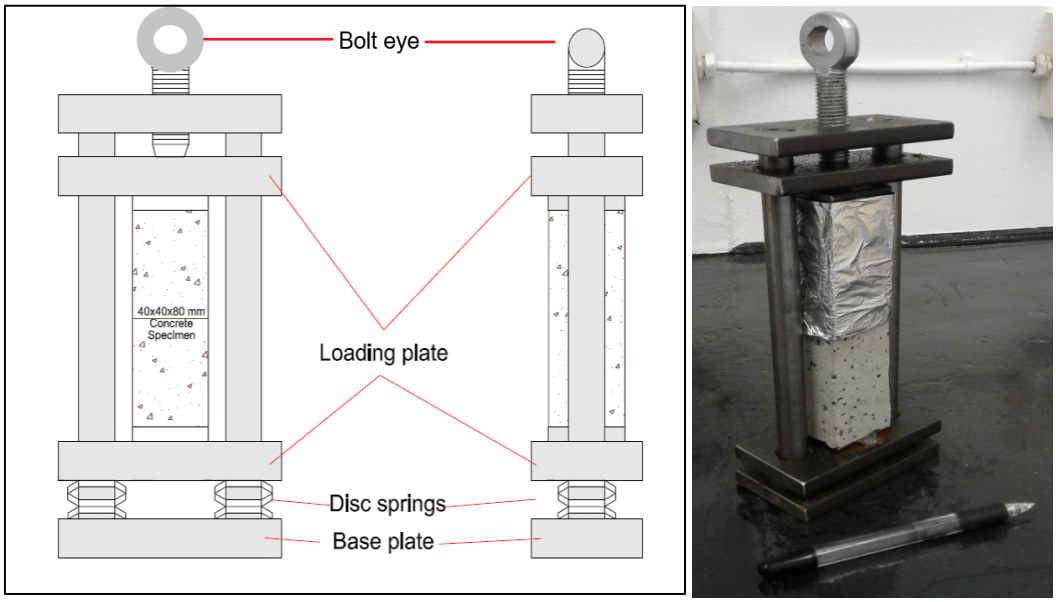

Figure 3.20: 80mm concrete specimen sustained loading rig

For each concrete mix 8 specimens were prepared. The specimens were unloaded after 52 weeks. For each micro-crack assessment there were 2 creep specimens and 2 shrinkage specimens, one was allowed to dry and the other sealed to resemble the 200 mm creep and shrinkage specimens in Section 3.3.4.

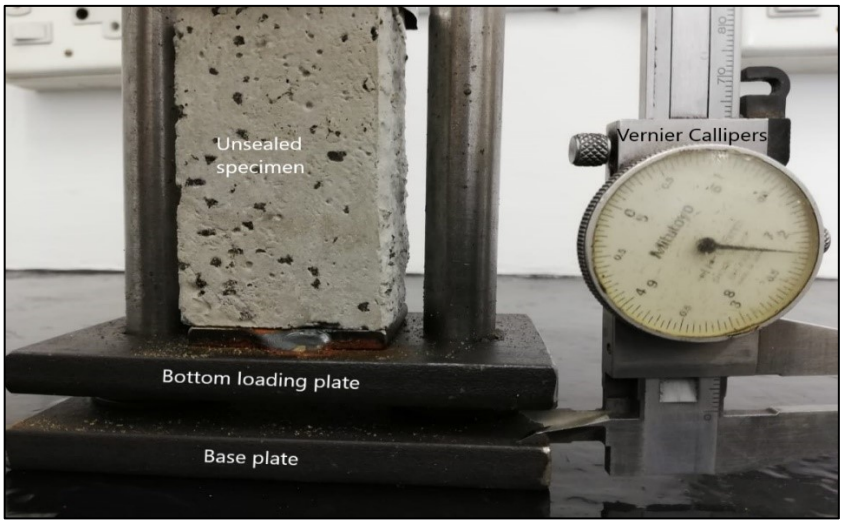

Figure 3.21: Measuring the distance between the base plate and the bottom loading plate

Microcrack identification

Before the fluorescence microscopy could be carried out the prisms were first immersed in ethanol which had been mixed with a fluorescent dye. The prisms were left in the ethanol dye mixture for 24 hours as shown in Figure 3.22. This was to allow the dye to penetrate as far into the specimen as possible. After 24 hours the prisms were allowed to air dry under room temperature. The prisms were then coated with an epoxy resin to prevent the specimens from breaking and disintegrating during the diamond saw cutting. 40 × 40 × 2 mm slices (Figure 3.23) were prepared for viewing under a fluorescent microscope.



Figure 3.22: Concrete specimens immersed in ethanol with fluorescent dye

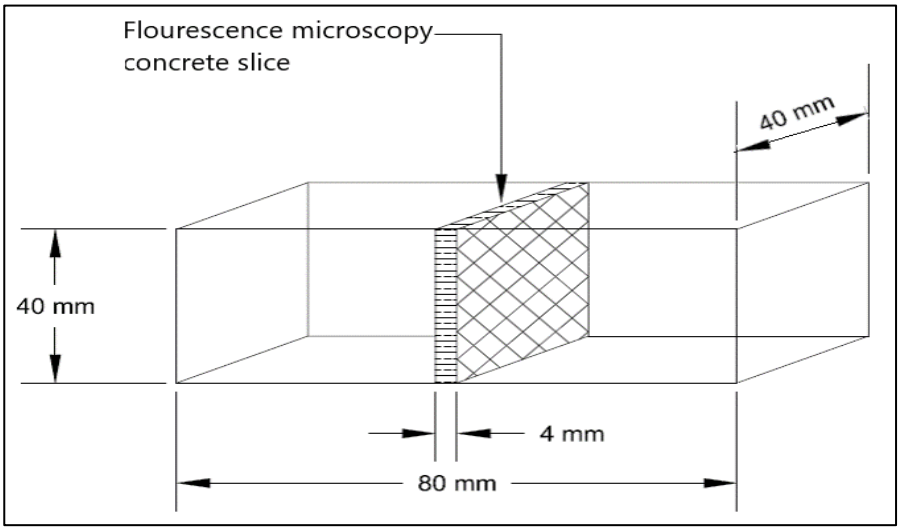

a) Typical slicing of concrete specimen for fluorescent microscopy



b) Fluorescent microscopy specimens (40 × 40 × 4 mm)

Figure 3.23: Fluorescence microscopy specimens

An EVOS FLoid fluorescent microscope was used to analyse the specimens and take micrographs of points of interest. The fluorescent microscope allowed viewing to be done under three illumination settings, green, blue and red. The micrographs were taken using any of one the three settings depending on which gave the best view for particular observations. The micrographs taken for each illumination setting could be superimposed in some instances to make one micrograph to better show some observations.

3.3.9 Concrete porosity determination

The concrete percent voids determination test was done in order to ascertain whether the use of crumb rubber particles in concrete increases the porosity of the concrete by increasing the voids content in hardened concrete.

Specimen preparation

The hardened concrete percent voids determination was carried out on the drying shrinkage specimens at the end of the 52 weeks. 55 mm thick slices were cut, using a diamond saw, from the middle of each of the 200 mm long drying shrinkage specimens to make 100 x 100 x 55 mm specimens. Three specimens were cut for each of the concrete mixes.

Test procedure

The hardened concrete voids determination was carried out in accordance with ASTM C642 (2013) which involves the removal of all moisture in the specimen by oven-drying at 110°C before filling up the voids by immersing it in 21°C tap water and thereafter boiling it for 5 hours. The complete details of the experimental procedures are presented in Appendix A.

CHAPTER FOUR: RESULTS AND ANALYSIS

4.1 INTRODUCTION

The chapter discusses the results of various experiments conducted on tyre crumb rubber particles and the concrete made from the crumb rubber particles with a view to evaluate properties of the hardened concrete. The specific investigation objectives were as follows:

a) Characterise the tyre crumb rubber with respect to its shape, size, surface texture and density.
b) Evaluate the effect of different crumb rubber size (2.36 mm, 1.18 mm, 0.425 mm) on basic creep, total creep and drying shrinkage behaviour of the structural concrete.
c) Evaluate the effect of crumb rubber surface modification by various crumb tyre rubber surface treatments on basic creep, total creep and drying shrinkage behaviour of structural rubberised concrete.
d) Assess the interaction of the crumb rubber particles with the concrete matrix undergoing shrinkage and creep deformations

The chapter is organised in a way that is intended to allow for a logical build-up of understanding the effects of crumb tyre rubber on hardened concrete properties. Hence, results of characterisation of the crumb rubber particles are presented first, followed by the results of the assessment of crumb rubber-concrete matrix interaction which was done by fluorescent microscopy. The results of the hardened concrete voids determination is presented thereafter followed by the elastic and time-dependent deformation results in that order. As mentioned before, this allows

for the use of observations made in the characterisation stage to be referenced in the time-dependent results discussion stage.

4.2 TYRE CRUMB RUBBER SHAPE AND TEXTURE CHARACTERISATION

The tyre crumb rubber particles were produced by a tyre recycling company using an ambient production process. The particles were characterised in terms of size, relative density, shape and texture. The characterisation results with respect to size and density are presented in Section 3.3.2. The elemental composition analysis of the untreated and treated tyre rubber is also presented in Section 3.2.2. This section presents the shape and texture characterisation.

4.2.1 Crumb rubber particle shape

The SEM microscopy revealed significant differences in the shape and surface texture of the crumb rubber sizes. Micrographs of the crumb rubber particles are shown in Figures 4.1, 4.2 and 4.3 at a magnification of 100 times.

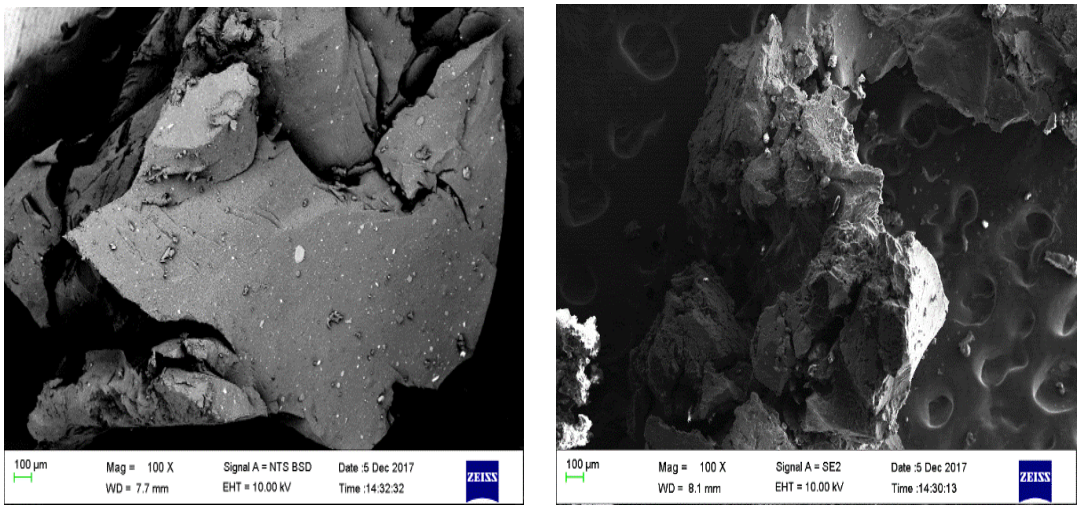

Regular shaped particle *b) Irregular shaped particle*

Figure 4.1: SEM micrograph of a 2.36 mm particle (magnification 100×)

The 2.36 mm crumb rubber particles generally have a more regular and well-defined angular shape with a few irregular shaped ones as shown in Figure 4.1. The edges are fairly clean-cut because the tyre rubber size at this stage is big enough to still be cut directly by the steel shredder teeth.

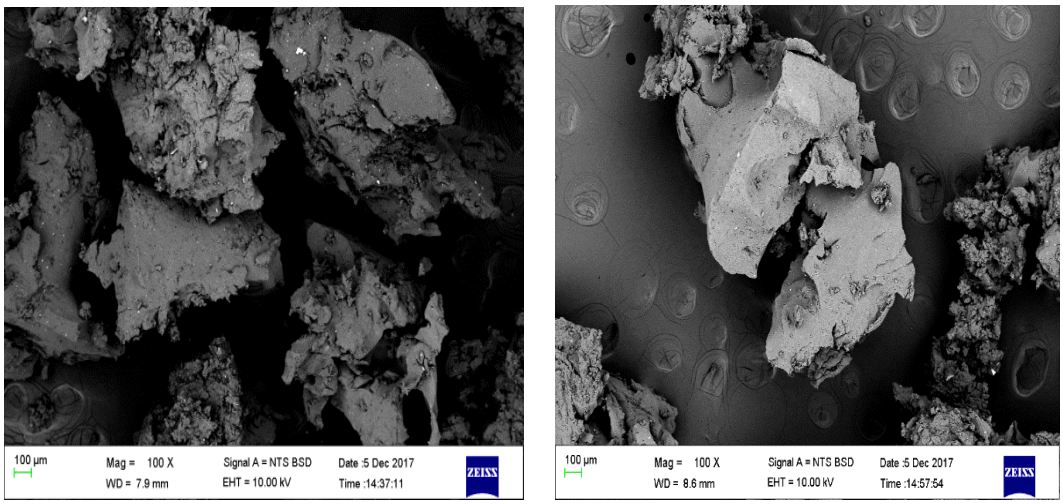

a) Irregular shaped particle *b) Regular shaped particle*

Figure 4.2: SEM micrograph of a 1.18 mm particle (magnification 100×)

The 1.18 mm crumb rubber particles also have a generally regular and well-defined, angular shape with a slightly higher proportion of irregularly-shaped particles due to the friction between the particles during the grinding process as shown in Figure 4.2.

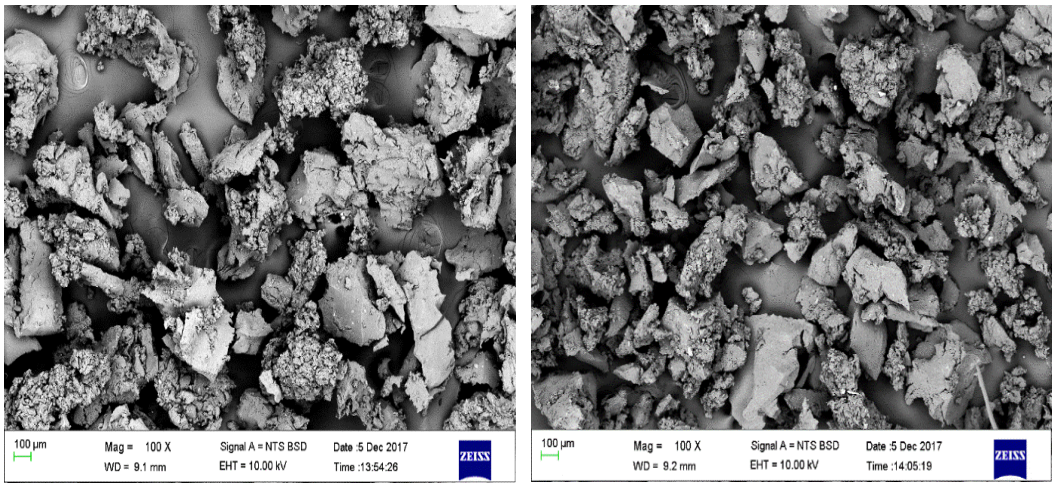

a) Bigger particles *b) Smaller particles*

Figure 4.3: SEM micrograph of 0.425 mm crumb rubber particles (magnification 100×)

The 0.425 mm crumb rubber particles have an irregular and more fibrous looking morphology as shown in Figure 4.3. The bulk of the particles are produced through the rubbing action of the particles against each other. The rubbing or friction action results in the particles tearing up, stretching until they snap or rolling up into a ball while breaking down. The crumb rubber particles' shape descriptions are in agreement with what is found in literature (Kara De Maeijer et al., 2021; Shulman, 2019), in keeping with the morpology of crumb rubber produced by the ambient mechanical method.

4.2.2 Surface texture

Texture variation for different particle sizes

Table 4.1 contains images showing the surface features of the different sizes of untreated crumb tyre rubber particles and brief descriptions of the surface features observed on each of the particles.

As previously discussed, there is a clear difference in surface texture for the different crumb rubber sizes. The surface texture is observed to be rougher as the crumb rubber becomes smaller with an increase in rough edges and crevices on the particle surface. This is mainly due to the production process of the particles which results in particles breaking down and snaping due to particles rubbering against each other as they become smaller instead to being cut by the teeth of the steel shredder.

Table 4.1: Micrographs showing the surface texture of the different crumb tyre rubber sizes (magnification 500×)

Micrographs	**Observations**
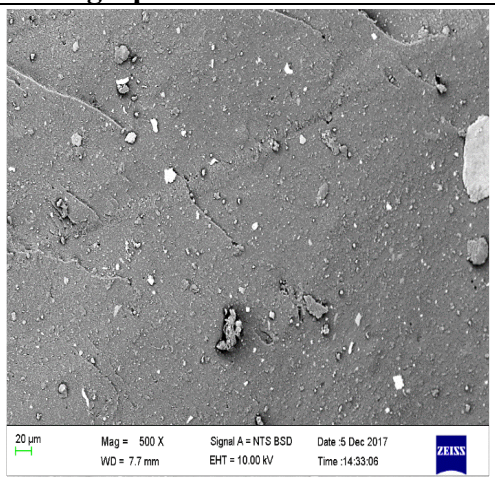 *a) 2.36 mm rubber particle micrograph*	The surface texture of the 2.36 mm crumb rubber particles is generally smooth with very little variation of the texture across the particles surface.
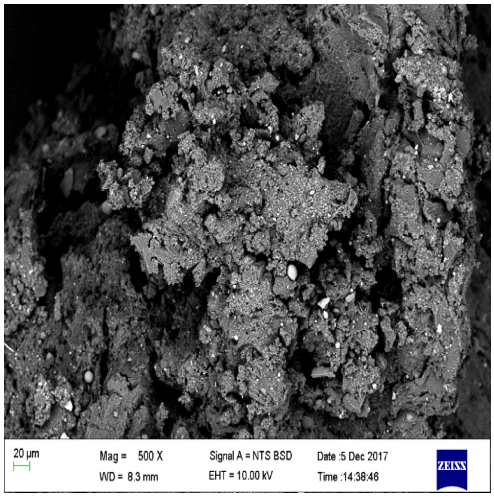 *b) 1.18 mm rubber particle micrograph*	The surface texture of the 1.18 mm crumb rubber particles is rough with a number of crevices and pores although there are some smooth portions on the particles.
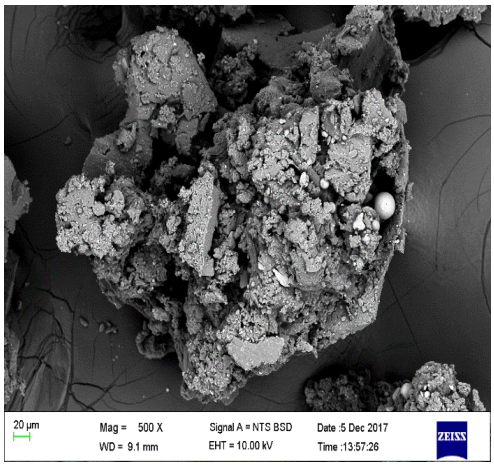 *c) 0.425 mm rubber particle micrograph*	The surface texture of the 0.425 mm crumb rubber particles is much rougher with a considerable number of crevices and pores all over the particle's surface.

Effect of surface treatment on surface texture

Tables 4.2, 4.3 and 4.4 give details of the observed surface features of the different crumb tyre rubber size particles. Each table details the observed effects of each of the two pretreatment methods used, namely; soaking in 0.1M NaOH and soaking in tap water.

Table 4.2: 2.36 mm tyre rubber micrographs with different pretreatment methods

Micrograph	**Observations**
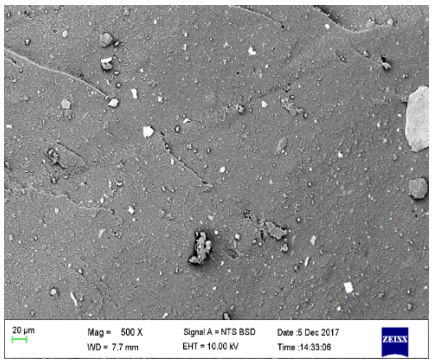 *a) Untreated*	The NaOH treated crumb rubber has a rougher surface texture when compared to the untreated and water-soaked crumb rubber. The water soaking of the crumb rubber had the effect of exposing the hidden pores of the rubber particles. The pretreatment methods resulted in changes to the surface texture of the crumb rubber though the effects are quite different. The water soaking simply cleaned the surface to reveal any hidden pores while for the NaOH treatment, the NaOH somehow reacted with the surface and made it rougher.
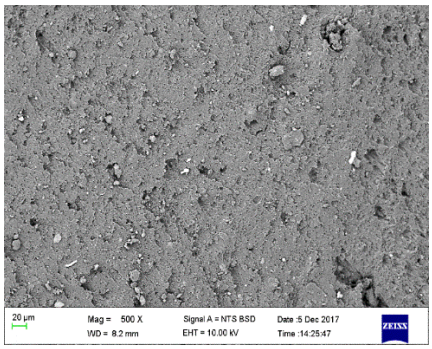 *b) 0.1M NaOH pretreatment*	
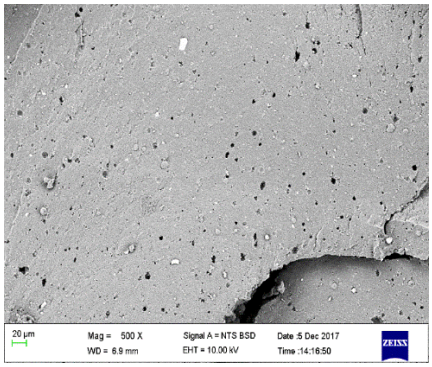 *c) Water soaked*	

Table 4.3: 1.18 mm tyre rubber micrographs with different pretreatment methods

Micrographs	**Observations**
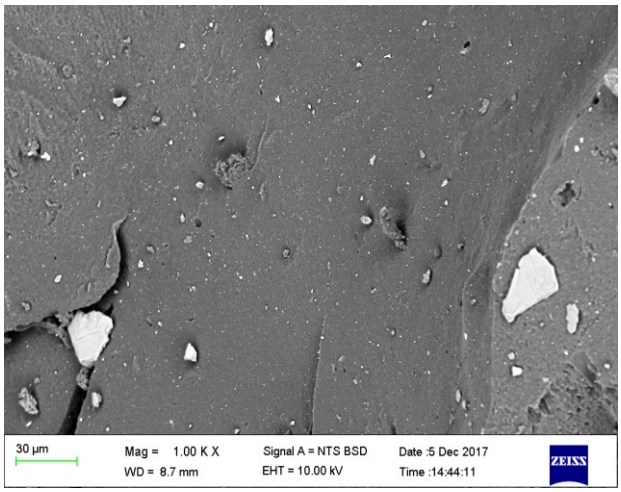 *a) Untreated*	The NaOH treated crumb rubber has a rougher surface texture when compared to the untreated but there is no clear difference with the water-soaked crumb rubber. The water-soaked crumb rubber is rougher than the NaOH treated rubber. The pretreatment methods both resulted in changes to the surface texture of the crumb rubber though the effects are not quite as clear as those observed for the bigger crumb tyre rubber size of 2.36 mm.
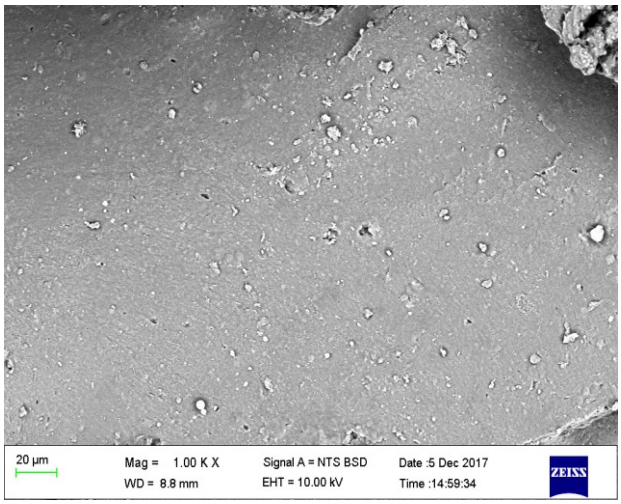 *b) 0.1M NaOH pretreatment*	
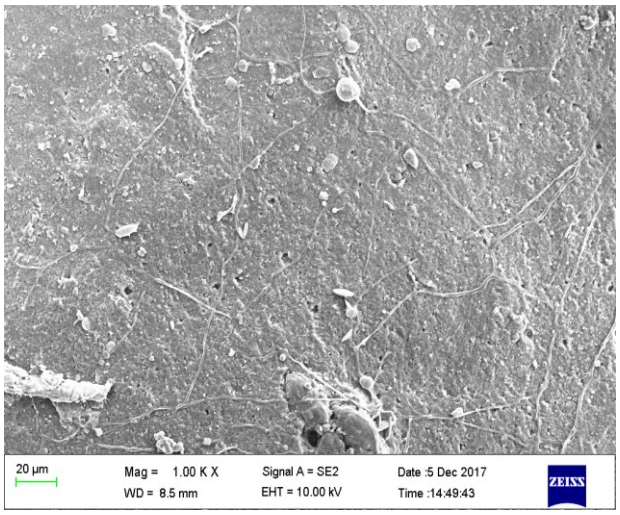 *c) Water soaked*	

Table 4.4: 0.425 mm tyre rubber micrographs with different pretreatment methods

Micrographs	**Observations**
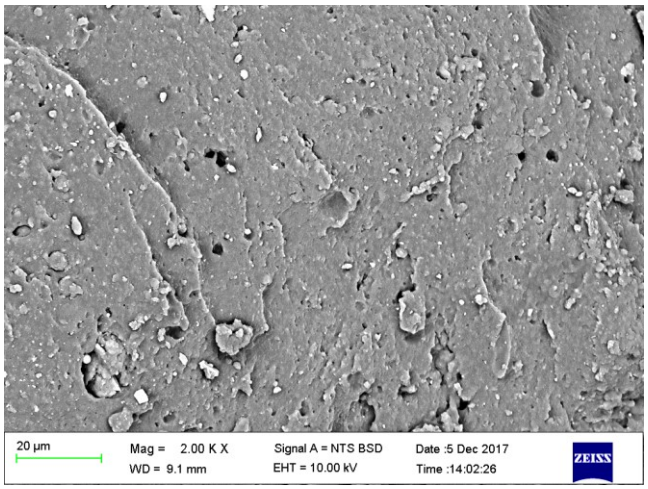 *a) Untreated*	The NaOH treated crumb rubber has a smoother surface texture when compared to the untreated and the water-soaked crumb rubber. The water-soaked particles have a texture more similar to the untreated crumb tyre rubber surface. The pretreatment methods both resulted in changes to the surface texture of the crumb tyre rubber. It appears though that the untreated surface is much rougher than both treated surfaces. The reason for this is not apparent.
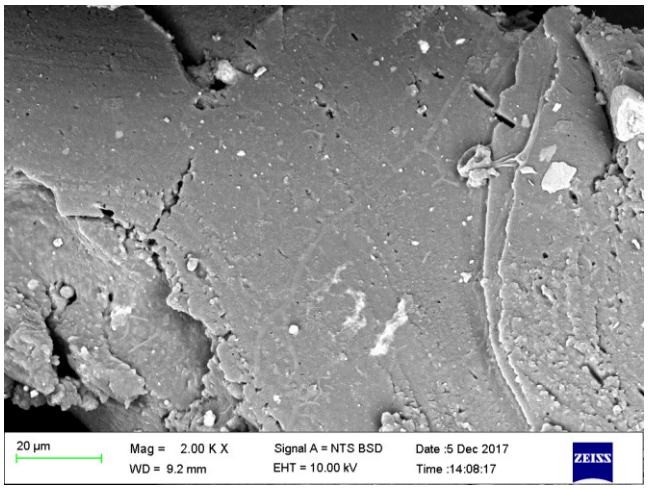 *b) 0.1M NaOH pretreatment*	
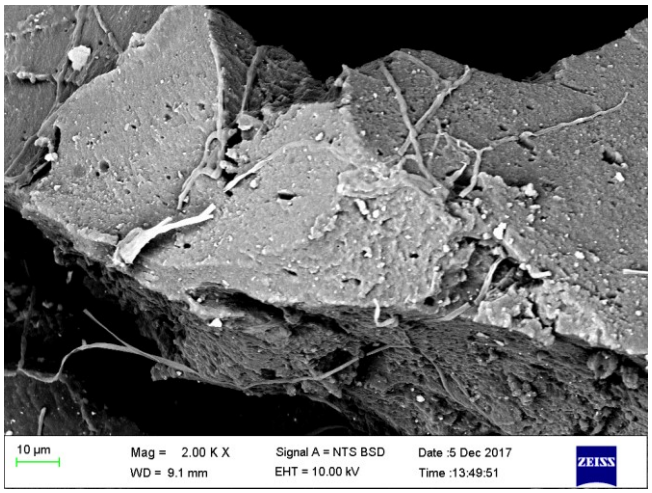 *c) Water soaked*	

The surface treatments had a visible effect on the surface texture of the tyre rubber particles. The effects however vary in magnitude depending on the size of the particle, with the bigger sizes showing the greatest change due to the treatment. As already noted in the previous discussion, the sodium hydroxide treatment had the effect of roughening the surface more and the water soaking cleaned the particle surfaces to reveal the pores on the particle surface, the same effects are reported by other researchers (Li et al., 2019; Mohammadi et al., 2014). These effects are also suggested by the results of the EDS that revealed a change in the chemical composition in the pretreated rubber particles. The reduction on the effect of the treatment on the smaller particles could be due to the increase of air voids around the particles as they get smaller, hence the contact between the treatment liquid and the particles is reduced.

4.3 FLUORESCENT MICROSCOPY RESULTS

This section discusses the results of the fluorescent microscopy work carried out on the reference and various rubberised concrete slices prepared to evaluate the interaction of the crumb tyre rubber particles with the matrix. The fluorescent microscopy aimed to identify microcracks mainly around the aggregates as a result of time-dependent deformations and assess the crumb rubber-matrix interface. The tests were carried out at the end of 52 weeks on sealed and unsealed creep and shrinkage specimens in an environment-controlled room.

4.3.1 Micro-cracking

The specimens were analysed for micro-cracking particularly around the bigger stiff mineral aggregates. This is because as the concrete deforms, stiffer aggregates act as restraints to the less stiffer matrix resulting in the formation of cracks in the matrix in the vicinity of the aggregate. It was observed that there was no identifiable micro-cracking in the concretes analysed, for both the reference concrete and the rubberised concretes. The micrographs taken of the reference concrete and rubberised concrete shown in Figure 4.4 and Figure 4.5 illustrate this observation.

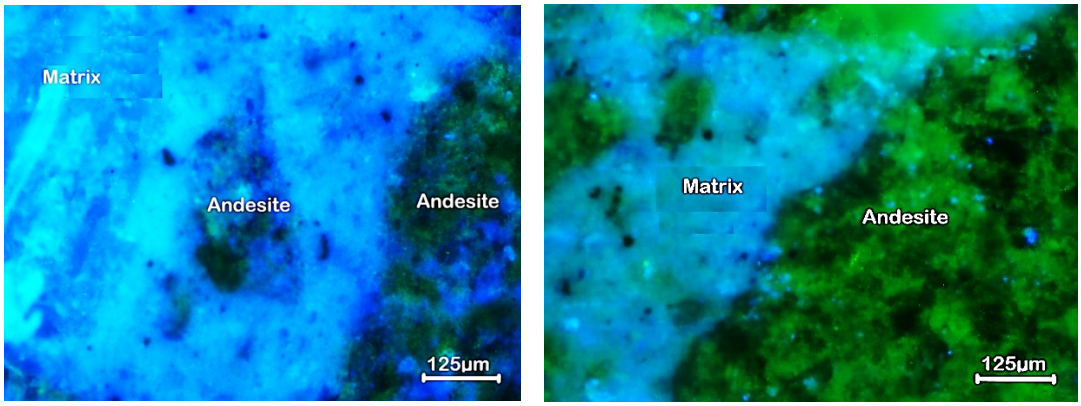

a) Slightly isolated aggregates *b) Aggregates closer together*

Figure 4.4: Reference concrete flourescent micrographs (blue and green light)

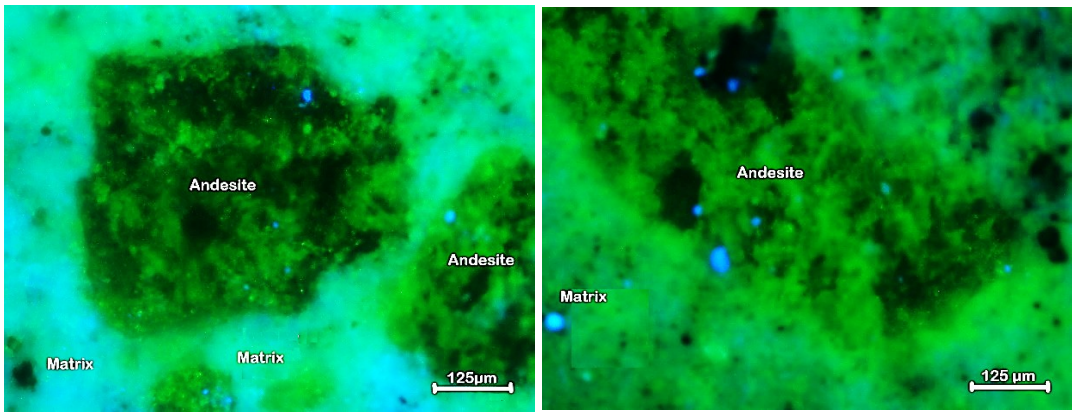

a) Andesite aggregates in M8 concrete *b) Andesite aggregates in M16 concrete*

Figure 4.5: Rubberised concrete fluorescent micrographs (blue and green light)

The fluorescent microscopy showed that there was no difference between the matrix in the vicinity of the aggregates for both the reference concrete and the

rubberised concrete. This suggests that the deformation experienced in rubberised concrete are not excessive to the point of causing notable micro-cracking within the period of the shrinkage and creep experiments. The introduction of crumb tyre rubber in concrete does not negatively change its micro-cracking potential of the during time-dependent deformations, if anything, according to work done by Pham et al. (2018) and Turatsinze et al. (2017) it improves cracking resistance. This means that even if there are excessive deformations in the concrete, in the presence of crumb rubber, it would take longer for cracking to occur.

4.3.2 Crumb rubber particle-matrix interaction

The area around the crumb rubber was viewed in order to have an insight on the nature of the embedding of the rubber aggregate in the concrete matrix. It was observed that, for most of the crumb rubber particles and for all sizes, air voids existed around the rubber particles. Figures 4.6 – 4.8 show micrographs taken of the different crumb rubber sizes. The presence of voids around the crumb rubber particles was observed more around the smaller size, M16 and M40, particles than the bigger, M8, particles as shown in the micrographs.

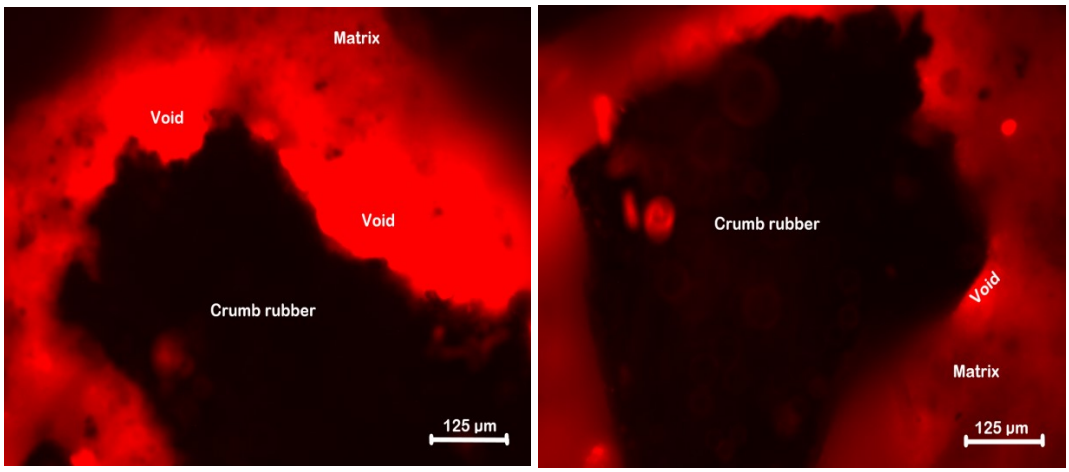

a) Voids around a rubber particle tip *b) Minimal voids around rubber particle*

Figure 4.6: M8 concrete flourescent micrographs (red light)

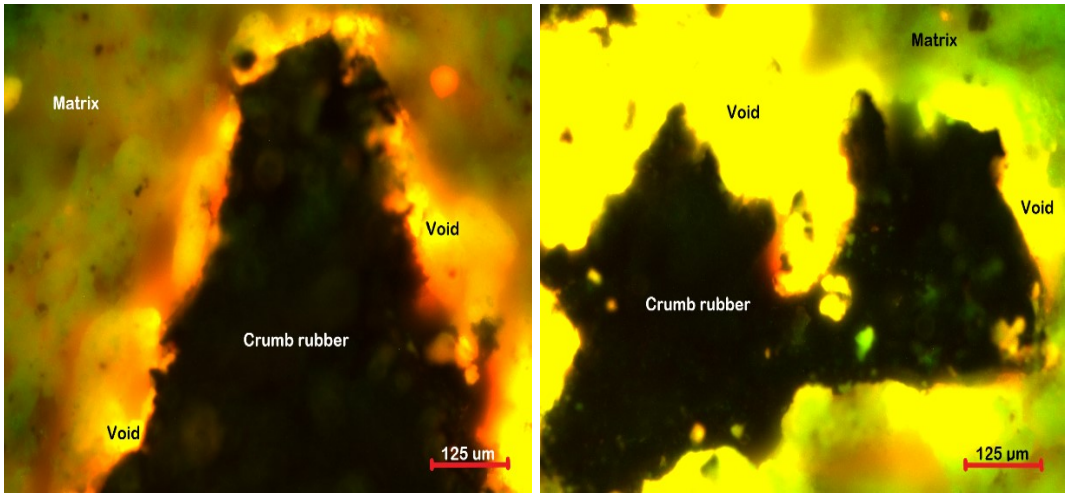

a) Voids around a rubber particle tip *b) Voids around two rubber particles*

Figure 4.7: M16 concrete flourescent micrographs (red and green light)

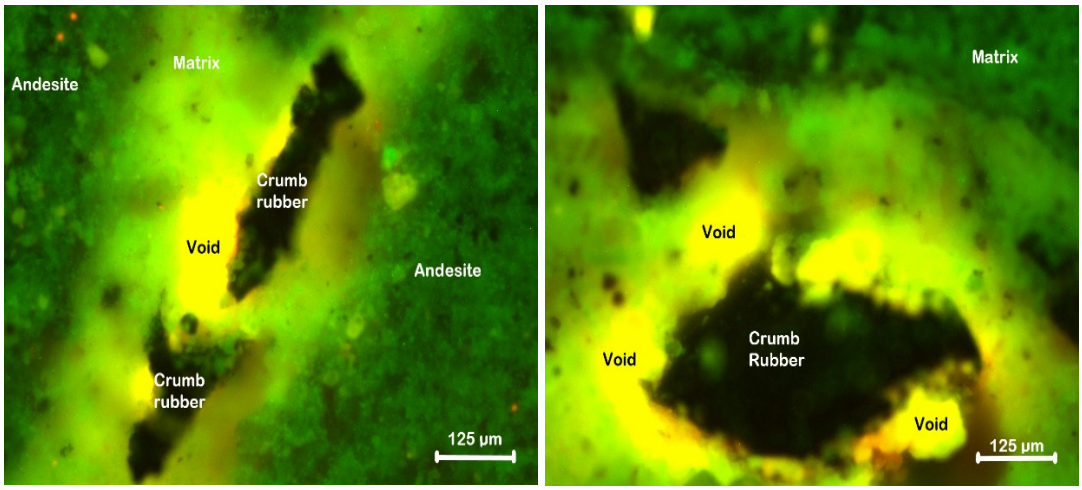

a) Rubber particles in-between aggregates *b) Voids around a rubber particle*

Figure 4.8: M40 concrete fluorescent micrographs (red and green light)

This is in agreement with work done by several researchers (Pham et al., 2018; Taha et al., 2008) on the rubber-cement matrix interface. The reason for this, as already explained in the previous section, is that bigger crumb tyre rubber particles have more regular and clean-cut edges, which do not allow for much air entrapment, compared to smaller particles. Pham et al. (2018) refers to this phenomenon that is caused by the air entrapment around the particle as bond defects. This observation implies that concrete with smaller crumb rubber particles

(≤1.18 mm) will inevitably have higher voids content than concrete with bigger particles (≥2.36 mm).

4.4 CONCRETE POROSITY

The porosity of the concrete was determined by assessing the hardened concrete percent voids using the total immersion and boiling method on drying shrinkage specimens at the end of the 52 weeks of drying. The results of the test are shown in Figure 4.9 and Figure 4.10. The Figure 4.9 shows the effect of crumb rubber size on the hardened concrete percent voids with one standard deviation error bars.

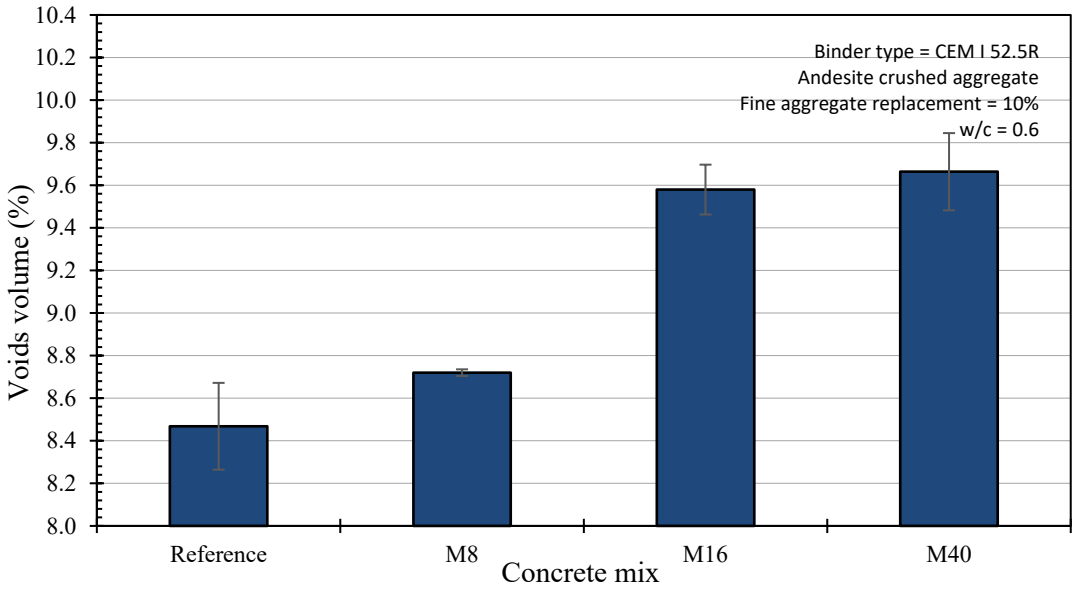

Figure 4.9: Effect of crumb rubber size on hardened concrete percent voids

There is an increase in hardened concrete percent voids with the inclusion of crumb rubber particles, which is agreement with what is reported literature (Youssf et al., 2020; Alisaif et al., 2018). The void percentage increases as the crumb rubber size decreases. Statistically, M8 crumb rubber has an insignificant ($p > 0.05$) effect on the percent voids in concrete relative to the reference concrete. However, the M16 and M40 crumb rubber particles have a statistically significant effect on the percent voids with reference to the reference and M8 concretes. But, between the two

concretes, M16 and M40, there is no statistically significant difference in percentage voids. This implies that the two sizes have a similar effect on the concrete porosity. The observations confirm findings by Zimmermann et al. (2016b), who found that using smaller particles resulted in more voids due to an increased specific surface area. This is in addition to what is reported in the preceding sections, that smaller crumb rubber particles, due to their surface texture, trap more air and thus increasing void content in concrete resulting in higher porosity. The effect of pretreatment on hardened concrete percent voids is shown Figure 4.10 with one standard deviation error bars.

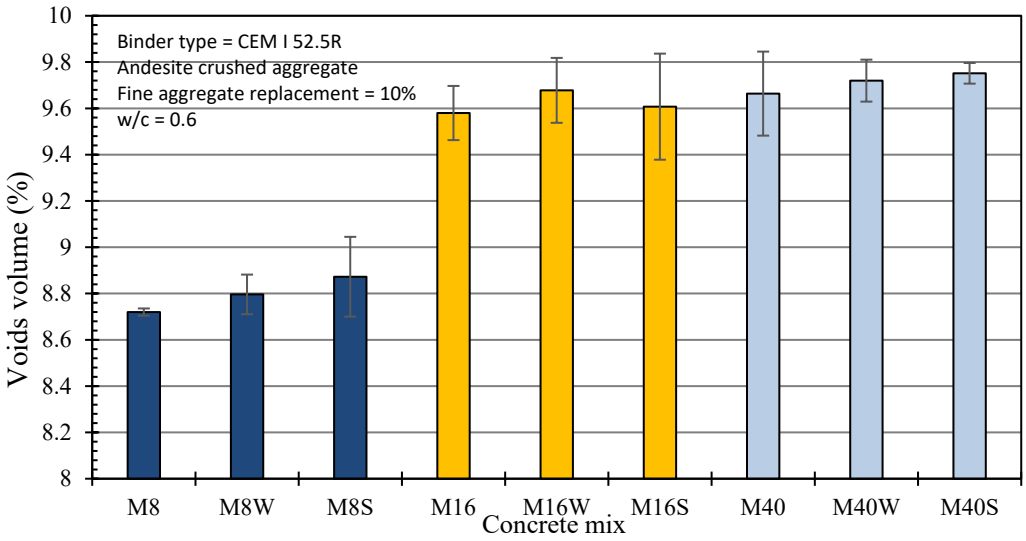

Figure 4.10: Effect of pretreatment on hardened percent voids

The pretreatment of the crumb rubber particles had no statistically significant effect on the hardened concrete percent voids for all sizes. This shows that the effects of the pretreatment process on the crumb rubber surface texture does not have an impact on the hardened concrete percent voids at each particle size level. Therefore, there is no difference in using pretreated concrete or untreated concrete with respect to changing hardened concrete percent voids.

4.5 ELASTIC MODULUS RESULTS

This section presents the results of the elastic modulus tests carried out on various mixes of rubberised concrete after 28 days of curing in water. The tests were carried out on normal concrete as a reference and rubberised concrete with untreated and pre-treated crumb tyre rubber aggregates. The fine aggregate replacement level for concrete with tyre rubber particles was 10%. The results of the tests are shown in Figure 4.11 with one standard deviation error bars.

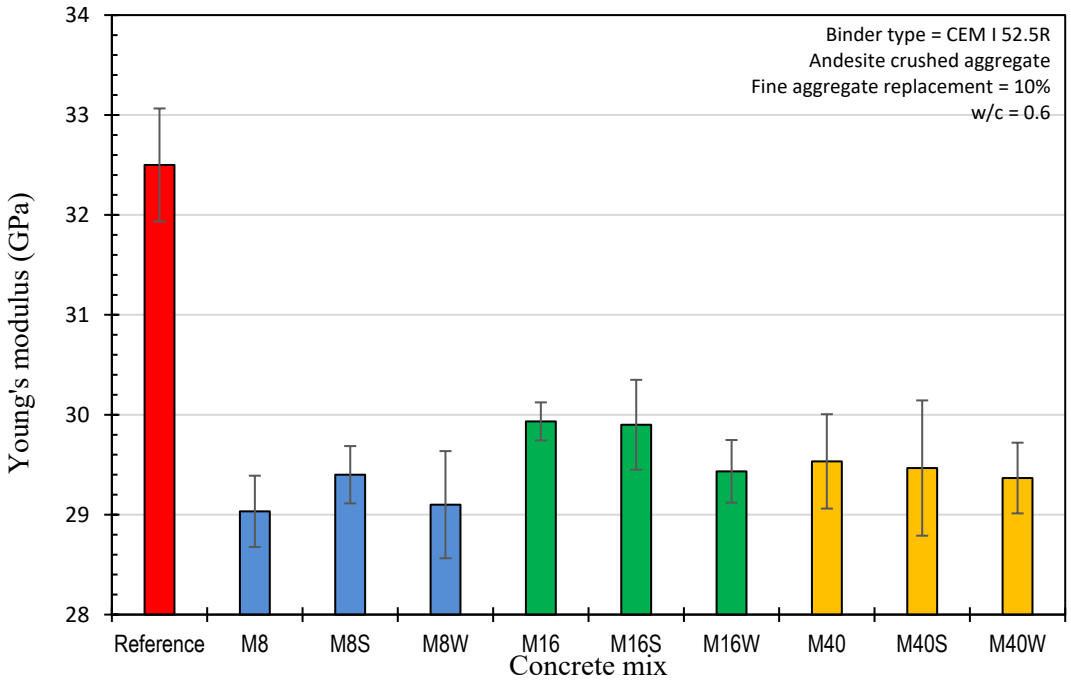

Figure 4.11: Effect of crumb rubber size and surface treatment on concrete elastic modulus

The use of crumb rubber as a partial replacement for fine mineral aggregate in concrete resulted in a significant decrease in the elastic modulus of the concrete, producing a more deformable concrete, similar to what has been reported in literature (Stukar et al., 2019; Khaloo et al., 2008; Ganjian et al., 2009). The reduction does not show any trend dependent on the size of the particles and the difference between the concretes of the different sizes are small (< 1 GPa). The M8 mix had the highest reduction of 11% while other mixes of M16 and M40 had 8%

and 9% respectively when compared with the reference concrete. The reduction in the elastic modulus of the rubberized concrete can be attributed to the low elastic modulus of the rubber particles, which reduces the restraining effect offered by the aggregate during deformation. It can also be attributed to the reduction in the stiffness of the hardened cement paste because of an increase in its porosity, due to the inclusion of crumb tyre rubber particles as shown by the percent void results. There is no statistically significant difference between the elastic modulus for the various crumb rubber sizes. This implies that statistically, the size of the crumb rubber does not have a notable effect on the elastic modulus of rubberised concrete, implying that regardless of which rubber size is used, the elastic variation will more or less be the same from the normal concrete. The pretreatment of the tyre rubber particles also did not have a significant effect on the on the elastic modulus of rubberised concrete.

4.6 SHRINKAGE RESULTS

This section presents the results of shrinkage tests carried out on various mixes of rubberised concrete after 28 days of curing in water. The tests were carried over a period of 52 weeks on sealed and unsealed specimens in an environment-controlled room. The few deviations that occurred with controlled-environment settings were thought to have not affected the shrinkage of the test specimens as the readings were noted to be stable.

4.6.1 Autogenous shrinkage

Free shrinkage tests were carried out on sealed concrete specimens to assess autogenous shrinkage. The autogenous shrinkage specimens were accompanied by

similar specimens being tested for basic creep. The crumb rubber replacement level of 10% was used for all the crumb rubber sizes because it was the highest replacement which achieved the target compressive strength.

Effect of crumb rubber size on autogenous shrinkage

The results of the tests to assess the effect of crumb rubber size on autogenous shrinkage of concrete are presented in Figure 4.12.

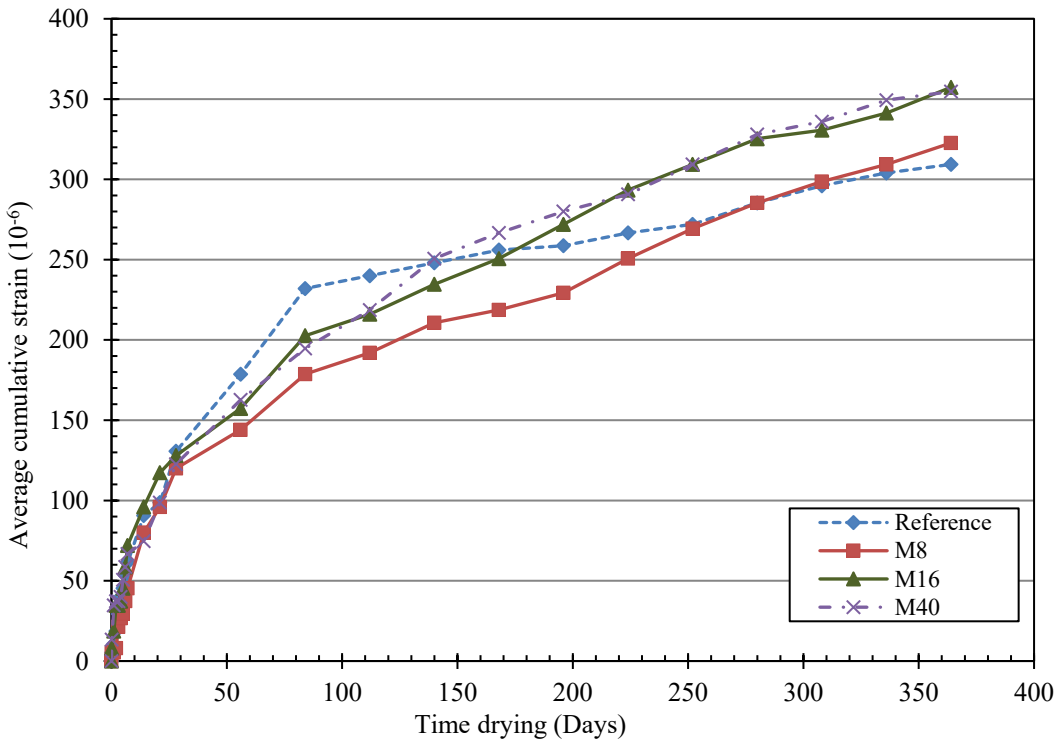

Figure 4.12: Effect of crumb rubber size on autogenous shrinkage

The autogenous shrinkage strains of the rubberised concrete mixes M8, M16 and M40 were all higher than those of the reference mix at the end of the monitoring period. The measured autogenous shrinkage strains at the end of the monitoring period of 52 weeks for the reference, M8, M16 and M40 mixes were 309με, 323με, 357με, 355με respectively. The percentage increase in the measured autogenous shrinkage for the M8, M16 and M40 is 5%, 16%, 15% compared to the reference

mix. The readings at the end of observation period do not reflect the behaviour of the rubberised concrete during the monitoring period. The reference mix had higher strains till at 140 days where the shrinkage rate reduces and the strains become lower than the rubberised concrete starting with the M40, then M16 at 168 days and lastly the M8 at 280 days. The trend implies that the crumb tyre rubber particles result in lower short-term autogenous shrinkage strains than normal concrete and an increase in long-term strains. The effect of the crumb rubber size on autogenous shrinkage is not clearly shown for the smaller crumb rubber sizes of 1.18 mm and 0.425 mm, as they exhibited similar strains. The observations are clearly illustrated by the equality graph in Figure 4.13. The incorporation of crumb rubber for all sizes results in a statistically insignificant variation on the autogenous shrinkage of concrete (Appendix E, Table E11).

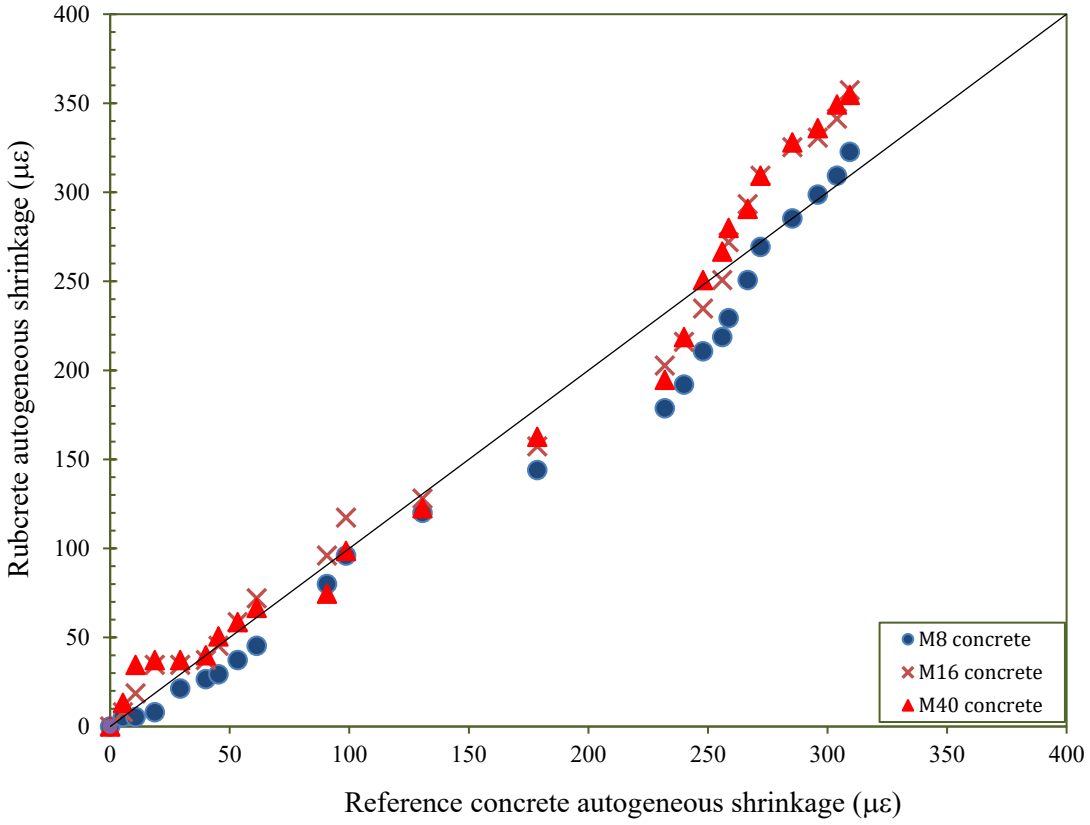

Figure 4.13: Autogenous shrinkage equality graph

The initial lower autogenous shrinkage rate of the rubberised concrete can be due to water being lodged in the rubber particles' crevices as noted Section 4.2. The poor bonding and voids between the cement paste and the rubber particle hinders the easy movement of the water (Taha et al., 2008; Pham et al., 2018). The mineral aggregate due to their superior bonding with the paste can easily transfer absorbed water to the paste earlier than the rubber particles. Therefore, during desiccation process as the cement hydrates, the available water in the reference mix is easily accessible and is accessed earlier hence the higher shrinkage rate at the beginning. When the water becomes more difficult to access, as it is deep inside the aggregate, the shrinkage rate decreases in the reference concrete, while in the rubberised concrete the "stored" water now starts being released slowly as the matrix contracts. The crevice-lodged water is quickly dislodged and used as the concrete contracts resulting in a continuous increase in shrinkage strain as water from finer pores gets used up to the end of the monitoring period. The generally higher strains exhibited by the rubberised concrete at the end of the 52 weeks can be explained by the increased number of pores, the lower water absorption and the lower restraining effect of the rubber particles as reported by Sukontasukkul and Tiamlom (2012). The lower stiffness and the increase in pores is reported to increase the compressibility of the concrete (Alsaif et al., 2018; Li et al., 2020). The lower water absorption of the rubber limits its ability to provide internal curing to concrete which the mineral aggregate can provide over a longer period. It is generally agreed that internal curing has the effect of reducing autogenous shrinkage (Bentz and Jensen, 2004; Šahinagić-Isović et al., 2012). Therefore, tyre crumb rubber particles by their shape, which creates more pores; low absorption, which reduces internal

curing, and stiffness, which reduces restraint, results in higher autogenous shrinkage in concrete.

Figure 4.14 shows the ratio of each of the rubberised concrete autogenous shrinkage strains ($\varepsilon_{a(rub)}$) to the reference concrete autogenous shrinkage strains ($\varepsilon_{a(ref)}$) over time from 7 days of drying to the end of observation period. The period prior to the 7 days is not shown as the ratios are more varied and much higher than the long-term shrinkage ratios, this would have given a distorted view.

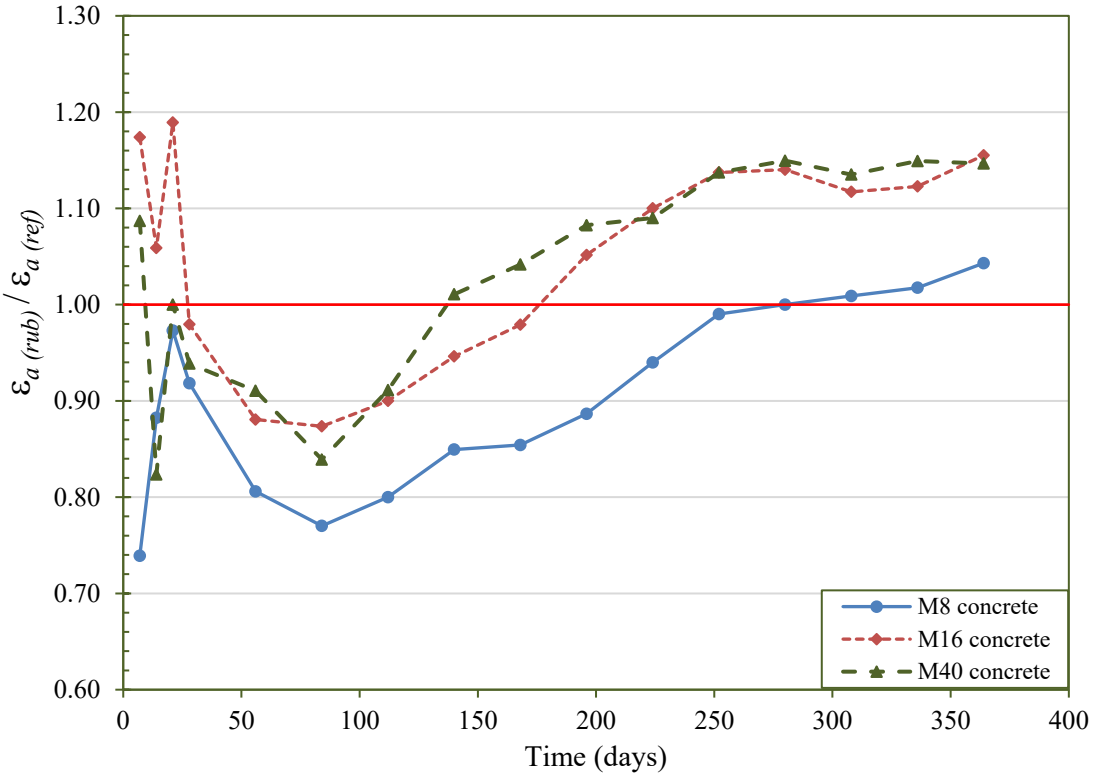

Figure 4.14: Ratio of rubberised concrete to reference concrete autogenous shrinkage

Autogenous shrinkage strains for M8, M16 and M40 rubberised concretes are a minimum of 0.74, 0.87 and 0.82 times that of the reference concrete and a maximum of 1.04, 1.19 and 1.15 times respectively. The medians of the M8, M16

and M40 ratios are 0.90, 1.08, 1.06 respectively while the means are 0.90, 1.05 and 1.03 respectively. Considering these statistics, indicating the distribution of the ratios, in structural design where rubberised concrete with crumb rubber mesh size 8 and smaller is to be used, a conservative multiplier of 1.2 can be applied to the autogenous shrinkage expected for plain normal strength concrete, that is:

$$\varepsilon_{a(rub)}(t) = 1.2\ \varepsilon_{a(ref)}(t), \qquad (t > 7\ days) \ldots\ldots\ldots\ldots\ldots\ldots \text{Eqn. 4.1}$$

Effect of surface treatment of crumb rubber

The results of the tests to assess the effect of the surface treaments of the crumb rubber on autogenous shrinkage deformation are presented in Figures 4.15 - 4.17.

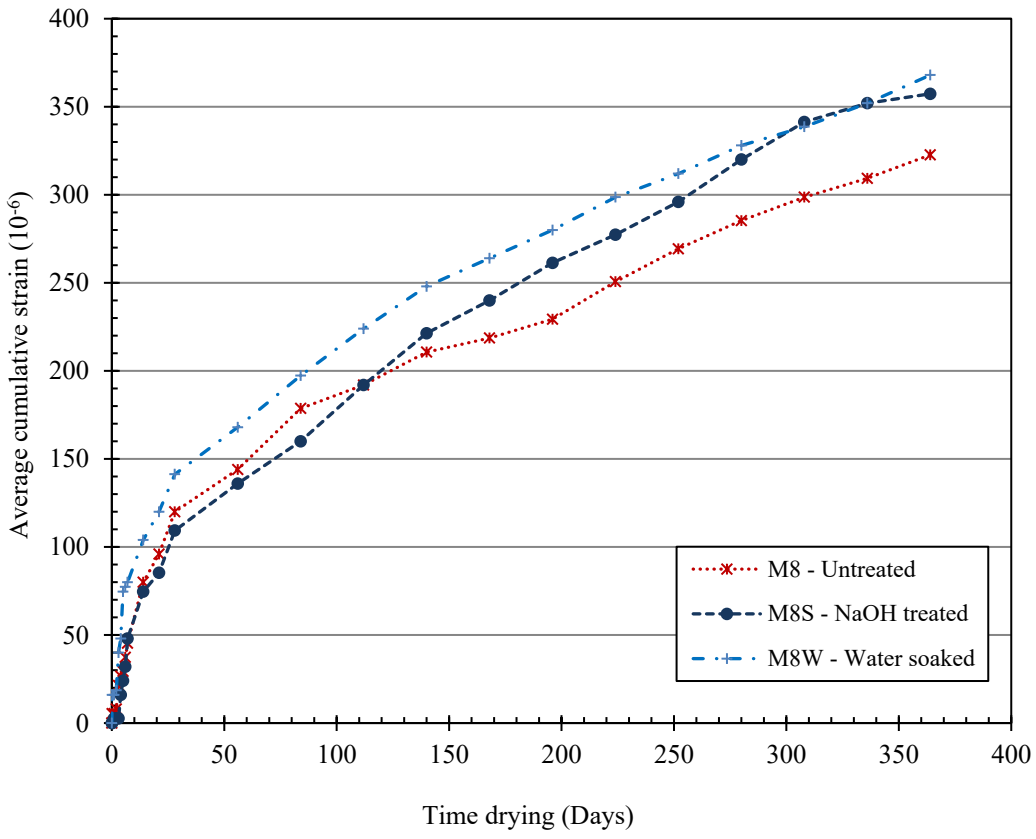

Figure 4.15: Effect of surface treatment of 2.36 mm crumb rubber on autogenous shrinkage

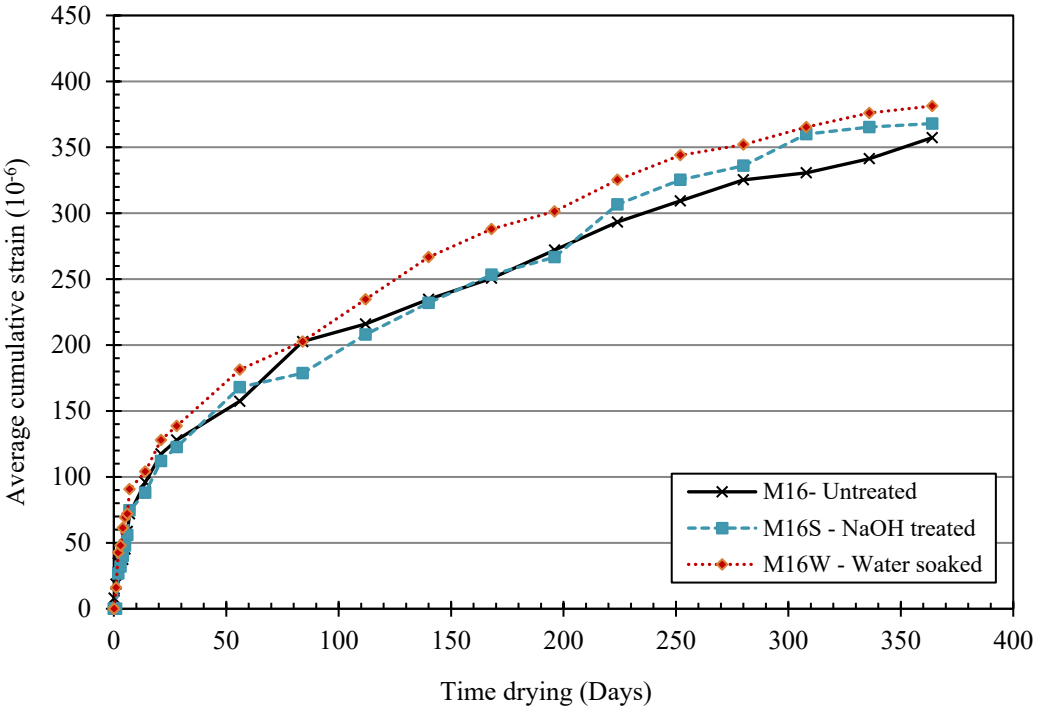

Figure 4.16: Effect of surface treatment of 1.18 mm crumb rubber on autogenous shrinkage

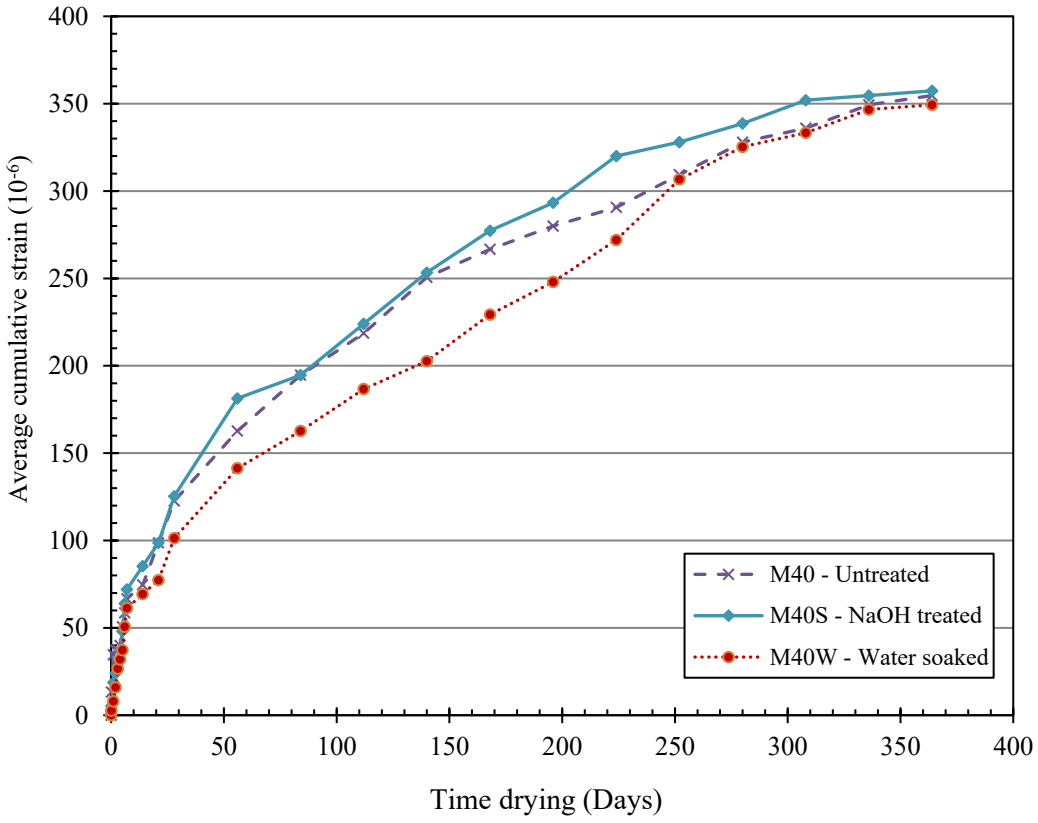

Figure 4.17: Effect of surface treatment of 0.425 mm crumb rubber on autogenous shrinkage

The autogenous shrinkage of the pretreated crumb rubber concretes are slightly higher than the untreated crumb rubber concretes. The increases in autogenous shrinkage of the concrete made from pretreated rubber increases are considered as insignificant for the M40 and M16 concretes as the increases are less than 7%. The percentage increases at 52 weeks for M8W, M8S, M16W, M16S, M40S concretes are 14%, 11%, 7%, 3%, and 1% respectively. The M40W concrete is the only one with an decrease of 1%. The larger crumb rubber size concretes have a higher increase in autogenous shrinkage which can be due to better bonding between cement and rubber particles that is encouraging more water movement from the rubber to the cement. However, pretreatment does not have a statistically significant effect on the autogenous shrinkage of the concrete (Appendix E, Table E13). This implies that the use of pretreatment with regards to improving autogenous shrinkage performance can be excluded.

4.6.2 Drying shrinkage

Free shrinkage tests were carried out on unsealed concrete specimens to assess the drying shrinkage of the concrete over the period stated in the section 4.5. The drying shrinkage specimens had similar corresponding creep specimens. The 10% replacement level was used as the optimum level for all crumb rubber sizes used in concrete.

Effect of crumb rubber size on drying shrinkage

The results of the tests to assess the effect of crumb tyre rubber size on drying shrinkage are presented in Figure 4.18.

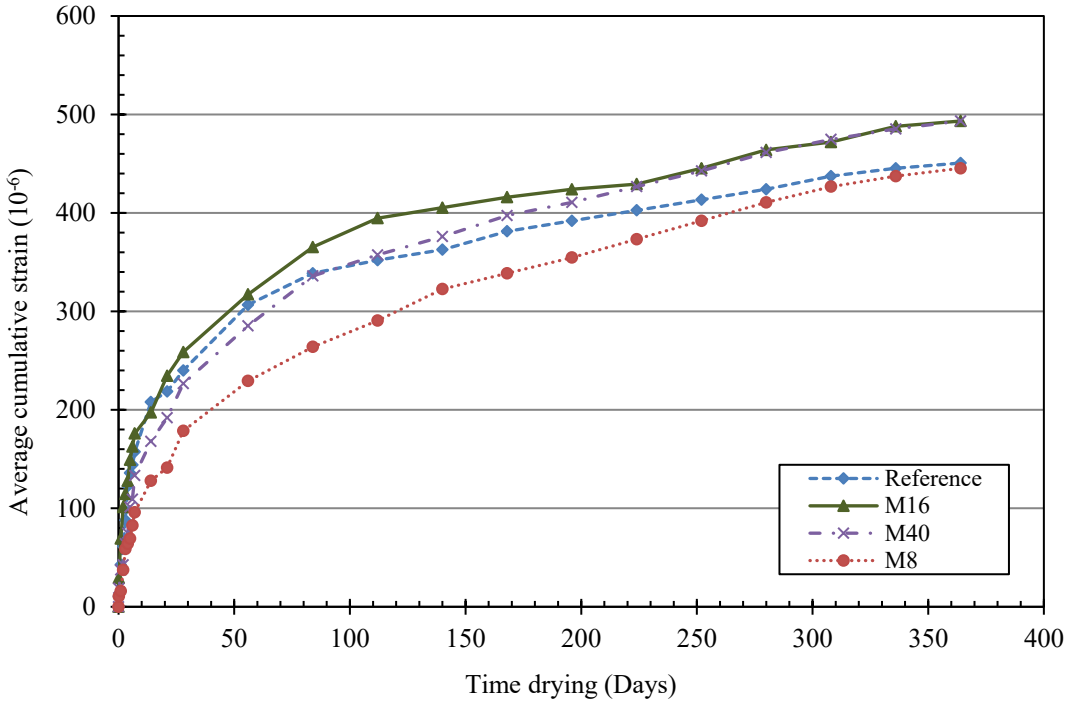

Figure 4.18: Effect of crumb rubber size on drying shrinkage

The drying shrinkage strains of the rubberised concrete mixes M16 and M40 at the end of the monitoring period are similar and are higher than those of the reference mix. Other researchers having used similar size crumb rubber tyre particles have reported similar findings (Alsaif et al., 2018; Li et al., 2020a). The M8 rubberised concrete drying shrinkage for the said period is similar to that of the reference mix. The measured drying shrinkage strains at the end of the monitoring period of 52 weeks for the reference, M8, M16 and M40 mixes are 451με, 445με, 493με, 493με respectively. The drying shrinkage of the M16 and M40 rubberised concrete increase by the same margin of 16% while that of M8 decreased by 1% when compared to the control concrete. The M8 rubberised concrete drying shrinkage is lower than the reference concrete for the duration of the monitoring period but the difference between the 2 reduces gradually towards the end. The other rubberised concretes with smaller rubber particles show higher shrinkage for the greater part of the monitoring period from 21 days and 112 days for the M16 and M40

respectively. These observations are illustrated more clearly by the equality graph in shown in Figure 4.19. The incorporation of crumb rubber for all sizes results in a statistically insignificant variation on the drying shrinkage of concrete (Appendix E, Table E12). Implying that, although there are variations in shrinkage strains with the inclusion of crumb rubber, the effects are not any different than when crumb rubber has not been used.

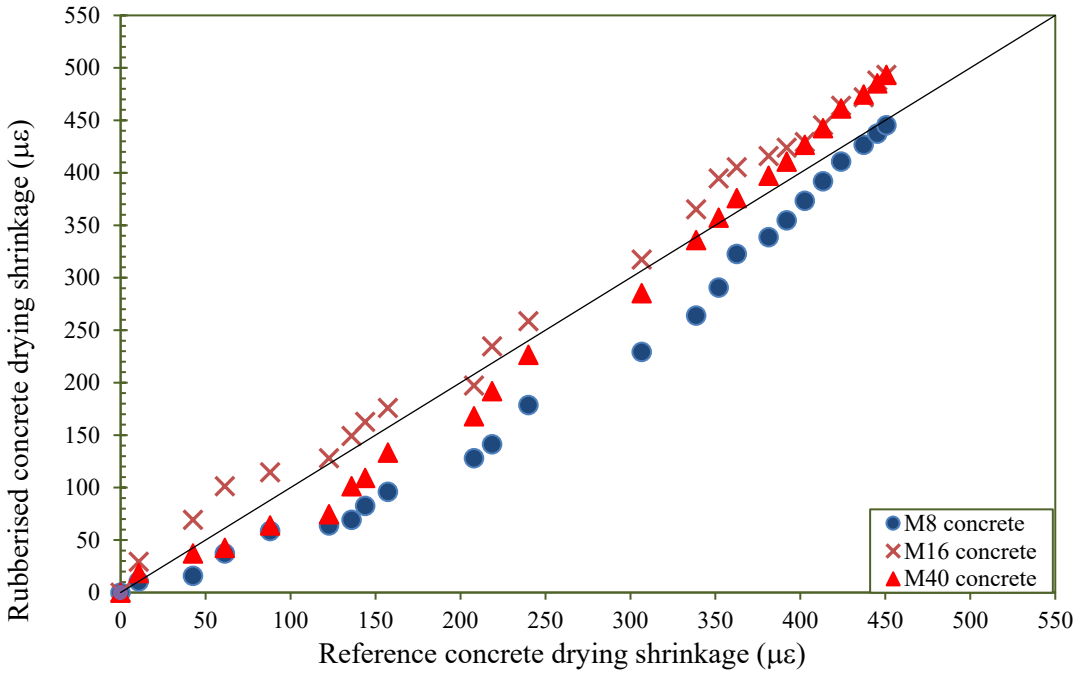

Figure 4.19: Drying shrinkage equality graph

The observed trend implies that larger crumb rubber size result in lower drying shrinkage compared to smaller crumb rubber particles. This is linked to the increase of air voids within the concrete with the use of smaller crumb rubber particles. Increased voids in concrete normally result in higher shrinkage strains which might be the case in this instance with the smaller crumb rubber (Owens, 2013; Šahinagić-Isović et al., 2012). This is because as water is removed from the capillary pores the increased voids make it easy for the water to evaporate from the concrete (Alsaif et al., 2018). The similarity in the M16 mix and the M40 mix drying shrinkage strains

can be explained by the results obtained from the hardened concrete percent void experiment that showed that the two concretes have similar void percentages. Although it is generally agreed that the lower rubber stiffness is the reason for the shrinkage strains in rubberised concrete, in this instance, air content and porosity seem to play a bigger role.

Figure 4.20 shows the ratio of each of the rubberised concrete drying shrinkage strains ($\varepsilon_{d(rub)}$) to the reference concrete drying shrinkage strains ($\varepsilon_{d(ref)}$) over time from 7 days drying to end of observation period. The period prior to the 7 days was not shown as the ratios vary widely and much higher than the long-term shrinkage ratios, this would have given a distorted view.

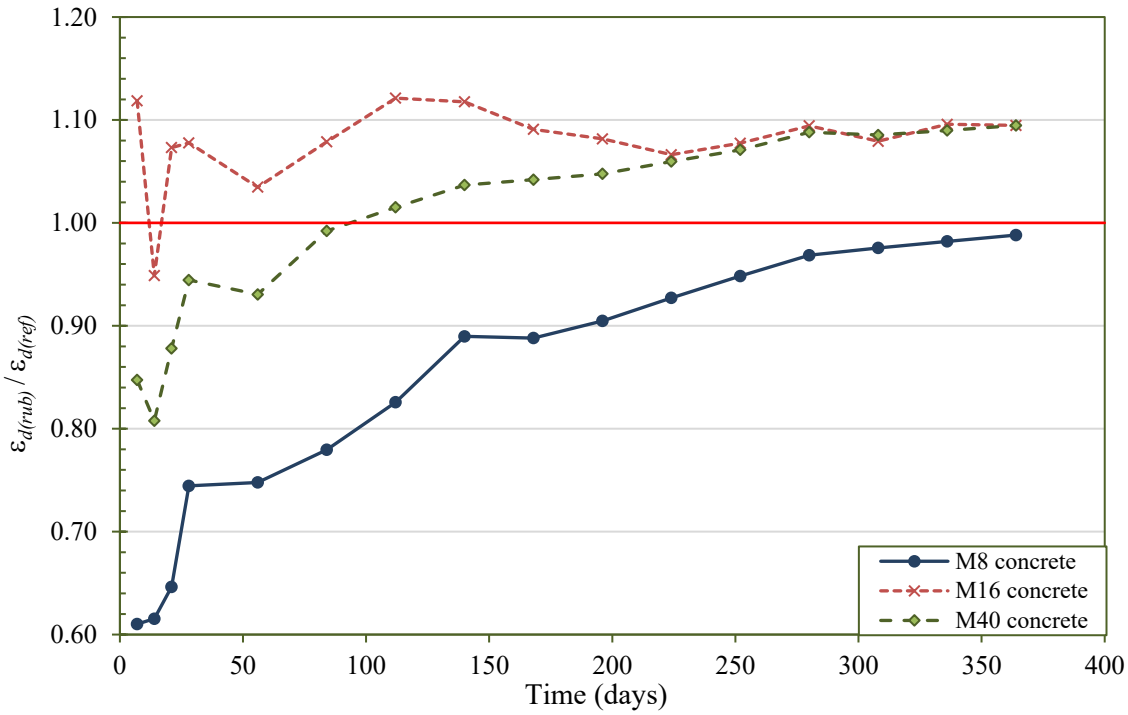

Figure 4.20: Ratio of rubberised concrete to reference concrete drying shrinkage

The drying shrinkage strains for M8, M16 and M40 rubberised concretes are a minimum of 0.61, 0.95 and 0.81 times that of the reference concrete and a maximum of 0.99, 1.12 and 1.09 times respectively. The medians of the M8, M16 and M40 ratios are 0.89, 1.08, 1.04 respectively while the means are 0.84, 1.08 and 1.04 respectively. Considering these statistics, indicating the distribution of the ratios, in structural design where rubberised concrete with crumb rubber mesh size 8 and smaller is to be used, a conservative multiplier of 1.15 can be applied to the drying shrinkage expected for plain normal strength concrete, that is:

$$\varepsilon_{d(rub)}(t) = 1.15\ \varepsilon_{d(ref)}(t), \qquad (t > 7\ days) \ldots\ldots\ldots\ldots\ldots\ldots\ldots\ldots \text{Eqn. 4.2}$$

Effect of surface treatment of crumb rubber on drying shrinkage

The results of the tests to assess the effect of the surface treaments of the crumb rubber on drying shrinkage deformation are presented in Figures 4.21 - 4.23.

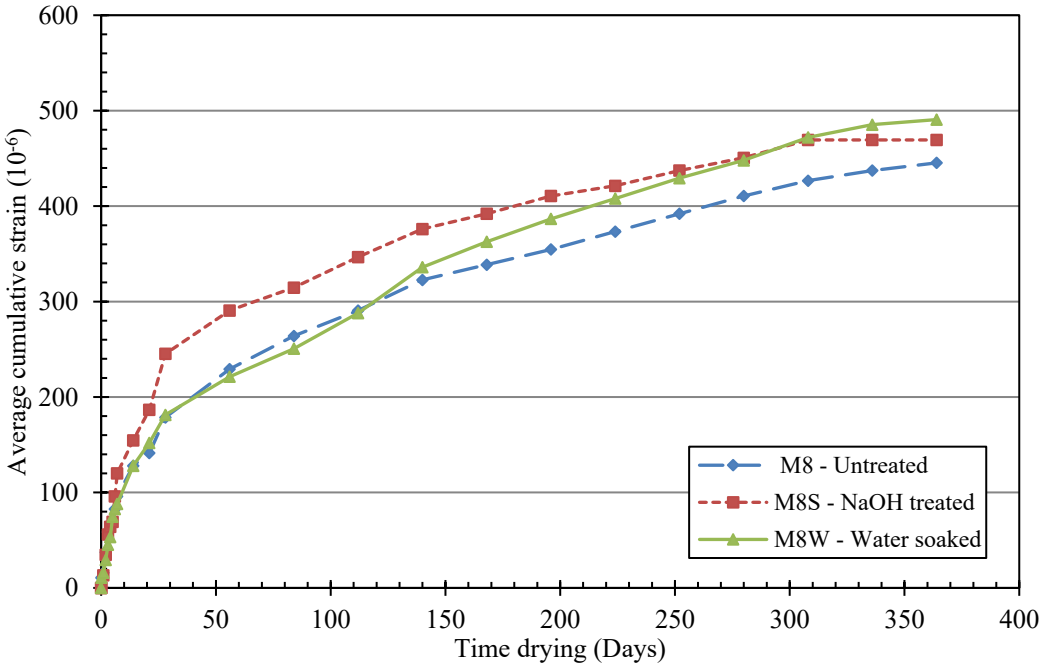

Figure 4.21: Effect of surface treatment of 2.36 mm crumb rubber on drying shrinkage

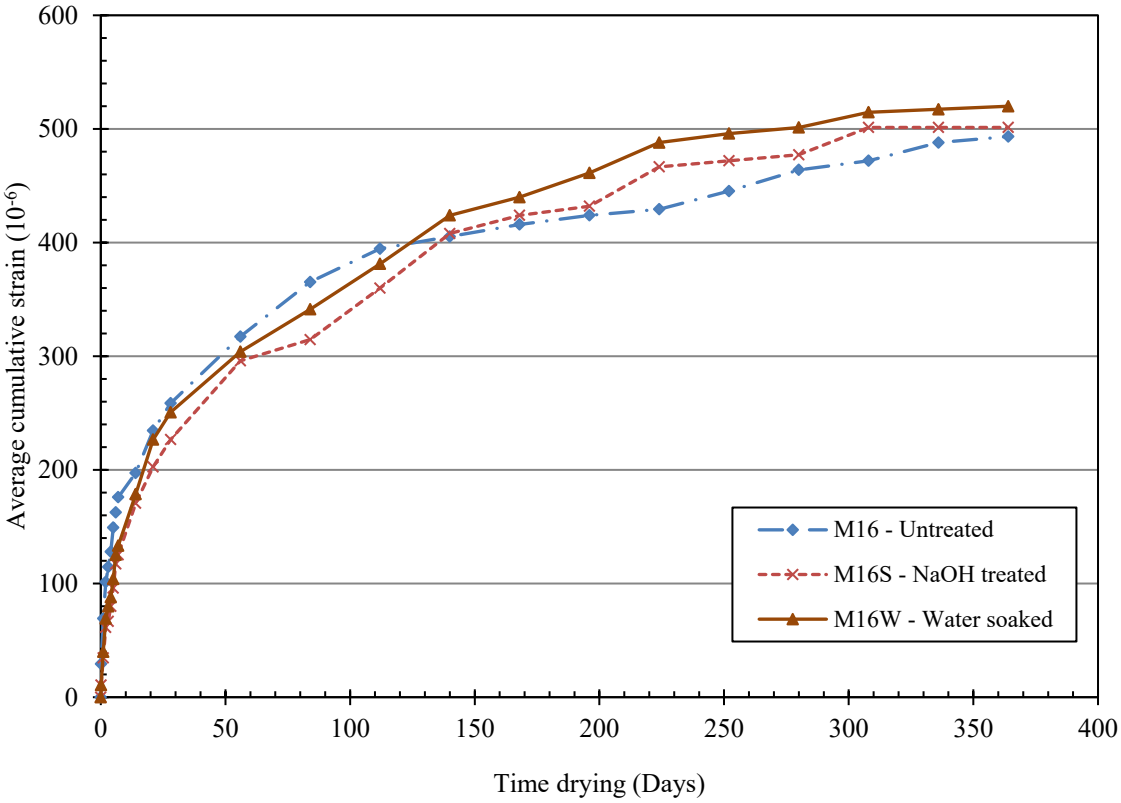

Figure 4.22: Effect of surface treatment of 1.18 mm crumb rubber on drying shrinkage

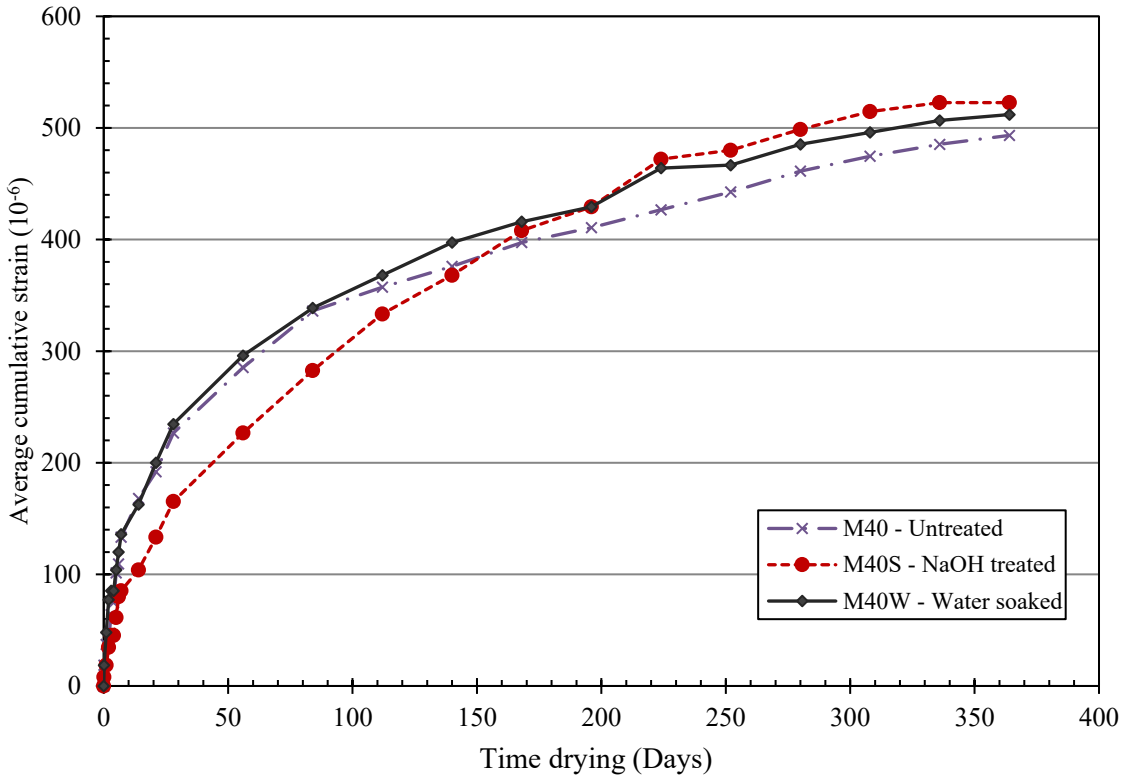

Figure 4.23: Effect of surface treatment of 0.425 mm crumb rubber on drying shrinkage

The drying shrinkage of the pretreated crumb rubber concretes are only slightly higher than the untreated crumb rubber concretes. The drying shrinkage increases are marginal for the M40 and M16 concretes at less than 6%. The percentage increases for M8W, M8S, M16W, M16S, M40W, M40S concretes are 10%, 5%, 5%, 2%, 4%and 6% respectively relative to their corresponding untreated rubber mixes. The M40W concrete is the only one with an increase of 10%, which could be considered significant. Again similar to the autogenous shrinkage results the larger crumb rubber size concretes have a higher increase in drying shrinkage which could be due to better bonding between cement and rubber particles brought about by the pretreatment process. This closer proximity of the rubber particles to the cement enables easier water movement from the rubber to the cement paste due improved bonding as reported in literature (Taha et al., 2008; Polydorou et al., 2020; Pham et al., 2018). However, in general, the pretreatment does not have a statistically significant effect on the drying shrinkage of the concrete as well (Appendix E, Table E14). This finding is contrary to what Li et al. (2020a) found in their study, where NaOH pretreated rubber perfomed better by 15%. The difference might be due to pretreatment procedures. In this study the particles were soaked for 24 hours while Li et al. (2020a) soaked theirs for 20 minutes. This points to a possible link between soaking time and concrete peformance, although this cannot be confirmed from just these two findings.

4.7 CREEP DEFORMATION RESULTS

This section discusses the results of creep deformation tests carried out on various rubberised concretes after 28 days of curing in water. The tests were carried over a

period of 52 weeks on sealed and unsealed specimens in an environment-controlled room. The temperature and humidity variations that occurred during the tests were thought to have not affected the creep behaviour of the specimens, as the readings were observed to be steady.

The measured creep strains were corrected by subtracting elastic strains and the shrinkage strains of the unloaded concrete prisms exposed to the same environmental conditions as the loaded prisms using Equation 2.6. The resulting creep strains $\varepsilon_c\,(t)$ were used to calculate the specific creep relating to the period under investigation. Specific creep is used to cater for the different stresses on the concretes.

The specific or the unit creep at any age, $\varepsilon_{sp}\,(t)$, according is computed as was given in Equation 2.9 but repeated here for ease of reference:

$$\varepsilon_{sp}(t) = \frac{\varepsilon_c(t)}{\sigma_c}$$

where:

$\varepsilon_{sp}\,(t)$ = specific creep strain,
$\varepsilon_c\,(t)$ = creep strain
σ_c = sustained constant stress on the specimen

In order to demonstrate the homogenity of the creep readings, the individual specimens creep strain readings are presented in Appendix F. The creep strains shown are the actual reading taken on the specimens before elastic and shrinkage strains are subtracted. The graphs generally show a similar trend and are stable throughout for the individual specimens, showing good homogenity and consistency in the readings.

4.7.1 Basic creep deformation

Creep tests were carried out on sealed concrete specimens to assess the basic creep of the concrete. These specimens were accompanied by similar specimens tested for autogenous shrinkage. The crumb rubber replacement level for all the crumb rubber sizes used in the concrete was also 10%.

Effect of crumb rubber size on basic creep

The results of the tests to assess the effect of crumb rubber size on basic creep are presented in Figure 4.24.

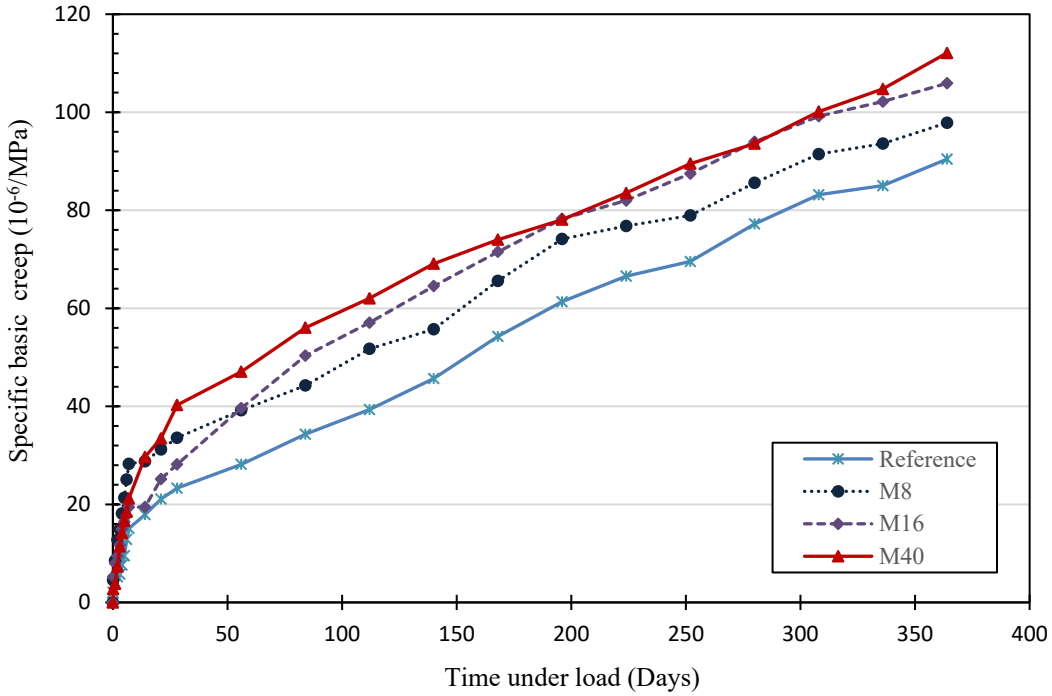

Figure 4.24: Effect of crumb rubber size on basic creep

The specific basic creep of the rubberised concretes M8, M16 and M40 are higher than those of the reference concrete. The percentage increase in the measured specific basic creep for the M8, M16 and M40 is 9%, 18%, 30% compared to the reference concrete. The trend is similar to one observed for autogenous shrinkage strains at the end of the monitoring period only that in this instance the difference in

the different concrete behaviours is consistent and clear throughout the monitoring period. The graphs show that as the crumb rubber size becomes smaller the specific basic creep increases, the trend can be observed clearly in Figure 4.25. The reason for the higher creep strains in concrete with smaller crumb rubber sizes is due to the higher hardened concrete percent voids which are associated with smaller crumb rubber particles as reported by Zimmermann et al. (2016b) This trend concurs with findings by Dhir et al. (2019) and Lopez (2005) who report that basic creep increases with an increase in concrete porosity although this effect it more pronounced for drying creep. The increase in voids reduces the ability of concrete to withstand loading due to the reduction in the stiffness of the hardened cement paste thus making the concrete more compressible.

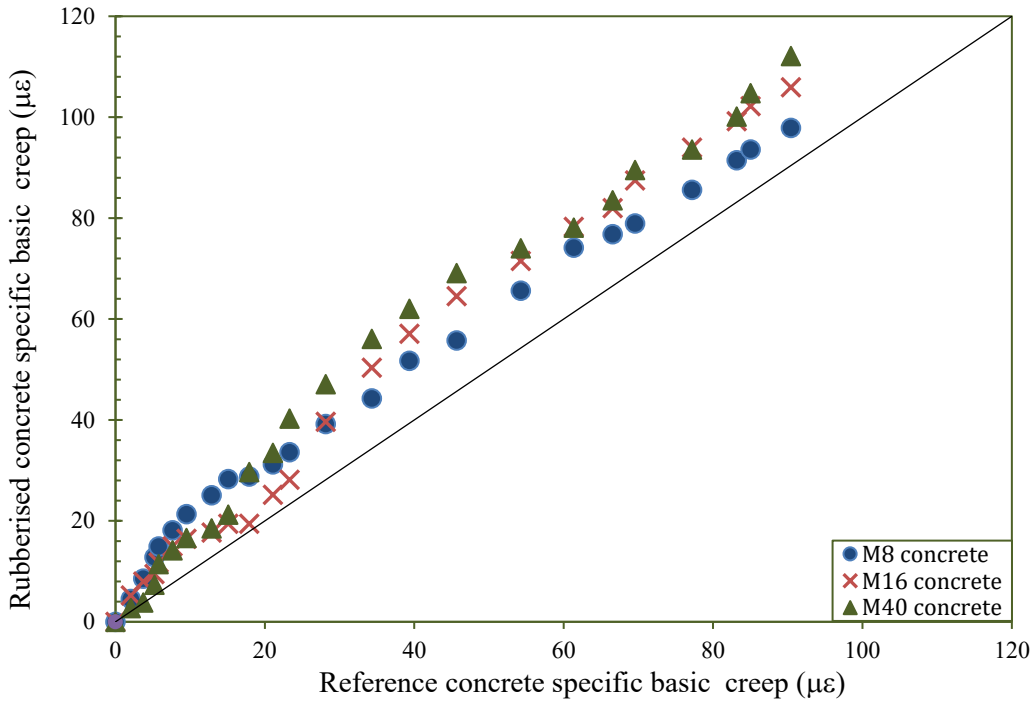

Figure 4.25: Specific basic creep equality graph

Figure 4.26 shows the ratio of each of the rubberised concrete specific basic creep strains ($\varepsilon_{bsp(rub)}$) to the reference concrete basic creep strains ($\varepsilon_{bsp(ref)}$) from 7 days under load to end of observation period. The period prior to the 7 days was not

shown as the ratios are vary widely and much higher than the long-term creep ratios, this would have given a distorted view.

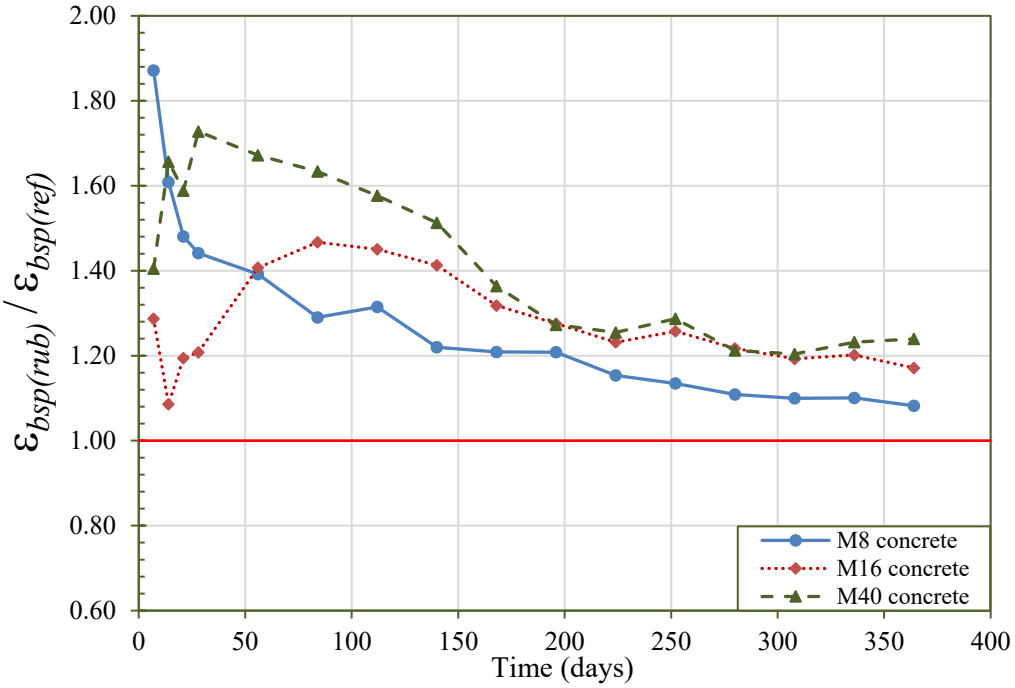

Figure 4.26: Ratio of rubberised concrete to reference concrete specific basic creep

The specific basic creep for M8, M16 and M40 rubberised concretes are a minimum of 1.08, 1.09 and 1.20 times respectively that of the reference concrete and a maximum of 1.87, 1.47 and 1.73 times respectively. The medians of the M8, M16 and M40 ratios are 1.21, 1.24, 1.38 respectively while the means are 1.29, 1.27 and 1.43 respectively. Considering these statistics, indicating the distribution of the ratios, in structural design where rubberised concrete with crumb rubber mesh size 8 and less is to be used, a conservative multiplier of 1.25 can be applied to the specific basic creep expected for plain normal strength concrete, that is:

$$\varepsilon_{bsp(rub)}(t) = 1.25\ \varepsilon_{bsp(ref)}(t), \qquad (t > 28 \text{ days}) \quad \text{.....Eqn. 4.3}$$

Effect of crumb rubber surface treatment on basic creep

The results of the tests to assess the effect of crumb rubber surface treatment on basic creep deformation of concrete are presented in Figures 4.27 – 4.29.

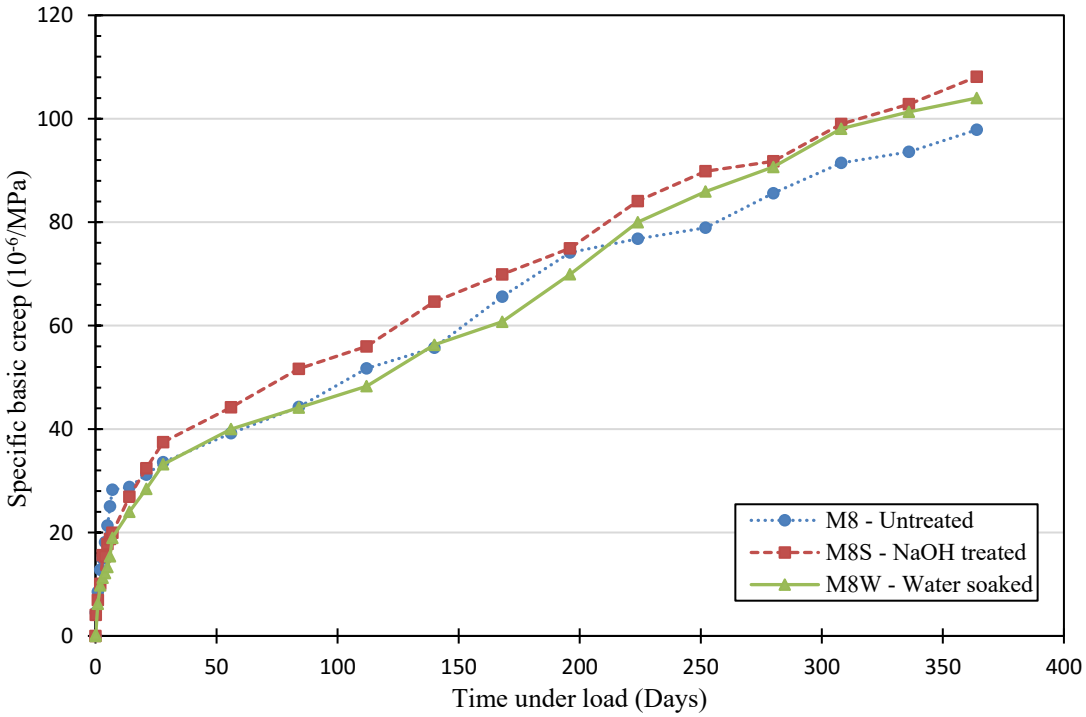

Figure 4.27: Effect of surface treatment of 2.36 mm crumb rubber on basic creep

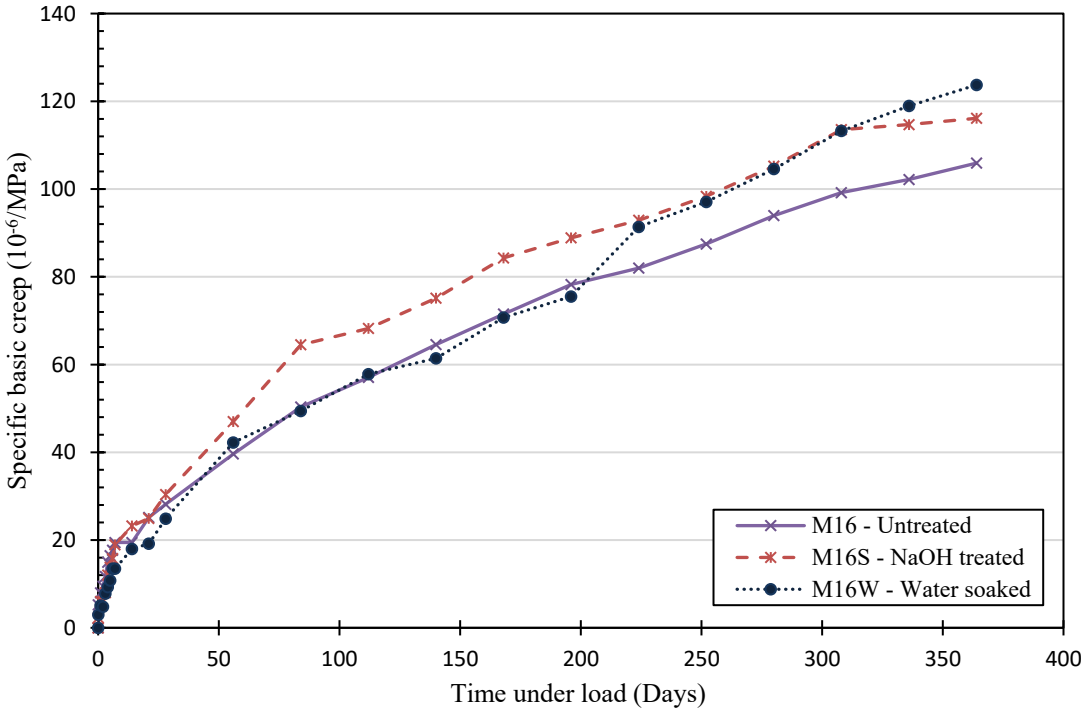

Figure 4.28: Effect of surface treatment of 1.18 mm crumb rubber on basic creep

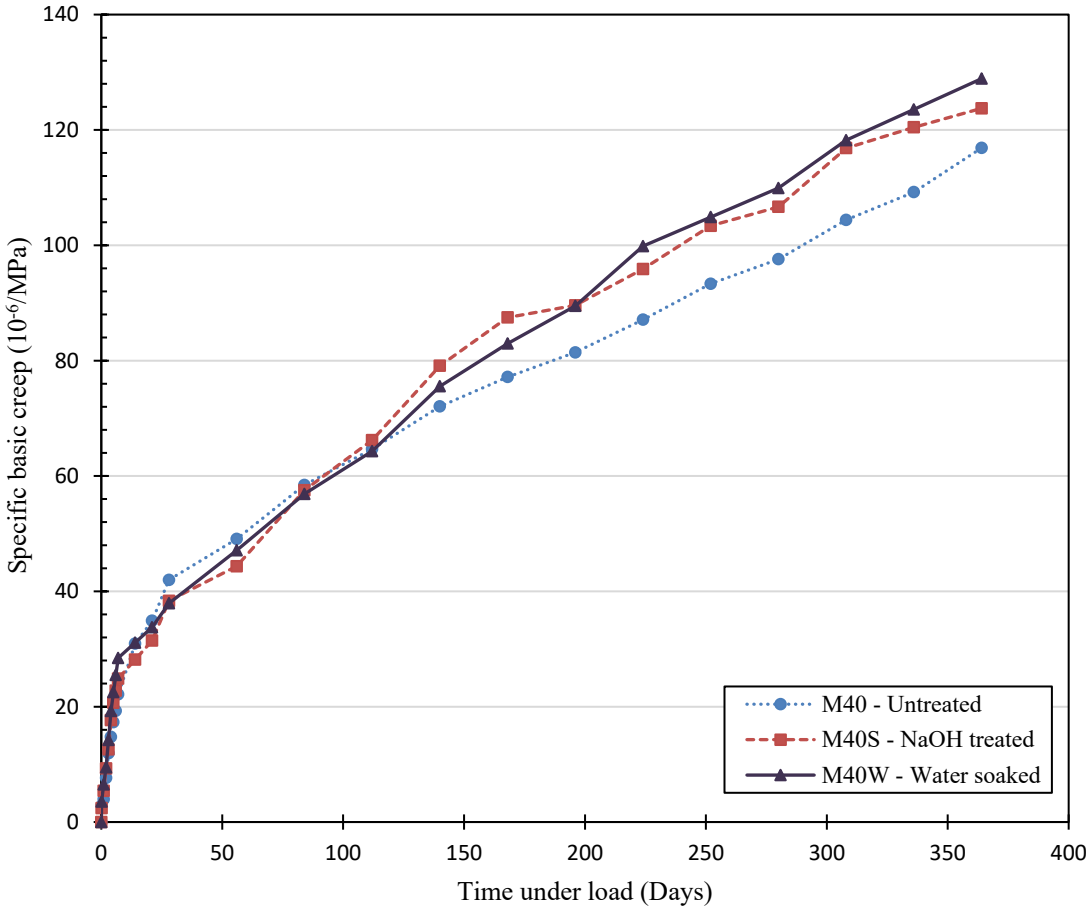

Figure 4.29: Effect of surface treatment of 0.425 mm crumb rubber on basic creep

The specific basic creep of the pretreated crumb rubber concretes, similar to shrinkage, are higher than those of the untreated crumb rubber concretes. The percentage increases for M8W, M8S, M16W, M16S, M40W, M40S concretes are 6%, 10%, 17%, 9%, 10% and 6% respectively. Again similar to the autogenous shrinkage results the larger crumb rubber size concretes have a higher increase in autogenous shrinkage is due to better bonding between cement and rubber particles brought about by the pretreatment process. This closer proximity of the rubber particles to the cement encourages more water movement from the rubber to the cement. However, in general, the pretreatment does not have a significant effect on the basic creep of the concrete as well.

4.7.2 Total creep deformation

Creep tests were carried out on unsealed specimens concrete specimens to assess the total creep deformation of the concrete over the period stated in the section above. These specimens had identical accompaning specimens tested for drying shrinkage. The crumb rubber replacement level for all the crumb rubber sizes used in the concrete was 10%.

Effect of crumb rubber size on total creep

The results of the tests to assess the effect of crumb rubber size on total creep are presented in Figure 4.30.

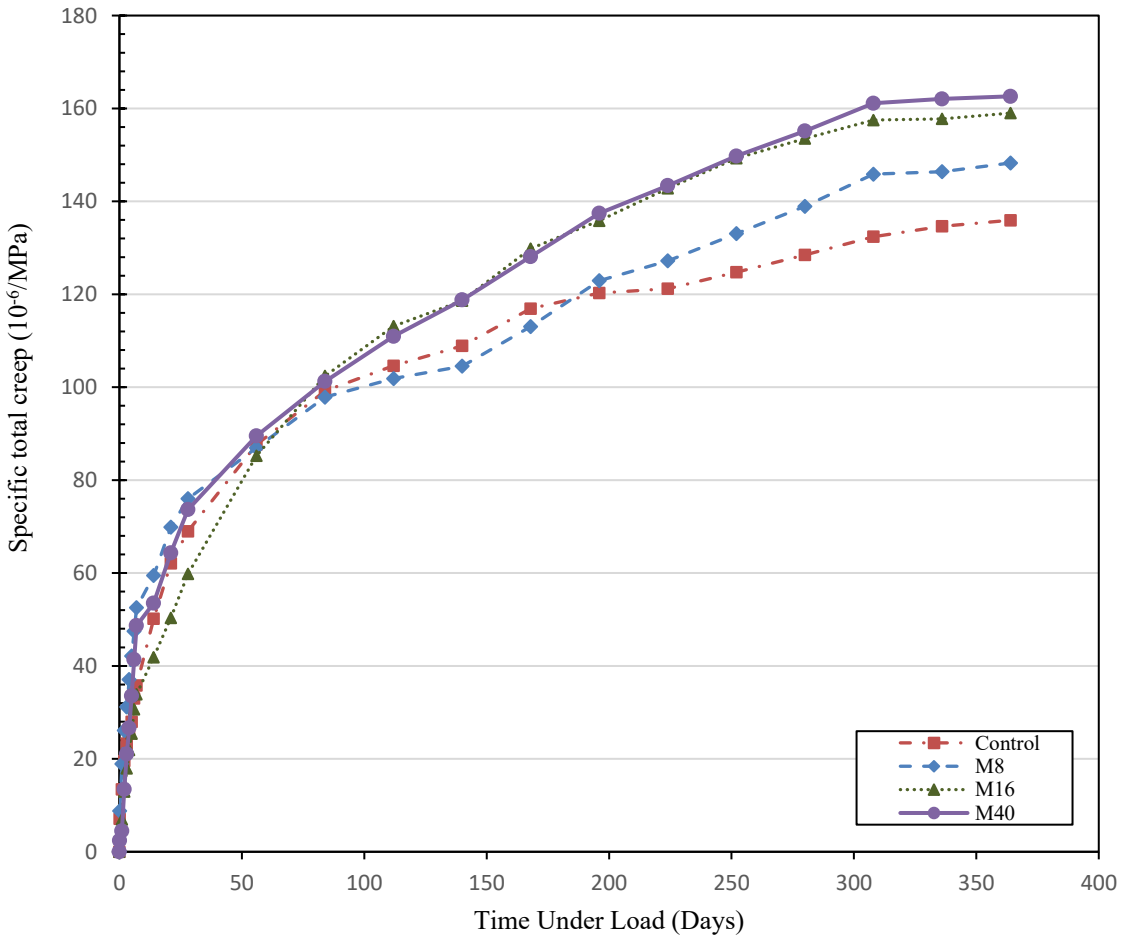

Figure 4.30: Effect of crumb rubber size on total creep

The specific total creep of the rubberised concretes M8, M16 and M40 are higher than those of the reference concrete. The percentage increase in the measured total specific creep for the M8, M16 and M40 is 9%, 17%, 20% compared to the reference concrete. For the period between the start of the test period and 80 days M8 and M40 rubberised concretes are higher than the reference concrete while M16 concrete is lower. After this period, all three rubberised concretes have higher specific creep values than the reference concrete. These trends are illustrated in Figure 4.31 for better visualisation.

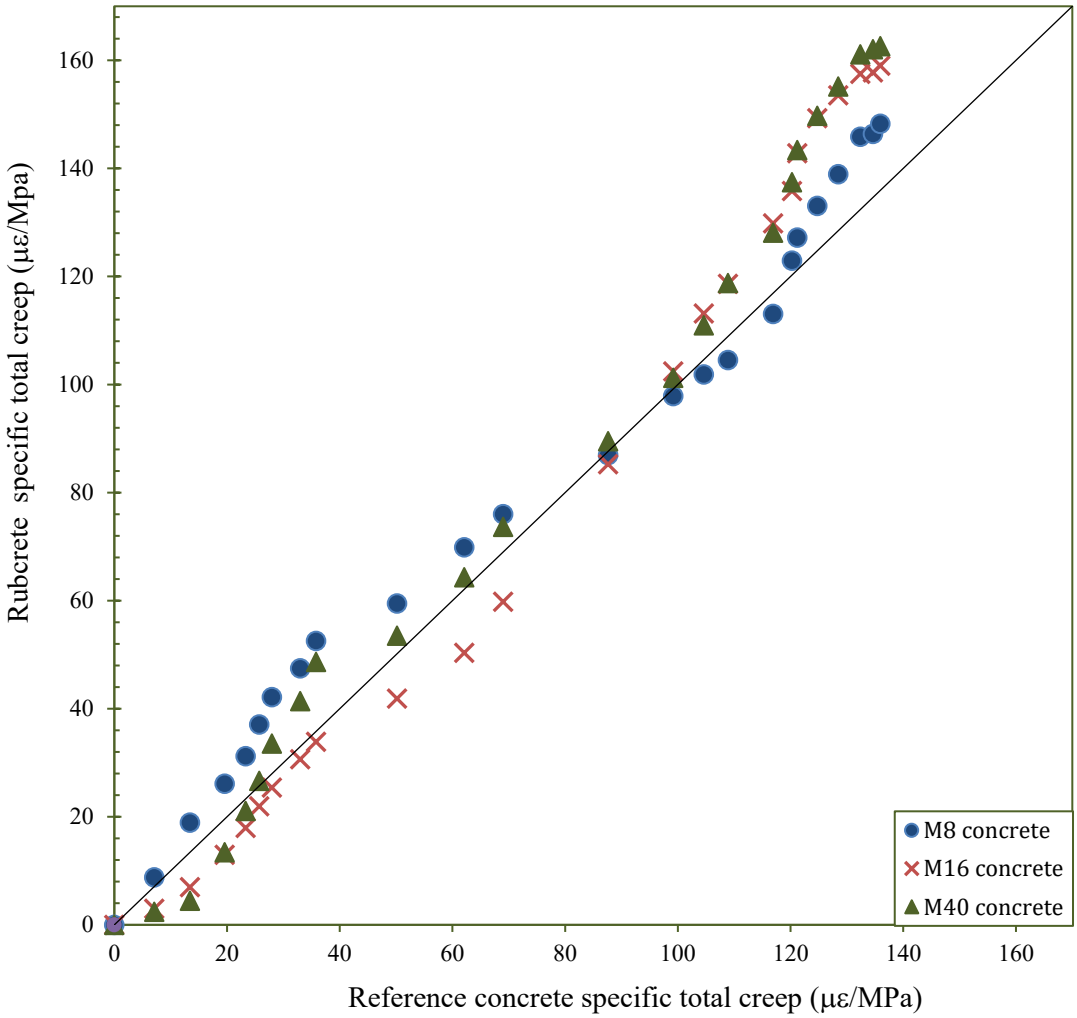

Figure 4.31: Specific total creep equality graph

The observed increase in creep is in agreement with what is reported in literature (Bompa and Elghazouli, 2019, Youssf et al., 2020). This is despite the use of varied concrete strength classes and varied crumb rubber sizes. In all instances, the high creep deformation is attributed the loss of aggregate restraint due to the low stiffness of the rubber particles and an increase in air voids which are associated with tyre rubber particles. Zimmermann et al. (2016) report that inclusion of crumb rubber in concrete increases the number of voids in the concrete thereby increasing concrete porosity. According to Ghuraiz et al. (2011) the increase in concrete voids results in higher concrete permeability which eases the viscous out-flow of capillary water and cement gel. The lower stiffness of the tyre rubber aggregates, and the air voids offer less restraint to the shrinking paste (Evans and Kong, 1996)

The smaller crumb rubber sizes have higher specific creep than the larger 2.36 mm crumb rubber concrete. The reason for the greater creep in the smaller crumb rubber size is attributed to the greater air voids shown to be in concretes with smaller crumb tyre rubber particles. The voids reduce the stiffness of the hardened cement paste which in turn increases compressibility of concrete. In addition, there is higher water loss as a result of having more voids as described in previous sections. This trend is also corroborated by Dhir et al. (2019) in his work that showed a strong correlation between creep and concrete porosity.

Figure 4.32 shows the ratio of each of the rubberised concrete specific total creep ($\varepsilon_{tsp(rub)}$) to the reference concrete specific total creep ($\varepsilon_{tsp(ref)}$) over time from 7 days under load to end of observation period. The period prior to the 7 days was not

shown as the ratios are quite unstable and much higher than the long-term creep ratios, this would have given a distorted view.

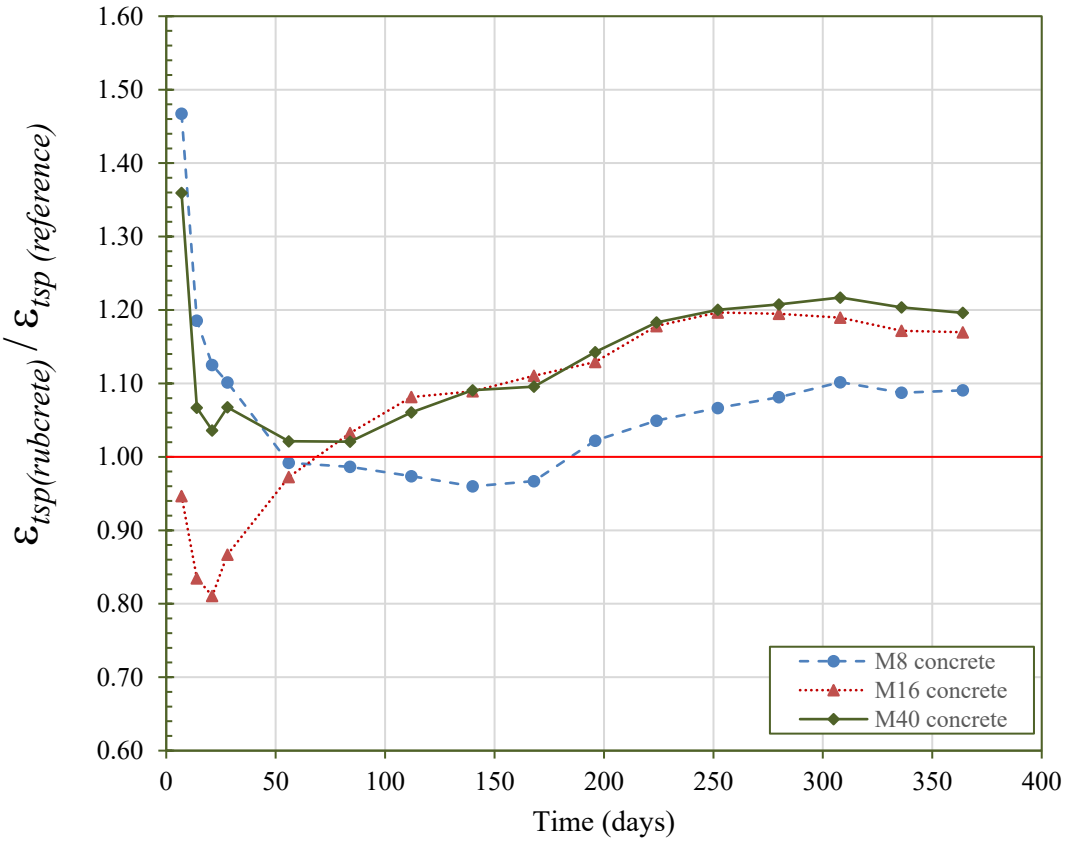

Figure 4.32: Ratio of rubberised concrete to reference concrete specific total creep

The total specific creep for M8, M16 and M40 rubberised concretes are a minimum of 0.96, 0.81 and 1.02 times that of the reference concrete respectively and a maximum of 1.47, 1.20 and 1.36 times respectively. The medians of the M8, M16 and M40 ratios are 1.07, 1.10, 1.12 respectively while the means are 1.08, 1.06 and 1.14 respectively. Considering these statistics, indicating the distribution of the ratios, for structural design where rubberised concrete with crumb rubber of mesh size 8 and less is to be used, a conservative multiplier of 1.2 can be applied to the total specific creep expected for plain normal strength concrete, that is:

$$\varepsilon_{tsp(rub)}\ (t) = 1.2\ \varepsilon_{tsp(ref)}\ (t), \qquad (for\ t > 28\ days) \ldots\ldots\ldots\ldots\ldots\ldots \text{Eqn. 4.4}$$

Effect of crumb rubber surface treatment on total creep

The results of the tests to assess the effect of crumb rubber surface treatment on basic creep deformation of concrete are presented in Figures 4.33 – 4.35.

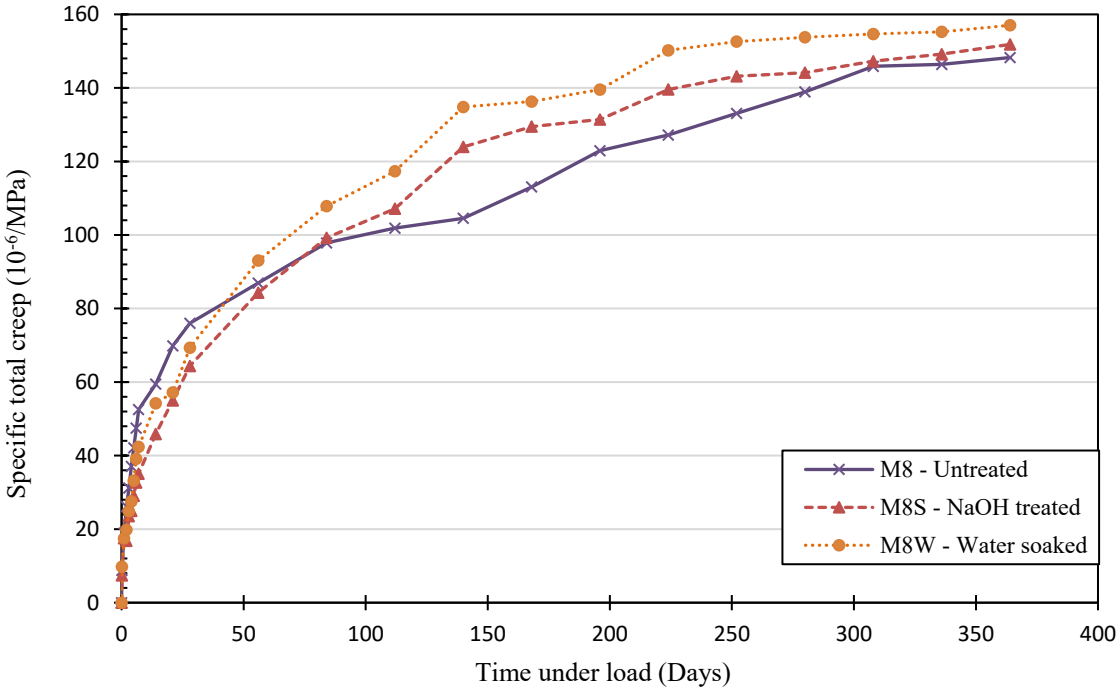

Figure 4.33: Effect of surface treatment of 2.36 mm crumb rubber on total creep

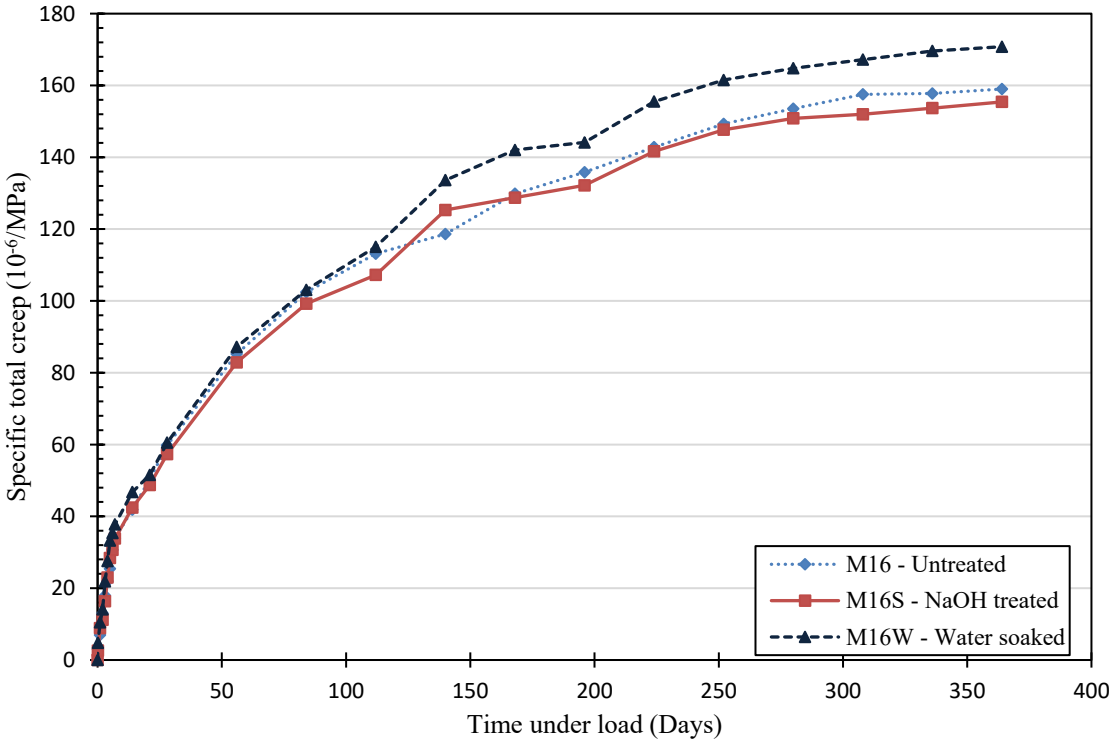

Figure 4.34: Effect of surface treatment of 1.18 mm crumb rubber on total creep

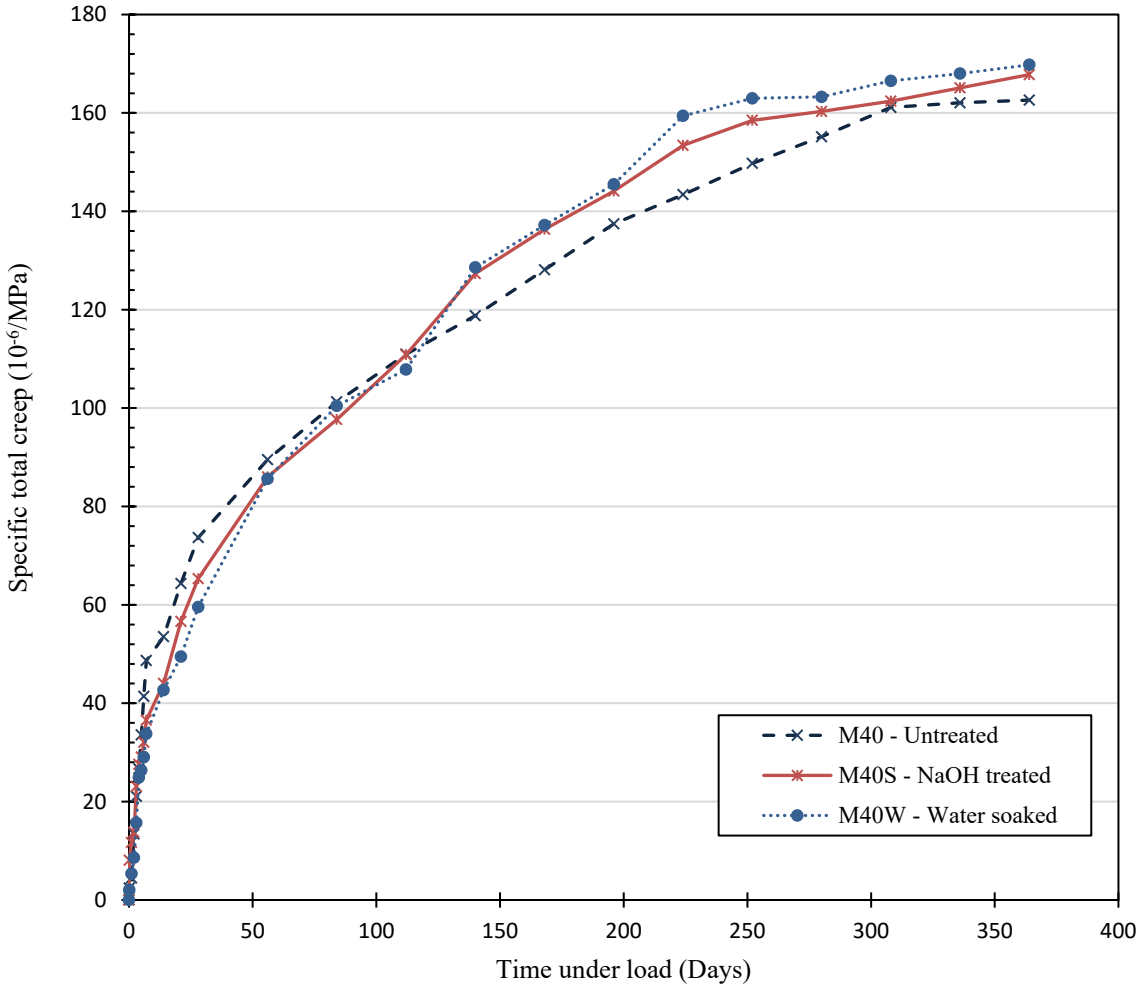

Figure 4.35: Effect of surface treatment of 0.425 mm crumb rubber on total creep

The total specific creep of the pretreated crumb rubber concretes, are comparable to total specific creep of untreated crumb tyre rubber concretes. The percentage increases for M8W, M8S, M16S, M40W, M40S concretes are 6%, 3%, 2%, 6%and 4% respectively when compared to the untreated crumb rubber concretes. The M16W concrete had a decrease of 7%. The differences were all within the 7 % range which is marginal. The effect of pretreatment does not show any trend related to the size of the particles. The marginal effect of pretreating tyre rubber particles on creep is similar to that reported for strength, elastic modulus and shrinkage. A similar insignificant effect is reported by Li et al. (2020a).

4.7.3 Creep coefficients

Figure 4.36 shows the variation of creep coefficients with time for a period up to 364 days for all the tested sealed concrete.

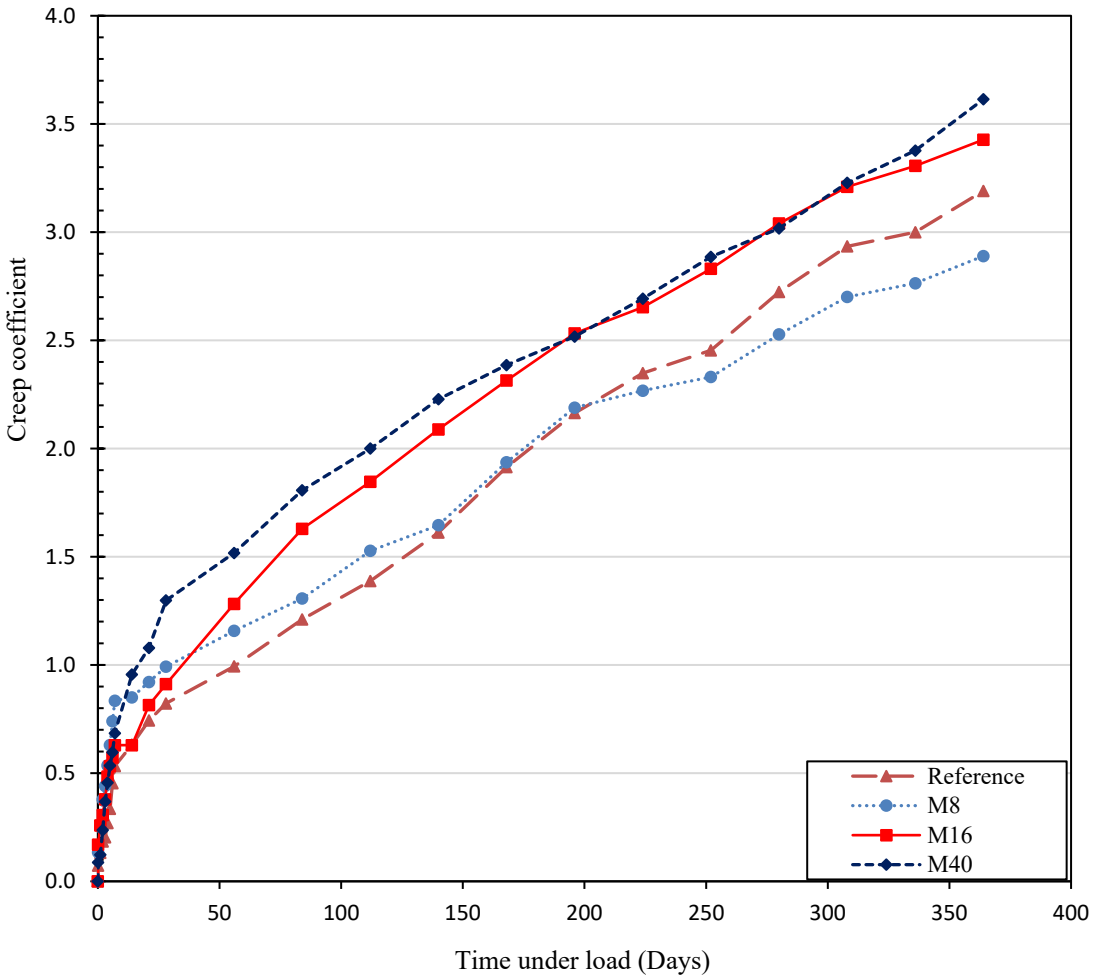

Figure 4.36: Effect of crumb rubber on basic creep coefficient

The rubberised concrete basic creep coefficients are higher than the control concrete up to 140 days after which the M8 concrete exhibits lower creep coefficient. At the end of the monitoring period of 364 days the rubberised concretes M16 and M40 were 24% and 42% respectively higher than control whilst M8 concrete was 30% lower than the control. The basic creep coefficients ranged between 2.7 and 3.7.

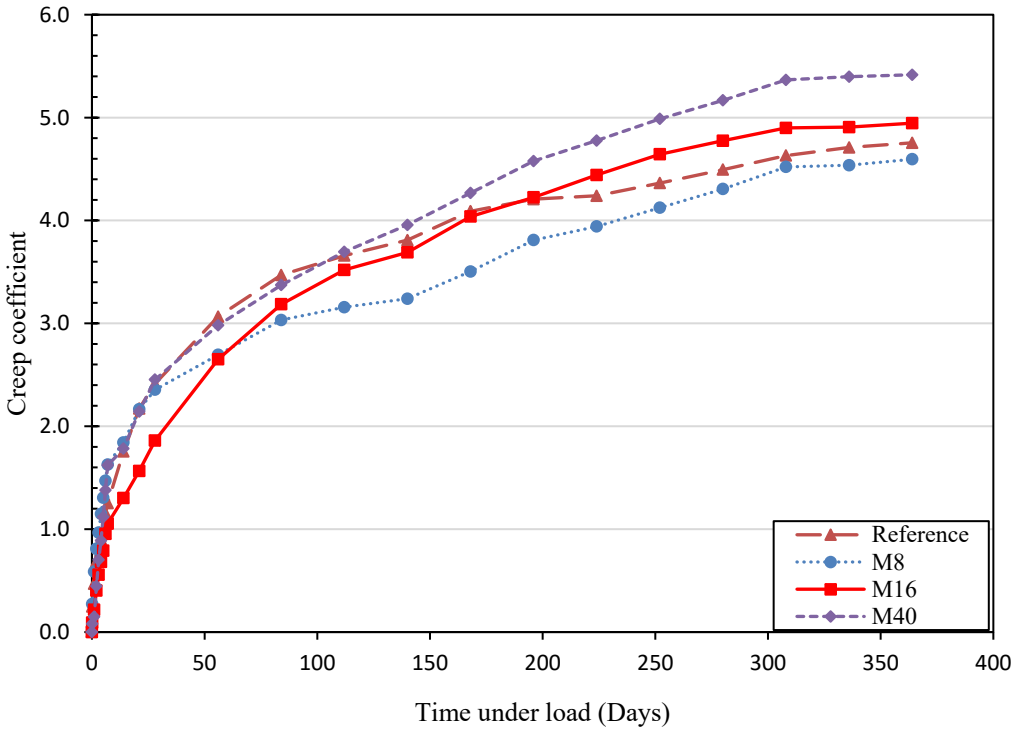

Figure 4.37: Effect of crumb rubber on total creep coefficient

Figure 4.37 shows the variation of creep coefficients with time for a period up to 364 days for all the tested unsealed concrete. The rubberised concrete total creep coefficients are higher than the control concrete up to 56 days after which the M8 concrete exhibits lower creep coefficient. At the end of the monitored period of 364 days the rubberised concretes M16 and M40 were 20% and 67% respectively higher than control whilst M8 concrete was 15% lower than the control. The basic creep coefficients ranged between 4.7 and 5.5. Bompa and Elghazouli (2019) also reported creep coefficient trends like the M16 and M40 which might be due to them also using very fine crumb particles. This assertion is to an extent confirmed by the Li et al. (2020a) findings that showed a lower to comparable creep coefficient for crumb rubber particle sizes similar to M8 concrete.

In both instances of basic and total creep coefficient plots the smaller sized crumb rubber aggregates exhibit higher numbers than the control concrete throughout the

test period with the smallest having the highest. The high creep coefficients for the concretes with smaller sized crumb rubber particles, resulting from lower HCP stiffness, can be attributed to higher air content and voids in the concrete associated with the smaller crumb rubber particles.

4.8 SUMMARY OF RESULTS

This section presents a summary of the results and discussions presented in this chapter.

a) Crumb tyre rubber properties considered integral to its effect on concrete behaviour, namely its shape and surface texture, were presented and discussed. The following were the main observations:

   i. There are notable differences in surface texture and shape amongst the 3 crumb rubber sizes mainly due to the production process which involves cutting, shredding and to a certain extent grinding. The larger crumb rubber particles are smoother with a more regular shape while the smaller crumb rubber particles are rougher and irregularly shaped.

   ii. The pretreatment of the crumb rubber particles with sodium hydroxide and by soaking in tap water, only influenced the surface texture of the crumb rubber particles and not the shape. Generally, for the bigger particles, the sodium hydroxide makes the rubber surfaces smoother while the water cleans the surfaces making the defects on the surfaces more visible. For the smaller particles the pretreated surfaces appeared rougher than the untreated surfaces.

b) Fluorescent microscopy on the rubber concrete slices revealed that:

i. Crumb tyre rubber particles in concrete do not result in immediately identifiable micro cracks.

ii. Voids are formed around crumb rubber particle of all sizes.

c) Hardened concrete percent void determination results revealed that;

i. Crumb tyre rubber particles in concrete increased the void volume of the concrete.

ii. The increase was indirectly proportional with the size of the crumb rubber particle.

d) The elastic moduli of concretes made from treated and untreated crumb rubber of various sizes was also presented, the following main observations were made:

i. There was a significant drop in the elastic modulus of the concrete when crumb rubber was used in the concrete.

ii. The reduction in the elastic modulus did not follow any trend related to crumb rubber size.

iii. The modulus of elasticity for all the rubberised concretes are similar for all sizes at the same replacement level.

iv. The pretreatment of the crumb tyre rubber does not result in any significant effect on the elastic modulus when compared to untreated crumb rubber concrete.

e) The autogenous and drying shrinkage of concrete made from treated and untreated crumb rubber of three different sizes was presented and the following observations were made:

i. Long-term (≥ 360 days) autogenous shrinkage for rubberised concrete was higher than normal concrete.

ii. Short-term (≤ 100 days) rubberised concrete autogenous shrinkage was lower than that of normal concrete.

iii. The rubberised concrete long-term shrinkage was higher for smaller crumb rubber sizes than the slightly bigger rubber sizes.

iv. Short-term and long-term drying shrinkage of rubberised concrete was higher than that of normal concrete. The smaller crumb tyre rubber particles sizes exhibited higher strains than the bigger particles.

v. The pretreatment of the crumb rubber particles does not have a significant effect on the autogenous and drying shrinkage of the rubberised concrete.

vi. The higher shrinkage of the rubberised concrete is attributed mainly to the higher air voids and the lower restraining capacity of the rubber particles.

f) The basic and total creep of concrete made from treated and untreated crumb rubber of three different sizes was presented and the following observations were made:

i. Rubberised concrete had higher total and basic creep strains than normal concrete

ii. Total and basic creep strains were higher for rubberised concrete with smaller crumb rubber particles

iii. Pretreating the rubber particles did not improve the performance of the crumb rubber.

iv. The lower stiffness of the rubber which should be more pronounced in bigger rubber particles plays a lesser role in the behaviour of the rubberised concrete compared to the air voids.

v. Smaller sized crumb rubber particles result in higher creep coefficients.

vi. Based on the shrinkage and creep results of this study, for practical application in design the following expressions can be used to estimate the expected deformation due to the use of crumb rubber particles of mesh size 8 and smaller (Otieno and Mushunje, 2021):

- Autogenous shrinkage:

$$\varepsilon_{a\ (rubberised\ concrete)}\ (t) = 1.2\ \varepsilon_{a\ (reference)}\ (t), \qquad (t > 7\ days) \ldots\ldots \text{Eqn. 4.1}$$

- Drying shrinkage:

$$\varepsilon_{d\ (rubberised\ concrete)}(t) = 1.15\ \varepsilon_{d\ (reference)}(t)\ , \qquad (t > 7\ days) \ldots\ldots \text{Eqn. 4.2}$$

- Basic creep

$$\varepsilon_{bsp\ (rubberised\ concrete)}\ (t) = 1.25\ \varepsilon_{bsp\ (reference)}\ (t), \qquad (t > 28\ days) \ldots\ldots \text{Eqn. 4.3}$$

- Total creep

$$\varepsilon_{tsp\ (rubberised\ concrete)}\ (t) = 1.2\ \varepsilon_{tsp\ (reference)}\ (t), \qquad (t > 28\ days) \ldots\ldots \text{Eqn. 4.4}$$

The results summary shows that the inclusion of crumb tyre rubber in concrete changes the porosity of the concrete and replaces a stiff aggregate with a compressible one which changes the mechanical behaviour of the concrete. These changes result in a less stiff concrete which deforms a maximum of about 25% more than plain normal strength concrete. These changes result in a concrete that can be used for applications where compressibility and lower crack potential is required.

CHAPTER FIVE: RHEOLOGICAL MODELLING THEORY

5.1 INTRODUCTION

This chapter discusses different rheological modelling and its significance in the representation of concrete creep behaviour. The development, application and limitations of rheological models is also discussed. The rheological modeling of rubberised concrete creep deformation assists to better assess if the physical properties of the concrete under loading reamain fundamentally the same when compared to that of plain normal strength concrete. This is because rheological modeling allows the overall deformation to be broken down into separate components.

5.2 RHEOLOGICAL MODELS

Concrete under sustained loading is thought to exhibit viscoelastic behaviour (Neville et al., 1983; Reiner, 1949). This viscoelastic behavior of concrete can be satisfactorily simulated using rheological models (Mehta and Monteiro, 2014). The rheological models give insight into the mechanics of the observed elastic and viscous behavior of the concrete under sustained loading (Fathifazl and Razaqpur, 2013). Neville et al. (1983) caution that rheological models should not be considered as showing the deformation mechanisms but should be understood as representing the physical properties of the whole element under loading, which is, the macroscopic view.

5.2.1 Basic rheological models

Rheological or mechanical models are representations of linear viscoelasticity constructed by making use of a combination of idealised linear elastic springs and linear viscous dash-pots (Neville et al., 1983; Pauw, 1971). The consitutive equation for linear elastic response of a material which is represented by a linear spring with elastic modulus, E, (see Figure 5.1) is given by Equation 5.1;

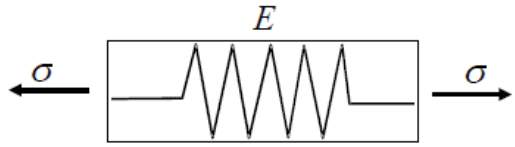

Figure 5.1: Linear elastic spring element (Kelly, 2019)

$$\varepsilon = \sigma/E \quad \text{.....Eqn. 5.1}$$

where: ε is the strain; σ is the applied stress

This type of material gives an instantaneous strain when stressed and maintans the deformation for the duration of the stress. It immediately relesases the strain when the stress is removed and does not show any signs of the stress having been applied (Nagataki and Yonekura, 1984; Özkaya et al., 2012; Roeder, 2013).

A material that has a viscous response visualised as a dashpot, a piston in a cylinder with a perforated bottom filled with a viscous fluid (see Figure 5.2). The movement of the piston in the cylinder is governed by the Newton's law of viscocity (Equation 5.2);

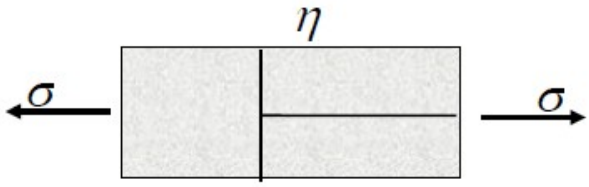

Figure 5.2: Linear dash-pot element (Kelly, 2019)

$$\dot{\varepsilon}(t) = \sigma(t)/\eta \quad \text{.....Eqn. 5.2}$$

where $\dot{\varepsilon}(t) = d\varepsilon/dt = strain\,rate$ *;* η *is the viscocity coefficient; t is the time*

The Newtonian fluid law states that stress is directly proportional to the rate of strain, implying that the larger the stress the faster the straining (Nielsen, 2007). Therefore, in the course of a creep experiement with constant stress, the rate of strain of the dashpot will be constant (Nagataki and Yonekura, 1984; Özkaya et al., 2012; Roeder, 2013).

In order to model real material behaviour a combination of springs and dashpots is necessary. The Kelvin (Voigt) model and the Maxwell models are the simplest and basic forms of rheological models (Figure 5.3). They are refered to as two element models. The Kelvin (Voigt) model comprises an ideal linear spring and a dash-pot in parallel (Figure 5.3a) while the Maxwell model has the same elements but in series as shown in Figure 5.3b (Barnes, 2000; Choi et al., 2007).

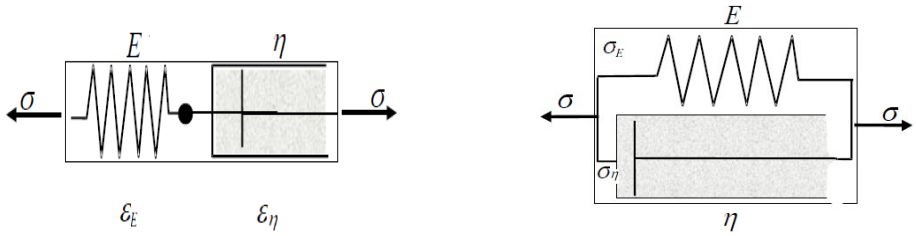

a) Maxwell model *b) Kelvin model*

Figure 5.3: Two-element Maxwell and Kelvin models (Kelly, 2019)

The two models are limited in their representation of the viscoelastic behavior of most materials. In the Maxwell model because the elements are in series they experience equal stress but variable strain thus, the spring has a strain, ε_E, and dash-pot, ε_η. To satisfy strain compatibility, Equation 5.3 applies;

$$\varepsilon(t) = \varepsilon_E(t) + \varepsilon_\eta(t)\ ; \qquad \varepsilon_E(t) = \sigma(t)/E\ ; \qquad \dot{\varepsilon}_\eta(t) = \sigma(t)/\eta \quad \text{.....Eqn. 5.3}$$

After differentiating the compatibility equation and spring deformation equations and substituting we get Equation 5.4,

$$\dot{\varepsilon}(t) = \sigma(t)/\eta + \dot{\sigma}(t)/E \text{.....Eqn. 5.4}$$

Equation 5.4 is the constitutive equation for the Maxwell model and the response of different time-dependent stress or strain patterns are found by solving it. Figure 5.4 shows the response of a Maxwell model. When a Maxwell material is loaded by a stress, σ_0, at time, t_0, the spring will stretch immediately independent of the dash-pot since it is in series with the dash-pot, the dash-pot responds slowly to the load depending on the resistance offered by the fluid to the piston's movement. When the load is removed at time, t_1, the spring contracts instantenously and the dashpot, without anything to push it back to its initial undeformed position, mantains the deformation (Barnes, 2000; Mezger, 2006)

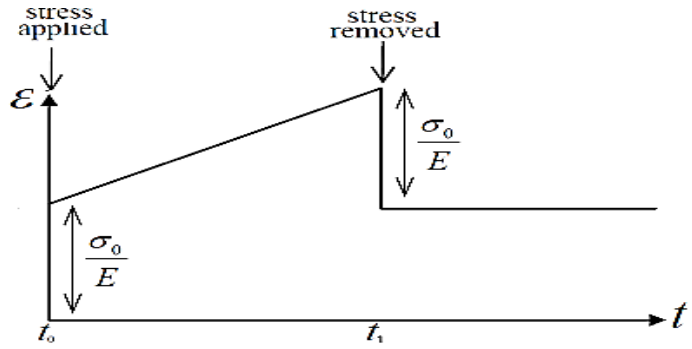

Figure 5.4: Maxwell model creep-recovery response (Kelly, 2019)

For the case of a creep expriement, with initial conditions $\sigma = \sigma_0$ at $t = t_0$, by integrating Equation 5.4 we get Equation 5.5:

$$\varepsilon(t) = \sigma_0/E + \sigma_0 t/\eta \text{ .....Eqn. 5.5}$$

The Maxwell model equation shows that the model is more suitable for fluids than for solids because it shows a constant deformation rate under sustained load. The model predicts boundless strain which is typical of fluids (Mehta and Monteiro, 2014).

Since the Kelvin Model elements are in parallel, they experience equal strain with variable stress of σ_E (spring) and σ_η (dash-pot). Therefore for equilibriumwe must satisfy Equation 5.6;

$$\sigma(t) = \sigma_E(t) + \sigma_\eta(t); \qquad \varepsilon(t) = \sigma_E/E\ ; \qquad \dot{\varepsilon}_\eta(t) = \sigma_\eta(t)/\eta \quad \text{…Eqn. 5.6}$$

Eliminating the variable stresses σ_E and σ_η we get the consitutive equation for Kelvin model, Equation 5.7:

$$\sigma(t) = E\varepsilon(t) + \eta\ \dot{\varepsilon}_\eta(t) \text{……Eqn. 5.7}$$

Equation 5.7 is used to predict the strain for a given stress history. Figure 5.5 shows the response of a material behavior as modeled by the Kelvin model. When a Kelvin model material is loaded, the spring's normal response would be to stretch instantaneously but because of its parallel connection to the dashpot, the stiffer dashpot dictates the response. Therefore the stress is initially absorbed by the dashpot and the creep graph is a curve. Upon unloading, again, the spring would want to contract instantenously but due to the dash-pot the response will be delayed dependent on the resistance of the viscous liquid. Ultimately, overtime the dash-pot will be slowly pulled to its original zero stress position by the spring. (Mehta and Monteiro, 2014; Ozkaya et al., 2012; Roeder, 2013; Kelly, 2019).

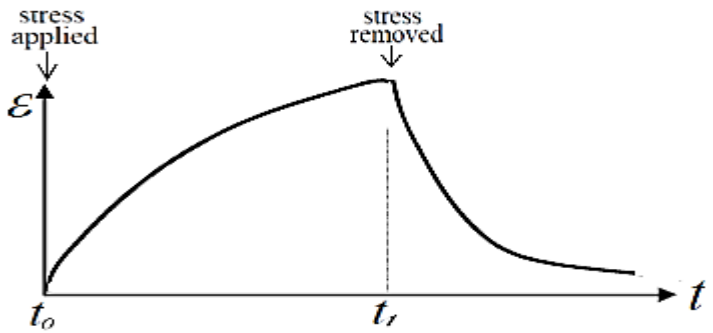

Figure 5.5: Kelvin model creep-recovery response (Kelly, 2019)

In the case of a creep test, integrating Equation. 5.7 for boundary conditions σ = σ_0 at time t_0= 0, the equation gives Equation 5.8:

$$\varepsilon(t) = \frac{\sigma_0}{E}\left(1 - e^{-Et/\eta}\right)$$……..……..……Eqn. 5.8

The downside of the Kelvin model is that it does not show permanent deformation that happens after removing the loading, which is what happens in real materials (Mehta and Monteiro, 2014).

5.2.2 Solid rheological models

Although the Kelvin and the Maxwell models are not ideal for real materials, they are the basic elements in most models. For most materials including concrete, more complex models are necessary to mimic more precisely the material behaviour (Choi et al, 2007; Mehta and Monteiro, 2014). An example is that of models refered to as "solids" which are varying versions of the standard solid model. These models react instantaneously as elastic materials and recover completely upon unloading. The one version comprises of a spring connected in series with a Kelvin element, the other version comprises a spring in parallel with Maxwell model as shown in Figure 5.6 (Choi et al, 2007).

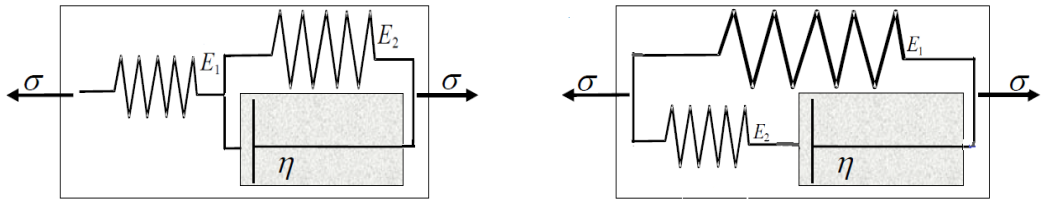

a) Model I *b) Model II*

Figure 5.6: Standard solid (Zener) models (Kelly, 2019)

These models are also refered to as 3-element models and the consitutive equations for the models are shown in Equations 5.9 and 5.10:

$\sigma + \eta\dot{\sigma}/(E_1 + E_2) = [E_1E_2\varepsilon/(E_1 + E_2)] + \eta\dot{\varepsilon}E_1/(E_1 + E_2)$ ……Eqn. 5.9

$\sigma + (\eta\dot{\sigma}/E_2) = E_1\varepsilon + \eta\dot{\varepsilon}(E_1 + E_2)/E_2$ ……..……..…Eqn. 5.10

The creep response of these models is also be determined by specifying stress history and then solving the differential equations for strain. The response of the standard solid model is shown in Figure 5.7 (Ozkaya et al., 2012; Roeder,2013).

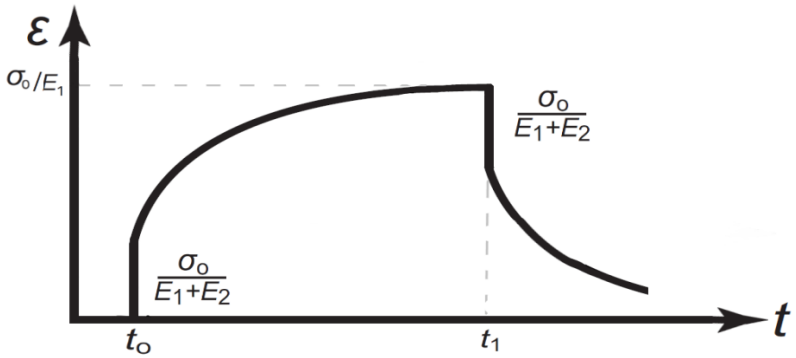

Figure 5.7: Typical standard solid model response (Roeder, 2013)

Another slightly more complex model built from the Kelvin and the Maxwell model is the Burgers model. It is a four element model which is a step up from the standard solid models and better resembles the creep deformation of concrete (Fathifazl and Razaqpur, 2013; Yoon et al., 2011). According to Neville et al, (1983) the Burgers model is the most basic model that qualitatively describes the deformation of concrete under sustained loading. The Burgers model consists of standard solid model I with a dashpot on the other end, as shown in Figure 5.8. Essentially, the Burgers model is a full combination of a Kelvin and Maxwell model.

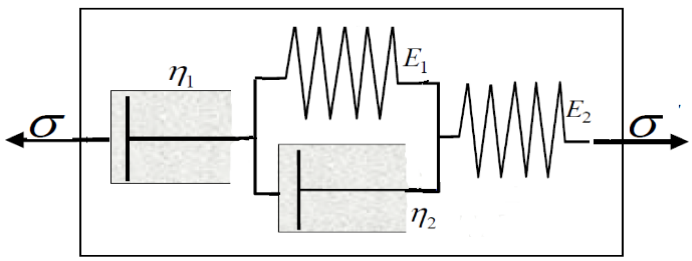

Figure 5.8: Burgers model (Kelly, 2019)

The response of a Burgers model is shown Figure 5.8. When a constant load is applied to a Burgers model material, there is an immediate elastic deformation that occurs, this is proceeded by a delayed time dependent strain that is increasing at a decreasing rate. Upon unloading, immediate elastic recovery occurs, followed by a slow delayed recovery tending to a straight line with does not approach complete recovery. This means that after unloading, the deformation under load is not fully recovered. By this behaviour, the Burgers model has been seen as the model that best qualitatively mimics the concrete creep behaviour (Yoon et al, 2011; Fathifazl and Razaqpur, 2013).

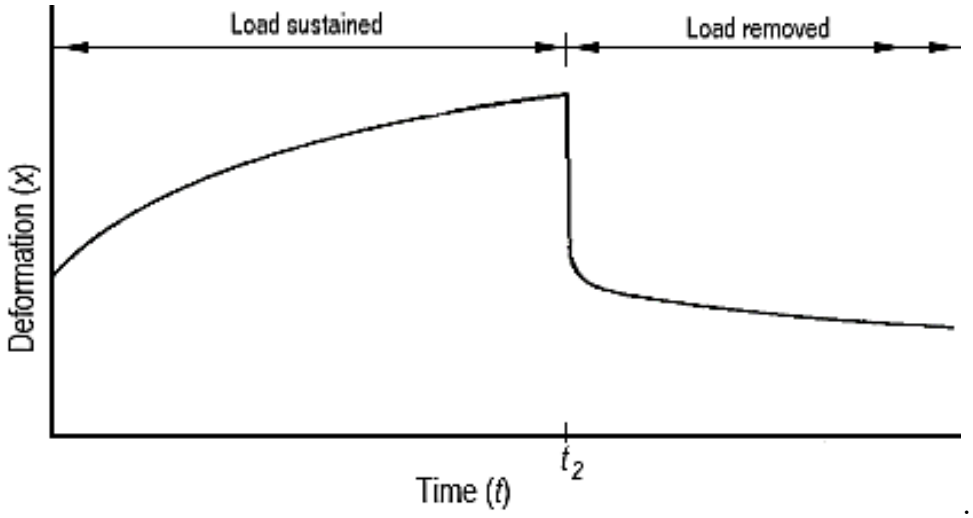

Figure 5.9: Typical Burgers model response (Neville et al, 1983)

The Burgers rheological model consitutive equation is given in Equation. 5.11;

$$\sigma + [(\eta_1/E_1) + (\eta_2/E_1) + (\eta_2/E_2)]\dot{\sigma} + \ddot{\sigma}(\eta_1\eta_2/E_1E_2) = \eta_2\dot{\varepsilon} + \ddot{\varepsilon}\ (\eta_1\eta_2/E_1) \quad \text{.....Eqn. 5.11}$$

A number of other more complex models exist that seek to qualitatively and quantitatively predict the concrete behaviour under sustained loading. These complex models usually take the form of the generalised Maxwell chain or the generalised Kelvin chain, shown in Figure 5.10. The generalised Maxwell model can comprise of N different Maxwell units in parallel or series similarly for the

Kelvin model, each unit has different parameter values (Mehta and Monterio, 2014). Ideally, the more elements the model has, the more accurate it should be. The vastness of the model comes with its own challenges in terms of consitutive equation complexity. Nonetheless, Reiner (1963) has shown that these complex models can be reduced to simpler forms. Therefore most researchers have sort to keep the models simpler and fairly basic also owing to the fact that the models are largely empirical.

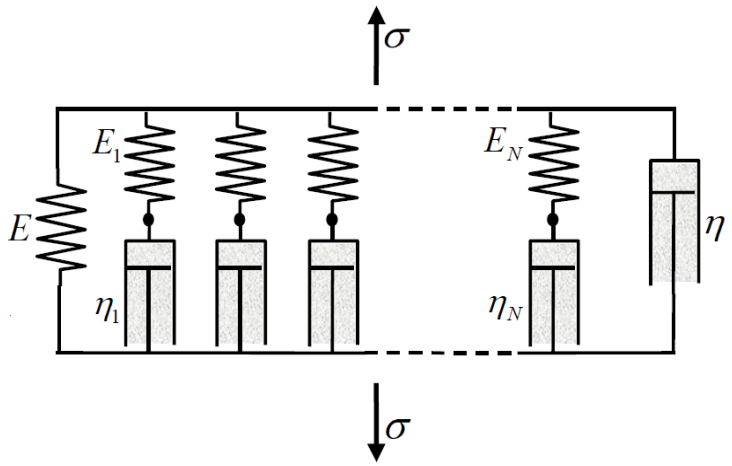

a) Generalised Maxwell model (in parallel)

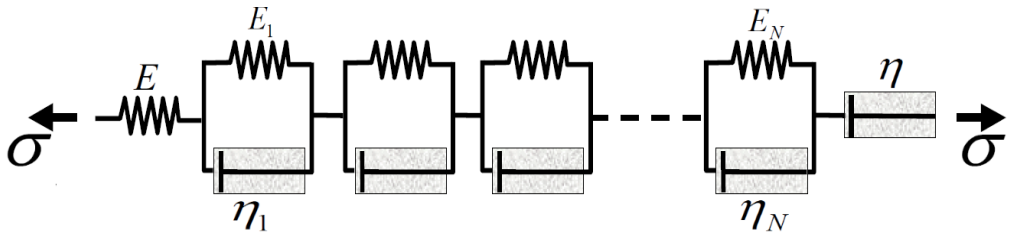

b) Generalised Kelvin model (in series)

Figure 5.10: Generalised rheological models (Kelly, 2019)

These rheological models are the basis for code-type creep prediction models. The CEB-FIP code method which was developed by Hubert Rusch from the work done by Dischinger is one such model (Hilsdorf, 1988). Dischinger made use of the aging Maxwell element and derived what is known as the rate-of-creep method. This method was further developed by Rusch and was later called the

Dischinger method. It is this method that found its way into the CEB-FIP codes and also the DIN code (Rusch et al., 1983). The ability to predict time dependent deformations using these models has made it possible to provide safe, economical and durable structures. It is important to be able to visualise the rheological behaviour of a material under sustained loading. The knowledge makes it easier to create mathematical models to predict the deformation behaviour of the particular material.

5.3 DEVELOPING A RHEOLOGICAL MODEL

Neville et al. (1983) citing Vaishan and Kesler suggests that for the rheological model to be at least qualitatively representative of concrete behaviour under sustained stress and when unloaded, it must possess the following features:

i. Initial set on application of load, partly constant and partly stress-dependent,
ii. Instantaneous elastic deformation,
iii. Delayed-elastic deformation
iv. A creep property dependent on stress and time
v. A permamnent (irrecoverable) time-dependent set, predominationg at stresses nearing the ultimate
vi. Instantenous elastic recovery and
vii. Permanent residual deformation

They state that concrete behaviour at the early stages of loading can be qualitatively simulated by the Kelvin Model , while the later behaviour can be simulated by the Maxwell model. Since the Burger Model is the only model that exclusively has both the Kelvin and Maxwell models, it better qualitatively

approximates concrete deformation under sustained loading (Nielsen, 2007). However, the model does not quantitatively predict concrete creep without matching it up with experiemental data. Therefore, inorder to fit the model to concrete behaviour, experimental data will have to be acquired and applied to the model. The downside of rheological modeling is that it normally gives macro scale deformation characteristics not the fundamental causes of behaviour.

In this study the a four element rheological model is used because the aim of the study was to have a basic understanding of the behaviour of the material and note how it differs in form from conventional concrete. For this purpose the Burgers model was chosen and the base model and emprical values were then derived to mimic the observe behaviour during experiments. The variations in the constants was then atributed to the different factors affecting the creep behaviour. Although this is a simplitic approach to the problem, it does shed some light on the key rubber attributes that might be responsible for the concrete behaviour.

CHAPTER SIX: CONCRETE CREEP RHEOLOGICAL MODELLING

6.1 INTRODUCTION

This chapter presents the rheological modeling of the creep behaviour of the test concrete. It details the procedures of fitting the data to the selected rheological model. It also explores the accuracy of the selected model to predict the creep behaviour quantitatively and qualitatively.

6.2 DETERMINATION OF MODEL PARAMETERS

The Burgers rheological model was used for the modeling of creep deformations in this research because of its reported ability to qualitatively mimic creep deformations to a great extent. Its inability to quantatively predict creep deformation in this research is mitigated by the fitting the model to actual experimental data. This was achieved by determining values for the Burgers model parameters as exhibited by the test specimens. Therefore, the model was developed to qualitatively and quantitatively model creep behaviour of the test specimens.

6.2.1 Application of Burgers model to measured creep data

The determination of the Burgers model parameters for the test specimens comprised of the following four main steps.

i. Dividing the Burgers model into 3 distinct parts (A, B and C) as shown in Figure 6.1.

ii. Assigning each part of the Burgers model to a particular section of the creep curve illustrated in Figure 6.2. This was done visually and later by trial and error using excel and matlab based on theory.

iii. The determination of the governing equation for each rheological unit(s).

iv. Solving of the governing equations to obtain the different paramters using the curve properties.

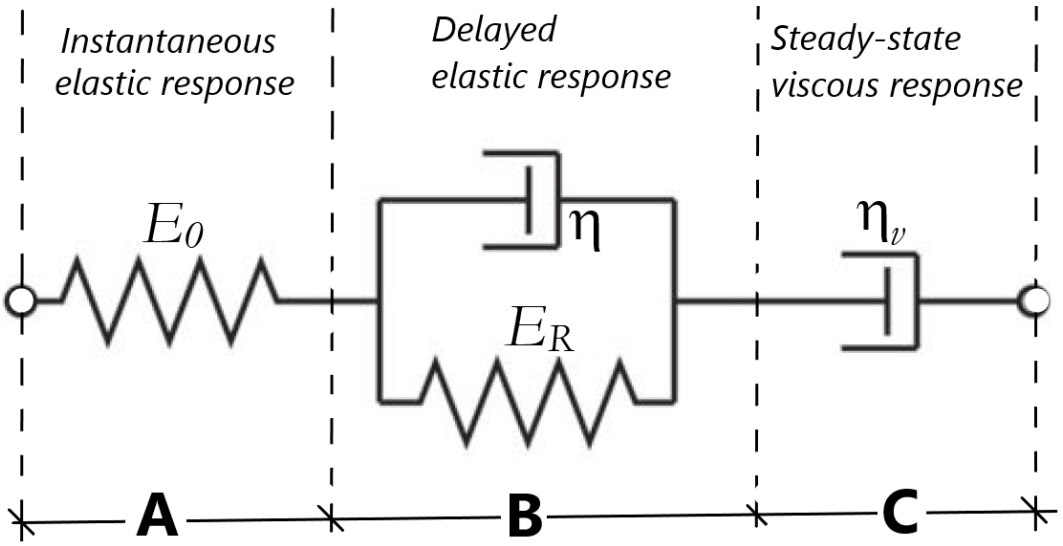

Figure 6.1: Division of Burgers model

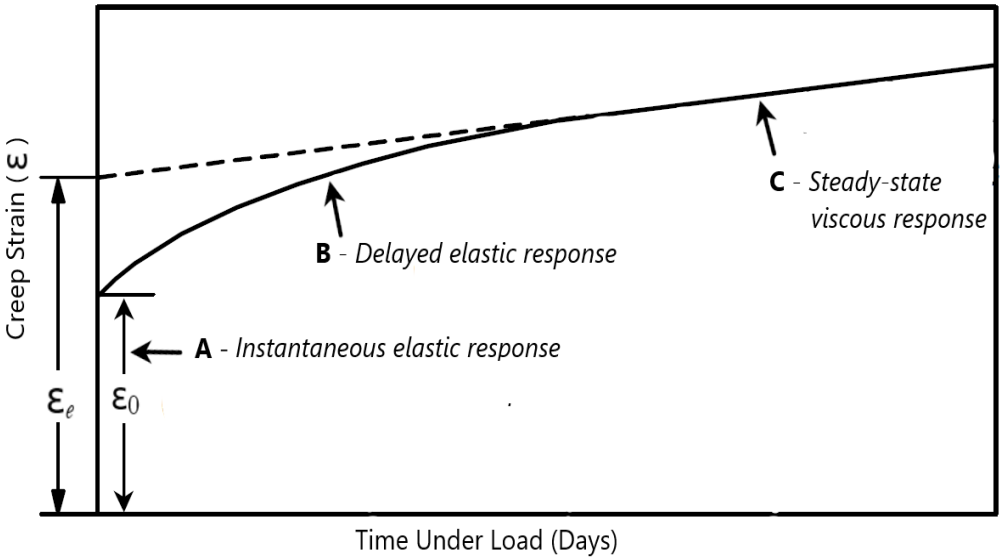

Figure 6.2: Assigning deformation response to curve sections

6.2.2 Model section governing equations

The equations governing the response of each of the three sections of the Burgers model are given in Equation 6.1 – 6.3.

Section A – The elastic response:

$$\varepsilon_0 = \sigma_0/E_0 \text{……..….Eqn. 6.1}$$

Section B – Delayed elastic response:

$$\varepsilon_{VE}(t) = \frac{\sigma_0}{E_R}\left(1 - e^{-E_R t/\eta}\right) \text{……..…..Eqn. 6.2}$$

Section C – Steady-state viscous response:

$$\varepsilon_V(t) = \sigma_0 t/\eta_v \text{…….……Eqn. 6.3}$$

In order to model the creep behaviour of the test specimens, the measured strains were used to determine the values for the Burgers model parameters, E_0, E_R, η and η_v.

The instantaneous elastic modulus, E_0, was obtained using Equation. 6.1 and the measured strain at time, $t = 0$. The retarded elastic modulus, E_R, was obtained by equating the retarded elastic strain, ε_R, portion of the section B response to the quotient of applied stress, σ_0, and elastic modulus, E_R, as shown in Equation. 6.4:

$$\varepsilon_e - \varepsilon_0 = \varepsilon_R = \sigma_0/E_R \text{ ……..Eqn. 6.4}$$

Since ε_e and ε_0 are measured strains read off the creep strain – time graph and σ_0 is known, then, the initial value for E_R, can be found. Having found E_R, Equation 6.2 is then used to solve for the retarded viscosity, η. These values are then used to come up with the most suited curve fitting values for the measured data curve.

Excel and Matlab were used to conduct the curve fitting exercise using an Equation. 6.5:

$$\varepsilon_{VE}(t) = \alpha\left(1 - e^{-\beta t}\right) \text{.....Eqn. 6.5}$$

where $\alpha = \sigma_0/E_R$ and $\beta = 1/T_R = E_R/\eta$, T_R is the retardation time.

The viscosity,η_v, for the steady state section was obtained by passing a regression line through the data points of Section C of the creep strain-time graph. The gradient, *m*, of the regression line was used in Equation 6.6:

$$\eta = \sigma_0/m \text{ .....Eqn. 6.6}$$

where $m = \Delta\varepsilon/\Delta t$ and read off the regression equation.

The model parameters were obtained assuming that the strains for the separate sections are additive and the creep equations governing each creep behaviour of the concrete do not come into effect at the same time. For basic creep strains including elastic strain the governing Equations 6.4 and 6.5 were applied from time, 0.13 days to 21 days. For total creep strains the equations were applied from time, 0.13 days to 56 days. From thereafter the strains from Equations 6.4 and 6.5 are added to strains from Equation 6.6 to get the final strain for time 84 days to 365 days. Table 6.1 shows the schematic application of the equations.

Table 6.1: Application of creep governing equations

Time under load (Days)	0	0.13	...	21	28	56	84	...	364
Basic creep strain equation	σ_0/E_0	$\frac{\sigma_0}{E_R}\left(1-e^{-E_R t/\eta_v}\right)+(\sigma_0/E_0)$			$\frac{\sigma_0}{E_R}\left(1-e^{-E_R t/\eta_v}\right)+(\sigma_0/E_0)+\sigma_0 t/\eta_i$				
Total creep strain equation	σ_0/E_0	$\frac{\sigma_0}{E_R}\left(1-e^{-E_R t/\eta_v}\right)+(\sigma_0/E_0)$					$\frac{\sigma_0}{E_R}\left(1-e^{-E_R t/\eta_v}\right)+(\sigma_0/E_0)+\sigma_0 t/\eta_i$		

The Burgers model parameter values obtained for the test data are given in Table 6.2 and Table 6.3.

Table 6.2: Burgers model parameters for basic creep

Parameter	**Reference**	**M8**	**M16**	**M40**
Spring compliance (E_0) [GPa]	35.3	29.5	32.3	30.9
Spring compliance (E_R) [GPa]	50.0	32.5	32.2	23.9
Viscocity (η_v) [GPa.day]	4820	5040	4460	4540
Viscocity (η) [GPa.day]	383	102	204	280
Retardation time (days)	7.7	3.2	6.3	11.7

The values of E_0 for the 3 rubberised concretes do not show a trend that can be attributed to crumb rubber size (Figure 6.3). However, all the rubberised concretes have lower elastic values than the reference. The E_R values do not follow the same trend as E_0. The E_0 value of the M8 concrete is the lowest whilst E_R values of the M40 concrete is the lowest of the three rubberised concretes. The E_0 values range from 29.5 to 35.3 GPa whilst the E_R values range from 23.9 to 50 GPa. The η_v value for the M8 concrete is the highest of all 4 concretes including the reference, whilst its η value is the least (Figure 6.4). Besides the M8 concrete values, all concretes had comparable values for η_v. The η value is highest for the reference and seems to increase with crumb rubber size (Figure 6.5).

The model parameter values are comparable with the values reported by Nagataki and Yonekura (1982) in their study on conventional structural concrete. However, the conclusions they arrived differ from those of this study. In their study they concluded that the bulk of the strain was in the visco-elastic region of the burger model, which is not the case in this study. The indications of the model show that

for basic creep the viscous region contributes the most to total strain. The difference in the conclusions could be as a result of the fact that their study was on drying creep not basic creep.

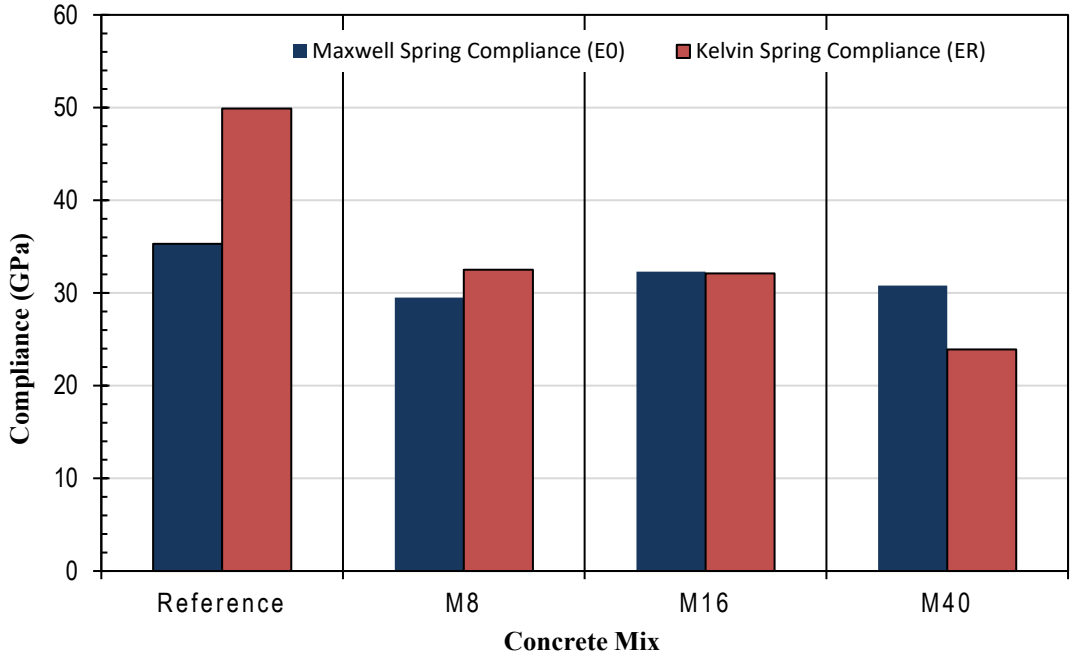

Figure 6.3: Spring compliance variation with crumb rubber size

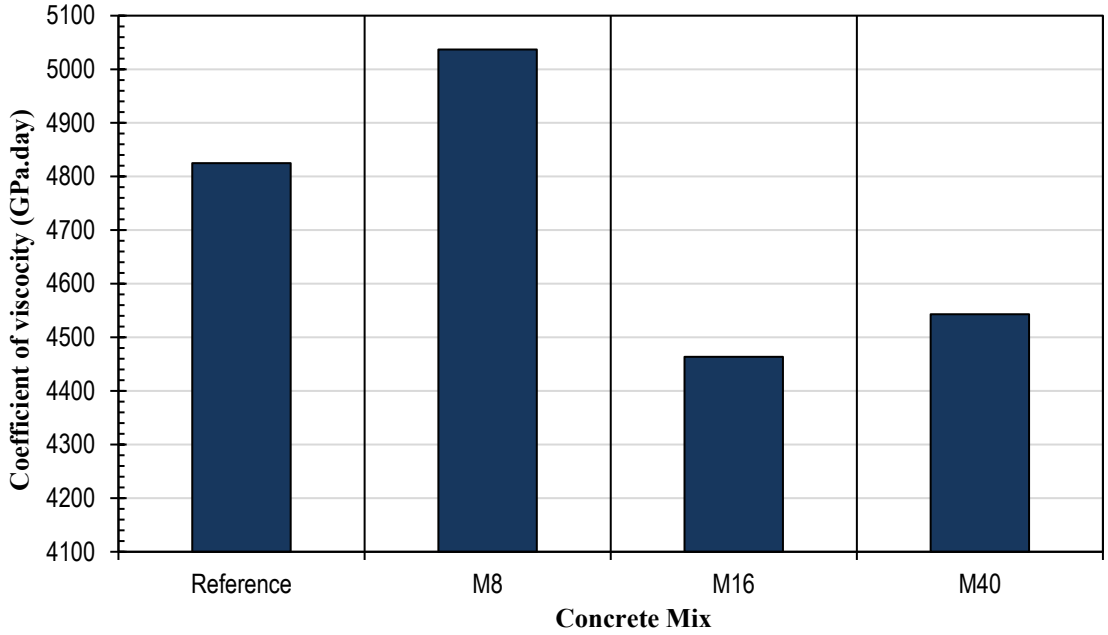

Figure 6.4: Maxwell model coefficient of viscosity variation with crumb rubber size

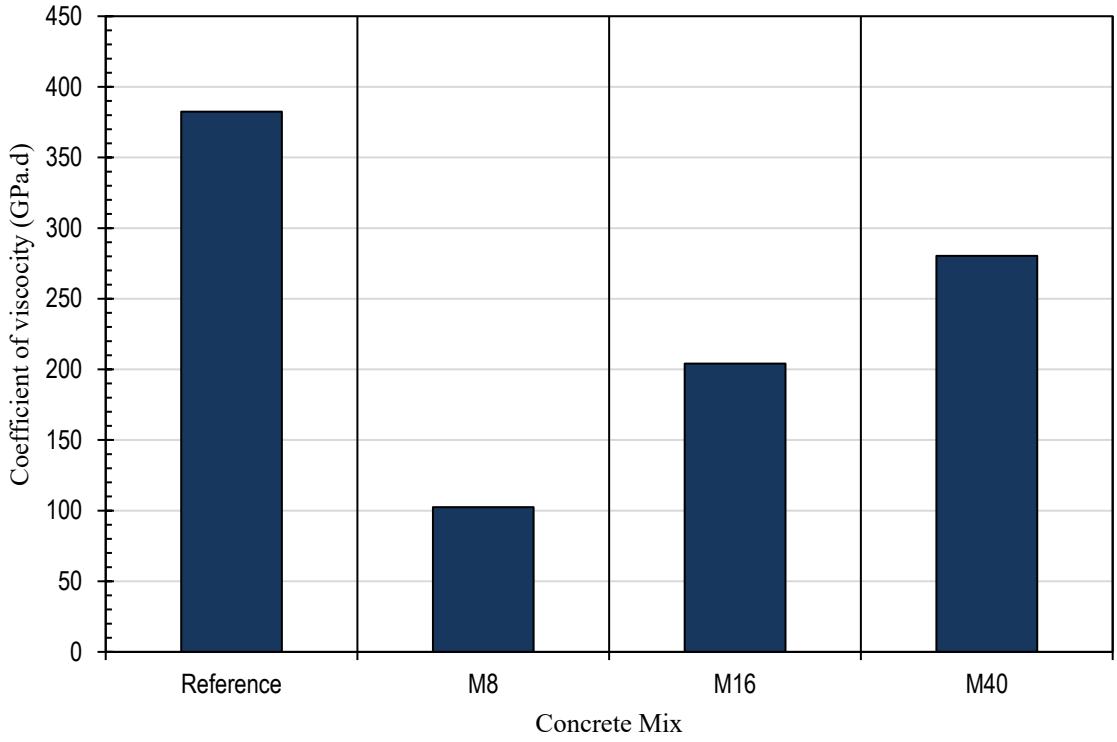

Figure 6.5: Kelvin model coefficient of viscosity variation with crumb rubber size

Table 6.3: Burgers model parameters for total creep

Parameter	**Reference**	**M8**	**M16**	**M40**
Maxwell spring compliance (E_0) [GPa]	34.9	31.0	31.1	33.3
Elastic modulus (E_R) [GPa]	10.7	11.8	10.3	11.7
Viscosity (η_v) [GPa.d]	7660	5000	4820	4010
Viscosity (η) [GPa.d]	185	130	195	139
Retardation time (days)	17.3	11.1	18.9	11.8

The E_0 and E_R values for the 3 rubberised concretes do not show a trend that can be attributed to crumb rubber size (Figure 6.6). All the concretes generally have comparable E_0 and E_R values with no significant variations, with values ranges from 31.1 – 34.9 GPa and 10.3 – 11.8 GPa respectively. The E_0 values for the reference and the M40 concretes are more comparable to each other whilst the M8 and M16 values are similar. The E_R values for the reference and M16 concretes

are similar whilst M8 and M40 values are similar in this case. The reference concrete has the highest η_v value of all 4 concretes. The values seem to decrease as the size of the crumb rubber becomes smaller. The η_v values range from 7700 to 4000 GPa·d. The η values do not show a similar trend as that of η_v (Figure 6.7-6.8). In this case reference value for η is similar to the M16 value whilst M8 and M40 have similar values. The η_v values range from 130 to 195 GPa·d.

The model parameter values are comparable with values reported by Nagataki and Yonekura (1982). The model also suggests similar creep behaviour and mechanism as reported in their study conventional structural concrete. The model shows that creep is predominantly visco-elastic given that the bulk of the strain is contributed by the visco-elastic component of the Burger's model.

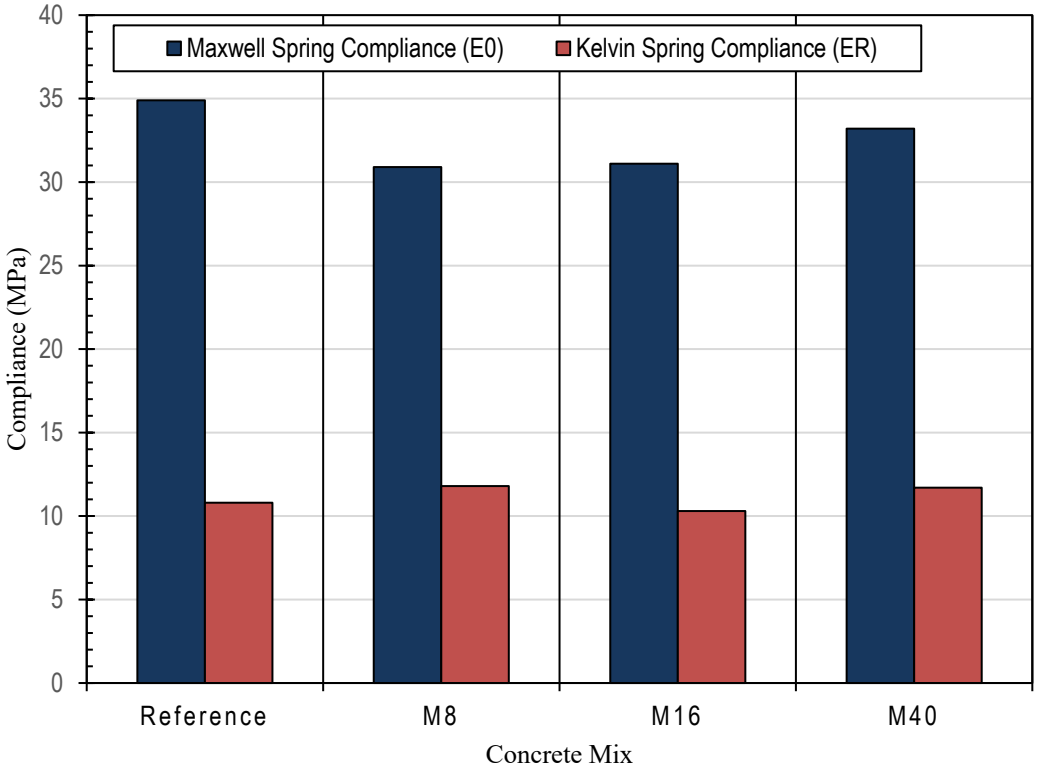

Figure 6.6: Spring compliance variation with crumb rubber size

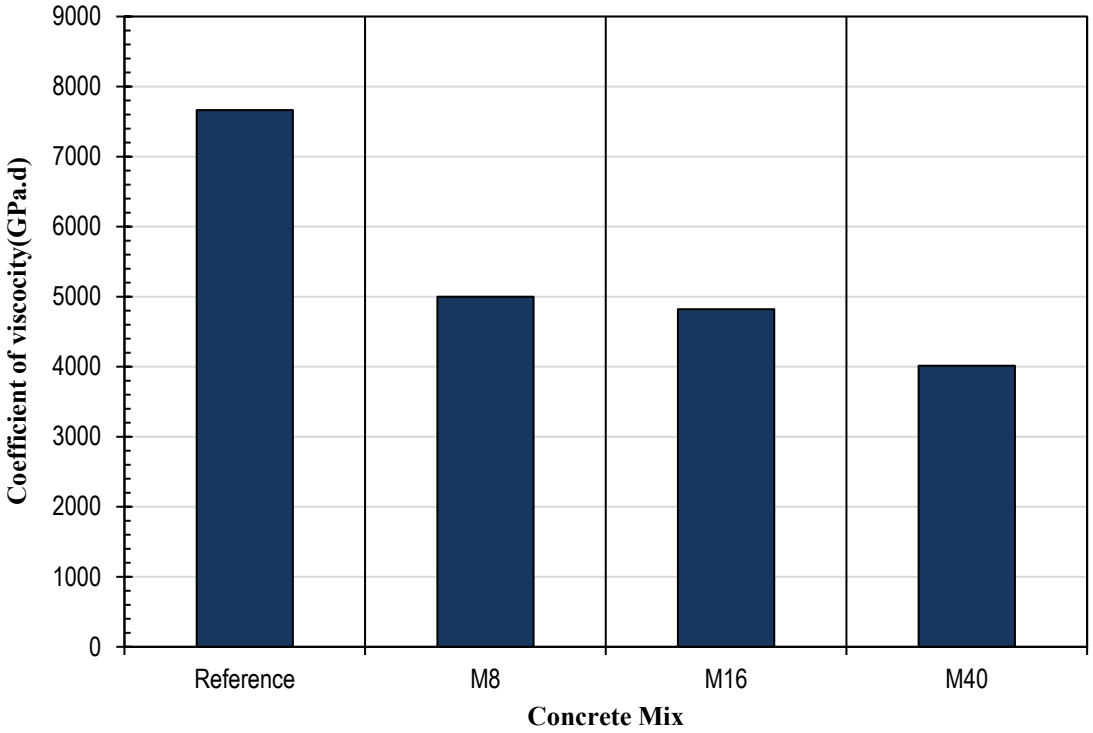

Figure 6.7: Maxwell model coefficient of viscosity variation with crumb rubber size

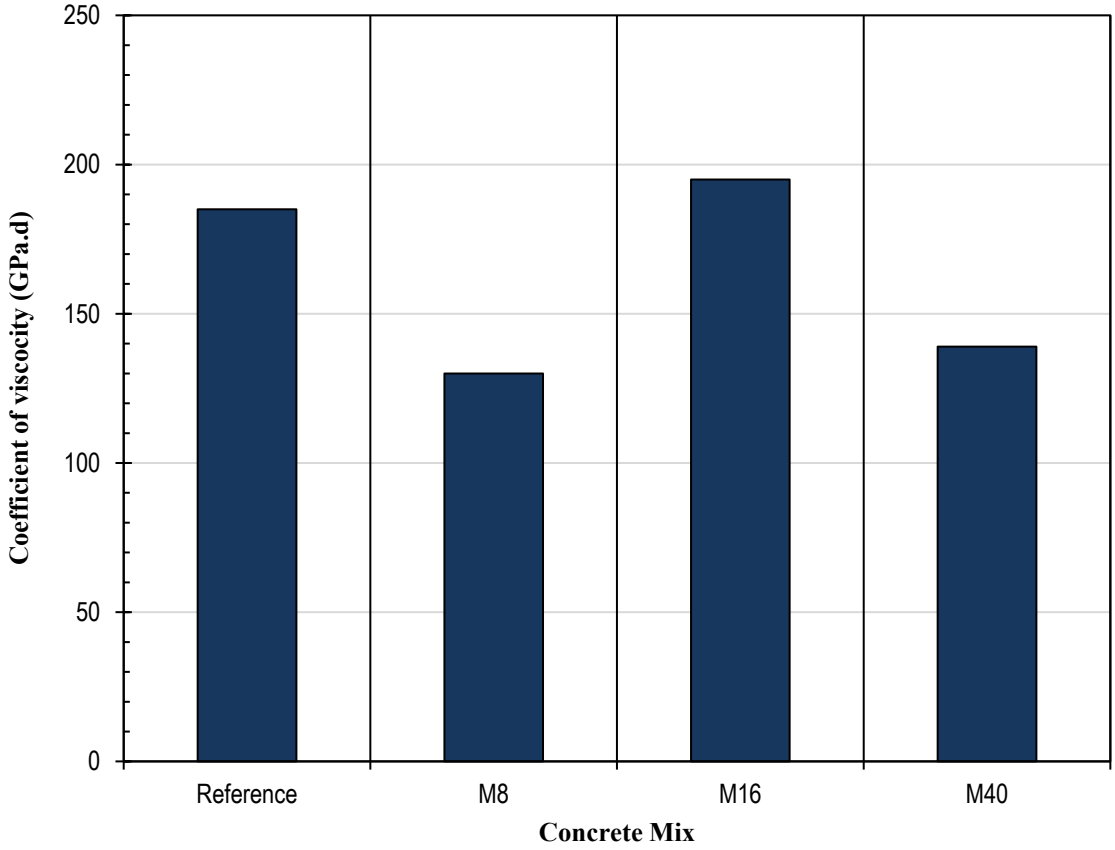

Figure 6.8: Kelvin model coefficient of viscosity variation with crumb rubber size

6.3 MODELLING CREEP BEHAVIOUR

The Burgers rheological model parameters given in Tables 6.2 and 6.3 were used to predict the creep behaviour of the concrete. The accurracy of the model was measured by calculating the prediction error (PE) in each case using Equation 6.7.

$$\text{PE} = \sqrt{\sum_{i=1}^{n} \frac{\left(\varepsilon_i^p - \varepsilon_i^m\right)^2}{n}} \quad \text{.....Eqn 6.7}$$

where ε_i^p and ε_i^m are the predicted and measured creep strains at particular time (i), respectively and n is the number of creep strain data points. The prediction model is considered more accurate the lower the PE value. The magnitude of the difference between the measured and predicted values is best demonstrated by expressing PE as a percentage of the measured strain at the end of the test period, ε_{364}^m as shown in Equation 6.8.

$$PEP\% = \frac{PE}{\varepsilon_{364}^m} \times 100 \text{.....Eqn. 6.8}$$

6.3.1 Basic Creep Prediction Model

The predicted values were plotted with the measured values and are shown in Figures 6.9 – 6.12 for basic creep strains. In general the measured and the predicted strains follow a similar trend as is expected, indicating a good qualitative model of concrete creep. There is a fairly good agreement between the predicted values and the measured values for all the concrete strains as shown by the low PE percentage (PEP). The PEP for the reference, M8, M16 and M40 concretes are 2%, 2%, 3% and 1% respectively. To visualise the deviation of the predicted strains to the mesured strains a plot of equality of the creep strains as shown in Figure 6.14. The scatter off the line of equality is minimal with

coefficients of correlations for reference, M8, M16 and M40 being 0.9969, 0.9928, 0.9899 and 0.9985 respectively. This indicates an acceptable fit of the mesured results to the Burgers model predicted strains and suggests good quantitative accuracy in predicting concrete creep.

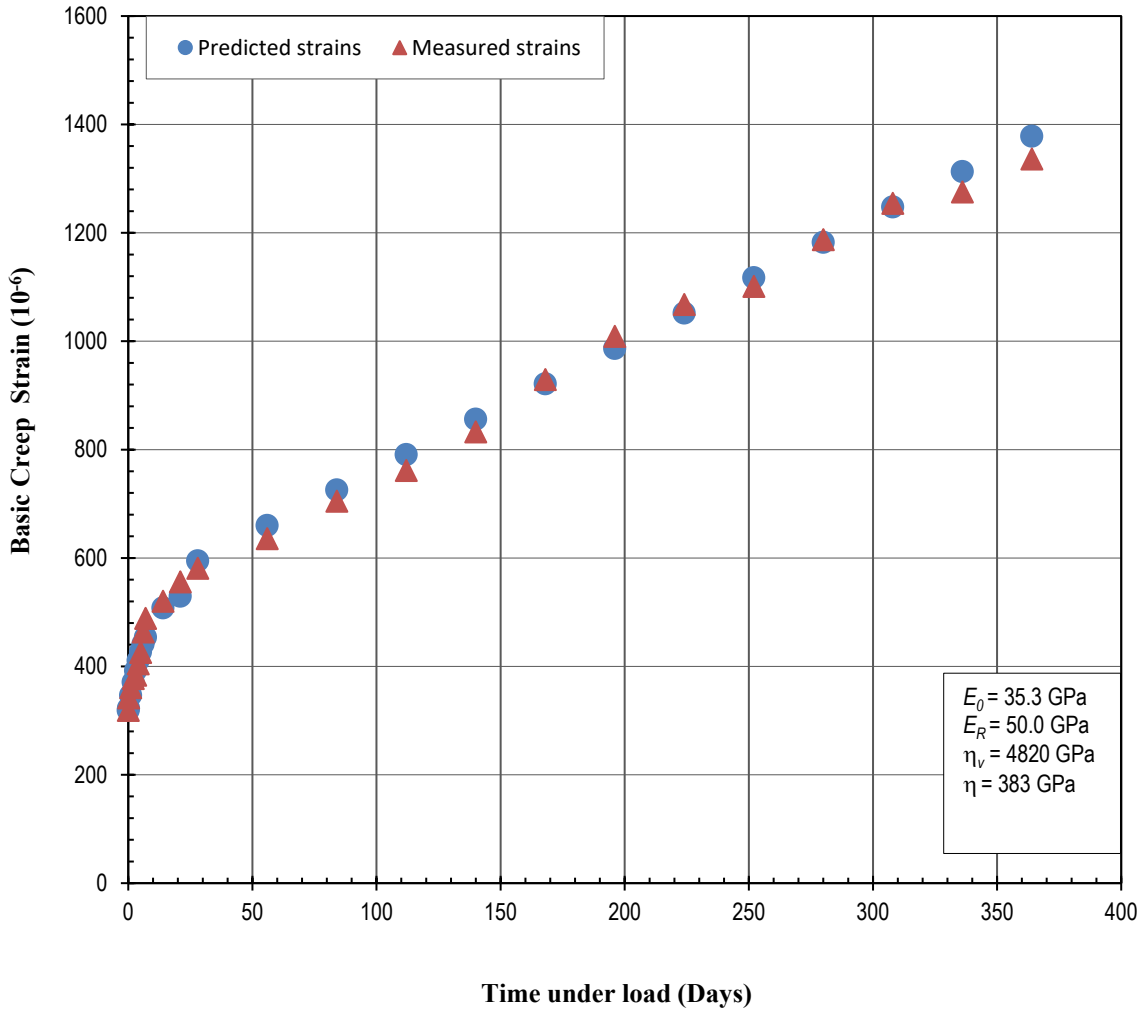

Figure 6.9: Predicted and measured basic creep strain for reference concrete

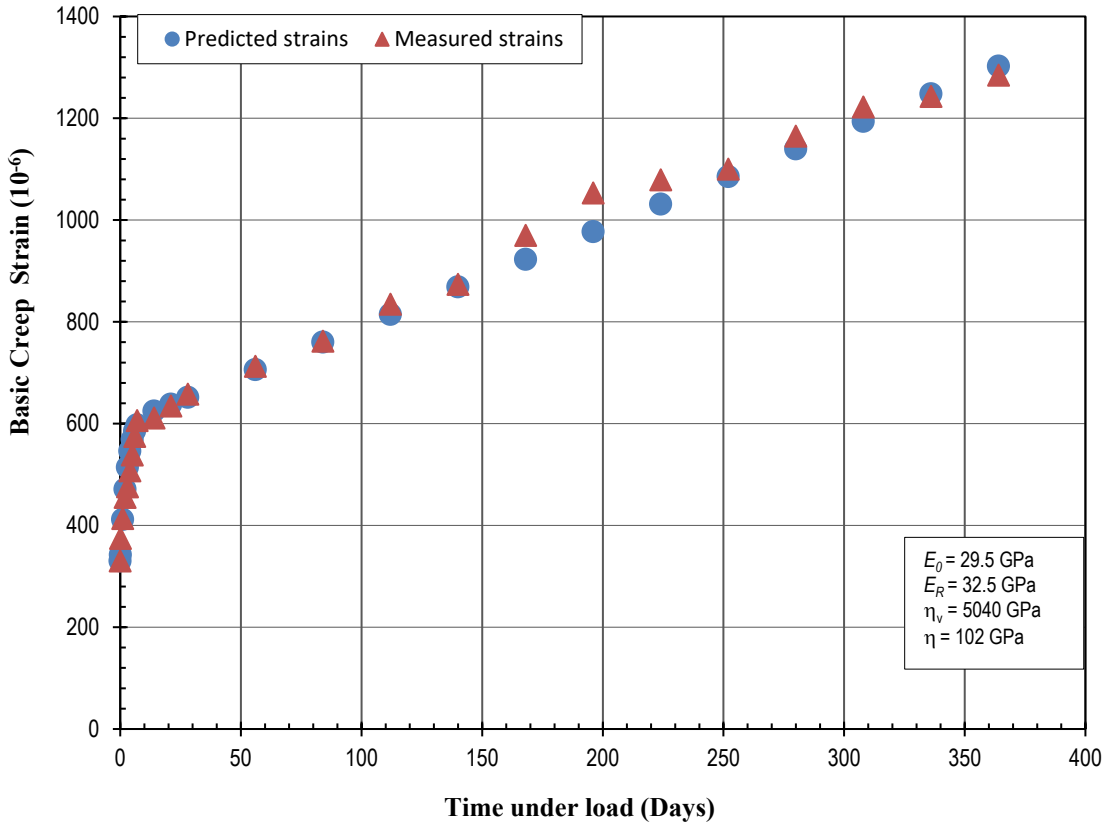

Figure 6.10: Predicted and measured asic creep strain for M8 concrete

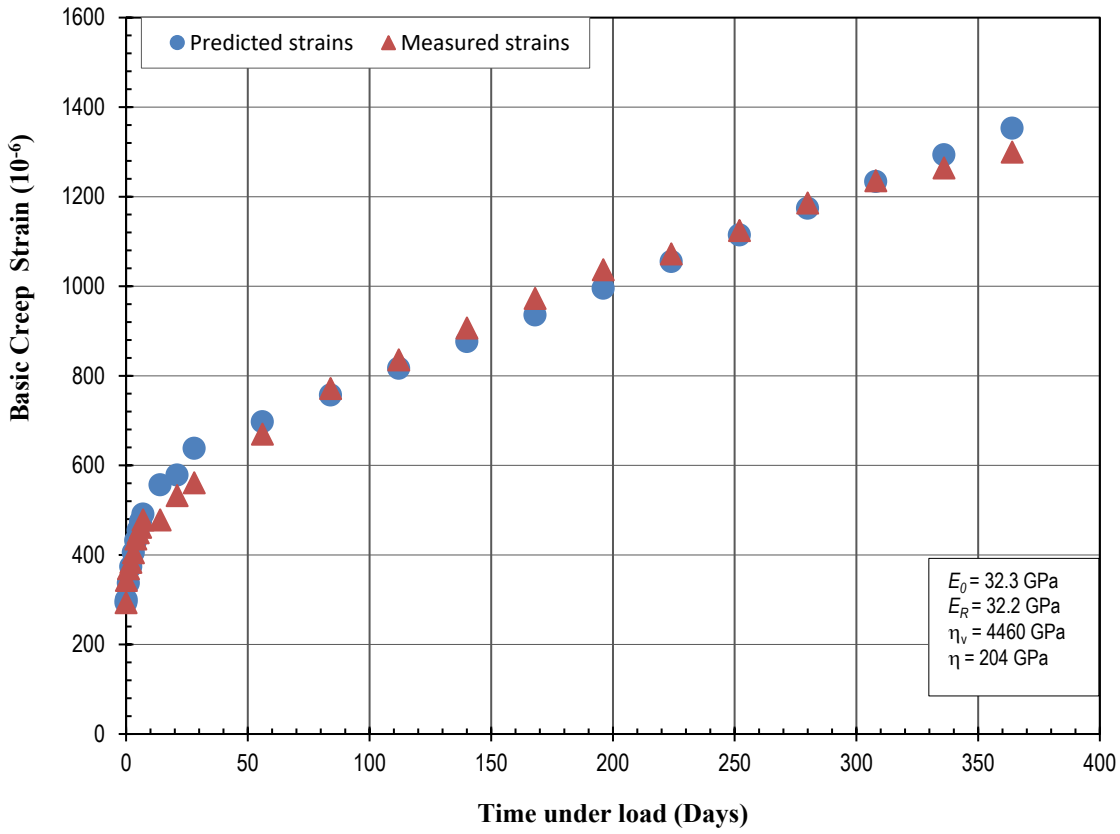

Figure 6.11: Predited and measured basic creep strain for M16 concrete

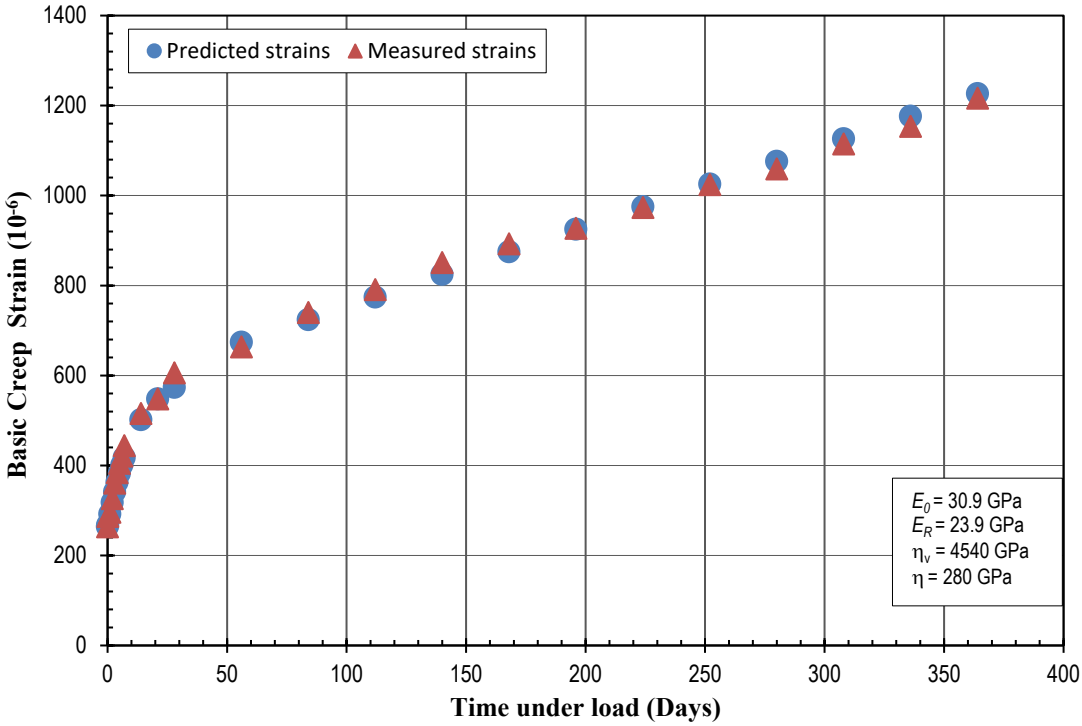

Figure 6.12: Predicted and measured basic creep strain for M40 concrete

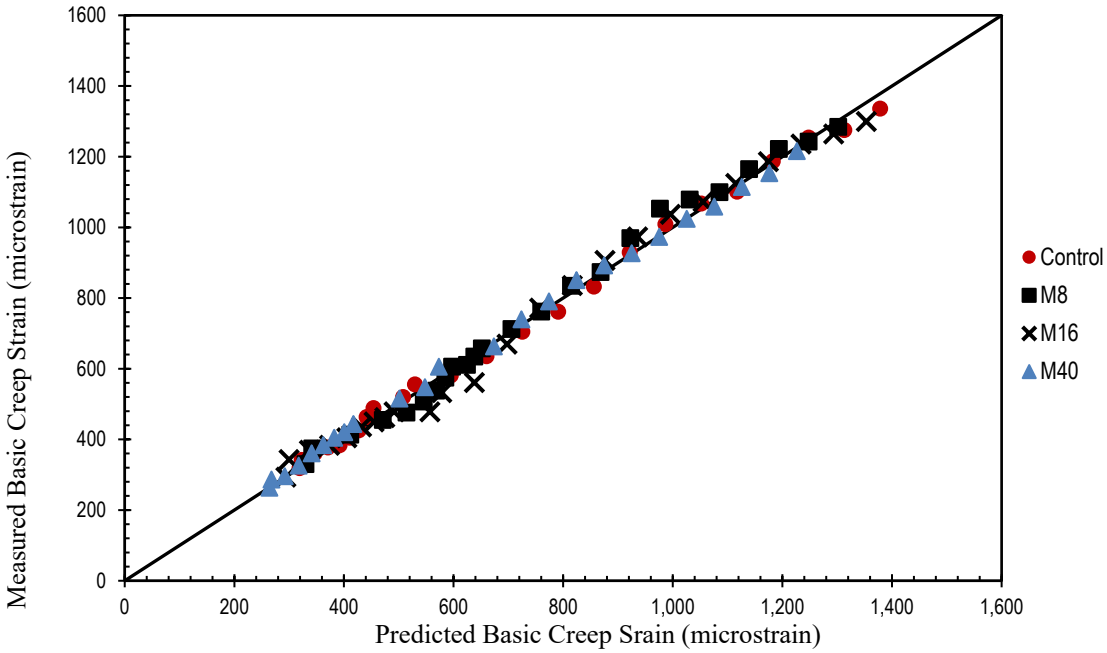

Figure 6.13: Line of equality for reference and rubberised basic creep strain

6.3.2 Total Creep Prediction Model

The predicted values were plotted with the measured values and are shown in Figures 6.14 – 6.17 for total creep strains. In general the measured and the

predicted strains follow a similar trend as is expected, indicating a good qualitative model of concrete creep. There is a fairly good agreement between the predicted values and the measured values for all the concrete strains as shown by the relatively low PE percentage (PEP). The PEP for the reference, M8, M16 and M40 concretes were 3%, 4%, 3% and 3% respectively. To visualise the deviation of the predicted strains to the mesured strains a plot of equality of the creep strains as shown in Figure 6.19. The scatter off the line of equality is minimal with coefficients of correlations for control, M8, M16 and M40 being 0.9944, 0.9917, 0.9896 and 0.9935 respectively, indicative of a good fit. It can be observed from the line of equality that although there is a generally good fit of the measured srains to the Burgers model predicted strains, there is a higher deviation for the reference and M8 strains for the strains at the early stages of the testing period. However, this does not seem to significantly affect the overall prediction accuracy of the model, particularly at later ages.

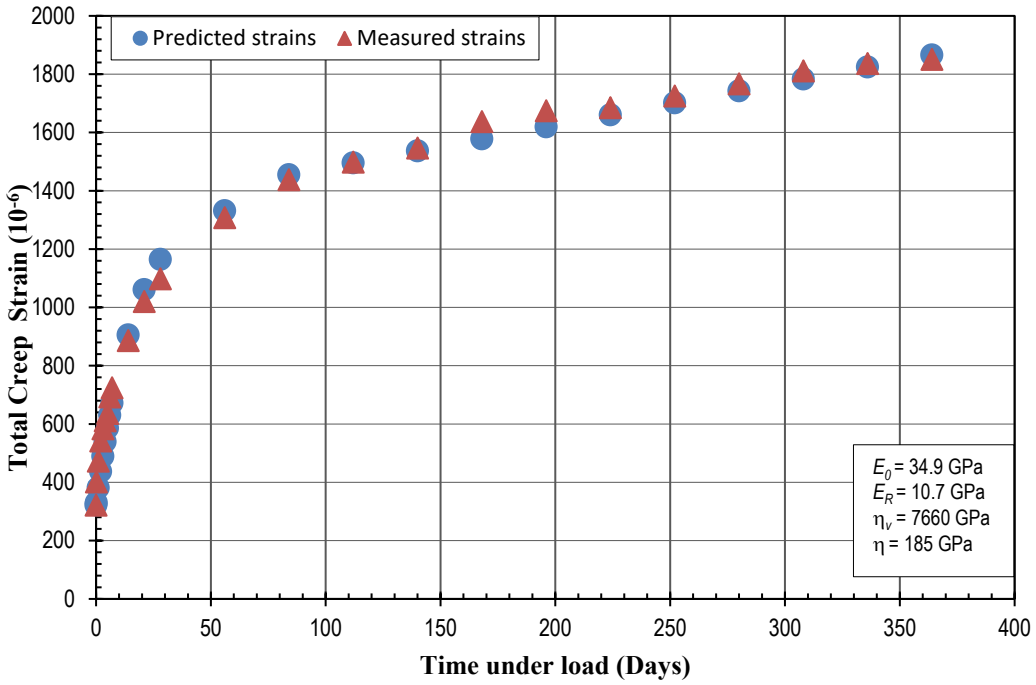

Figure 6.14: Predicted and measured total creep strain for reference concrete

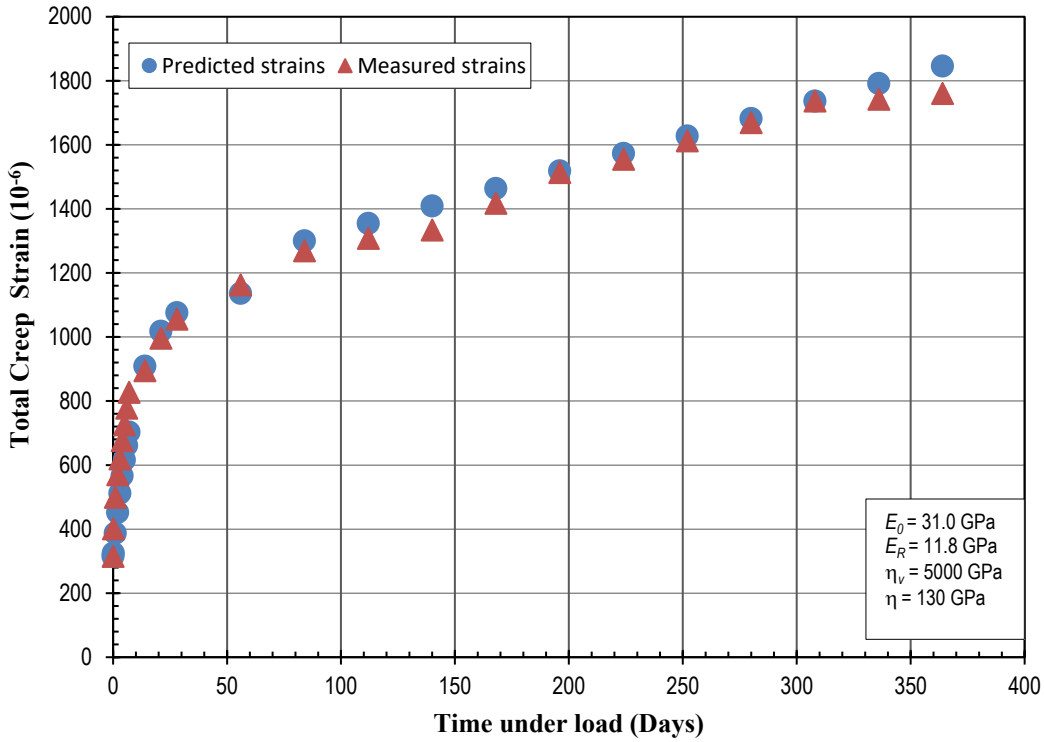

Figure 6.15: Predicted and measured total creep strain for M8 concrete

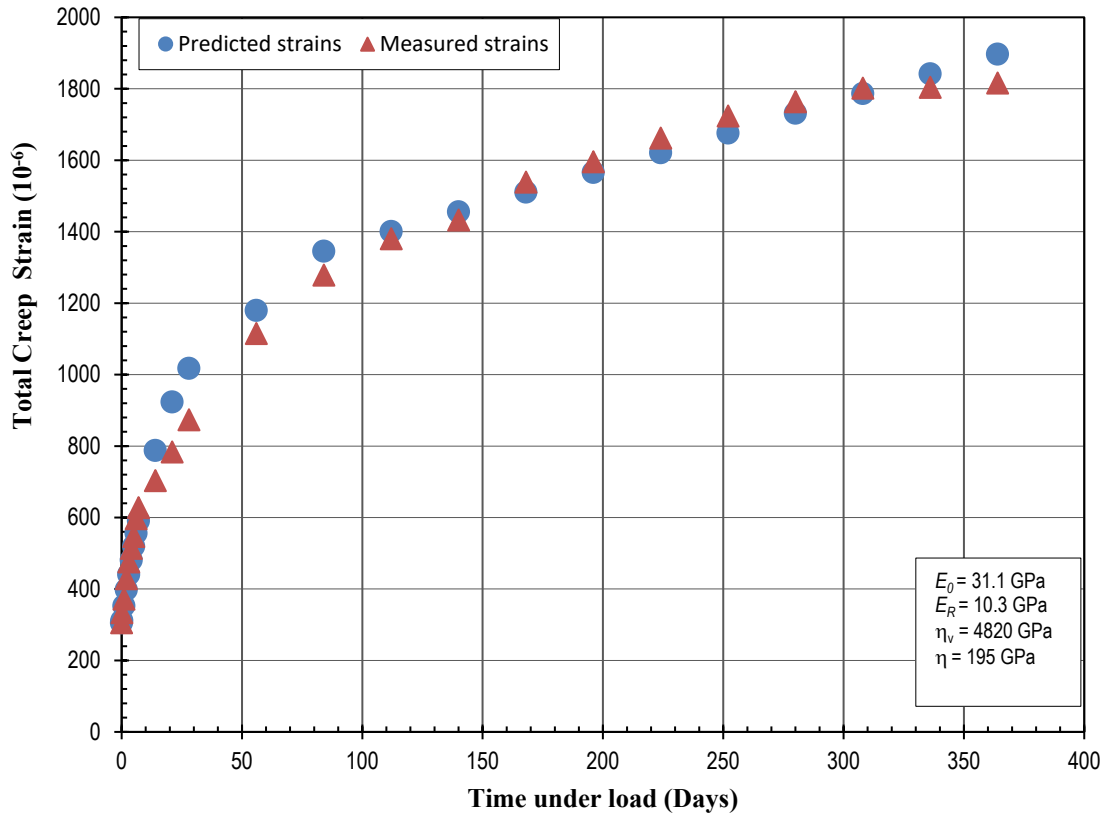

Figure 6.16: Predicted and measured total creep strain for M16 concrete

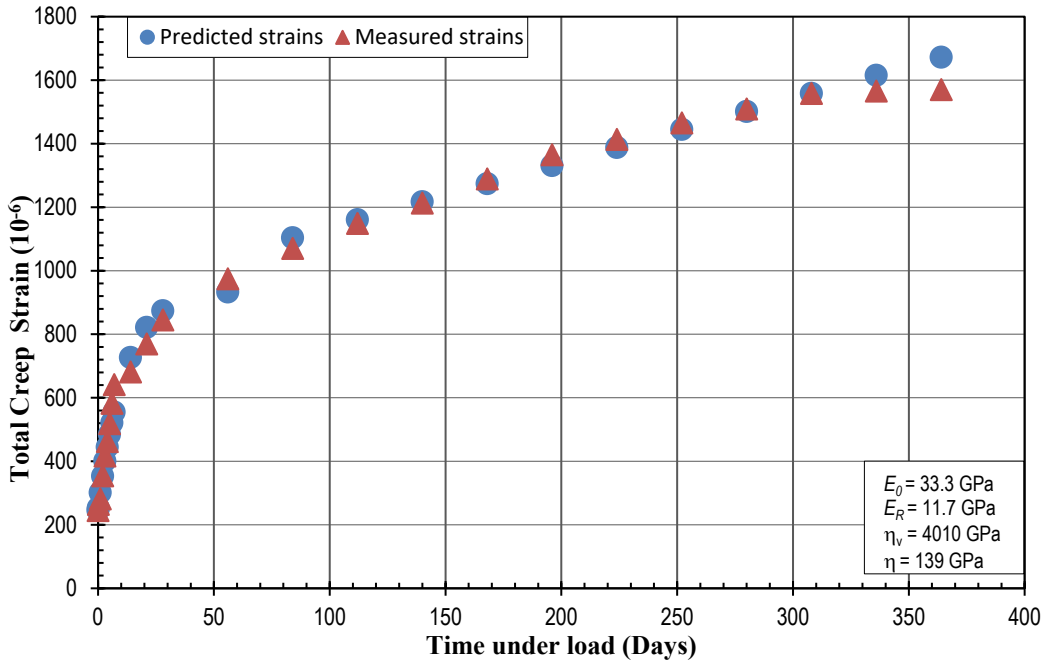

Figure 6.17: Predicted and measured total creep strain for M40 concrete

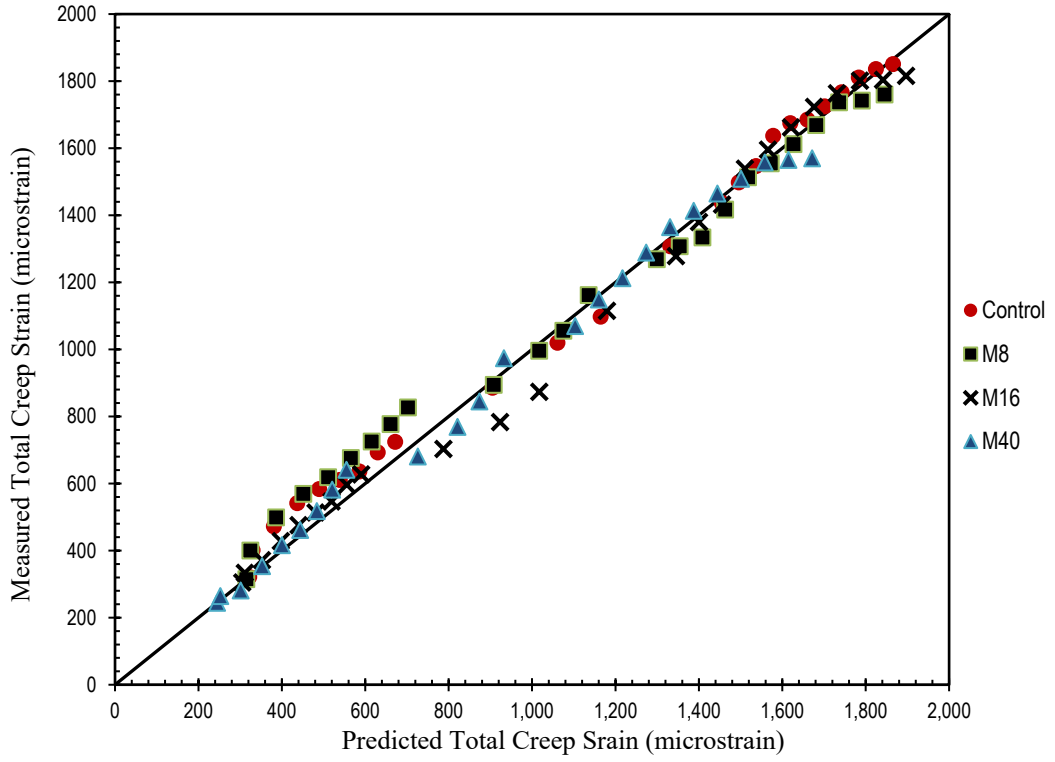

Figure 6.18: Line of equality for reference and rubberised total creep

6.4 CREEP MODELLING SUMMARY

The Burgers rheological model was applied to the measured creep strains for normal and rubberised concrete with 3 different crumb rubber sizes, the following is a summary of observations and conclusions.

- The model can not be applied the same way for both basic and total creep. The model components apply at different stages for the different creeps.
- Based on the Burgers model, basic creep is dominated by viscous component while total creep is dominated by visco-elastic component.
- The model can be successfully used to predict both basic and total creep.
- The model shows that rubberised concrete fundamentally exhibits the same physical behaviour as plain normal strength concrete under sustained loading.

CHAPTER SEVEN: CONCLUSIONS & RECOMMENDATIONS

7.1 INTRODUCTION

The main objective of the research was to investigate the effect of crumb tyre rubber particles on the shrinkage and creep deformation of concrete. The motivation for the research was the increasing interest in the use of rubberised concrete for structural applications. Time-dependent deformations are some of the most crucial hardened concrete properties that must be known before a material can confidently used for structural applications. This aspect of the rubberised concrete behaviour has however not been adequately researched to give confidence to the application of the material for this intended use, hence the need for this research.

The main observations and conclusions of the investigations to better understand the time-dependent behaviour of the rubberised concrete are summarised in this chapter. The observations and conclusions are presented in order of significance, starting with the primary outcomes ending with the secondary outcomes that support the primary outcomes. Therefore, time-dependent deformations test outcomes are presented first, followed by crumb tyre rubber characteristics affecting concrete performance and then the other mechanical properties of concrete. The concluding section of this chapter provides recommendations for further research gaps identified in the course of this research.

7.2 CONCLUSIONS

7.2.1 Time-dependent deformation of structural rubberised concrete

The primary investigation of characterising time-dependent deformations in rubberised concrete revealed some clear patterns relating to crumb tyre rubber particle size. In all instances, the response of the concrete with respect to time-dependent deformation characteristics to the inclusion of crumb tyre rubber was similar largely due to the concrete changes at a meso and micro level as summarised in the following sections.

a) Shrinkage characteristics of structural rubberised concrete

Autogeous shrinkage results showed that crumb tyre rubber increased the overall autogenous shrinkage strains of concrete. It was found that finer crumb rubber particles (<2.36 mm) result in higher shrinkage (≥10%) than coarser crumb rubber particles (≥ 2.36 mm). The rubberised concrete autogenous shrinkage rates are initially lower than for plain concrete but gradually increase to be much higher (>10%) at later stages (>150 days). The observed changes in the autogenous shrinkage characteristics due to the inclusion of the crumb tyre rubber particles in concrete are attributed to

i. the reduction in the restraining effect of the aggregates due to the low stiffness of the rubber particles,
ii. the lower water absoption of the rubber particles, which reduces the amount of water available for internal curing of concrete over a longer period of time.

iii. the rugged and irregular shape of the crumb rubber particles which increases concrete porosity makes it more compressible and also eases the removal of water from the concrete.

Drying shrinkage results showed that crumb tyre rubber generally increases the drying shrinkage of concrete. Similar to autogenous shrinkage, finer crumb tyre rubber particles are also found to increase drying shrinkage strains in concrete. The main cause of the increase in rubberised concrete drying shrinkage is the higher concrete porosity induced by the finer crumb rubber particles, which create voids in concrete due to their shape. The higher porosity makes water-loss to the environment through evaporation easier after being removed from the capillary pores. In addition, the increased porosity reduces the stiffness of the hardened cement paste making it more compressible allowing it to contract more easily.

The autogenous and drying shrinkage deformations are affected more by the crumb tyre rubber development of voids in the concrete. This is confirmed by the lower shrinkage strains observed for rubberised concrete with the coarse crumb rubber particles (2.36 mm), which develops less voids relative to the finer crumb tyre rubber (<2.36 mm).

The expressions for calculating the expected autogenous and drying shrinkage for rubberised concrete with crumb tyre rubber size no greater than 2.36 mm at a 10% fine aggregate replacement level by volume is given in Equations 7.1 and 7.2:

$$\varepsilon_{a\,(rub)}(t) = 1.2\,\varepsilon_{a\,(ref)}(t), \qquad (t > 7\ days) \ldots\ldots\ldots\ldots\ldots \text{Eqn. 7.1}$$

$\varepsilon_{d\,(rub)}(t) = 1.15\ \varepsilon_{d\,(ref)}(t)$, $(t > 7\ days)$……..Eqn. 7.2

where:

$\varepsilon_{a\,(rub)}\ (t)$ – Rubberised concrete autogenous shrinkage strain

$\varepsilon_{d\,(rub)}\ (t)$ - Rubberised concrete drying shrinkage strain

$\varepsilon_{a\,(ref)}\ (t)$ – Plain concrete autogenous strain

$\varepsilon_{d\,(ref)}\ (t)$ – Plain concrete drying shrinkage strain

The expressions illustrate the quantitative implications of the conclusions discussed in this section with regards to crumb tyre rubber particle effect on shrinkage strains. It can also be deduced from the conclusions that shrinkage strains for rubberised concrete can be limited by using coarser rubber particles (>2.36 mm).

b) Creep deformation of structural rubberised concrete

Basic creep results showed that rubberised concrete specific basic creep is higher than for plain concrete. Finer crumb tyre rubber particles (<2.36 mm) were found to result in higher specific basic creep than coarser crumb tyre rubber particles (2.36 mm). The increases are attributted to the reduced restraining effect of the aggregate, due to the low tyre rubber stiffness, and the lower hardened cement paste (HCP) stiffness, due to the increased porosity.

Similarly, total creep results showed that crumb tyre rubber particles increase the specific total creep of concrete. The use of finer crumb rubber particles results in higher specific total creep compared to the coarser crumb rubber particles. This is attributed to a number of factors, namely; the lower aggregate restraint due to low

rubber agregate stiffness, the increase in concrete porosity which eases viscous out-flow of capillary water and also reduces the HCP stiffness.

The expressions for calculating the expected basic and total specific creep for rubberised concrete with crumb tyre rubber size not greater than 2.36 mm at a 10% fine aggregate replacement level by volume is given in Equations 7.3 and 7.4:

$$\varepsilon_{bsp\,(rub)}(t) = 1.25\,\varepsilon_{bsp\,(ref)}(t), \qquad (t > 28 \text{ days}) \ldots\ldots\ldots \text{Eqn. 7.3}$$

$$\varepsilon_{tsp\,(rub)}(t) = 1.2\,\varepsilon_{tsp\,(ref)}(t), \qquad (t > 28 \text{ days}) \ldots\ldots\ldots\ldots \text{Eqn. 7.4}$$

where

$\varepsilon_{bsp\,(rub)}(t)$ – Rubberised concrete basic specific creep

$\varepsilon_{tsp\,(rub)}(t)$ – Rubberised concrete total specific creep

$\varepsilon_{bsp\,(ref)}(t)$ – Plain concrete basic specific creep

$\varepsilon_{tsp\,(ref)}(t)$ – Plain concrete total specific creep

The expressions illustrate the quantitative implications of the conclusions discussed in this section with regards to crumb tyre rubber particle effect on creep deformation. It can also be deduced from the conclusions that creep strains for rubberised concrete can be limited by using coarser rubber particles (>2.36 mm). In fact, when expressing creep in terms of creep coefficient, coarser crumb tyre rubber particles show even lower figures than plain concrete. In addition, rheological modelling also confirmed that crumb tyre rubber does not fundamentally alter the time dependent deformation characteristics of concrete. Basically, the rheological components used to describe creep of plain concrete can be successfully used for rubberised concrete.

c) Creep and shrinkage induced micro-cracking characteristics of structural rubberised concrete

Flourescent microscopy results showed that the increase in shrinkage and creep deformation does not result in increased micro-cracking of concrete. In terms of time dependent deformation induced micro-cracking there was no observable difference in the internal appearance of both plain concrete and the rubberised concrete. This means that the time-dependent deformation of rubberised concrete are comparable with plain concrete deformations therefore the use of rubberised concrete is not limited in use with respect to micro-cracking.

7.2.2 Effect of properties of crumb rubber on time dependent deformation characteristics of rubberised structural concrete

The characterisation of crumb tyre rubber particles showed that smaller sized crumb rubber particles are irregularly shaped, rugged-edged and have a rough surface texture in contrast to the bigger crumb rubber particles that are regularly shaped, have clean cut edges and smoother surface texture. The shape and texture of the crumb rubber is responsible for the increased porosity of the concrete which increases the time-dependent deformations in concrete by firstly reducing the stiffness of the HCP and secondly, by enhancing mechanisms by which water is lost in the concrete during shrinkage and creep. The other tyre rubber property found to be of consequence in the investigation is the stiffness of the rubber, which limits the ability of the crumb tyre rubber to act as a restraint in the concrete during deformation. These conclusions imply that concrete properties sensitive to porosity and fine aggregate stiffness will be significantly affected by the use of crumb tyre rubber in concrete.

7.2.3 Strength and stiffness characteristics of structural rubberised concrete

(a) Compressive strength of rubberised concrete

Crumb tyre rubber negatively affects the compressive strength of concrete. Compressive strength of concrete decreases with reduction in crumb tyre rubber sizes and an increase in crumb tyre rubber content. The strength reduction is attributed to the increased concrete porosity, reduced rubber-paste bond and the low crumb tyre rubber stiffness. These observations imply that the use of rubberised concrete is feasible only to the extent to which replacement levels as well as particle sizes can be limited.

(b) Stiffness of rubberised concrete

The elastic modulus results showed that crumb tyre rubber significantly reduces the elastic modulus of the concrete. Concrete stiffness is not very sensitive to crumb rubber size as the stiffness results showed comparable reductions. The reduction in concrete stiffness is attributed to the increased concrete porosity and the low crumb tyre rubber stiffness.

7.2.4 Significance and practical implications of the study

The use of rubberised concrete for structural purposes has been hindered by the lack of data on the long-term behaviour of the rubberised concrete under sustained loading in a drying environment. The general sentiment has been that rubberised concrete would most likely result in excessive deformations that would render it undesirable for structural applications. This study has shown that rubberised

concrete can be optimised to limit time dependent deformations to acceptable levels which would allow it to be used for structural purposes without the use of admixtures. The study has also quantified the extent to which crumb rubber particles will affect creep determination calculations in structural design. The other concern with the use of rubberised concrete has been the perception that creep deformation manifestations would be different requiring special models and analysis tools to simulate it. This study has shown that already existing rheological models can be used to simulate creep deformation of rubberised concrete. This study having provided guidance on the use of rubberised concrete for time-dependent deformation sensitive applications, it is envisaged that there will be a wider acceptance of the use of the material. This will go a long way in also alleviating the scourge of tyre waste as civil engineering concstruction has the potential of absorbing a very large proportion of this waste.

7.3 RECOMMENDATIONS

Due to the limited scope as a result of time and financial constraints some aspects of interest that arose during the research could not be pursued. This highlighted some areas further research in the following:

i. A five-year time dependent monitoring study of rubberised concrete for a wider range of crumb rubber sizes to better understand the effect of size over a longer period of time.
ii. Investigate the recovery phase of the time dependent deformation of rubberised concrete to fully understand aspects affected by the inclusion of rubber.

iii. Extensive microstructural analysis of rubberised concrete undergoing time dependent deformation to better understand the interaction between the rubber and th HCP during deformation.

iv. Investigate the time dependent behaviour of rubberised concrete with different SCMs that are able to refine the pore structure of the concrete inorder to evaluate the effect of porosity.

REFERENCES

Adamu, M., Mohammed, B.S., Liew, M.S., 2018. Effect of crumb rubber and nano silica on the creep and drying shrinkage of roller compacted concrete pavement. Int. J. GEOMATE 15, 58–65.

Aiello, M.A., Leuzzi, F., 2010. Waste tyre rubberized concrete: Properties at fresh and hardened state. Waste Manag. 30, 1696–1704. https://doi.org/10.1016/j.wasman.2010.02.005

Albano, C., Camacho, N., Reyes, J., Feliu, J.L., Hernández, M., 2005. Influence of scrap rubber addition to Portland I concrete composites: Destructive and non-destructive testing. Compos. Struct. 71, 439–446. https://doi.org/10.1016/j.compstruct.2005.09.037

Alexander, M., Beushausen, H., 2009. Deformation and volume change of hardened concrete, in: Owens, G. (Ed.), Fulton's Concrete. Cement & Concrete Institute, Midrand, South Africa, pp. 111–154.

Alexander, M., Mindess, S., 2015. Aggregates in Concrete. Taylor & Francis, London and New York.

Alexander, M.G., 1994. Deformation properties of blended cement concretes containing blastfurnace slag and condensed silica fume. Adv. Cem. Res. 6, 73–81. https://doi.org/10.1680/adcr.1994.6.22.73

Alexander, M.G., Davis, D.E., 1992. The influence of aggregates on the compressive strength and elastic modulus of concrete. Civ. Eng. South Afr. 34, 161–170.

Ali, F., Khan, M.A., Qurashi, M.A., Shah, S.A.R., Khan, N.M., Khursheed, Z., Rahim, H.S., Arshad, H., Farhan, M., Waseem, M., 2020. Utilization of

Pyrolytic Carbon Black Waste for the Development of Sustainable Materials. Processes 8, 174. https://doi.org/10.3390/pr8020174

Alsaif, A., Koutas, L., Bernal, S.A., Guadagnini, M., Pilakoutas, K., 2018. Mechanical performance of steel fibre reinforced rubberised concrete for flexible concrete pavements. Constr. Build. Mater. 172, 533–543. https://doi.org/10.1016/j.conbuildmat.2018.04.010

American Concrete Institute, 2017. 233R-17: Guide to the Use of Slag Cement in Concrete and Mortar.

American Concrete Institute, 2005. ACI 209.1 R-2 Report on Factors Affecting Shrinkage and Creep of Hardened Concrete.

American Concrete Institute, 2000. ACI 116R-00 Cement and Concrete Terminology.

Arreguia, I.I., 2017. New approaches to recycling tyres needed. The Herald.

Arthur, E., Prosper Dorfiah, Inga Hilbert, Vincent Nartey Kyere, Paul Kwesi Ocran, 2020. Waste tyre management: Baseline Study for Ghana. Sustainable Recycling Industries.

Asadi, I., Shafigh, P., Abu Hassan, Z.F.B., Mahyuddin, N.B., 2018. Thermal conductivity of concrete – A review. J. Build. Eng. 20, 81–93. https://doi.org/10.1016/j.jobe.2018.07.002

ASTM International, 2015. ASTM C512 / C512M-15, Standard Test Method for Creep of Concrete in Compression.

ASTM International, 2013. C642: Test Method for Density, Absorption, and Voids in Hardened Concrete. https://doi.org/10.1520/C0642-13

Atahan, A.O., Sevim, U.K., 2008. Testing and comparison of concrete barriers containing shredded waste tire chips. Mater. Lett. 62, 3754–3757. https://doi.org/10.1016/j.matlet.2008.04.068

Azevedo, F., Pacheco-Torgal, F., Jesus, C., Barroso de Aguiar, J.L., Camões, A.F., 2012. Properties and durability of HPC with tyre rubber wastes. Constr. Build. Mater. 34, 186–191. https://doi.org/10.1016/j.conbuildmat.2012.02.062

Balaha, M., Badawy, A., Hashish, M., 2007. Effect of using ground waste tire rubber as fine aggregate on the behaviour of concrete mixes. Indian J. Eng. Mater. 14, 427–435.

Ballim, Y., 1983. The concrete making properties of andesite lavas from the Langeleven formation of the Ventersdorp Supergroup (MSc). University of the Witwatersrand, Johannesburg.

Banzibaganye, G., 2014. Investigation of the use of waste tyre shreds in reinforcement of sandy soils in South Africa (MSc). University of Cape Town.

Barnes, H.A., 2000. A handbook of elementary rheology. Univ. of Wales, Institute of Non-Newtonian Fluid Mechanics, Aberystwyth.

Bažant, Z.P., Cusatis, G., Cedolin, L., 2004. Temperature Effect on Concrete Creep Modeled by Microprestress-Solidification Theory. J. Eng. Mech. 130, 691–699. https://doi.org/10.1061/(ASCE)0733-9399(2004)130:6(691)

Bažant, Z.P., Hauggaard, A.B., Baweja, S., Ulm, F.-J., 1997. Microprestress-solidification theory for concrete creep. I: Aging and drying effects. J.

Eng. Mech. 123, 1188–1194. https://doi.org/10.1061/(ASCE)0733-9399(1997)123:11(1188)

Bažant, Z.P., Panula, L., 1984. Practical prediction of creep and shrinkage of high strength concrete. Matér. Constr. 17, 375–378. https://doi.org/10.1007/BF02478710

Bazant, Z.P., Xi, Y.-P., 1994. Drying creep of concrete constitutive model and new experiments separating its mechanisms. Mater. Struct. 27, 3–14.

Bentz, D.P., Jensen, O.M., 2004. Mitigation strategies for autogenous shrinkage cracking. Cem. Concr. Compos. 26, 677–685. https://doi.org/10.1016/S0958-9465(03)00045-3

Bhatt, B., 2017. Experimental Study of Crumb Rubber in Concrete. GRD J. Eng. 2, 5.

Biel, T., Lee, H., 1996. Magnesium Oxychloride Cement Concrete with Recycled Tire Rubber. Transp. Res. Rec. 1561, 6–12. https://doi.org/10.3141/1561-02

Bisschop, J., van Mier, J.G.M., 2002. Effect of aggregates on drying shrinkage microcracking in cement-based composites. Mater. Struct. 35, 453–461.

Bissonnette, B., Pierre, P., Pigeon, M., 1999. Influence of key parameters on drying shrinkage of cementitious materials. Cem. Concr. Res. 29, 1655–1662. https://doi.org/10.1016/S0008-8846(99)00156-8

Bjegovic, D., Lakusic, S., Baricevic, A., Serdar, M., Haladin, I., 2013. Innovative use of waste tyres for sustainable concrete technology, in: International Advances in Cement and Concrete Technology in Africa. Presented at the International Advances in Cement and Concrete Technology in Africa,

BAM Federal Institute of Materials Research and Testing, Johannesburg, pp. 535–542.

Blumenthal, M.H., 1996. Producing Ground Scrap Tire Rubber: A Comparison Between Ambient and Cryogenic Technologies, in: 17th Biennial. Presented at the Waste Processing Conference, ASME.

Bompa, D.V., Elghazouli, A.Y., 2019. Creep properties of recycled tyre rubber concrete. Constr. Build. Mater. 209, 126–134. https://doi.org/10.1016/j.conbuildmat.2019.03.127

Bosscher, P.J., Edil, T.B., Eldin, N.N., 1992. Construction and performance of a shredded waste tire test embankment. Transp. Res. Rec. 44–52.

Boudaoud, Z., Beddar, M., 2012. Effects of Recycled Tires Rubber Aggregates on the Characteristics of Cement Concrete. Open J. Civ. Eng. 02, 193–197. https://doi.org/10.4236/ojce.2012.24025

Bravo, M., de Brito, J., 2012. Concrete made with used tyre aggregate: durability-related performance. J. Clean. Prod. 25, 42–50. https://doi.org/10.1016/j.jclepro.2011.11.066

British Standards Institute, 1983. BS 1881-121: Testing concrete. Method for determination of static modulus of elasticity in compression.

Cement Concrete & Aggregates, 2002. Drying Shrinkage of Cement and Concrete.

Cement Concrete and Aggregates, 2005. Plastic Shrinkage Cracking.

Choi, K.-K., Lissel, S.L., Reda Taha, M.M., 2007. Rheological modelling of masonry creep. Can. J. Civ. Eng. 34, 1506–1517. https://doi.org/10.1139/L07-062

Chou, L. H., Lin, C. N., Lu, C. K., Lee, C. H., Lee, M. T., 2010. Improving rubber concrete by waste organic sulfur compounds. Waste Manag. Res. J. Int. Solid Wastes Public Clean. Assoc. ISWA 28, 29–35. https://doi.org/10.1177/0734242X09103843

Chowdhary, P., Sharma, R.K., 2013. Effect of relative humidity on creep-shrinkage behaviour of composite tall buildings. Lat. Am. J. Solids Struct. 10, 571–584. https://doi.org/10.1590/S1679-78252013000300007

Clarke, C., 2009. Concrete shrinkage prediction using maturity and activation energy (MSc). University of Maryland.

Combrinck, R., Boshoff, W., 2009. Plastic Shrinkage Cracking of fresh Concrete (Techincal Report No. ISI2009-3). Institute of Strctural Engineers, Stellenbosch University.

Coutinho, S.A., 1977. A contribution to the mechanism of concrete creep. Matér. Constr. 10, 3–16. https://doi.org/10.1007/BF02473583

Crow, J.M., 2008. The concrete conundrum. Chem. World 5, 62–66.

Davis, H.E., 1940. Autogenous volume change of concrete. Am. Soc. Test. Mater. Proc. 40, 1103–1110.

Davis, H.E., Davis, R.E., Hamilton, J.S., 1934. Plastic flow of concrete under sustained stress. Am. Soc. Test. Mater. Proc. 34, 354–386.

Department of Environmental Affairs, 2012. Integrated Industry Waste Tyre Management Plan of the Recycling and Economic Development Initiative of South Africa, ACT NO. 59 OF 2008.

Dhir, R.K., de Brito, J., Silva, R.V., Lye, C.Q., 2019. 9 - Deformation of Concrete Containing Recycled Concrete Aggregate, in: Dhir, R.K., de Brito, J.,

Silva, R.V., Lye, C.Q. (Eds.), Sustainable Construction Materials, Woodhead Publishing Series in Civil and Structural Engineering. Woodhead Publishing, pp. 283–363. https://doi.org/10.1016/B978-0-08-100985-7.00009-1

Edeskär, T., 2004. Technical and Environmental Properties of Tyre Shreds Focusing on Ground Engineering Applications (Technical Report No. 2004/5). Lulea University of Tachnology.

Elchalakani, M., 2015. High strength rubberized concrete containing silica fume for the construction of sustainable road side barriers. Structures 1, 20–38. https://doi.org/10.1016/j.istruc.2014.06.001

Eldin, N.N., Senouci, A.B., 1993. Rubber-Tire Particles as Concrete Aggregate. J. Mater. Civ. Eng. 5, 478–496. https://doi.org/10.1061/(ASCE)0899-1561(1993)5:4(478)

Esping, O., 2007. Early age properties of self-compacting concrete: effects of fine aggregate and limestone filler (PhD). Chalmers Univ. of Technology, Göteborg.

Evans, A., Evans, R., 2006. The Composition of a Tyre: Typical Components (Technical Report No. TYR0009- 02). The Waste & Resources Action Programme, United Kingdom.

Evans, R.H., Kong, F.K., 1966. Estimation of creep of concrete in R.C and P.C. design. Civ. Eng. Public Works Rev. 61, 593–596.

Ezema, I.C., 2019. Materials, in: Tam, V.W.Y., Le, K.N. (Eds.), Sustainable Construction Technologies. Butterworth-Heinemann, pp. 237–262. https://doi.org/10.1016/B978-0-12-811749-1.00007-9

Fang, G., Bahrami, H., Zhang, M., 2018. Mechanisms of autogenous shrinkage of alkali-activated fly ash-slag pastes cured at ambient temperature within 24 h. Constr. Build. Mater. 171, 377–387. https://doi.org/10.1016/j.conbuildmat.2018.03.155

Fanourakis, G.C., 2011. Validation of International concrete prediction models by application to South African concretes. South Afr. Inst. Civ. Eng. 53, 23–30.

Fanourakis, G.C., Ballim, Y., 2006. The influence of aggregate stiffness on the creep of concrete. Concr. Beton 5–12.

Fathifazl, G., Razaqpur, A.G., 2013. Creep Rheological Models for Recycled Aggregate Concrete. Mater. J. 110, 115–126. https://doi.org/10.14359/51685526

Fiore, A., Marano, G.C., Marti, C., Molfetta, M., 2014. On the Fresh/Hardened Properties of Cement Composites Incorporating Rubber Particles from Recycled Tires. Adv. Civ. Eng. 2014, 1–12. https://doi.org/10.1155/2014/876158

Forrest, M., 2017. Developments in Recycling and Re-use of Waste Rubber (Technical Report No. MPG9). Smithers.

Freyssinet, E., 1936. Une révolution dans les techniques du béton. Librairie de l'Enseignement Technique.

Gesoğlu, M., Güneyisi, E., 2007. Strength development and chloride penetration in rubberized concretes with and without silica fume. Mater. Struct. 40, 953–964. https://doi.org/10.1617/s11527-007-9279-0

Ghedan, R.H., Hamza, D.M., 2011. Effect of Rubber Treatment on Compressive Strength and Thermal Conductivity Of Modified Rubberized Concrete. J. Eng. Dev. 15, 21–29.

Ghuraiz, Y.S., Swellam, M.H., Ragab, A.M., Garas, G.L.K., 2011. The effect of recycled aggregates on creep behavior of structural concrete : Gaza Strip - a case study. J. Emerg. Trends Eng. Appl. Sci. 2, 308–313.

Gilbert, R.I., 1988. Time effects in concrete structures. Elsevier.

Gilbert, R.I., Ranzi, G., 2010. Time-Dependent Behaviour of Concrete Structures. CRC Press.

Glanville, W.H., Collins, A.R., Matthews, D.D., 1947. The Grading of Aggregates and Workability of Concrete, 2nd ed, Department of Scientific and Industrial Research. Road Research Laboratory. Technical Paper. no. 5.

Grieve, G., 1991. The influence of two South African fly ashes on the engineering properties of concrete (PhD). University of the Witwatersrand, Johanesburg.

Güneyisi, E., Gesoğlu, M., Özturan, T., 2004. Properties of rubberized concretes containing silica fume. Cem. Concr. Res. 34, 2309–2317. https://doi.org/10.1016/j.cemconres.2004.04.005

Gupta, T., Chaudhary, S., Sharma, R.K., 2016. Mechanical and durability properties of waste rubber fiber concrete with and without silica fume. J. Clean. Prod. 112, 702–711. https://doi.org/10.1016/j.jclepro.2015.07.081

Gupta, T., Chaudhary, S., Sharma, R.K., 2014. Assessment of mechanical and durability properties of concrete containing waste rubber tire as fine

aggregate. Constr. Build. Mater. 73, 562–574. https://doi.org/10.1016/j.conbuildmat.2014.09.102

Haibo, Z., Mifeng, G.O.U., Xiaoxing, L.I.U., Xuemao, G., 2014. Effect of Rubber Particle Modification on Properties of Rubberized Concrete. J. Wuhan Univ. Technol. Sci. Ed. 763–768.

Han, N., 1996. Time Dependent Behaviour of High Strength Concrete (PhD). Delft University of Technology.

Hansen, T.C., Mattock, A.H., 1966. Influence of Size and Shape of Member on the Shrinkage and Creep of Concrete. J. Proc. 63, 267–290. https://doi.org/10.14359/7622

He, L., Ma, Y., Liu, Q., Mu, Y., 2016. Surface modification of crumb rubber and its influence on the mechanical properties of rubber-cement concrete. Constr. Build. Mater. 120, 403–407. https://doi.org/10.1016/j.conbuildmat.2016.05.025

Heitzman, M., 1992. Design and Construction of Asphalt paving materials with crumb rubber, in: Kassabian, N. (Ed.), Recycled Tire Rubber in Asphalt Pavements, Transportation Research Record. Transportation Research Board, National Research Council, Washington, D.C, pp. 1–8.

Hernández-Olivares, F., Barluenga, G., 2004. Fire performance of recycled rubber-filled high-strength concrete. Cem. Concr. Res. 34, 109–117. https://doi.org/10.1016/S0008-8846(03)00253-9

Hobbs, D.W., 1971. The dependence of the bulk modulus, Young's modulus, creep, shrinkage and thermal expansion of concrete upon aggregate

volume concentration. Matér. Constr. 4, 107–114. https://doi.org/10.1007/BF02473965

Hobbs, D.W., Parrott, L.J., 1979. Prediction of drying shrinkage. Cem. Concr. Assoc. 13, 19–24.

Holmes, N., Browne, A., Montague, C., 2014. Acoustic properties of concrete panels with crumb rubber as a fine aggregate replacement. Constr. Build. Mater. 73, 195–204. https://doi.org/10.1016/j.conbuildmat.2014.09.107

Holt, E., 2001. Early age autogenous shrinkage (Technical Report No. Espoo 2001). Technical Research Centre of Finland.

Hooton, D., Stanish, K., Prusinski, J., 2014. The Effect of Ground, Granulated Blast Furnace Slag (Slag Cement) on the Drying Shrinkage of Concrete-A Critical Review of the Literature, in: Eighth CANMET/ACI Eighth CANMET/AC. Presented at the Fly Ash, Silica Fume, Slag and Natural Pozzolans in Concrete.

Howells, R.W., Lark, R.J., Barr, B.I.G., 2005. A sensitivity study of parameters used in shrinkage and creep prediction models. Mag. Concr. Res. 57, 589–602. https://doi.org/10.1680/macr.2005.57.10.589

Hsu, T., 1965. Inelastic behavior of concrete under short time loading (Technical Report No. 322), Colloquim on the Nature of Inelasticity of Concrete and its Structural Effects. Cornwell University, New York.

Huang, B., Shu, X., Cao, J., 2013. A two-staged surface treatment to improve properties of rubber modified cement composites. Constr. Build. Mater., Special Section on Recycling Wastes for Use as Construction Materials 40, 270–274. https://doi.org/10.1016/j.conbuildmat.2012.11.014

ISO, 2012. ISO 1382: Rubber - Vocabulary.

ISO Technical Committee, 2016. Strategic business plan (Techincal Report No. ISO/TC 71). International Organization for Standardization.

Jain, S., 2014. To Study on Waste Tyre Rubber as Concrete. Int. J. Res. Eng. Technol. Manag. 1–4.

Janotka, I., Martauz, P., Bačuvčík, M., 2021. Design of Concrete Made with Recycled Brick Waste and Its Environmental Performance. Minerals 11, 463–483. https://doi.org/10.3390/min11050463

Jedidi, M., Boulila, A., Benjeddou, O., Soussi, C., 2014. Crumb Rubber Effect on Acoustic Properties of Self-Consolidating Concrete. Int. J. Therm. Environ. Eng. 8, 69–76.

Jensen, R.S., Richart, F.E., 1938. Short-Time Creep Test of Concrete in Compression, in: ASTM Proceedings. pp. 410–417.

Kara De Maeijer, P., Craeye, B., Blom, J., Bervoets, L., 2021. Crumb Rubber in Concrete—The Barriers for Application in the Construction Industry. Infrastructures 6, 116–136. https://doi.org/10.3390/infrastructures6080116

Kardos, A.J., Durham, S.A., 2015. Strength, durability, and environmental properties of concrete utilizing recycled tire particles for pavement applications. Constr. Build. Mater. 98, 832–845. https://doi.org/10.1016/j.conbuildmat.2015.08.065

Kelly, P., 2019. Rheological Models, in: Introduction to Solid Mechanics. University of Auckland, pp. 292–301.

Khairallah, R.S., 2009. Analysis of Autogenous and Drying Shrinkage of Concrete (MSc). McMaster University.

Khalaf, F.M., 2004. Recycling of clay bricks as aggregate in asphalt concrete, in: Proceedings of International RILEM Conference on the Use of Recycled Materials in Buildings and Structures, Barcelona, Spain. pp. 56–65.

Khaloo, A.R., Dehestani, M., Rahmatabadi, P., 2008. Mechanical properties of concrete containing a high volume of tire–rubber particles. Waste Manag., Pay as you throw: a tool fo urban waste management 28, 2472–2482. https://doi.org/10.1016/j.wasman.2008.01.015

Khatib, Z.K., Bayomy, F.M., 1999. Rubberized Portland Cement Concrete. J. Mater. Civ. Eng. 11, 206–213. https://doi.org/10.1061/(ASCE)0899-1561(1999)11:3(206)

Kim, H.K., Lee, H.K., 2010. Influence of cement flow and aggregate type on the mechanical and acoustic characteristics of porous concrete. Appl. Acoust. 71, 607–615. https://doi.org/10.1016/j.apacoust.2010.02.001

Kocak, S., 2016. Interaction between recycled tire rubber, polymers and high amount of reclaimed asphalt pavements (PhD). Michigan State University.

Kotresh, K., Belachew, M.G., 2014. Study On Waste Tyre Rubber As Concrete Aggregates. Int. J. Sci. Eng. Technol. 3, 433–436.

Lee, H.S., Lee, H., Moon, J.S., Jung, H.W., 1998. Development of Tire Added Latex Concrete. ACI Mater. J. 95. https://doi.org/10.14359/378

L'Hermite, R., 1959. What do we know about plastic deformation and creep of concrete? RILEM Bull. 21–25.

Li, D., Xiao, J., Zhuge, Y., Mills, J.E., Senko, H., Ma, X., 2020a. Experimental study on crumb rubberised concrete (CRC) and reinforced CRC slabs

under static and impact loads. Aust. J. Struct. Eng. 21, 294–306. https://doi.org/10.1080/13287982.2020.1809811

Li, D., Zhuge, Y., Gravina, R., Benn, T., Mills, J.E., 2020b. Creep and drying shrinkage behaviour of crumb rubber concrete (CRC). Aust. J. Civ. Eng. 18, 187–204. https://doi.org/10.1080/14488353.2020.1761510

Li, G., Wang, Z., Leung, C.K.Y., Tang, S., Pan, J., Huang, W., Chen, E., 2016. Properties of rubberized concrete modified by using silane coupling agent and carboxylated SBR. J. Clean. Prod. 112, 797–807. https://doi.org/10.1016/j.jclepro.2015.06.099

Li, L., Ruan, S., Zeng, L., 2014. Mechanical properties and constitutive equations of concrete containing a low volume of tire rubber particles. Constr. Build. Mater. 70, 291–308. https://doi.org/10.1016/j.conbuildmat.2014.07.105

Li, Y., Zhang, X., Wang, R., Lei, Y., 2019. Performance enhancement of rubberised concrete via surface modification of rubber: A review. Constr. Build. Mater. 227, 116691. https://doi.org/10.1016/j.conbuildmat.2019.116691

Lopez, M., 2005. Creep and Shrinkage of High Performance Lightweight Concrete: A Multi-Scale Investigation (PhD). Georgia Institute of Technology.

Lura, P., Jensen, O.M., van Breugel, K., 2003. Autogenous shrinkage in high-performance cement paste: An evaluation of basic mechanisms. Cem. Concr. Res. 33, 223–232. https://doi.org/10.1016/S0008-8846(02)00890-6

Lynam, C.G., 1934. Growth and movement in portland cement concrete. Oxford University Press, London.

Ma, Q.W., Yue, J.C., 2013. Effect on Mechanical Properties of Rubberized Concrete due to Pretreatment of Waste Tire Rubber with NaOH. Appl. Mech. Mater. 357–360, 897–904. https://doi.org/10.4028/www.scientific.net/AMM.357-360.897

Mahlangu, M.L., 2009. Waste tyre management problems in South Africa and the possible opportunities that can be created through the recycling thereof (MSc). University of South Africa.

Malladi, K.S., 2004. Studies on rubberized cement concrete (MSc). Indian Instisute of Technology Kharagpur, India.

Maney, G.A., 1941. Concrete under sustained working loads. Evidence that shrinkage dominates time yield. ASTM 41, 1021–1030.

Marques, A.C., Akasaki, J.L., Trigo, A.P.M., Marques, M.L., 2008. Influence of the surface treatment of tire rubber residues added in mortars. Ibracon Struct. Mater. J. 1, 113–120.

Mavroulidou, M., Figueiredo, J., 2010. Discarded tyre rubber as concrete aggregate: a possible outlet for used tyres. Glob. NEST J. 12, 359–367.

Maxxis Tires, 2018. How a Tire is Made [WWW Document]. URL https://www.maxxis.com/technology/how-a-tire-is-made (accessed 4.19.18).

McDonald, M., 2009. Control of concrete quality, in: Owens, G. (Ed.), Fulton's Concrete. Cement & Concrete Institute, Midrand, South Africa, pp. 111–154.

McNeil, K., Kang, T.H.-K., 2013. Recycled Concrete Aggregates: A Review. Int. J. Concr. Struct. Mater. 7, 61–69. https://doi.org/10.1007/s40069-013-0032-5

Mead, N.V., 2019. A brief history of concrete: from 10,000BC to 3D printed houses. The Guardian.

Mehta, K.P., Monteiro, P.J.M., 2014. Concrete: Microstructure, Properties, and Materials, 4th ed. McGraw-Hill.

Meyers, B.L., 1967. Time-dependent strains and microcracking of plain concrete (PhD). Cornell University, New York.

Mezger, T.G., 2006. The Rheology Handbook: For Users of Rotational and Oscillatory Rheometers. Vincentz Network GmbH & Co KG.

Mindess, S., Young, F.J., Darwin, D., 2003. Concrete, 2nd ed. Prentice Hall.

Mmereki, D., Machola, B., Mokokwe, K., 2019. Status of waste tires and management practice in Botswana. J. Air Waste Manag. Assoc. 69, 1230–1246. https://doi.org/10.1080/10962247.2017.1279696

Mohammadi, I., Khabbaz, H., 2015. Shrinkage Performance of Crumb Rubber Concrete Prepared by Water-soaking Treatment Method for Rigid Pavements. Cem. Concr. Compos. 62, 106–116.

Mohammadi, I., Khabbaz, H., Vessalas, K., 2016. Enhancing mechanical performance of rubberised concrete pavements with sodium hydroxide treatment. Mater. Struct. 49, 813–827. https://doi.org/10.1617/s11527-015-0540-7

Mohammed, B.S., Anwar Hossain, K.M., Eng Swee, J.T., Wong, G., Abdullahi, M., 2012. Properties of crumb rubber hollow concrete block. J. Clean. Prod. 23, 57–67. https://doi.org/10.1016/j.jclepro.2011.10.035

Moonen, P., Pedersen, R.R., Simone, A., Sluys, L.J., Carmeliet, J., 2008. Mesoscopic analysis of drying shrinkage damage in a cementitious material. Presented at the Concrete Modelling CONMOD`08 - Proceedings of the International RILEM Symposium, pp. 691–698.

Mors, R.M., 2011. Cementitious materials containing BFS (MSc). Delft University of Technology.

Mushunje, K., Otieno, M., Ballim, Y., 2018a. A review of Waste Tyre Rubber as an Alternative Concrete Consituent Material. MATEC Web Conf. 199, 11003. https://doi.org/10.1051/matecconf/201819911003

Mushunje, K., Otieno, M., Ballim, Y., 2018b. Partial replacement of conventional fine aggregate with crumb tyre rubber in structural concrete – effect of particle size on compressive strength and time dependent deformations. MATEC Web Conf. 199, 11002. https://doi.org/10.1051/matecconf/201819911002

Muzenda, E., 2014. A discussion on waste generation and management trends in South Africa. Int. J. Chem. Environ. Biol. Sci. 2, 105–112.

Nagataki, S., Yonekura, A., 1984. The mechanisms of drying shrinkage and creep of concrete. Concr. Libr. Jpn. Soc. Civ. Eng. 177–191.

Naik, T.R., Singh, S.S., 1991. Utilization of discrded tires as construction materials for transportation facilities (Technical Report No. CBU-1991-

02), Center for By - Products Utilization. The University of Wisconsin, Milwaukee.

National Ready Mixed Concrete Association, 2014. Plastic shrinkage cracking (No. 5), concrete in practice. National Ready Mixed Concrete Association.

Nawa, T., Horita, T., 2005. A mechanism of autogenous shrinkage of cementitious materials, in: Cement Combinations for Durable Concrete. Thomas Telford Publishing, pp. 425–434. https://doi.org/10.1680/ccfdc.34013.0047

Nehdi, M., Khan, A., 2001. Cementitious composites containing recycled tire rubber: an overview of engineering properties and potential applications. Cem. Concr. Aggreg. 23, 3–10.

Nemati, K.M., 2015. Volume changes and creep of concrete, in: Concrete Technology. University of Washington, pp. 1–8.

Neubauer, C.M., Jennings, H.M., Garboczi, E.J., 1997. Mapping drying shrinkage deformations in cement-based materials. Cem. Concr. Res. 27, 1603–1612.

Neville, A.M., 2011. Properties of concrete, 5th ed. ed. Pearson, Harlow, England ; New York.

Neville, A.M., 1964. Creep of concrete as a function of its cement paste content. Mag. Concr. Res. 16, 21–30. https://doi.org/10.1680/macr.1964.16.46.21

Neville, A.M., 1959. Role of Cement in the Creep of Mortar. J. Proc. 55, 963–984. https://doi.org/10.14359/11405

Neville, A.M., 1955. Theories of Creep in Concrete. J. Proc. 52, 47–60. https://doi.org/10.14359/11585

Neville, A.M., Brooks, J.J., Dilger, W.H., 1983. Creep of plain and structural concrete. Construction Press, London ; New York.

Neville, A.M., Dilger, W.H., 1970. Creep of concrete: plain, reinforced, and prestressed. North-Holland Pub. Co, Amsterdam.

Neville, A.M., Meyers, B.L., 1964. Creep of Concrete: Influencing Factors and Prediction. Spec. Publ. 9, 1–33. https://doi.org/10.14359/17218

Nielsen, L.F., 2007. Composite creep analysis of concrete (No. BYG-DTU R-178). Danmarks Tekniske Universitet.

Nissen, T., 2016. Chloride Ingress in Concrete (MSc). Norwegian Universoty of Science and Technology, Trondheim.

Nkosi, N., Muzenda, E., Belaid, M., Mateescu, C., 2021. A Critical Analysis of the Integrated Industry Waste Tyre Management Plan of South Africa. Adv. Sci. Technol. Eng. Syst. J. 6, 1046–1054. https://doi.org/10.25046/aj0602119

Nkosi, N., Zvimba, J., Muzenda, E., Pilusa, J., 2013. The Waste Tyre Problem in South Africa: An Analysis of the REDISA Plan. Presented at the International Conference on Chemical and Environmental Engineering, Johannesburg, pp. 42–46.

Ocholi, A., Ejeh, S.P., Yinka, S.M., 2014. An Investigation into the Thermal Performance of Rubber-Concrete. Acad. J. Interdiscip. Stud. 3, 29–38.

Oikonomou, N., Mavridou, S., 2009. Improvement of chloride ion penetration resistance in cement mortars modified with rubber from worn automobile tires. Cem. Concr. Compos. 31, 403–407. https://doi.org/10.1016/j.cemconcomp.2009.04.004

Onuaguluchi, O., Panesar, D.K., 2014. Hardened properties of concrete mixtures containing pre-coated crumb rubber and silica fume. J. Clean. Prod. 82, 125–131. https://doi.org/10.1016/j.jclepro.2014.06.068

Otieno, M., Mushunje, K., 2021. Creep deformation characteristics of rubberised structural concrete. Constr. Build. Mater. 312, 125418. https://doi.org/10.1016/j.conbuildmat.2021.125418

Owens, G., 2013. Fundamentals of concrete, 3rd ed. Cement and Concrete Institute, Midrand, South Africa.

Özkaya, N., Nordin, M., Goldsheyder, D., Leger, D., 2012. Mechanical Properties of Biological Tissues, in: Fundamentals of Biomechanics. Springer New York, New York, NY, pp. 221–236. https://doi.org/10.1007/978-1-4614-1150-5_15

Pacheco-Torgal, F., Ding, Y., Jalali, S., 2012. Properties and durability of concrete containing polymeric wastes (tyre rubber and polyethylene terephthalate bottles): An overview. Constr. Build. Mater. 30, 714–724. https://doi.org/10.1016/j.conbuildmat.2011.11.047

Panda, K.C., Parhi, P.S., Jena, T., 2012. Scrap-Tyre-Rubber Replacement for Aggregate in Cement Concrete: Experimental Study. Int. J. Earth Sci. Eng., 1 5, 1692–1701.

Park, S.B., Seo, D.S., Lee, J., 2005. Studies on the sound absorption characteristics of porous concrete based on the content of recycled aggregate and target void ratio. Cem. Concr. Res. 35, 1846–1854. https://doi.org/10.1016/j.cemconres.2004.12.009

Pauw, A., 1971. Time-Dependent Deformations of Concrete (Technical Report No. 71–1). University of MIssouri, Columbia.

Pelisser, F., Zavarise, N., Longo, T.A., Bernardin, A.M., 2010. Concrete Made with Recycled Tire Rubber: Effect of Alkaline Activation and Silica Fume Addition. J. Clean. Prod. 1–7.

Pham, N.-P., Toumi, A., Turatsinze, A., 2018. Rubber aggregate-cement matrix bond enhancement: Microstructural analysis, effect on transfer properties and on mechanical behaviours of the composite. Cem. Concr. Compos. 94, 1–12. https://doi.org/10.1016/j.cemconcomp.2018.08.005

Pickett, G., 1956. Effect of aggregate on shrinkage of concrete and hypothesis concerning shrinkage. Portland Cement Association, Chicago.

Pierce, C.E., Blackwell, M.C., 2003. Potential of scrap tire rubber as lightweight aggregate in flowable fill. Waste Manag. 23, 197–208.

Pilkington, B., 2021. Tackling the Global Tire Waste Problem with Pretred [WWW Document]. AZoCleantech. URL https://www.azocleantech.com/article.aspx?ArticleID=1227

Polydorou, T., Constantinides, G., Neocleous, K., Kyriakides, N., Koutsokeras, L., Chrysostomou, C., Hadjimitsis, D., 2020. Effects of pre-treatment using waste quarry dust on the adherence of recycled tyre rubber particles to cementitious paste in rubberised concrete. Constr. Build. Mater. 254, 119325. https://doi.org/10.1016/j.conbuildmat.2020.119325

Rajayogan, V., 2009. Autogenous shrinkage in cementitious systems (PhD). The UNiversity of New Wales, Australia.

Rana, J., Rughooputh, R., 2014. Partial Replacement of Fine Aggregates by Rubber in Concrete. J. Emerg. Trends Eng. Appl. Sci. 5, 312–317.

Rangdale, P., Chandak, K.R., Bagade, G., 2018. Non Pneumatic Tyre. Int. J. Eng. Sci. Res. Technol. 7, 61–68. https://doi.org/10.5281/zenodo.1165624

Rashad, A.M., 2016. A comprehensive overview about recycling rubber as fine aggregate replacement in traditional cementitious materials. Int. J. Sustain. Built Environ. 5, 46–82. https://doi.org/10.1016/j.ijsbe.2015.11.003

Recycling Research Institute, 2017. Scrap Tire News | The source for news and information about the scrap tire and rubber recycling industry. [WWW Document]. URL http://www.scraptirenews.com/crumb.php#manufacturing (accessed 2.16.17).

Reiner, M., 1949. Twelve lectures on theoretical rheology: North-Holland Pub. Co.

Richardson, A., Coventry, K., Dave, U., Pienaar, J., 2011. Freeze/thaw performance of concrete using granulated rubber crumb. J. Green Build. 6, 83–92.

Richardson, A., Coventry, K., Edmondson, V., Dias, E., 2016. Crumb rubber used in concrete to provide freeze–thaw protection (optimal particle size). J. Clean. Prod. 112, 599–606. https://doi.org/10.1016/j.jclepro.2015.08.028

Roeder, R.K., 2013. Mechanical Characterization of Biomaterials, in: Characterization of Biomaterials. Elsevier, pp. 49–104. https://doi.org/10.1016/B978-0-12-415800-9.00003-6

Rostami, H., Lepore, J., Silverstraim, T., Zundi, I., 1993. Use of recycled rubber tires in concrete, in: Proceedings of the International Conference on Concrete 2000. Presented at the Proceedings of the International Conference on Concrete 2000, University of Dundee, Scotland, pp. 391–399.

Roy, S.K., Liam Kok Chye, Northwood, D.O., 1993. Chloride ingress in concrete as measured by field exposure tests in the atmospheric, tidal and submerged zones of a tropical marine environment. Cem. Concr. Res. 23, 1289–1306. https://doi.org/10.1016/0008-8846(93)90067-J

Rubber Manufacturers Association, 2016. 2015 U.S. Scrap Tire Management Summary. Washington.

Ruwona, W., Danha, G., Muzenda, E., 2019. A Review on Material and Energy Recovery from Waste Tyres. Procedia Manuf., The 2nd International Conference on Sustainable Materials Processing and Manufacturing, SMPM 2019, 8-10 March 2019, Sun City, South Africa 35, 216–222. https://doi.org/10.1016/j.promfg.2019.05.029

SAB Standards, 2017. SANS 50197 Cement Part 2: Conformity evaluation.

SAB Standards, 2013. SANS 50197 Cement Part 1: Composition, specifications and conformity criteria for common cements.

Sadiqul Islam, G.M., Gupta, S.D., 2016. Evaluating plastic shrinkage and permeability of polypropylene fiber reinforced concrete. Int. J. Sustain. Built Environ. 5, 345–354. https://doi.org/10.1016/j.ijsbe.2016.05.007

Safiuddin, Md., Alengaram, U.J., Rahman, Md.M., Salam, Md.A., Jumaat, Mohd.Z., 2013. Use of recycled concrete aggregate in concrete: a review.

J. Civ. Eng. Manag. 19, 796–810. https://doi.org/10.3846/13923730.2013.799093

Šahinagić-Isović, M., Bijedić, D., Markovski, G., 2012. Shrinkage strain of concrete - causes and types. Građevinar 64, 727–734.

Savas, B., Ahmad, S., Fedroff, D., 1997. Freeze-Thaw Durability of Concrete with Ground Waste Tire Rubber. Transp. Res. Rec. J. Transp. Res. Board 1574, 80–88. https://doi.org/10.3141/1574-11

Sayahi, F., 2016. Plastic Shrinkage Cracking in Concrete (PhD). Luleå University of Technology, Sweden.

Sebola, M.R., Mativenga, P.T., Pretorius, J., 2018. A Benchmark Study of Waste Tyre Recycling in South Africa to European Union Practice. Procedia CIRP 69, 950–955. https://doi.org/10.1016/j.procir.2017.11.137

Segre, N., Joekes, I., 2000. Use of tire rubber particles as addition to cement paste. Cem. Concr. Res. 30, 1421–1425. https://doi.org/10.1016/S0008-8846(00)00373-2

Segre, N., Monteiro, P.J.M., Sposito, G., 2002. Surface Characterization of Recycled Tire Rubber to Be Used in Cement Paste Matrix. J. Colloid Interface Sci. 248, 521–523. https://doi.org/10.1006/jcis.2002.8217

Sellin, J.-P., Barthélémy, J.-F., Bondonet, G., Torrenti, B.C.& J.-M., 2015. Delayed deformations of concrete structures: The Savines bridge and the Cheviré bridge, in: Pedro Pacheco, Filipe Magalhaes (Eds.), Multi-Span Large Bridges. CRC Press, pp. 21–29.

Sherwood, P.T., 1995. The Use of Waste and Recycled Materials in Roads. Proc. Inst. Civ. Eng. - Transp. 111, 116–124. https://doi.org/10.1680/itran.1995.27579

Shulman, V.L., 2019. Tire Recycling, in: Waste. Elsevier, pp. 489–515. https://doi.org/10.1016/B978-0-12-815060-3.00026-8

Siddique, R., Naik, T.R., 2004. Properties of concrete containing scrap-tire rubber – an overview. Waste Manag. 24, 563–569. https://doi.org/10.1016/j.wasman.2004.01.006

Sinha, D.A., 2012. Thermal Properties of Concrete. Indian J. Res. 3, 90–91. https://doi.org/10.15373/22501991/FEB2014/27

Sohrabi, M.R., Karbalaie, M., 2011. An Experimental Study on the Compressive Strength of Concrete Containing Crumb Rubber. Int. J. Civ. Environ. Eng. 11, 23–27.

Soroushian, P., Ravanbakhsh, S., 1998. Control of plastic shrinkage cracking with specialty cellulose fibers. ACI Mater. J. 95, 429–435.

South African Tyre Recycling Process Company, 2013. SATRP Waste Tyre Industry Plan.

Strukar, K., Kalman Šipoš, T., Miličević, I., Bušić, R., 2019. Potential use of rubber as aggregate in structural reinforced concrete element – A review. Eng. Struct. 188, 452–468. https://doi.org/10.1016/j.engstruct.2019.03.031

Su, H., Yang, J., Ghataora, G.S., Dirar, S., 2015a. Surface modified used rubber tyre aggregates: effect on recycled concrete performance. Mag. Concr. Res. 67, 680–691. https://doi.org/10.1680/macr.14.00255

Su, H., Yang, J., Ling, T.-C., Ghataora, G.S., Dirar, S., 2015b. Properties of concrete prepared with waste tyre rubber particles of uniform and varying sizes. J. Clean. Prod. 91, 288–296. https://doi.org/10.1016/j.jclepro.2014.12.022

Sukontasukkul, P., Tiamlom, K., 2012. Expansion under water and drying shrinkage of rubberized concrete mixed.pdf 29, 520–526.

Sun, X., Wu, S., Yang, J., Yang, R., 2020. Mechanical properties and crack resistance of crumb rubber modified cement-stabilized macadam. Constr. Build. Mater. 259, 119708. https://doi.org/10.1016/j.conbuildmat.2020.119708

Swenson, E.G., Sereda, P.J., 1968. Mechanism of the carbonatation shrinkage of lime and hydrated cement. J. Appl. Chem. 18, 111–117. https://doi.org/10.1002/jctb.5010180404

Taha, M.M.R., El-Dieb, A.S., Abdel-Hameed, M., Abd El-Wahab, M.A., 2008. Mechanical, Fracture, and Microstructural Investigations of Rubber Concrete. J. Mater. Civ. Eng. 20, 640–649. https://doi.org/10.1061/(ASCE)0899-1561(2008)20:10(640)

Taylor, R., 1991. Thermal Conductivity, in: Brook, R. (Ed.), Concise Encyclopedia of Advanced Ceramic Materials. Pergamon, Oxford, pp. 472–475. https://doi.org/10.1016/B978-0-08-034720-2.50130-1

Tazawa, E. (Ed.), 1999. Autogenous shrinkage of concrete: proceedings of the international workshop. Routledge, New York.

Tazawa, E., Miyazawa, S., 1995a. Influence of cement and admixture on autogeneous shrinkage of cement paste. Cem. Concr. Res. 25, 281–287.

Tazawa, E., Miyazawa, S., 1995b. Experimental study on mechanism of autogenous shrinkage of concrete. Cem. Concr. Res. 25, 1633–1638. https://doi.org/10.1016/0008-8846(95)00159-X

Teychenné, D.C., Franklin, R.E., Erntroy, H.C., 1997. Design of normal concrete mixes, 2nd ed, Building Research Establishment. Constructions Research Communications, London.

The Concrete Society, 2021. Non-structural concrete [WWW Document]. URL https://www.concrete.org.uk/fingertips-nuggets.asp?cmd=display&id=5 (accessed 11.25.21).

Thomas, B.S., Gupta, R.C., 2016. A comprehensive review on the applications of waste tire rubber in cement concrete. Renew. Sustain. Energy Rev. 54, 1323–1333. https://doi.org/10.1016/j.rser.2015.10.092

Thomas, B.S., Gupta, R.C., Kalla, P., Cseteneyi, L., 2014. Strength, abrasion and permeation characteristics of cement concrete containing discarded rubber fine aggregates. Constr. Build. Mater. 59, 204–212. https://doi.org/10.1016/j.conbuildmat.2014.01.074

Thomas, B.S., Gupta, R.C., Mehra, P., Kumar, S., 2015. Performance of high strength rubberized concrete in aggressive environment. Constr. Build. Mater. 83, 320–326. https://doi.org/10.1016/j.conbuildmat.2015.03.012

Thomas, F.G., 1937. Creep of concrete under load, in: London Congress. International Association for Testing Materials, pp. 292–294.

Topçu, lker B., Avcular, N., 1997. Analysis of rubberized concrete as a composite material. Cem. Concr. Res. 27, 1135–1139. https://doi.org/10.1016/S0008-8846(97)00115-4

Topçu, İ.B., Demir, A., 2007. Durability of Rubberized Mortar and Concrete. J. Mater. Civ. Eng. 173–178. https://doi.org/10.1061

Torrenti, J.-M., Le Roy, R., 2018. Analysis of some basic creep tests on concrete and their implications for modeling. Struct. Concr. 19, 483–488. https://doi.org/10.1002/suco.201600197

Troxell, G.E., Davis, H.E., Kelly, J.W., 1968. Composition and properties of concrete, 2nd ed, Civil Engineering Series. McGraw-Hill, New York.

Troxell, G.E., Raphael, J.M., Davis, R.E., 1958. Long-Time Creep and Shrinkage Tests of Plain and Reinforced Concrete. ASTM Proceeding 58, 1101–1120.

United Nations, 2012. Basel Convention Technical Guidelines, 2012. Secretariat of the Basel Convention, Châtelaine.

van Breugel, K., van Tuan, N., 2014. Autogenous Shrinkage of HPC and Ways to Mitigate it. Key Eng. Mater. 629–630, 3–20. https://doi.org/10.4028/www.scientific.net/KEM.629-630.3

van Staden, P., 2012. A feasibility study to establish the preferred environmentally-friendly utilisation option in respect of waste tyre materials in South Africa (MBA). University of Stellenbosch.

Vengatesan, M.R., Varghese, A.M., Mittal, V., 2018. Chapter 3 - Thermal properties of thermoset polymers, in: Guo, Q. (Ed.), Thermosets (Second Edition). Elsevier, pp. 69–114. https://doi.org/10.1016/B978-0-08-101021-1.00003-4

Vidal, T., Sellier, A., Ladaoui, W., Bourbon, X., 2013. Effect of temperature on basic creep of High Performance Concretes heated between 20 ° C and 80

° C, in: The 3rd International Conference on Sustainable Construction Materials and Technologies. pp. 20–30.

Wang, J.C., 1984. Young's modulus of porous materials. J. Mater. Sci. 19, 809–814. https://doi.org/10.1007/BF00540452

Watts, J., 2019. Concrete: the most destructive material on Earth. The Guardian.

Wittmann, F.H., 1973. Interaction of Hardened Cement Paste and Water. J. Am. Ceram. Soc. 56, 409–415. https://doi.org/10.1111/j.1151-2916.1973.tb12711.x

Wu, L., Farzadnia, N., Shi, C., Zhang, Z., Wang, H., 2017. Autogenous shrinkage of high performance concrete: A review. Constr. Build. Mater. 149, 62–75. https://doi.org/10.1016/j.conbuildmat.2017.05.064

Xi, Y.-P., Jennings, H.M., 1992. Relationships between microstructure and creep and shrinkage of cement paste. Mater Sci Concr IIIpp 37.

Yang, H., Xu, X., Cui, H., Lin, Z., Lo, T.Y., 2016. Effect of Cured Time on Creep of Lightweight Aggregate Concrete, in: Proceedings of the 5th International Conference on the Durability of Concrete Structures. Presented at the International Conference on the Durability of Concrete Structures, Purdue University Press. https://doi.org/10.5703/1288284316122

Yang, M., Jin, S., Gong, J., 2020. Concrete Creep Analysis Method Based on a Long-Term Test of Prestressed Concrete Beam. Adv. Civ. Eng. 2020, e3825403. https://doi.org/10.1155/2020/3825403

Yasin, A.A., 2012. Using Shredded Tires as an Aggregate in Concrete. Contemp. Eng. Sci. 5, 473–480.

Ye, H., 2015. Creep Mechanisms of Calcium–Silicate–Hydrate: An Overview of Recent Advances and Challenges. Int. J. Concr. Struct. Mater. 9, 453–462. https://doi.org/10.1007/s40069-015-0114-7

Yokohama tyres, 2018. Nomenclature for Passenger Car Tire / for Truck and Bus Tire | Tire Knowledge | LEARN | YOKOHAMA TIRE Global Website [WWW Document]. URL http://www.y-yokohama.com/global/product/tire/learn/knowledge/nomenclature/ (accessed 7.12.18).

Yoon, Y.-S., Lee, S.-K., Lee, M.-S., Kim, J.-K., Kwon, K.-Y., 2011. Rheological concrete creep prediction model for prestressed concrete bridges constructed by the free cantilever method. Mag. Concr. Res. 63, 645–653. https://doi.org/10.1680/macr.2011.63.9.645

Youssf, O., Mills, J.E., Benn, T., Zhuge, Y., Ma, X., Roychand, R., Gravina, R., 2020. Development of Crumb Rubber Concrete for Practical Application in the Residential Construction Sector – Design and Processing. Constr. Build. Mater. 260, 119813. https://doi.org/10.1016/j.conbuildmat.2020.119813

Youssf, O., Mills, J.E., Hassanli, R., 2016. Assessment of the mechanical performance of crumb rubber concrete. Constr. Build. Mater. 125, 175–183. https://doi.org/10.1016/j.conbuildmat.2016.08.040

Yuan, R.L., Cook, J.E., 1983. Study of a Class C Fly Ash Concrete. Spec. Publ. 79, 307–320. https://doi.org/10.14359/6698

Zaoiai, S., Makani, A., Tafraoui, A., Benmerioul, F., 2016. Optimisation & Mechanical Characterisation of SCC Incoparationg Rubber Aggregates. Asian J. Civ. Eng. 17, 817–829.

Zhang, W., Zakaria, M., Hama, Y., 2013. Influence of aggregate materials characteristics on the drying shrinkage properties of mortar and concrete. Constr. Build. Mater. 49, 500–510. https://doi.org/10.1016/j.conbuildmat.2013.08.069

Zheng, L., Huo, X.S., Yuan, Y., 2008. Strength, Modulus of Elasticity, and Brittleness Index of Rubberised Concrete. J. Mater. Civ. Eng. 20, 692–699.

Zhu, X., Miao, C., Liu, J., Hong, J., 2012. Influence of Crumb Rubber on Frost Resistance of Concrete and Effect Mechanism. Procedia Eng., 2011 Chinese Materials Conference 27, 206–213. https://doi.org/10.1016/j.proeng.2011.12.445

Zimmermann, A., Koenders, E.A.B., Yang, S., 2016a. Crumb Rubber as a Concrete Additive: Effect of Specific Surface on Air Void Content. Presented at the 3rd international conference on Microstructure related Durability properties of Cementitious Composites, RILEM, Nanjing, China.

Zimmermann, A., Röser, F., Koenders, E.A.B., 2016b. Formation of Air Pores in Concrete due to the addition of Tire Crumb Rubber. Presented at the II International Conference on Concrete Sustainability, RILEM, Madrid, Spain, pp. 236–242.

APPENDIX A: EXPERIMENTAL TEST PROCEDURES

A.1 RELATIVE DENSITY

The relative density of the crumb rubber was determined by the pycnometer method in accordance with SANS 5844:2014 using 100 ml volumetric flasks. The crumb rubber was first washed with tap water in order to reduce its hydrophobic behaviour. It was placed in a dry and tared volumetric flask and its mass determined (m_a) as shown in Figure A.1. De-aired distilled water was then introduced, just enough to cover the crumb rubber particles. The flask contents were gently shaken and rolled in order to dispel all entrapped air. A low vacuum pump (<13kPa) was used to dispel the remaining entrapped air. The flask was placed in the vacuum pump until all the air had been expelled which was about 8 hours (Figure A,2). The flask was then filled to its calibrated capacity and weighed (m_c). After weighing, the crumb rubber was removed; the flask was washed and filled with water to calibrated capacity.

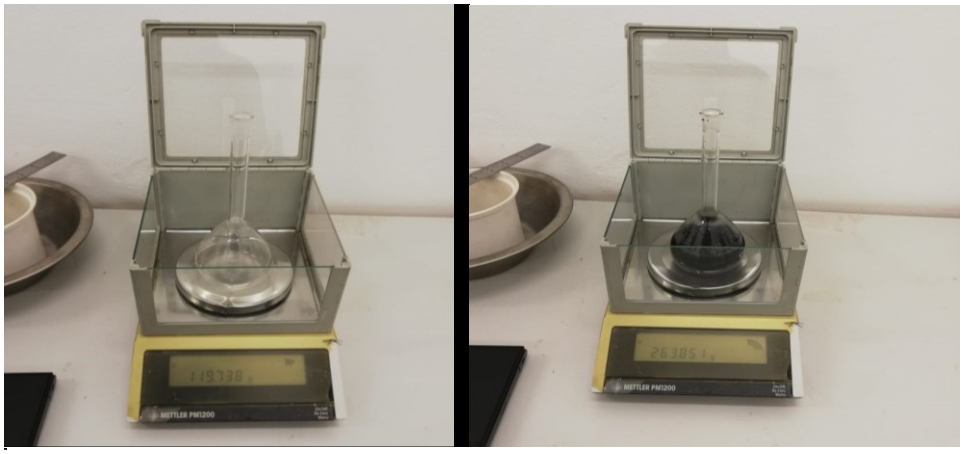

Figure A.1: Volumetric flask on the scale with and without crumb rubber

The mass of the volumetric flask with water was determined (m_d). The relative density of the material was then determined using the formula.

$$\textit{Relative density of particles} = m_a/[(m_d + m_a) - m_c] \ldots\ldots \text{ Eqn. A.1}$$

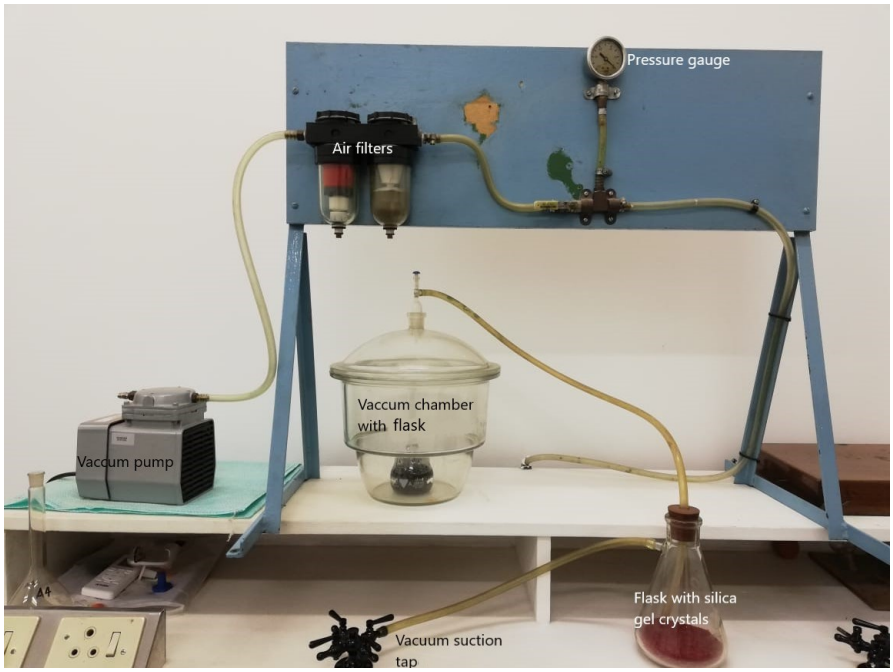

Figure A.2: Air suction apparatus arrangement

A.2 HARDENED CONCRETE POROSITY

The hardened concrete percent voids determination experiment was conducted in accordance with the ASTM C642-97. 100 × 100 × 55 mm concrete specimens, each weighing approximately 1500 g, were used. These specimens were cut from the 100 × 100 × 200 mm drying shrinkage specimens. The specimens were weighed and placed in an oven to dry at a temperature of 110°C for 24 hours. After 24 hours the specimens were removed from the oven and allowed to cool in a desiccator to a temperature of 20 to 25°C before being weighed again. If the specimen mass after drying was within 0.5% of the specimen mass before drying then the mass was adopted as the “over-dry mass” (A) of the specimen. However, if the masses were not within 0.5% of each other the specimen was placed back in the oven and re-dried. This was done until the masses were within 0.5% of each other. After obtaining the final oven-dry mass, the specimens were immersed in tap water at about 21°C for at least 48 hours until two successive 24-hour surface-

dried specimen masses are within 0.5% of each other. The specimens were removed from the water, dried with a towel to obtain the saturated mass after immersion (B). After obtaining mass B, the specimens were placed in a bucket of tap water and boiled for 5 hours. The specimens were then allowed to cool by natural loss of heat for not less than 14 hours to a final temperature of 20 to 25 °C before being removed from the water towel dried and weighed to obtain the "saturated mass after boiling" (C). Thereafter, the specimens were tied with a wire and suspended in water to determine the apparent mass in water (D).

The percent concrete voids were determined using the formula:

$$\textit{Volume of permeable pore space (voids), \%} = (C - A)/(C - D) \times 100 \quad \text{...Eqn. A.2}$$

APPENDIX B: COMPRESSIVE STRENGTH RESULTS

B.1 COMPRESSIVE STRENGTH RESULTS DISCUSSION

The results of the compressive strength tests carried out on various mixes of rubberised concrete are presented in this section. These compressive strength tests were carried out during the preliminary stages when the appropriate mix was being determined. The results on the effect of size and content on the concrete compressive strength are presented and discussed first, then the effect of surface treatment on the effect of tyre rubber particles on compressive strength are presented and discussed thereafter.

B.1.1 Effect of crumb tyre rubber size and content

The 28-day compressive strength of concrete made from different percentages (0%, 5%, 10% and 15%) of crumb tyre rubber of three different sizes (0.425 mm, 1.18 mm and 2.36 mm) was determined and the results are presented in Figure B.1 with standard deviation error bars. The crumb tyre rubber replaced the fine mineral aggregate by volume in the concrete.

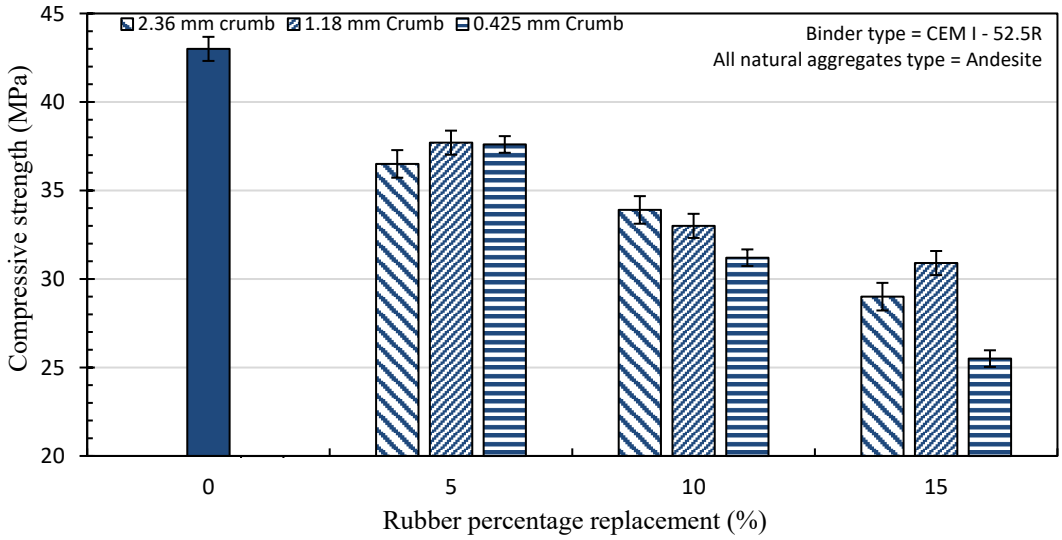

Figure B.1: Effect of crumb rubber content and size on concrete compresive strength

The compressive strength of the concrete decreases with an increase in crumb rubber content. This trend is in agreement with what is reported by other researchers (Naik, and Singh, 1991; Malladi, 2004; Zheng et al., 2008; Jain, 2014; Elchalakani, 2015). They attribute the reduction in compressive strength to the low stiffnes of the rubber and the lack of bond between the rubber and the cement. From Figure B.1 it can be seen that all crumb rubber sizes and replacement levels result in a reduction in compressive strength of concrete. All of the mixes were within the structural concrete strength range and only two, the 15% replacement level for 2.38 mm and 0.425 mm, were below the target strength of 30 MPa. In general, the differences in the compressive strengths due to change in rubber content for the different crumb tyre rubber sizes are statistically significant. However, comparison of the results between the replacement level pairs for each size revealed that in some cases the differences are not significant. Table B.1 shows the results of the t-test used to compare the results.

Table B.1: Statistical differences between different percentage replacement levels per rubber size

Significant difference		**Insignificant difference**	
M8 (5/15)	**[p =0.00005]**	M8 (5/10)	[p = 0.09]
M8 (10/15)	**[p = 0.0002]**	M16 (10/15)	[p = 0.08]
M16 (5/10)	**[p =0.01]**		
M16 (5/15)	**[p = 0.0002]**		
M40(5/10)	**[p = 0.0003]**		
M40 (5/15)	**[p = 0,000009]**		
M40 (10/15)	**[p = 0.006]**		

KEY: M40 (10/15)[p = 0.006] – "M40" is the concrete mix name
"(10/15)" are percentages being compared, in this case, 10% and 15%.
"[p = 0.006]" is the p-value from pairwise t-test

The statisical analysis of variance shows that for most of the mixes, the difference between them is significant meaning that the change in rubber content had an effect on the strength of the concrete. This was the case for all but 2 mixes. The implication of the insignificant difference is that the increase of the rubber content does not have a detectable effect on the compressive strength therefore it may be possible to replace a 5% M8 mix with a 10% or a 10% M16 mix with a 15%. This was in fact, the reasoning used in selecting the 10% replacement level for the testing specimens used in the creep and shrinkage investigations. Figure B.2 shows the ratio of rubberised concrete strength to reference concrete strength for the three crumb rubber sizes for each replacement level.

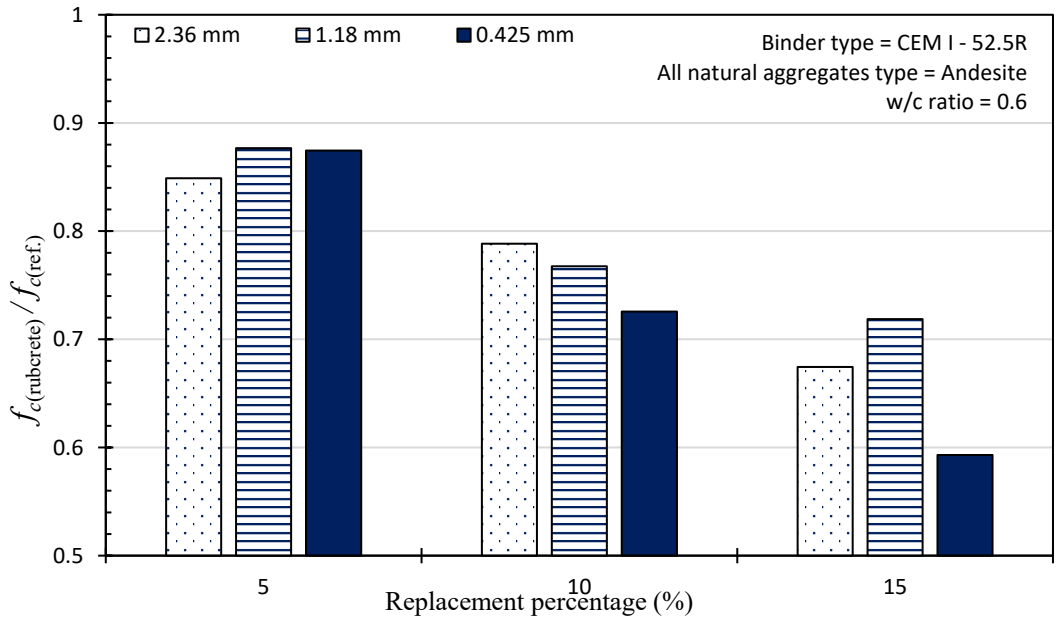

Figure B.2: Ratio of rubberised concrete strength to reference concrete strength for different rubber content and size

At 5% replacement level, the 2.36 mm and 0.425 mm crumb rubber mixes both have almost similar percentage strength loss of 12% and 13% respectively, while the 1.18 mm crumb rubber mix had a 15% strength loss. The strength reduction does not exhibit any obvious trend with regards to crumb rubber size. The expectation was that the smaller crumb tyre rubber would have higher strength

reduction due to its shape which results in an increase in the air content in the concrete. The increase in air content results in a decrease in compressive strength due to an increase in air voids in the concrete. However, the smaller size having a more irregular fibrous shape and slightly rougher surface can also exhibit lower strength reduction due to its ability to bond and to easily anchor into cement matrix. None of the results clearly show this ascertion. In fact, the results are a mix of the smaller size rubber particles (1.18 mm and 0.425 mm) showing a higher reduction for the 10% and 15% replacement level, and showing an almost comparable or lower reduction compared to bigger particle sizes for the 5% replacement level. Relating the strength observations to slump test shown in Figure B.2, it can be seen that for slump as well there is no trend that can be related to the size of the crumb rubber particles. However, the general increase in workability shown by the slump is in keeping with what is reported by other reserchers (Aiello and Leuzzi, 2010; Kotresh and Belachew, 2014). This is attributed to the increase in air bubbles in the concrete which is reported to increase workability (Zimmermann et al., 2016a).

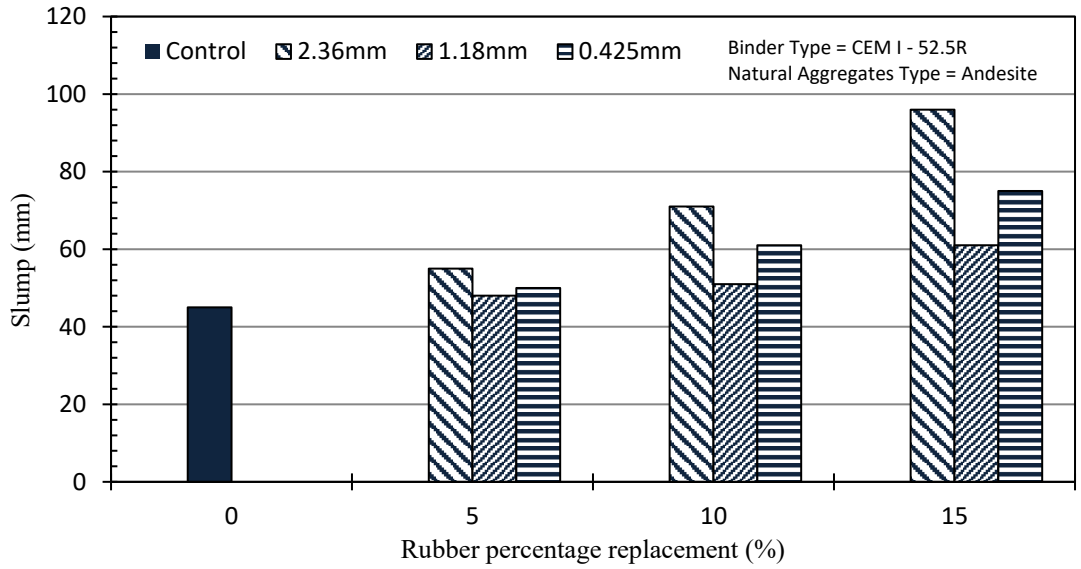

Figure B.3: Slump test

The 10% replacement level results are the only results that show an expected trend with regards to effect of size on the strength reduction. The results, although not showing similar trends for the different replacement levels, show that there is an optimum crumb rubber size that produces more consistent mix and results. This is due to the difference in the way the particles move around, interact with other concrete constituents during the mixing process and how they eventually disperse within the concrete matrix. The 2.36 mm being bigger would normally be evenly spread out through the concrete matrix while the smaller particles, particularly the 0.425 mm crumb rubber tends to clump up and stick onto the bigger coarse aggregates. The crumb rubber clumps create points of weakness in concrete due to this high concentration of low stiffness aggregates in one area the sticking of the tiny rubber particles arond the coarse aggregates has a potential to increase the porous nature of the interfacial transitional zone (ITZ) thereby further weakening it. The 2.36 mm results in lower strengths due to its bigger size which can act like the smaller crumb rubber sizes clump up together with the expection of addition air voids, thereby not resulting in as high strength reduction as a clump of the same size.. The 1.18 mm being intermediate size can considered the optimum crumb rubber size given the more consistent concrete strength performance it exhibits.

Statistically there are no significant differences in strength with regards to the size of the crumb tyre rubber for the 5% and 10% replacement. These results suggest that the change of crumb rubber sizes does not necessarily have an effect of the expected strength reduction, which means that the strength reduction might be

linked more to crumb rubber content rather than crumb rubber size particularly if the crumb rubber sizes are not very varied and the for replacement levels less than 10%. Based on the compressive strength results the optimum crumb tyre rubber content was take as 10% for the elastic modulus, shrinkage and creep tests.

B.1.2 Effect of crumb tyre rubber surface treatment

The results of the 28-day compressive strength tests of concrete made from 3 crumb tyre rubber size particles with a 15% fine aggregate replacement level by volume are presented in Figure B.4 with standard deviation error bars. The 15% replacemnt level was used for pretreatment tests because it was the replacement level that had produced concrete with strength less than target, therefore by pretreating it it was hoped that these mixes would achieve target strength. The crumb tyre rubber particles were surface treated by 2 methods firstly, by soaking them in 0.1M sodium hydroxide and secondly, by soaking in tap water, for 24 hours and then used to make rubberised concrete.

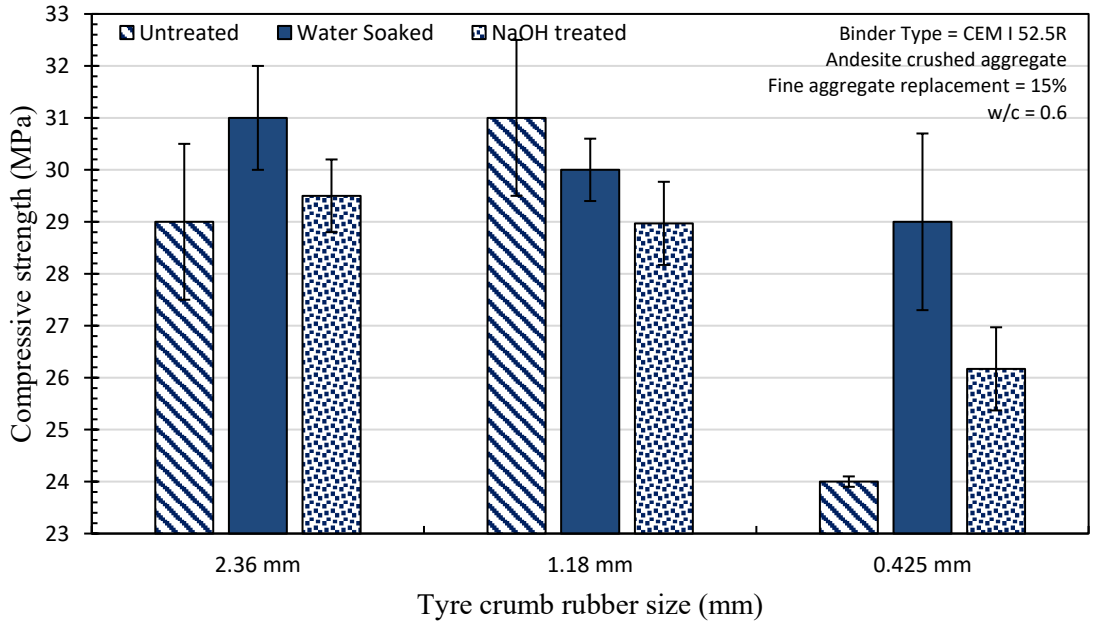

Figure B.4: Effect of crumb rubber pretreatment on concrete compresive strength

In this investigation the treatment methods did not yield the expected results of significantly increasing the compressive strength of the rubberized concrete as reported by other researchers (Mohammadi et al., 2016; Rostami et al., 1993; Segre and Joekes, 2000). Table B.2 shows the compressive strength increase due to pretreatment.

Table B.2: Percentage strength gain due to crumb rubber pretreatment

	Percentage strength increase	
Crumb rubber size (mm)	*NaOH treated*	*Water soaked*
2.36	6	2
1.18	(5)	(7)
0.425	16	6

In all instances the water soaked rubber was observed to have produced concrete with slightly better compressive strengths than the sodium hydroxide treated tyre rubber, this was probably due to the fact that for smaller particles ITZ quality influence on strength is less crucial than porosity of the matrix. The NaOH tends to increase particle-cement bond which plays a negligible where fine aggregates are concerned in concrete while water soaking treatment deals with mitigating the development of voids in the concrete, which plays a bigger role. In addition, the concrete with 0.425 mm tyre rubber particles is the only concrete that showed a statically significant difference with the use of pretreated rubber particles. The concrete with other rubber particle sizes did not show any change that could be associated pretreatment (Figure B.4). This implies that for rubberised concretes pretreating the rubber particles or not, before use would result in similar results. These findings are in agreement with work reported by other researchers (Albano et al., 2005; Marques et al., 2008; Su et al., 2015a) who also found that there is no

significant improvement in the compressive strength performance when the rubber was pretreated with NaOH or water. The reason for this is not very clear at this point. The lack of the pretreatment to significantly affect the strength performance of the concrete positively shows that rubber-cement paste bond for smaller rubber particles plays a less significant role when compared to stiffness of the particles particles as highlighted by Taha et al., (2008) and the increase in porosity due to hydrophobic nature of the rubber which results in more air voids.

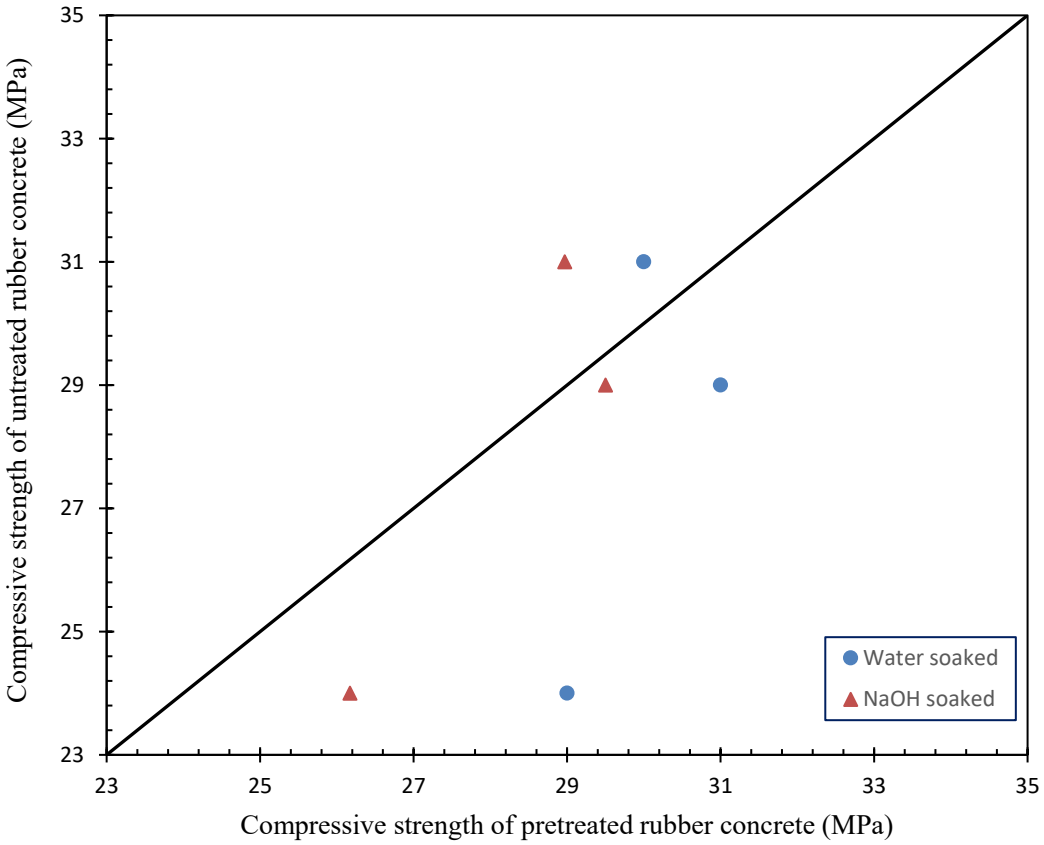

Figure B.4: Equality graph for effect of crumb rubber pretreatment on concrete compresive strength

B.2 RAW COMPRESSIVE STRENGTH RESULTS

Table B.3: Compressive strength of concrete with different crumb rubber content percentage

	CONTROL						
Rubber Content (%)	**Parameter**	**1**	**2**	**3**	**Mean**	**S.D**	**CoV**
0	Weight	2.6	2.5	2.6	2.57	0.06	2.2
	Strength	44	41.7	43.3	**43**	**1.18**	**2.7**
	M8						
5	Weight	2.5	2.46	2.46	2.47	0.02	0.9
	Strength	38.1	35.7	35.8	**37**	**1.36**	**3.7**
10	Weight	2.48	2.44	2.52	2.48	0.04	1.6
	Strength	34.8	32	34.9	**34**	**1.65**	**4.9**
15	Weight	2.38	2.36	2.44	2.39	0.04	1.7
	Strength	28.3	30.7	28.0	**29**	**1.48**	**5.1**
	M16						
5	Weight	2.48	2.56	2.52	2.52	0.04	1.6
	Strength	36.5	39.2	37.5	**38**	**1.37**	**3.6**
10	Weight	2.46	2.56	2.54	2.52	0.05	2.1
	Strength	32.2	32.8	34.8	**33**	**1.36**	**4.1**
15	Weight	2.44	2.46	2.44	2.45	0.01	0.5
	Strength	31.3	31	30.5	**31**	**0.40**	**1.3**
	M40						
5	Weight	2.48	2.52	2.5	2.50	0.02	0.8
	Strength	37.8	38.3	36.7	**38**	**0.82**	**2.2**
10	Weight	2.46	2.46	2.46	2.46	0.00	0.0
	Strength	31.9	29.8	31.8	**31**	**1.18**	**3.8**
15	Weight	2.48	2.46	2.44	2.46	0.02	0.8
	Strength	24.3	25.6	26.6	**26**	**1.15**	**4.5**

Table B.4: Compressive strength of pretreated crumb rubber concrete

	M8		M8W		M8S	
Sample No.	**Strength**	**Mass**	**Strength**	**Mass**	**Strength**	**mass**
1	28.3	2.36	31.8	2.44	29.4	2.4
2	30.7	2.48	30.7	2.46	30.2	2.44
3	28	2.42	29.8	2.5	28.9	2.48
Mean	**29**	2.42	**31**	2.47	**29.5**	2.44
S.D	**1.48**	0.06	**1.00**	0.03	**0.66**	0.04
CoV	**5.10**	2.48	**3.26**	1.24	**2.22**	1.64
	M40		**M40W**		**M40S**	
1	24.2	2.42	29	2.52	25.5	2.5
2	26.3	2.4	28	2.46	27	2.44
3	23.5	2.38	29	2.48	26	2.46
Mean	**24.7**	2.40	**29**	2.49	**26.17**	2.47
S.D	**1.46**	0.02	**0.58**	0.03	**0.76**	0.03
CoV	**5.91**	0.83	**2.01**	1.23	**2.92**	1.24
	M16		**M16W**		**M16S**	
1	31.1	2.42	28.4	2.44	28	2.42
2	31.2	2.48	31.5	2.42	29.4	2.54
3	31.3	2.44	28.8	2.46	29.5	2.48
Mean	**31.2**	2.45	**30**	2.44	**28.97**	2.48
S.D	**0.10**	0.03	**1.69**	0.02	**0.84**	0.06
CoV	**0.32**	1.25	**5.70**	0.82	**2.90**	2.42

B.3 STATISTICAL ANALYSIS OF COMPRESSIVE STRENGTH RESULTS

Table B.5-a: ANOVA results for compressive strengths of M8 concrete with different percentage crumb rubber

Source	*SS*	*df*	*MS*	*F-value*	*p-value*
Between Groups	87.7	2	43.8	19.5	0.002
Within Groups	13.5	6	2.2		
Total	101.2	8			

Table B.5-b: p-values of t-test result for compressive strength of M8 concrete with different crumb rubber percentages

Crumb %		**15%**	**10%**	**5%**
	Strength (MPa)	**29.0**	**33.9**	**36.5**
15%	**29.0**			
10%	**33.9**	0.007		
5%	**36.5**	0.001	0.075	

Table B.6: ANOVA results for compressive strengths of M8 concrete with pre-treated crumb rubber

Source	*SS*	*df*	*MS*	*F-value*	*p-value*
Between Groups	5.0	2	2.5	2.06	0.21
Within Groups	7.2	6	1.2		
Total	12.2	8			

Table B.7-a: ANOVA results for compressive strengths of M16 concrete with different percentage crumb rubber

Source	*SS*	*df*	*MS*	*F-value*	*p-value*
Between Groups	71.6	2	35.8	27.7	0.0009
Within Groups	7.8	6	1.3		
Total	79.4	8			

Table B.7-b: p-values of t-test result for compressive strength of M16 concrete with different crumb rubber percentages

Crumb %		**15%**	**10%**	**5%**
	Strength (MPa)	**30.9**	**33.3**	**37.7**
15%	**30.9**			
10%	**33.3**	0.007		
5%	**37.7**	0.001	0.075	

Table B.8: ANOVA results for compressive strengths of M16 concrete with pre-treated crumb rubber

Source	*SS*	*df*	*MS*	*F-value*	*p-value*
Between Groups	8.0	2.0	4.0	3.38	0.10
Within Groups	7.1	6.0	1.2		
Total	15.1	8.0			

Table B.9-a: ANOVA results for compressive strengths of M40 concrete with different percentage crumb rubber

Source	*SS*	*df*	*MS*	*F-value*	*p-value*
Between Groups	219.9	2	110.0	96.9	3E-05
Within Groups	6.8	6	1.1		
Total	226.7	8			

Table B.9-b: p-values of t-test result for compressive strength of M40 concrete with different crumb rubber percentages

Crumb %		**15%**	**10%**	**5%**
	Strength (MPa)	**25.5**	**31.2**	**37.6**
15%	**25.5**			
10%	**31.2**	0.00062		
5%	**37.6**	0.00001	0.00031	

Table B.10-a: ANOVA results for compressive strengths of M40 concrete with pre-treated crumb rubber

Source	*SS*	*df*	*MS*	*F-value*	*p-value*
Between Groups	24.5	2.0	12.3	12.1	0.008
Within Groups	6.1	6.0	1.0		
Total	30.6	8.0			

Table B.10-b: p-values of t-test result for compressive strength of M40 concrete with pre-treated crumb rubber

Crumb %		**M40**	**M40S**	**M40W**
	Strength (MPa)	**24.7**	**26.2**	**29.0**
M40	**24.7**			
M40S	**26.2**	0.118		
M40W	**29.0**	0.003	0.02	

APPENDIX C: HARDENED CONCRETE POROSITY RESULTS

Table C.1: Hardened concrete percent voids experimental data

		Specimen Number			Percent Voids				
Specimen ID	**Mass Designation**	**1**	**2**	**3**	**1**	**2**	**3**	**Mean**	**SD**
Reference	**A**	1533.5	1387.9	1466.9	8.24	8.62	8.55	**8.47**	**0.204**
	C	1615.1	1464.3	1548.1					
	D	624.4	578.1	598					
M8	**A**	1505.2	1404.7	1510.7	8.71	8.74	8.71	**8.72**	**0.016**
	C	1591.2	1483.2	1594.8					
	D	604.2	584.8	629.1					
M16	**A**	1420.7	1321.9	1390	9.66	9.63	9.45	**9.58**	**0.117**
	C	1504.9	1403.1	1474.2					
	D	633.4	560.1	582.8					
M40	**A**	1378.8	1600.1	1390	9.59	9.53	9.87	**9.66**	**0.181**
	C	1462.9	1697.7	1477.9					
	D	586.3	673.3	587.3					
M8W	**A**	1537.5	1478.9	1522.8	8.73	8.77	8.89	**8.80**	**0.085**
	C	1622	1561.1	1608					
	D	654	623.5	649.9					
M8S	**A**	1547	1622.3	1644.2	8.79	8.76	9.07	**8.87**	**0.172**
	C	1634	1712.2	1738.7					
	D	644.1	685.7	696.9					
M16W	**A**	1738.8	1547.3	1497.6	9.59	9.84	9.60	**9.68**	**0.140**
	C	1845.4	1644.2	1588.9					
	D	734	659.4	638.1					
M16S	**A**	1446.8	1538.8	1416.3	9.53	9.43	9.87	**9.61**	**0.229**
	C	1529.7	1631.4	1505					
	D	659.7	649.2	605.9					
M40W	**A**	1505.3	1488.7	1525.3	9.62	9.76	9.78	**9.72**	**0.091**
	C	1597	1580.4	1620.7					
	D	643.4	640.7	645.7					
M40S	**A**	1558.2	1530	1598.2	9.79	9.70	9.76	**9.75**	**0.045**
	C	1654.4	1624.5	1697.4					
	D	671.7	650.5	681.3					

APPENDIX D: STATISTICAL ANALYSIS OF HARDENED CONCRETE POROSITY

Table D.1-a: ANOVA of hardened concrete percent void results of reference and rubberised concrete

Source	*SS*	*Degress of freedom*	*MS*	*F*	*p-value*
Between Groups	3.27	3.00	1.09	49.37	1.66E-05
Within Groups	0.18	8.00	0.02		
Total	3.45	11.00			

Table D.1-b: p-values for t-tests result for hardened concrete percent void results of reference and rubberised concrete

Specimen ID		**Reference**	**M8**	**M16**	**M40**
	Percent void	**8.5**	**8.7**	**9.6**	**9.7**
Reference	**8.5**				
M8	**8.7**	0.07172			
M16	**9.6**	0.00002	0.00010		
M40	**9.7**	0.00001	0.00005	0.50928	

Table D.2: ANOVA results of hardened percent voids for M8 concrete with pre-treated crumb rubber

Source	*SS*	*Degrees of freedom*	*MS*	*F-value*	*P-value*	*F crit*
Between Groups	0.035	2	0.017	1.405	0.316	5.143
Within Groups	0.075	6	0.012			
Total	0.110	8				

Table D.3: ANOVA results of hardened percent voids for M16 concrete with pre-treated crumb rubber

Source	*SS*	*Degrees of freedom*	*MS*	*F-value*	*P-value*	*F crit*
Between Groups	0.015	2	0.008	0.268	0.774	5.143
Within Groups	0.172	6	0.029			
Total	0.187	8				

Table D.4: ANOVA results of hardened percent voids for M40 concrete with pre-treated crumb rubber

Source	*SS*	*Degrees of freedom*	*MS*	*F-value*	*P-value*	*F crit*
Between Groups	0.012	2	0.006	0.412	0.680	5.143
Within Groups	0.086	6	0.014			
Total	0.098	8				

APPENDIX E: SHRINKAGE RESULTS

Table E.1: Shrinkage Strain measurements for control prisms

			Unloaded Samples															
			Sealed								Unsealed							
			Sample Number and Side						Average Incremental strain (10^{-6})	Average cumulative Strain ($x10^{-6}$)	Sample Number and Side						Average Incremental strain (10^{-6})	Average cumulative Strain ($x10^{-6}$)
			1		2		3				1		2		3			
Age (Days)	Temp (°C)	RH (%)	A	B	A	B	A	B			A	B	A	B	A	B		
0	22.1	62	0	0	0	0	0	0	0	0	0	0	0	0	0	0	0	0
0.13	22	62	1	0	0	0	1	0	5	5	2	0	0	2	0	0	11	11
1	21.5	62	0	1	1	0	0	0	5	11	1	2	2	2	2	3	32	43
2	22	62	1	0	1	1	0	0	8	19	2	3	1	0	1	0	19	61
3	22	63	1	0	0	2	0	1	11	29	1	0	2	3	1	3	27	88
4	22.1	63	0	1	1	0	2	0	11	40	2	2	3	1	3	2	35	123
5	21.6	62	0	1	0	1	0	0	5	45	2	0	2	0	1	0	13	136
6	22.1	61	1	0	0	0	0	2	8	53	0	1	0	1	1	0	8	144
7	22.2	61	0	0	1	0	2	0	8	61	2	0	1	0	1	1	13	157
14	22	60	1	1	2	3	2	2	29	91	2	1	5	4	4	3	51	208
21	18	49	1	0	1	1	0	0	8	99	0	2	0	1	1	0	11	219
28	**19.4**	**62**	**1**	**2**	**2**	**2**	**3**	**2**	**32**	**131**	**1**	**2**	**1**	**2**	**1**	**1**	**21**	**240**
56	16.6	64	2	4	3	4	3	2	48	179	7	3	4	3	5	3	67	307
84	15.8	64	2	1	3	5	5	4	53	232	1	3	2	2	3	1	32	339
112	12.3	66	1	1	0	1	0	0	8	240	1	2	0	1	1	0	13	352
140	12.2	65	0	0	0	1	1	1	8	248	1	1	1	0	0	1	11	363
168	12.2	41	1	1	0	0	1	0	8	256	2	1	2	0	1	1	19	381
196	18.2	65	0	0	0	0	0	1	3	259	0	2	1	0	0	1	11	392
224	12.9	61	0	1	1	0	1	0	8	267	1	0	2	0	1	0	11	403
252	13	60	1	0	1	1	1	-2	5	272	0	1	1	1	0	1	11	413
280	19.8	60	1	0	0	1	1	2	13	285	1	0	1	0	1	1	11	424
308	19	63	0	1	1	0	1	1	11	296	1	2	1	1	0	0	13	437
336	21	63	1	0	0	1	0	1	8	304	0	0	0	1	1	1	8	445
364	20	49	0	1	0	0	1	0	5	309	1	0	1	0	0	0	5	451

Table E.2: Shrinkage Strain measurements for M8 prisms

			Unloaded Samples															
			Sealed								Unsealed							
			Sample Number and Side						Average Incremental strain (10^{-6})	Average cumulative Strain ($x10^{-6}$)	Sample Number and Side						Average Incremental strain (10^{-6})	Average cumulative Strain ($x10^{-6}$)
			1		2		3				1		2		3			
Age (Days)	Temp (°C)	RH (%)	A	B	A	B	A	B			A	B	A	B	A	B		
0	21.6	63	0	0	0	0	0	0	0	0	0	0	0	0	0	0	0	0
0.13	21.6	62	0	0	0	2	0	0	5	5	1	0	1	1	1	0	11	11
1	22	62	0	0	0	0	0	0	0	5	1	1	1	0	-1	0	5	16
2	22.1	62	0	0	0	0	0	1	3	8	2	1	1	1	1	2	21	37
3	22.1	63	1	0	0	1	1	2	13	21	1	3	1	1	1	1	21	59
4	22.1	63	0	0	0	0	1	1	5	27	0	1	0	0	0	1	5	64
5	22.1	62	0	0	0	0	1	0	3	29	0	0	0	1	0	1	5	69
6	22.2	61	0	0	1	2	0	0	8	37	1	1	1	0	1	1	13	83
7	19.9	47	1	2	0	0	0	0	8	45	1	2	0	0	1	1	13	96
14	17.6	56	1	3	2	3	2	2	35	80	3	1	3	1	0	4	32	128
21	17.4	52	2	1	1	0	2	0	16	96	2	1	1	0	1	0	13	141
28	**21.6**	**69**	**3**	**1**	**2**	**1**	**1**	**1**	**24**	**120**	**2**	**2**	**2**	**3**	**3**	**2**	**37**	**179**
56	16.6	63	0	2	2	1	2	2	24	144	4	5	0	2	4	4	51	229
84	12.3	64	2	2	2	3	2	2	35	179	3	1	2	1	3	3	35	264
112	12.2	66	1	1	1	1	1	0	13	192	3	2	1	3	1	0	27	291
140	12.3	66	2	1	0	0	2	2	19	211	1	3	1	2	3	2	32	323
168	12.1	41	0	1	2	0	0	0	8	219	2	1	0	1	2	0	16	339
196	18.1	62	2	0	1	0	1	0	11	229	1	1	3	1	1	-1	16	355
224	17.9	62	2	2	1	1	2	0	21	251	0	2	0	3	1	1	19	373
252	18.1	63	-1	2	1	1	1	3	19	269	1	2	1	1	2	0	19	392
280	18.1	66	1	1	0	2	1	1	16	285	1	0	1	2	1	2	19	411
308	19.1	60	2	1	0	2	-1	1	13	299	1	1	1	2	1	0	16	427
336	21	61	0	1	1	0	1	1	11	309	1	0	1	0	1	1	11	437
364	21	63	0	0	2	1	1	1	13	323	1	0	1	0	0	1	8	445

Table E.3: Shrinkage Strain measurements for M16 prisms

			Unloaded Samples															
			Sealed								Unsealed							
			Sample Number and Side						Average Incremental strain (10^{-6})	Average cumulative Strain ($x10^{-6}$)	Sample Number and Side						Average Incremental strain (10^{-6})	Average cumulative Strain ($x10^{-6}$)
			1		2		3				1		2		3			
Age (Days)	Temp (^{o}C)	RH (%)	A	B	A	B	A	B			A	B	A	B	A	B		
0	22	63	0	0	0	0	0	0	0	0	0	0	0	0	0	0	0	0
0.13	21.9	62	1	1	1	0	0	0	8	8	3	2	2	1	2	1	29	29
1	22.1	61	1	2	0	0	0	1	11	19	1	3	2	3	3	3	40	69
2	21.9	63	1	0	1	1	2	1	16	35	1	2	2	3	2	2	32	101
3	22.1	63	0	0	0	0	0	0	0	35	0	1	1	1	1	1	13	115
4	22.2	62	1	0	0	0	0	0	3	37	1	2	1	1	0	0	13	128
5	22.2	62	1	1	0	0	1	0	8	45	1	1	0	2	1	3	21	149
6	19.9	47	1	1	2	0	-1	2	13	59	0	2	2	0	1	0	13	163
7	19	55	1	0	0	2	2	0	13	72	1	1	0	0	2	1	13	176
14	17	59	1	2	3	1	0	2	24	96	0	3	1	1	1	2	21	197
21	17.9	61	1	2	1	2	1	1	21	117	2	3	3	3	2	1	37	235
28	**19.2**	**58**	**1**	**1**	**0**	**1**	**1**	**0**	**11**	**128**	**2**	**2**	**1**	**1**	**1**	**2**	**24**	**259**
56	16.7	64	3	2	2	2	1	1	29	157	4	4	4	4	3	3	59	317
84	17	64	4	3	2	3	3	2	45	203	3	4	2	3	3	3	48	365
112	12.7	66	1	1	1	0	1	1	13	216	2	3	2	1	1	2	29	395
140	12.3	66	1	1	2	1	1	1	19	235	0	1	1	1	1	0	11	405
168	13.1	41	1	1	1	1	1	1	16	251	2	0	1	1	0	0	11	416
196	18	63	1	1	2	2	1	1	21	272	0	2	1	1	-1	0	8	424
224	12.9	66	0	2	1	2	2	1	21	293	-1	0	0	1	0	2	5	429
252	13	60	2	1	1	1	0	1	16	309	1	1	1	1	1	1	16	445
280	18	60	2	1	1	0	1	1	16	325	1	1	3	1	1	0	19	464
308	18.1	61	0	1	0	1	0	0	5	331	1	0	1	0	1	0	8	472
336	22	60	-2	2	1	1	1	1	11	341	2	2	1	0	1	0	16	488
364	20	62	3	1	0	1	0	1	16	357	0	1	0	0	1	0	5	493

Table E.4: Shrinkage Strain measurements for M40 prisms

			Unloaded Samples															
			Sealed								Unsealed							
			Sample Number and Side						Average Incremental strain (10^{-6})	Average cumulative Strain ($x10^{-6}$)	Sample Number and Side						Average Incremental strain (10^{-6})	Average cumulative Strain ($x10^{-6}$)
			1		2		3				1		2		3			
Age (Days)	Temp (^{o}C)	RH (%)	A	B	A	B	A	B			A	B	A	B	A	B		
0	22	63	0	0	0	0	0	0	0	0	0	0	0	0	0	0	0	0
0.13	21.9	62	1	0	0	1	1	2	13	13	1	2	1	0	3	0	19	19
1	22.1	61	2	1	0	1	2	2	21	35	1	1	2	1	1	1	19	37
2	21.9	63	0	0	0	1	0	0	3	37	0	-1	0	2	1	0	5	43
3	22.1	63	0	0	0	0	0	0	0	37	1	2	1	0	2	2	21	64
4	22.2	62	0	0	0	0	1	0	3	40	1	2	0	0	1	0	11	75
5	22.2	62	0	0	2	2	0	0	11	51	2	1	1	2	1	3	27	101
6	19.9	47	1	1	1	0	0	0	8	59	0	1	0	0	2	0	8	109
7	19	55	0	2	0	1	0	0	8	67	2	2	1	1	1	2	24	133
14	17	59	-1	0	2	3	0	-1	8	75	3	3	1	2	2	2	35	168
21	17.9	61	2	1	1	1	2	2	24	99	2	2	2	1	1	1	24	192
28	**19.2**	**58**	**1**	**1**	**2**	**3**	**1**	**1**	**24**	**123**	**3**	**3**	**1**	**2**	**2**	**2**	**35**	**227**
56	16.7	64	3	2	3	2	3	2	40	163	4	3	4	4	3	4	59	285
84	17	64	2	2	2	2	1	3	32	195	3	4	2	2	4	4	51	336
112	12.7	66	1	1	3	2	2	0	24	219	1	3	1	2	1	0	21	357
140	12.3	66	1	2	2	3	2	2	32	251	1	1	1	1	1	2	19	376
168	13.1	41	2	1	2	1	0	0	16	267	2	1	2	2	0	1	21	397
196	18	63	2	1	1	0	1	0	13	280	2	1	0	1	1	0	13	411
224	12.9	66	0	0	0	0	3	1	11	291	2	0	1	2	1	0	16	427
252	13	60	1	1	2	1	1	1	19	309	1	2	1	1	0	1	16	443
280	18	60	1	2	1	1	1	1	19	328	1	1	2	1	1	1	19	461
308	18.1	61	0	1	0	1	0	1	8	336	2	0	2	0	1	0	13	475
336	22	60	0	2	1	1	0	1	13	349	1	0	1	1	0	1	11	485
364	20	62	0	1	0	0	1	0	5	355	1	0	0	1	0	1	8	493

Table E.5: Shrinkage Strain measurements for M8S prisms

			Unloaded Samples															
			Sealed								Unsealed							
			Sample Number and Side						Average Incremental strain (10^{-6})	Average cumulative Strain ($x10^{-6}$)	Sample Number and Side						Average Incremental strain (10^{-6})	Average cumulative Strain ($x10^{-6}$)
			1		2		3				1		2		3			
Age (Days)	Temp (^{o}C)	RH (%)	A	B	A	B	A	B			A	B	A	B	A	B		
0	12.3	66	0	0	0	0	0	0	0	0	0	0	0	0	0	0	0	0
0.13	12.3	66	0	0	0	0	0	0	0	0	0	0	0	0	0	0	0	0
1	13.1	65	0	0	0	0	1	0	3	3	1	1	1	1	0	1	13	13
2	14.1	66	0	0	0	0	0	0	0	3	1	2	1	1	2	1	21	35
3	13.3	69	0	1	0	-1	0	0	0	3	0	0	1	3	2	2	21	56
4	12.8	70	0	1	1	2	0	1	13	16	1	0	1	1	0	0	8	64
5	13.7	69	1	1	1	0	0	0	8	24	0	0	0	0	2	0	5	69
6	13.8	68	1	0	1	1	0	0	8	32	2	1	2	2	1	2	27	96
7	13.8	60	3	0	2	0	1	0	16	48	1	2	2	2	1	1	24	120
14	13.2	68	3	1	2	1	1	2	27	75	1	2	2	2	4	2	35	155
21	12.1	61	0	1	0	1	2	0	11	85	2	1	2	4	3	0	32	187
28	**13**	**55**	**1**	**2**	**1**	**2**	**2**	**1**	**24**	**109**	**3**	**4**	**5**	**3**	**4**	**3**	**59**	**245**
56	17.1	55	1	2	2	1	2	2	27	136	2	3	2	4	2	4	45	291
84	17.9	64	3	2	1	1	1	1	24	160	1	2	1	2	1	2	24	315
112	15.1	64	2	2	1	2	2	3	32	192	1	2	2	1	3	3	32	347
140	17.1	60	3	2	2	1	1	2	29	221	2	1	2	2	1	3	29	376
168	18.5	60	2	1	1	1	1	1	19	240	1	1	2	1	1	0	16	392
196	19.2	62	1	1	1	1	3	1	21	261	1	2	0	1	1	2	19	411
224	17.8	63	1	2	0	2	0	1	16	277	1	1	0	1	0	1	11	421
252	19.5	51	3	1	1	2	0	0	19	296	2	2	1	0	1	0	16	437
280	22	61	0	2	1	2	2	2	24	320	2	0	0	2	1	0	13	451
308	22	62	0	1	1	2	3	1	21	341	1	2	0	2	1	1	19	469
336	21	63	2	2	0	0	0	0	11	352	0	0	0	0	0	0	0	469
364	20	60	1	1	0	0	0	0	5	357	0	0	0	0	0	0	0	469

Table E.6: Shrinkage Strain measurements for M8W prisms

			Unloaded Samples															
			Sealed								Unsealed							
			Sample Number and Side						Average Incremental strain (10^{-6})	Average cumulative Strain ($x10^{-6}$)	Sample Number and Side						Average Incremental strain (10^{-6})	Average cumulative Strain ($x10^{-6}$)
			1		2		3				1		2		3			
Age (Days)	Temp (^{o}C)	RH (%)	A	B	A	B	A	B			A	B	A	B	A	B		
0	12.3	66	0	0	0	0	0	0	0	0	0	0	0	0	0	0	0	0
0.13	12.3	66	2	0	1	2	1	0	16	16	1	1	0	0	1	1	11	11
1	13.1	65	0	0	0	0	0	0	0	16	2	0	0	0	0	0	5	16
2	14.1	66	-2	1	0	1	0	1	3	19	1	0	1	1	1	1	13	29
3	13.3	69	2	1	0	2	2	1	21	40	1	2	1	2	0	0	16	45
4	12.8	70	0	0	1	0	1	1	8	48	0	0	1	0	1	1	8	53
5	13.7	69	2	1	1	2	2	2	27	75	1	1	2	1	2	1	21	75
6	13.8	68	0	0	1	0	0	0	3	77	0	1	0	1	0	1	8	83
7	13.8	60	1	0	0	0	0	0	3	80	0	1	0	0	1	0	5	88
14	13.2	68	2	0	1	2	3	1	24	104	3	1	2	1	5	3	40	128
21	12.1	61	1	1	1	1	1	1	16	120	1	2	1	2	1	2	24	152
28	**13**	**55**	**2**	**1**	**1**	**1**	**2**	**1**	**21**	**141**	**2**	**1**	**2**	**2**	**2**	**2**	**29**	**181**
56	17.1	55	1	2	1	2	3	1	27	168	3	1	4	2	3	2	40	221
84	17.9	64	2	3	2	2	1	1	29	197	4	3	1	2	1	0	29	251
112	15.1	64	1	2	1	2	2	2	27	224	3	2	4	2	2	1	37	288
140	17.1	60	3	1	1	1	2	1	24	248	5	2	3	3	3	2	48	336
168	18.5	60	1	0	1	1	1	2	16	264	1	2	2	1	2	2	27	363
196	19.2	62	1	0	2	0	2	1	16	280	1	1	2	1	3	1	24	387
224	17.8	63	3	2	1	1	-1	1	19	299	2	1	2	3	-1	1	21	408
252	19.5	51	2	1	0	1	0	1	13	312	1	2	1	1	2	1	21	429
280	22	61	1	0	1	1	2	1	16	328	2	-2	2	1	3	1	19	448
308	22	62	1	1	0	1	1	0	11	339	1	2	2	1	1	2	24	472
336	21	63	1	1	0	1	1	1	13	352	0	1	0	1	3	0	13	485
364	20	60	2	1	0	1	1	1	16	368	0	0	0	0	2	0	5	491

Table E.7: Shrinkage Strain measurements for M16S prisms

			Unloaded Samples															
			Sealed								Unsealed							
			Sample Number and Side						Average Incremental strain (10^{-6})	Average cumulative Strain ($x10^{-6}$)	Sample Number and Side						Average Incremental strain (10^{-6})	Average cumulative Strain ($x10^{-6}$)
			1		2		3				1		2		3			
Age (Days)	Temp (^{o}C)	RH (%)	A	B	A	B	A	B			A	B	A	B	A	B		
0	17.8	69	0	0	0	0	0	0	0	0	0	0	0	0	0	0	0	0
0.13	17.9	69	0	0	0	0	0	0	0	0	1	1	1	0	0	1	11	11
1	13.8	68	-4	1	0	2	1	0	0	0	1	1	2	2	1	2	24	35
2	13.8	60	2	1	2	2	1	2	27	27	1	2	1	2	2	2	27	61
3	13.8	61	0	0	1	0	0	1	5	32	0	1	0	1	0	0	5	67
4	13.7	61	-1	0	1	1	1	1	8	40	1	0	1	0	2	1	13	80
5	15.2	58	1	0	1	1	0	0	8	48	1	0	2	1	1	1	16	96
6	14.1	62	1	0	1	0	1	0	8	56	1	1	1	2	0	3	21	117
7	13.5	66	1	1	1	0	2	2	19	75	0	1	0	2	0	0	8	125
14	12.2	65	1	2	1	1	0	0	13	88	4	3	2	3	3	2	45	171
21	13	60	2	0	1	2	2	2	24	112	1	3	3	2	1	2	32	203
28	**13**	**55**	**1**	**1**	**1**	**0**	**0**	**1**	**11**	**123**	**2**	**1**	**1**	**2**	**2**	**1**	**24**	**227**
56	18.8	43	3	3	2	3	3	3	45	168	4	6	5	2	5	4	69	296
84	17.9	64	0	0	-1	2	0	3	11	179	2	0	0	4	1	0	19	315
112	15.1	64	2	1	1	2	2	3	29	208	3	2	3	4	3	2	45	360
140	17.1	60	1	2	2	2	1	1	24	232	2	2	4	4	2	4	48	408
168	18.5	60	2	3	1	0	1	1	21	253	0	1	1	1	2	1	16	424
196	21	61	1	0	0	1	1	2	13	267	1	0	1	0	1	0	8	432
224	17.5	62	3	2	2	1	3	4	40	307	1	3	3	3	1	2	35	467
252	19.5	62	1	1	1	1	2	1	19	325	0	0	0	1	0	1	5	472
280	22	61	0	1	0	0	0	3	11	336	0	0	1	0	1	0	5	477
308	20	63	2	1	1	2	2	1	24	360	4	1	1	0	0	3	24	501
336	21	61	1	0	0	1	0	0	5	365	0	0	0	0	0	0	0	501
364	22	62	0	0	1	0	0	0	3	368	0	0	0	0	0	0	0	501

Table E.8: Shrinkage Strain measurements for M16W prisms

			Unloaded Samples															
			Sealed								Unsealed							
			Sample Number and Side						Average Incremental strain (10^{-6})	Average cumulative Strain ($x10^{-6}$)	Sample Number and Side						Average Incremental strain (10^{-6})	Average cumulative Strain ($x10^{-6}$)
			1		2		3				1		2		3			
Age (Days)	Temp (^{o}C)	RH (%)	A	B	A	B	A	B			A	B	A	B	A	B		
0	17.8	69	0	0	0	0	0	0	0	0	0	0	0	0	0	0	0	0
0.13	17.9	69	0	0	0	0	0	0	0	0	1	0	1	0	1	1	11	11
1	13.8	68	2	1	0	2	1	0	16	16	1	1	2	2	3	2	29	40
2	13.8	60	2	1	2	2	1	2	27	43	1	2	1	2	3	2	29	69
3	13.8	61	0	0	1	0	0	1	5	48	0	1	1	1	0	1	11	80
4	13.7	61	1	0	1	1	1	1	13	61	-1	0	1	0	2	1	8	88
5	15.2	58	1	0	1	1	0	0	8	69	1	0	2	1	1	1	16	104
6	14.1	62	-1	0	1	0	1	0	3	72	1	1	1	2	0	3	21	125
7	13.5	66	1	1	1	0	2	2	19	91	0	1	0	1	0	1	8	133
14	12.2	65	1	2	1	1	0	0	13	104	1	3	2	3	3	5	45	179
21	13	60	2	0	1	2	2	2	24	128	3	4	3	2	0	6	48	227
28	**13**	**55**	**1**	**1**	**1**	**0**	**0**	**1**	**11**	**139**	**2**	**1**	**1**	**2**	**2**	**1**	**24**	**251**
56	18.8	43	3	3	2	3	3	2	43	181	3	5	4	2	2	4	53	304
84	17.9	64	1	0	1	2	1	3	21	203	2	3	1	3	2	3	37	341
112	15.1	64	2	3	3	2	1	1	32	235	3	2	3	4	1	2	40	381
140	17.1	60	1	2	2	2	3	2	32	267	2	2	2	4	2	4	43	424
168	18.5	60	2	3	1	0	1	1	21	288	0	1	1	1	2	1	16	440
196	21	61	1	0	0	1	1	2	13	301	1	3	1	1	1	1	21	461
224	17.5	62	1	2	1	2	1	2	24	325	1	2	3	1	1	2	27	488
252	19.5	62	1	1	1	1	2	1	19	344	1	0	0	1	0	1	8	496
280	22	61	0	0	0	0	0	3	8	352	1	2	0	-1	0	0	5	501
308	20	63	1	1	1	0	1	1	13	365	2	1	1	0	0	1	13	515
336	21	61	1	0	0	2	1	0	11	376	1	0	0	0	0	0	3	517
364	22	62	0	0	0	1	1	0	5	381	1	0	0	0	0	0	3	520

Table E.9: Shrinkage Strain measurements for M40S prisms

			Unloaded Samples															
			Sealed								Unsealed							
			Sample Number and Side						Average Incremental strain (10^{-6})	Average cumulative Strain ($x10^{-6}$)	Sample Number and Side						Average Incremental strain (10^{-6})	Average cumulative Strain ($x10^{-6}$)
			1		2		3				1		2		3			
Age (Days)	Temp (°C)	RH (%)	A	B	A	B	A	B			A	B	A	B	A	B		
0	15.4	59	0	0	0	0	0	0	0	0	0	0	0	0	0	0	0	0
0.13	14.1	59	1	0	0	1	0	0	5	5	1	0	1	0	1	0	8	8
1	13.6	62	1	1	1	0	1	1	13	19	1	0	1	1	1	0	11	19
2	13.5	66	0	1	0	0	1	0	5	24	1	2	0	1	0	2	16	35
3	13.2	97	0	1	1	0	1	0	8	32	1	1	0	1	1	0	11	45
4	13	69	0	1	0	0	0	1	5	37	0	0	0	0	0	0	0	45
5	12.5	66	1	1	1	0	1	0	11	48	0	0	2	1	1	2	16	61
6	12.6	59	2	1	2	1	0	0	16	64	2	1	0	1	1	2	19	80
7	12.6	58	0	0	1	0	1	1	8	72	0	0	2	0	0	0	5	85
14	12.9	58	1	1	1	1	1	0	13	85	1	1	1	2	1	1	19	104
21	13	62	2	1	1	0	0	1	13	99	3	2	2	1	2	1	29	133
28	**18.8**	**55**	**1**	**2**	**1**	**1**	**2**	**3**	27	125	**2**	**4**	**2**	**2**	**1**	**1**	**32**	**165**
56	17.8	65	3	3	5	3	4	3	56	181	2	3	4	5	4	5	61	227
84	15.1	64	2	1	1	1	0	0	13	195	2	3	5	3	6	2	56	283
112	17	64	1	2	2	2	2	2	29	224	4	2	4	1	6	2	51	333
140	17.5	60	2	3	2	1	2	1	29	253	2	0	2	1	6	2	35	368
168	21	60	1	2	1	2	1	2	24	277	2	3	1	2	4	3	40	408
196	19.5	62	0	2	1	2	0	1	16	293	0	2	0	2	3	1	21	429
224	19.5	63	2	2	1	2	1	2	27	320	3	3	2	3	2	3	43	472
252	22	63	0	2	0	0	0	1	8	328	1	1	1	0	0	0	8	480
280	21	63	1	0	1	1	0	1	11	339	1	1	1	1	2	1	19	499
308	20	61	1	1	0	1	1	1	13	352	1	0	1	2	2	0	16	515
336	22	60	0	0	1	0	0	0	3	355	0	0	0	0	1	2	8	523
364	22	62	0	0	1	0	0	0	3	357	0	0	0	0	0	0	0	523

Table E.10: Shrinkage Strain measurements for M40W prisms

			Unloaded Samples															
			Sealed								Unsealed							
			Sample Number and Side						Average Incremental strain (10^{-6})	Average cumulative Strain ($x10^{-6}$)	Sample Number and Side						Average Incremental strain (10^{-6})	Average cumulative Strain ($x10^{-6}$)
			1		2		3				1		2		3			
Age (Days)	Temp (°C)	RH (%)	A	B	A	B	A	B			A	B	A	B	A	B		
0	15.4	59	0	0	0	0	0	0	0	0	0	0	0	0	0	0	0	0
0.13	14.1	59	0	0	1	0	0	0	3	3	1	1	2	1	2	0	19	19
1	13.6	62	0	1	0	0	0	1	5	8	2	2	0	2	4	1	29	48
2	13.5	66	1	0	0	1	0	1	8	16	2	2	3	2	0	2	29	77
3	13.2	97	0	1	1	1	0	1	11	27	0	1	0	0	1	1	8	85
4	13	69	0	1	0	1	0	0	5	32	0	0	0	0	0	0	0	85
5	12.5	66	0	1	0	0	1	0	5	37	1	2	1	1	1	1	19	104
6	12.6	59	0	1	0	1	1	2	13	51	3	2	1	-1	0	1	16	120
7	12.6	58	1	0	1	2	0	0	11	61	1	0	0	3	1	1	16	136
14	12.9	58	1	1	0	0	1	0	8	69	2	2	1	2	2	1	27	163
21	13	62	1	1	0	1	0	0	8	77	2	2	2	1	5	2	37	200
28	**18.8**	**55**	**2**	**1**	**1**	**2**	**2**	**1**	**24**	**101**	**2**	**3**	**3**	**2**	**1**	**2**	**35**	**235**
56	17.8	65	3	3	2	2	3	2	40	141	4	1	3	6	6	3	61	296
84	15.1	64	1	1	2	1	1	2	21	163	2	3	5	2	2	2	43	339
112	17	64	1	2	2	1	2	1	24	187	2	2	2	3	1	1	29	368
140	17.5	60	1	1	1	1	1	1	16	203	2	2	1	1	3	2	29	397
168	21	60	2	2	1	1	2	2	27	229	2	1	0	1	1	2	19	416
196	19.5	62	1	1	1	2	1	1	19	248	2	0	2	0	1	0	13	429
224	19.5	63	1	1	2	1	3	1	24	272	3	2	3	2	2	1	35	464
252	22	63	2	1	2	2	3	3	35	307	0	0	0	0	0	1	3	467
280	21	63	1	1	1	1	1	2	19	325	1	2	1	1	1	1	19	485
308	20	61	1	0	1	0	0	1	8	333	0	1	0	2	1	0	11	496
336	22	60	1	1	1	0	1	1	13	347	1	1	0	1	1	0	11	507
364	22	62	0	0	0	0	1	0	3	349	0	0	0	1	0	1	5	512

Table E.11: ANOVA results of autogenous shrinkage of concrete with different crumb rubber sizes

Days drying	*Source*	*SS*	*Degrees of freedom*	*MS*	*F-value*	*P-value*
28	**Between Groups**	213.33	3	71.111	0.87	.4952
	Within Groups	653.33	8	81.667		
	Total	866.67	11			
56	**Between Groups**	1,850.67	3	616.889	0.61	.6260
	Within Groups	8,064.00	8	1,008.000		
	Total	9,914.67	11			
112	**Between Groups**	3,472.00	3	1,157.333	0.63	.6175
	Within Groups	14,762.67	8	1,845.333		
	Total	18,234.67	11			
224	**Between Groups**	3,728.00	3	1,242.667	0.72	.5657
	Within Groups	13,738.67	8	1,717.333		
	Total	17,466.67	11			
364	**Between Groups**	5,077.33	3	1,692.444	0.74	.5557
	Within Groups	18,218.67	8	2,277.333		
	Total	23,296.00	11			

Table E.12: ANOVA results of drying shrinkage of concrete with different crumb rubber sizes

Days drying	*Source*	*SS*	*Degrees of freedom*	*MS*	*F-value*	*P-value*
28	**Between Groups**	10,512.00	3	3,504.000	3.08	.0901
	Within Groups	9,088.00	8	1,136.000		
	Total	19,600.00	11			
56	**Between Groups**	13,840.00	3	4,613.333	2.87	.1034
	Within Groups	12,842.67	8	1,605.333		
	Total	26,682.67	11			
112	**Between Groups**	16,698.67	3	5,566.222	2.22	.1638
	Within Groups	20,096.00	8	2,512.000		
	Total	36,794.67	11			
224	**Between Groups**	6,101.33	3	2,033.778	0.75	.5520
	Within Groups	21,674.67	8	2,709.333		
	Total	27,776.00	11			
364	**Between Groups**	6,208.00	3	2,069.333	0.71	.5711
	Within Groups	23,210.67	8	2,901.333		
	Total	29,418.67	11			

Table E.13: ANOVA results of autogenous shrinkage of concrete with pretreated crumb rubber at 364 days

Days drying	*Source*	*SS*	*Degrees of freedom*	*MS*	*F-value*	*P-value*
M8	**Between Groups**	3,370.67	2	1,685.333	1.02	.4165
	Within Groups	9,941.33	6	1,656.889		
	Total	13,312.00	8			
M16	**Between Groups**	867.56	2	433.778	0.16	.8542
	Within Groups	16,085.33	6	2,680.889		
	Total	16,952.89	8			
M40	**Between Groups**	99.56	2	49.778	0.03	.9710
	Within Groups	10,112.00	6	1,685.333		
	Total	10,211.56	8			

Table E.14: ANOVA results of drying shrinkage of concrete with pretreated crumb rubber at 364 days

Days drying	*Source*	*SS*	*Degrees of freedom*	*MS*	*F-value*	*P-value*
M8	**Between Groups**	3,086.22	2	1,543.111	0.99	.4248
	Within Groups	9,344.00	6	1,557.333		
	Total	12,430.22	8			
M16	**Between Groups**	1,123.56	2	561.778	0.31	.7438
	Within Groups	10,837.33	6	1,806.222		
	Total	11,960.89	8			
M40	**Between Groups**	1,322.67	2	661.333	0.21	.8142
	Within Groups	18,645.33	6	3,107.556		
	Total	19,968.00	8			

APPENDIX F: CREEP RESULTS

Table F.1: Creep Strain measurements for Control prisms

			Unloaded Samples															
			Sealed								Unsealed							
			Sample Number and Side						Average Incremental strain (10^{-6})	Average cumulative Strain (10^{-6})	Sample Number and Side						Average Incremental strain (10^{-6})	Average cumulative Strain (10^{-6})
			1		2		3				1		2		3			
Age (Days)	Temp (°C)	RH (%)	A	B	A	B	A	B			A	B	A	B	A	B		
0	22.1	62	0	0	0	0	0	0	0	0	0	0	0	0	0	0	0	0
0.13	22	62	1	1	1	4	3	3	35	35	9	6	11	4	5	7	112	112
1	21.5	62	1	2	2	2	2	2	29	64	8	7	10	7	5	9	123	235
2	22	62	3	1	1	2	2	2	29	93	8	6	8	6	6	6	107	341
3	22	63	1	1	2	1	1	1	19	112	6	4	7	4	4	5	80	421
4	22.1	63	4	2	3	3	1	1	37	149	4	4	5	4	4	5	69	491
5	21.6	62	2	1	5	2	1	1	32	181	4	3	2	2	3	3	45	536
6	22.1	61	3	4	4	3	6	1	56	237	5	2	4	7	8	4	80	616
7	22.2	61	3	4	1	4	2	1	40	277	2	3	4	4	4	3	53	669
14	22	60	4	5	3	5	5	4	69	347	18	13	18	16	13	18	256	925
21	18	49	3	2	2	3	7	3	53	400	12	11	16	7	9	13	181	1107
28	**19.4**	**62**	**3**	**4**	**2**	**4**	**6**	**5**	**64**	**464**	**10**	**6**	**8**	**7**	**7**	**7**	**120**	**1227**
56	16.6	64	8	9	5	9	5	8	117	581	13	19	28	19	23	23	333	1560
84	15.8	64	7	6	7	8	8	17	141	723	14	11	15	9	13	12	197	1757
112	12.3	66	5	6	2	6	5	6	80	803	8	5	6	2	5	8	91	1848
140	12.2	65	6	5	6	6	7	7	99	901	3	4	7	6	3	4	72	1920
168	12.2	41	7	8	6	8	10	10	131	1032	9	8	9	9	7	8	133	2053
196	18.2	65	5	6	5	8	8	7	104	1136	4	2	4	6	3	3	59	2112
224	12.9	61	6	8	4	5	3	5	83	1219	1	1	2	2	1	2	24	2136
252	13	60	1	1	5	3	4	4	48	1267	6	3	4	3	5	2	61	2197
280	19.8	60	6	5	5	11	8	11	123	1389	4	3	5	3	3	6	64	2261
308	19	63	5	5	6	7	8	5	96	1485	5	6	1	7	3	4	69	2331
336	21	63	1	1	0	3	4	4	35	1520	3	4	3	4	0	1	40	2371
364	20	49	6	5	5	3	6	6	83	1603	0	2	1	1	3	2	24	2395

Table F.2: Creep Strain measurements for M8 prisms

			Unloaded Samples															
			Sealed								Unsealed							
			Sample Number and Side						Average Incremental strain (10^{-6})	Average cumulative Strain (10^{-6})	Sample Number and Side						Average Incremental strain (10^{-6})	Average cumulative Strain (10^{-6})
			1		2		3				1		2		3			
Age (Days)	Temp (^{o}C)	RH (%)	A	B	A	B	A	B			A	B	A	B	A	B		
0	21.6	63	0	0	0	0	0	0	0	0	0	0	0	0	0	0	0	0
0.13	21.6	62	4	3	5	3	2	2	51	51	6	8	7	6	6	4	99	99
1	22	62	3	4	2	2	2	2	40	91	7	8	6	6	6	7	107	205
2	22.1	62	1	3	3	4	2	4	45	136	5	7	8	5	6	4	93	299
3	22.1	63	2	2	3	2	1	3	35	171	6	4	5	4	5	3	72	371
4	22.1	63	3	2	3	3	1	2	37	208	6	7	3	3	3	2	64	435
5	22.1	62	1	2	3	2	3	2	35	243	5	3	6	3	2	2	56	491
6	22.2	61	3	3	4	3	3	1	45	288	7	2	6	3	4	3	67	557
7	19.9	47	4	3	4	1	2	1	40	328	2	5	3	4	4	6	64	621
14	17.6	56	3	2	2	3	2	3	40	368	5	9	5	8	6	5	101	723
21	17.4	52	2	3	2	3	3	2	40	408	7	8	9	7	8	5	117	840
28	**21.6**	**69**	**4**	**3**	**5**	**3**	**1**	**2**	**48**	**456**	**5**	**3**	**13**	**5**	**6**	**5**	**99**	**939**
56	16.6	63	6	6	5	5	5	3	80	536	11	13	10	9	9	8	160	1099
84	12.3	64	7	6	5	6	4	4	85	621	9	10	9	6	12	8	144	1243
112	12.2	66	6	8	6	3	5	5	88	709	2	6	4	6	3	4	67	1309
140	12.3	66	5	4	2	5	3	3	59	768	4	3	4	3	4	4	59	1368
168	12.1	41	9	9	8	4	6	4	107	875	7	8	6	8	6	3	101	1469
196	18.1	62	8	7	6	4	6	5	96	971	9	8	5	7	5	9	115	1584
224	17.9	62	3	3	3	4	3	2	48	1019	4	3	3	5	5	3	61	1645
252	18.1	63	2	4	4	3	1	1	40	1059	9	5	2	3	6	4	77	1723
280	18.1	66	6	7	5	4	5	4	83	1141	5	6	4	6	4	4	77	1800
308	19.1	60	5	6	4	4	4	4	72	1213	5	7	6	6	5	3	85	1885
336	21	61	3	2	2	1	2	2	32	1245	0	1	2	1	2	0	16	1901
364	21	63	2	1	5	3	6	4	56	1301	1	2	2	0	3	2	27	1928

Table F.3: Creep Strain measurements for M16 prisms

			Unloaded Samples															
			Sealed								Unsealed							
			Sample Number and Side						Average Incremental strain (10^{-6})	Average cumulative Strain (10^{-6})	Sample Number and Side						Average Incremental strain (10^{-6})	Average cumulative Strain (10^{-6})
			1		2		3				1		2		3			
Age (Days)	Temp (°C)	RH (%)	A	B	A	B	A	B			A	B	A	B	A	B		
0	22	63	0	0	0	0	0	0	0	0	0	0	0	0	0	0	0	0
0.13	21.9	62	3	4	5	3	5	4	64	64	4	3	4	3	4	5	61	61
1	22.1	61	2	2	3	3	2	3	40	104	6	5	7	4	5	4	83	144
2	21.9	63	2	1	1	2	4	2	32	136	7	7	5	6	7	4	96	240
3	22.1	63	1	2	2	1	1	2	24	160	5	4	6	3	5	2	67	307
4	22.2	62	3	2	2	3	1	3	37	197	4	4	6	2	1	4	56	363
5	22.2	62	3	1	1	2	1	1	24	221	4	3	5	2	5	3	59	421
6	19.9	47	1	2	2	2	2	1	27	248	5	5	6	3	5	2	69	491
7	19	55	2	1	2	1	3	3	32	280	2	2	3	5	3	3	48	539
14	17	59	3	2	2	1	0	1	24	304	7	6	7	9	6	5	107	645
21	17.9	61	4	6	5	5	6	5	83	387	9	8	9	8	8	6	128	773
28	**19.2**	**58**	**3**	**3**	**2**	**2**	**3**	**3**	**43**	**429**	**8**	**8**	**9**	**8**	**9**	**5**	**125**	**899**
56	16.7	64	5	11	11	8	12	10	152	581	21	23	16	20	23	21	331	1229
84	17	64	11	9	11	7	13	9	160	741	16	14	18	10	16	13	232	1461
112	12.7	66	6	5	6	4	6	5	85	827	10	5	14	9	9	7	144	1605
140	12.3	66	6	7	7	6	7	4	99	925	5	4	3	4	8	2	69	1675
168	13.1	41	4	5	6	9	5	5	91	1016	9	8	9	7	8	8	131	1805
196	18	63	4	7	6	6	5	7	93	1109	8	2	7	2	4	4	72	1877
224	12.9	66	5	5	4	2	4	3	61	1171	6	5	7	5	5	2	80	1957
252	13	60	3	6	6	5	4	4	75	1245	6	6	4	5	7	4	85	2043
280	18	60	5	5	4	7	6	5	85	1331	5	6	4	2	3	4	64	2107
308	18.1	61	4	4	4	2	5	4	61	1392	2	9	2	1	4	1	51	2157
336	22	60	3	4	2	2	4	1	43	1435	1	2	1	0	1	2	19	2176
364	20	62	5	3	5	3	2	3	56	1491	1	0	3	0	2	1	19	2195

Table F.4: Creep Strain measurements for M40 prisms

			Unloaded Samples															
			Sealed								Unsealed							
			Sample Number and Side						Average Incremental strain (10^{-6})	Average cumulative Strain (10^{-6})	Sample Number and Side						Average Incremental strain (10^{-6})	Average cumulative Strain (10^{-6})
			1		2		3				1		2		3			
Age (Days)	Temp (°C)	RH (%)	A	B	A	B	A	B			A	B	A	B	A	B		
0	22	63	0	0	0	0	0	0	0	0	0	0	0	0	0	0	0	0
0.13	21.9	62	2	3	2	4	2	2	40	40	3	3	2	5	3	4	53	53
1	22.1	61	2	1	4	1	2	2	32	72	2	2	2	0	7	5	48	101
2	21.9	63	4	2	2	1	3	2	37	109	9	7	13	9	3	9	133	235
3	22.1	63	2	3	2	2	4	2	40	149	6	8	7	7	12	9	131	365
4	22.2	62	1	2	2	1	2	3	29	179	8	6	3	7	2	8	91	456
5	22.2	62	3	2	3	1	3	1	35	213	7	9	7	9	8	7	125	581
6	19.9	47	3	1	1	1	2	2	27	240	7	6	5	13	8	6	120	701
7	19	55	1	1	4	2	1	4	35	275	9	9	7	11	3	9	128	829
14	17	59	8	4	8	6	6	2	91	365	6	5	5	4	12	7	104	933
21	17.9	61	6	4	4	1	6	2	61	427	13	11	12	9	13	9	179	1112
28	**19.2**	**58**	**8**	**5**	**6**	**4**	**6**	**5**	**91**	**517**	**13**	**11**	**9**	**11**	**10**	**9**	**168**	**1280**
56	16.7	64	7	6	8	5	8	6	107	624	21	18	13	21	19	15	285	1565
84	17	64	5	5	10	9	9	7	120	744	10	15	11	19	18	9	219	1784
112	12.7	66	5	5	5	5	6	5	83	827	12	8	13	13	9	5	160	1944
140	12.3	66	8	8	3	8	6	5	101	928	9	7	9	8	8	8	131	2075
168	13.1	41	4	4	8	4	2	2	64	992	12	8	13	9	10	6	155	2229
196	18	63	3	6	3	3	2	3	53	1045	6	7	9	13	9	11	147	2376
224	12.9	66	3	7	4	4	2	4	64	1109	5	8	4	6	7	8	101	2477
252	13	60	4	3	7	6	3	6	77	1187	7	4	8	4	8	9	107	2584
280	18	60	2	2	3	7	6	2	59	1245	3	8	6	7	6	6	96	2680
308	18.1	61	6	3	6	5	4	3	72	1317	7	2	8	8	6	6	99	2779
336	22	60	2	3	8	4	1	4	59	1376	1	2	0	3	2	1	24	2803
364	20	62	7	7	4	7	1	3	77	1453	1	2	1	0	2	0	16	2819

Table F.5: Creep Strain measurements for M8S prisms

			Unloaded Samples															
			Sealed								Unsealed							
			Sample Number and Side						Average Incremental strain (10^{-6})	Average cumulative Strain (10^{-6})	Sample Number and Side						Average Incremental strain (10^{-6})	Average cumulative Strain (10^{-6})
			1		2		3				1		2		3			
Age (Days)	Temp (^{o}C)	RH (%)	A	B	A	B	A	B			A	B	A	B	A	B		
0	12.3	66	0	0	0	0	0	0	0	0	0	0	0	0	0	0	0	0
0.13	12.3	66	7	0	2	2	3	3	45	45	5	5	5	7	4	5	83	83
1	13.1	65	7	1	3	2	0	0	35	80	10	6	11	6	7	7	125	208
2	14.1	66	4	2	0	2	4	1	35	115	1	1	2	2	-3	2	13	221
3	13.3	69	6	2	4	3	4	4	61	176	6	4	8	5	5	8	96	317
4	12.8	70	1	0	1	0	2	0	11	187	2	2	3	1	0	1	24	341
5	13.7	69	4	2	2	0	4	1	35	221	3	2	2	4	3	5	51	392
6	13.8	68	2	2	1	2	0	0	19	240	4	3	3	2	10	3	67	459
7	13.8	60	3	2	1	2	1	2	29	269	4	2	5	4	0	4	51	509
14	13.2	68	11	5	7	4	8	4	104	373	12	8	13	9	6	10	155	664
21	12.1	61	7	3	5	3	6	3	72	445	11	6	12	9	4	8	133	797
28	**13**	**55**	**6**	**4**	**8**	**5**	**4**	**3**	**80**	**525**	**24**	**5**	**13**	**3**	**13**	**3**	**163**	**960**
56	17.1	55	8	6	4	5	7	8	101	627	19	12	28	12	16	13	267	1227
84	17.9	64	7	9	6	6	6	6	107	733	18	6	18	8	11	10	189	1416
112	15.1	64	2	3	6	5	9	5	80	813	15	2	5	3	8	12	120	1536
140	17.1	60	6	13	8	6	6	8	125	939	14	12	10	15	15	15	216	1752
168	18.5	60	3	5	9	2	5	5	77	1016	9	2	8	1	5	4	77	1829
196	19.2	62	8	3	8	3	6	1	77	1093	3	0	7	1	3	1	40	1869
224	17.8	63	9	8	5	7	6	9	117	1211	3	4	9	5	9	8	101	1971
252	19.5	51	7	2	6	5	7	4	83	1293	6	2	6	1	3	3	56	2027
280	22	61	1	1	8	1	5	1	45	1339	1	8	0	0	0	0	24	2051
308	22	62	6	5	7	7	9	4	101	1440	4	5	5	1	3	2	53	2104
336	21	63	3	7	3	0	5	2	53	1493	3	0	2	0	2	1	21	2125
364	20	60	4	6	5	0	8	1	64	1557	3	1	2	2	2	1	29	2155

Table F.6: Creep Strain measurements for M8W prisms

			Unloaded Samples															
			Sealed								Unsealed							
			Sample Number and Side						Average Incremental strain (10^{-6})	Average cumulative Strain (10^{-6})	Sample Number and Side						Average Incremental strain (10^{-6})	Average cumulative Strain (10^{-6})
			1		2		3				1		2		3			
Age (Days)	Temp (°C)	RH (%)	A	B	A	B	A	B			A	B	A	B	A	B		
0	12.3	66	0	0	0	0	0	0	0	0	0	0	0	0	0	0	0	0
0.13	12.3	66	5	1	0	0	0	1	19	19	4	1	16	6	5	5	99	99
1	13.1	65	7	4	5	1	3	0	53	72	5	2	7	3	6	5	75	173
2	14.1	66	6	6	0	1	0	0	35	107	2	0	5	2	2	2	35	208
3	13.3	69	5	0	3	0	3	2	35	141	3	1	8	2	5	4	61	269
4	12.8	70	0	1	1	1	2	1	16	157	4	2	3	1	1	1	32	301
5	13.7	69	3	1	3	1	5	1	37	195	9	2	7	2	4	3	72	373
6	13.8	68	4	1	0	1	2	0	21	216	5	5	3	5	3	2	61	435
7	13.8	60	3	2	1	3	4	0	35	251	2	0	4	0	4	3	35	469
14	13.2	68	5	3	9	4	2	3	69	320	3	7	12	8	14	11	147	616
21	12.1	61	8	1	1	3	8	0	56	376	4	1	7	1	4	2	51	667
28	**13**	**55**	**5**	**4**	**6**	**2**	**4**	**3**	64	**440**	**10**	**6**	**14**	**4**	**10**	**8**	**139**	**805**
56	17.1	55	6	5	6	5	7	4	88	528	18	6	32	8	19	12	253	1059
84	17.9	64	4	6	4	3	5	3	67	595	14	3	18	4	14	8	163	1221
112	15.1	64	4	4	4	5	4	3	64	659	13	5	14	3	7	4	123	1344
140	17.1	60	7	8	7	5	4	5	96	755	19	7	10	8	21	12	205	1549
168	18.5	60	5	3	4	2	3	4	56	811	2	4	5	1	2	1	40	1589
196	19.2	62	8	5	6	7	5	6	99	909	8	5	3	2	0	2	53	1643
224	17.8	63	5	9	7	6	6	8	109	1019	10	4	11	3	11	5	117	1760
252	19.5	51	6	2	7	3	3	4	67	1085	4	0	6	1	3	2	43	1803
280	22	61	5	2	6	4	3	2	59	1144	0	7	1	0	3	0	29	1832
308	22	62	4	7	5	5	4	4	77	1221	3	2	2	1	2	2	32	1864
336	21	63	5	2	3	1	3	2	43	1264	2	1	2	0	1	1	19	1883
364	20	60	3	2	3	2	3	2	40	1304	1	0	2	1	3	1	21	1904

Table F.7: Creep Strain measurements for M16S prisms

			Unloaded Samples															
			Sealed								Unsealed							
			Sample Number and Side						Average Incremental strain (10^{-6})	Average cumulative Strain (10^{-6})	Sample Number and Side						Average Incremental strain (10^{-6})	Average cumulative Strain (10^{-6})
			1		2		3				1		2		3			
Age (Days)	Temp (°C)	RH (%)	A	B	A	B	A	B			A	B	A	B	A	B		
0	17.8	69	0	0	0	0	0	0	0	0	0	0	0	0	0	0	0	0
0.13	17.9	69	2	2	2	1	1	0	21	21	3	3	0	1	4	2	35	35
1	13.8	68	1	0	2	3	5	2	35	56	5	4	7	5	7	3	83	117
2	13.8	60	3	0	1	2	2	2	27	83	3	3	4	2	3	3	48	165
3	13.8	61	2	0	0	2	2	3	24	107	4	3	4	3	5	1	53	219
4	13.7	61	3	3	2	3	3	3	45	152	4	2	5	6	5	6	75	293
5	15.2	58	2	2	1	1	1	2	24	176	3	5	6	4	4	3	67	360
6	14.1	62	2	0	1	1	2	4	27	203	3	5	3	3	1	1	43	403
7	13.5	66	3	2	4	3	2	4	48	251	1	3	3	4	2	1	37	440
14	12.2	65	4	3	4	1	5	3	53	304	7	8	5	9	10	8	125	565
21	13	60	3	4	2	1	2	3	40	344	6	3	10	4	7	4	91	656
28	**13**	**55**	**5**	**4**	**4**	**3**	**3**	**4**	**61**	**405**	**6**	**8**	**6**	**6**	**6**	**7**	**104**	**760**
56	18.8	43	16	14	15	9	8	13	200	605	20	16	25	14	24	16	307	1067
84	17.9	64	13	9	11	10	12	10	173	779	13	10	12	12	11	6	171	1237
112	15.1	64	5	4	3	5	3	4	64	843	11	8	5	7	4	10	120	1357
140	17.1	60	6	4	7	5	6	5	88	931	16	14	12	13	19	7	216	1573
168	18.5	60	9	6	7	7	5	6	107	1037	3	2	5	3	3	2	48	1621
196	21	61	4	4	5	3	4	1	56	1093	2	1	5	2	4	1	40	1661
224	17.5	62	5	9	3	5	4	3	77	1171	7	7	11	7	8	6	123	1784
252	19.5	62	7	3	5	5	3	3	69	1240	4	3	5	6	2	3	61	1845
280	22	61	6	5	5	3	4	5	75	1315	1	1	2	3	3	3	35	1880
308	20	63	8	7	6	6	7	4	101	1416	2	2	3	3	2	1	35	1915
336	21	61	1	1	1	1	1	1	16	1432	1	1	1	1	1	1	16	1931
364	22	62	1	1	1	1	1	1	16	1448	1	1	1	1	1	1	16	1947

Table F.8: Creep Strain measurements for M16W prisms

			Unloaded Samples															
			Sealed								Unsealed							
			Sample Number and Side						Average Incremental strain (10^{-6})	Average cumulative Strain (10^{-6})	Sample Number and Side						Average Incremental strain (10^{-6})	Average cumulative Strain (10^{-6})
			1		2		3				1		2		3			
Age (Days)	Temp (^{o}C)	RH (%)	A	B	A	B	A	B			A	B	A	B	A	B		
0	17.8	69	0	0	0	0	0	0	0	0	0	0	0	0	0	0	0	0
0.13	17.9	69	2	2	2	1	1	2	27	27	3	3	7	1	4	2	53	53
1	13.8	68	1	0	2	3	5	2	35	61	5	4	6	5	7	3	80	133
2	13.8	60	3	0	1	2	1	2	24	85	3	3	4	2	3	8	61	195
3	13.8	61	0	2	3	2	2	3	32	117	6	5	6	1	6	6	80	275
4	13.7	61	1	1	2	3	2	1	27	144	7	2	3	6	3	1	59	333
5	15.2	58	2	1	1	1	1	2	21	165	3	5	6	4	4	3	67	400
6	14.1	62	2	0	1	1	2	4	27	192	1	4	3	5	1	1	40	440
7	13.5	66	1	0	0	1	2	3	19	211	1	3	3	1	2	1	29	469
14	12.2	65	4	3	4	1	5	3	53	264	7	8	5	9	10	8	125	595
21	13	60	1	3	3	2	2	2	35	299	6	3	10	4	7	4	91	685
28	**13**	**55**	**5**	**4**	**4**	**3**	**3**	**4**	**61**	**360**	**6**	**8**	**6**	**6**	**6**	**7**	**104**	**789**
56	18.8	43	18	11	13	11	12	9	197	557	20	16	25	14	18	16	291	1080
84	17.9	64	6	4	6	5	6	5	85	643	12	11	12	14	12	6	179	1259
112	15.1	64	5	4	3	5	3	4	107	749	12	8	10	11	10	4	147	1405
140	17.1	60	8	9	4	6	7	5	64	813	9	11	12	13	19	14	208	1613
168	18.5	60	9	6	7	7	5	6	104	917	7	2	7	8	8	2	91	1704
196	21	61	4	4	5	3	4	1	56	973	2	1	5	2	4	1	40	1744
224	17.5	62	12	9	11	10	11	9	165	1139	9	7	11	7	8	6	128	1872
252	19.5	62	7	3	5	5	3	3	69	1208	4	3	6	5	2	3	61	1933
280	22	61	6	5	5	3	4	5	75	1283	1	1	2	3	3	3	35	1968
308	20	63	6	7	6	6	5	4	91	1373	2	2	3	3	2	1	35	2003
336	21	61	4	4	5	3	3	4	61	1435	2	1	2	1	2	1	24	2027
364	22	62	4	2	3	3	4	2	48	1483	1	0	2	0	2	0	13	2040

Table F.9: Creep Strain measurements for M40S prisms

			Unloaded Samples															
			Sealed								Unsealed							
			Sample Number and Side						Average Incremental strain (10^{-6})	Average cumulative Strain (10^{-6})	Sample Number and Side						Average Incremental strain (10^{-6})	Average cumulative Strain (10^{-6})
			1		2		3				1		2		3			
Age (Days)	Temp (^{o}C)	RH (%)	A	B	A	B	A	B			A	B	A	B	A	B		
0	15.4	59	0	0	0	0	0	0	0	0	0	0	0	0	0	0	0	0
0.13	14.1	59	1	3	2	1	1	2	27	27	6	5	6	5	5	3	80	80
1	13.6	62	3	2	2	4	3	1	40	67	4	1	3	3	2	3	43	123
2	13.5	66	4	4	3	1	2	1	40	107	2	1	3	2	3	2	35	157
3	13.2	97	2	3	2	3	3	1	37	144	7	7	6	5	5	5	93	251
4	13	69	1	3	3	4	3	5	51	195	1	3	2	2	3	4	40	291
5	12.5	66	3	2	3	1	1	4	37	232	3	2	2	2	1	1	29	320
6	12.6	59	5	1	2	1	3	1	35	267	3	4	3	2	3	2	45	365
7	12.6	58	0	2	3	1	3	1	27	293	3	2	4	3	2	3	45	411
14	12.9	58	1	3	2	4	2	4	43	336	9	6	4	5	4	4	85	496
21	13	62	7	2	2	1	1	3	43	379	10	13	10	6	9	5	141	637
28	**18.8**	**55**	**8**	**5**	**6**	**6**	**3**	**5**	**88**	**467**	**10**	**2**	**9**	**8**	**8**	**4**	**109**	**747**
56	17.8	65	7	4	8	7	7	8	109	576	18	10	14	14	18	18	245	992
84	15.1	64	10	7	9	11	6	6	131	707	11	16	12	7	10	4	160	1152
112	17	64	7	6	7	6	8	6	107	813	13	13	11	13	5	8	168	1320
140	17.5	60	8	7	12	6	8	13	144	957	11	10	12	15	8	12	181	1501
168	21	60	9	7	6	4	6	5	99	1056	10	11	12	7	3	2	120	1621
196	19.5	62	2	1	2	2	2	4	35	1091	6	5	8	5	7	3	91	1712
224	19.5	63	5	4	3	6	5	8	83	1173	7	6	7	7	12	8	125	1837
252	22	63	3	5	4	3	6	7	75	1248	2	3	1	4	4	6	53	1891
280	21	63	4	1	3	2	2	3	40	1288	2	1	4	2	3	1	35	1925
308	20	61	7	7	6	4	7	8	104	1392	4	3	3	1	2	0	35	1960
336	22	60	2	2	1	2	3	3	35	1427	2	2	2	2	3	1	32	1992
364	22	62	2	2	1	1	2	4	32	1459	1	2	2	2	1	1	24	2016

Table F.10: Creep Strain measurements for M40W prisms

			Unloaded Samples															
			Sealed								Unsealed							
			Sample Number and Side						Average Incremental strain (10^{-6})	Average cumulative Strain (10^{-6})	Sample Number and Side						Average Incremental strain (10^{-6})	Average cumulative Strain (10^{-6})
			1		2		3				1		2		3			
Age (Days)	Temp (°C)	RH (%)	A	B	A	B	A	B			A	B	A	B	A	B		
0	15.4	59	0	0	0	0	0	0	0	0	0	0	0	0	0	0	0	0
0.13	14.1	59	2	2	0	5	0	4	35	35	1	2	2	4	1	4	37	37
1	13.6	62	2	3	1	2	1	3	32	67	2	7	2	3	5	3	59	96
2	13.5	66	3	3	2	2	2	1	35	101	4	3	4	5	3	3	59	155
3	13.2	97	3	4	2	5	1	5	53	155	2	7	3	5	4	6	72	227
4	13	69	4	4	2	3	3	3	51	205	5	6	7	4	4	5	83	309
5	12.5	66	1	1	4	1	2	4	35	240	1	2	3	3	2	1	32	341
6	12.6	59	5	2	2	3	1	2	40	280	1	4	2	4	3	1	40	381
7	12.6	58	3	1	3	1	4	2	37	317	3	3	4	3	5	4	59	440
14	12.9	58	2	2	1	3	1	3	32	349	8	6	6	6	6	8	107	547
21	13	62	1	3	1	6	1	0	32	381	13	8	3	6	4	3	99	645
28	**18.8**	**55**	**5**	**5**	**3**	**2**	**2**	**6**	**61**	**443**	**10**	**8**	**6**	**8**	**8**	**7**	**125**	**771**
56	17.8	65	6	7	9	7	9	8	123	565	18	20	14	22	16	21	296	1067
84	15.1	64	8	7	6	4	7	9	109	675	3	18	6	15	11	13	176	1243
112	17	64	6	6	6	7	4	5	91	765	6	8	4	8	4	6	96	1339
140	17.5	60	8	5	8	6	9	8	117	883	9	13	12	18	13	16	216	1555
168	21	60	8	5	7	4	5	6	93	976	2	16	1	8	4	5	96	1651
196	19.5	62	3	5	2	5	8	6	77	1053	5	6	7	6	7	2	88	1739
224	19.5	63	8	9	6	9	5	7	117	1171	6	15	7	12	9	11	160	1899
252	22	63	6	4	6	5	4	5	80	1251	0	4	2	3	1	3	35	1933
280	21	63	4	6	2	4	1	7	64	1315	0	3	0	3	1	1	21	1955
308	20	61	5	6	7	4	5	4	83	1397	1	4	2	4	2	2	40	1995
336	22	60	2	3	4	7	4	3	61	1459	1	2	1	2	1	2	24	2019
364	22	62	3	2	3	3	2	6	51	1509	1	3	0	2	1	1	21	2040

Table F.11: Results of basic creep results (a)

Mix ID	Reference			M8			M16			M40		
Applied stress	14.3 MPa			10 Mpa			10.7 Mpa			9.8 Mpa		
Stress/strength ratio	30%			30%			30%			30%		
Age (days)	Average cumulative strain ($\times 10^6$)	Specific creep ($\times 10^{-6}$ Mpa)	Creep coefficient (Creep factor)	Average cumulative strain ($\times 10^6$)	Specific creep ($\times 10^{-6}$ Mpa)	Creep coefficient (Creep factor)	Average cumulative strain ($\times 10^6$)	Specific creep ($\times 10^{-6}$ Mpa)	Creep coefficient (Creep factor)	Average cumulative strain ($\times 10^6$)	Specific creep ($\times 10^{-6}$ Mpa)	Creep coefficient (Creep factor)
1	53	4	0.1	85	9	0.3	85	8	0.3	37	4	0.1
2	75	5	0.2	128	13	0.4	101	9	0.3	72	7	0.2
3	83	6	0.2	149	15	0.4	125	12	0.4	112	11	0.4
4	109	8	0.3	181	18	0.5	160	15	0.5	139	14	0.5
5	136	10	0.3	213	21	0.6	176	16	0.5	163	17	0.5
6	184	13	0.5	251	25	0.7	189	18	0.6	181	19	0.6
7	216	15	0.5	283	28	0.8	208	19	0.6	208	21	0.7
14	256	18	0.6	288	29	0.9	208	19	0.6	291	30	1.0
21	301	21	0.7	312	31	0.9	269	25	0.8	328	33	1.1
28	333	23	0.8	336	34	1.0	301	28	0.9	395	40	1.3
56	403	28	1.0	392	39	1.2	424	40	1.3	461	47	1.5
84	491	34	1.2	443	44	1.3	539	50	1.6	549	56	1.8
112	563	39	1.4	517	52	1.5	611	57	1.8	608	62	2.0
140	653	46	1.6	557	56	1.6	691	65	2.1	677	69	2.2
168	776	54	1.9	656	66	1.9	765	72	2.3	725	74	2.4
196	877	61	2.2	741	74	2.2	837	78	2.5	765	78	2.5
224	952	67	2.3	768	77	2.3	877	82	2.7	819	84	2.7
252	995	70	2.5	789	79	2.3	936	87	2.8	877	90	2.9
280	1104	77	2.7	856	86	2.5	1005	94	3.0	917	94	3.0
308	1189	83	2.9	915	91	2.7	1061	99	3.2	981	100	3.2
336	1216	85	3.0	936	94	2.8	1093	102	3.3	1027	105	3.4
364	1293	90	3.2	979	98	2.9	1133	106	3.4	1099	112	*3.6*

Table F.12: Results of basic creep results (b)

Mix ID	M8S			M8W			M16S		
Applied stress	11.1 MPa			9 MPa			9.3 MPa		
Stress/strength ratio	30%			30%			30%		
Age (days)	Average cumulative strain ($\times 10^6$)	Specific creep ($\times 10^{-6}$ MPa)	Creep coefficient (Creep factor)	Average cumulative strain ($\times 10^6$)	Specific creep ($\times 10^{-6}$ MPa)	Creep coefficient (Creep factor)	Average cumulative strain ($\times 10^6$)	Specific creep ($\times 10^{-6}$ MPa)	Creep coefficient (Creep factor)
1	77	7	0.2	56	6	0.16	56	6	0.15
2	112	10	0.3	88	10	0.25	56	6	0.15
3	173	16	0.5	101	11	0.28	75	8	0.20
4	171	15	0.5	109	12	0.31	112	12	0.30
5	197	18	0.5	120	13	0.34	128	14	0.35
6	208	19	0.6	139	15	0.39	147	16	0.40
7	221	20	0.6	171	19	0.48	176	19	0.48
14	299	27	0.8	216	24	0.60	216	23	0.59
21	360	32	1.0	256	28	0.72	232	25	0.63
28	416	37	1.1	299	33	0.84	283	30	0.77
56	491	44	1.3	360	40	1.01	437	47	1.19
84	573	52	1.6	397	44	1.11	600	65	1.63
112	621	56	1.7	435	48	1.22	635	68	1.72
140	717	65	1.9	507	56	1.42	699	75	1.90
168	776	70	2.1	547	61	1.53	784	84	2.13
196	832	75	2.3	629	70	1.76	827	89	2.25
224	933	84	2.5	720	80	2.01	864	93	2.35
252	997	90	2.7	773	86	2.16	915	98	2.49
280	1019	92	2.8	816	91	2.28	979	105	2.66
308	1099	99	3.0	883	98	2.47	1056	114	2.87
336	1141	103	3.1	912	101	2.55	1067	115	2.90
364	1200	108	3.3	936	104	2.62	1080	116	2.93

Table F.13: Results of basic creep results (c)

Mix ID	M16W			M40S			M40W		
Applied stress	9.8 MPa			10.7 MPa			9.8 MPa		
Stress/strength ratio	30%			30%			30%		
Age (days)	Average cumulative strain ($\times 10^6$)	Specific creep ($\times 10^{-6}$ MPa)	Creep coefficient (Creep factor)	Average cumulative strain ($\times 10^6$)	Specific creep ($\times 10^{-6}$ MPa)	Creep coefficient (Creep factor)	Average cumulative strain ($\times 10^6$)	Specific creep ($\times 10^{-6}$ MPa)	Creep coefficient (Creep factor)
1	45	5	0.13	48	5	0.14	59	7	0.17
2	43	5	0.12	83	9	0.23	85	9	0.24
3	69	8	0.19	112	13	0.32	128	14	0.37
4	83	9	0.23	157	18	0.45	173	19	0.50
5	96	11	0.27	184	21	0.52	203	23	0.58
6	120	13	0.33	203	23	0.58	229	25	0.66
7	120	13	0.33	221	25	0.63	256	28	0.73
14	160	18	0.44	251	28	0.71	280	31	0.80
21	171	19	0.47	280	31	0.80	304	34	0.87
28	221	25	0.61	341	38	0.97	341	38	0.98
56	376	42	1.04	395	44	1.12	424	47	1.21
84	440	49	1.22	512	58	1.45	512	57	1.47
112	515	58	1.43	589	66	1.67	579	64	1.66
140	547	61	1.52	704	79	2.00	680	76	1.95
168	629	71	1.75	779	87	2.21	747	83	2.14
196	672	76	1.87	797	90	2.27	805	89	2.31
224	813	91	2.26	853	96	2.42	899	100	2.57
252	864	97	2.40	920	103	2.61	944	105	2.70
280	931	105	2.59	949	107	2.70	989	110	2.83
308	1008	113	2.80	1040	117	2.95	1064	118	3.05
336	1059	119	2.94	1072	120	3.05	1112	124	3.18
364	1101	124	3.06	1101	124	3.13	1160	129	3.32

Table F.14: Results of total creep results (a)

Mix ID	Reference			M8			M16			M40		
Applied stress	14.3 MPa			10 MPa			10.7 MPa			9.8 MPa		
Stress/strength ratio	30%			30%			30%			30%		
Age (days)	Average cumulative strain ($\times 10^6$)	Specific creep ($\times 10^{-6}$ MPa)	Creep coefficient (Creep factor)	Average cumulative strain ($\times 10^6$)	Specific creep ($\times 10^{-6}$ MPa)	Creep coefficient (Creep factor)	Average cumulative strain ($\times 10^6$)	Specific creep ($\times 10^{-6}$ MPa)	Creep coefficient (Creep factor)	Average cumulative strain ($\times 10^6$)	Specific creep ($\times 10^{-6}$ MPa)	Creep coefficient (Creep factor)
1	192	13	0.47	189	19	0.59	75	7	0.22	64	4	0.15
2	280	20	0.68	261	26	0.81	139	13	0.40	192	13	0.45
3	333	23	0.82	312	31	0.97	192	18	0.56	301	21	0.70
4	368	26	0.90	371	37	1.15	235	22	0.68	381	27	0.89
5	400	28	0.98	421	42	1.31	272	25	0.79	480	34	1.12
6	472	33	1.15	475	47	1.47	328	31	0.95	592	41	1.38
7	512	36	1.25	525	53	1.63	363	34	1.05	696	49	1.62
14	717	50	1.75	595	59	1.84	448	42	1.30	765	54	1.78
21	888	62	2.17	699	70	2.17	539	50	1.57	920	64	2.14
28	987	69	2.41	760	76	2.36	640	60	1.86	1053	74	2.45
56	1253	88	3.07	869	87	2.69	912	85	2.65	1280	90	2.98
84	1419	99	3.47	979	98	3.03	1096	102	3.19	1448	101	3.37
112	1496	105	3.66	1019	102	3.16	1211	113	3.52	1587	111	3.70
140	1557	109	3.81	1045	105	3.24	1269	119	3.69	1699	119	3.96
168	1672	117	4.09	1131	113	3.50	1389	130	4.04	1832	128	4.27
196	1720	120	4.21	1229	123	3.81	1453	136	4.22	1965	137	4.58
224	1733	121	4.24	1272	127	3.94	1528	143	4.44	2051	143	4.78
252	1784	125	4.36	1331	133	4.12	1597	149	4.64	2141	150	4.99
280	1837	128	4.49	1389	139	4.31	1643	154	4.78	2219	155	5.17
308	1893	132	4.63	1459	146	4.52	1685	158	4.90	2304	161	5.37
336	1925	135	4.71	1464	146	4.54	1688	158	4.91	2317	162	5.40
364	1944	136	4.75	1483	148	4.60	1701	159	4.95	2325	163	5.42

Table F.15: Results of total creep results (b)

Mix ID	M8S			M8W			M16S		
Applied stress	11.1 MPa			9.0 MPa			9.3 MPa		
Stress/strength ratio	30%			30%			30%		
Age (days)	Average cumulative strain ($\times 10^6$)	Specific creep ($\times 10^{-6}$ MPa)	Creep coefficient (Creep factor)	Average cumulative strain ($\times 10^6$)	Specific creep ($\times 10^{-6}$ MPa)	Creep coefficient (Creep factor)	Average cumulative strain ($\times 10^6$)	Specific creep ($\times 10^{-6}$ MPa)	Creep coefficient (Creep factor)
1	195	18	0.58	157	17	0.45	83	9	0.27
2	187	17	0.56	179	20	0.51	104	11	0.34
3	261	24	0.78	224	25	0.64	152	16	0.50
4	277	25	0.83	248	28	0.71	213	23	0.70
5	323	29	0.96	299	33	0.85	264	28	0.86
6	363	33	1.08	352	39	1.01	285	31	0.93
7	389	35	1.16	381	42	1.09	315	34	1.03
14	509	46	1.52	488	54	1.40	395	42	1.29
21	611	55	1.82	515	57	1.47	453	49	1.48
28	715	64	2.13	624	69	1.79	533	57	1.74
56	936	84	2.79	837	93	2.40	771	83	2.51
84	1101	99	3.28	971	108	2.78	923	99	3.01
112	1189	107	3.54	1056	117	3.02	997	107	3.25
140	1376	124	4.10	1213	135	3.47	1165	125	3.80
168	1437	129	4.28	1227	136	3.51	1197	129	3.90
196	1459	131	4.34	1256	140	3.60	1229	132	4.01
224	1549	140	4.61	1352	150	3.87	1317	142	4.30
252	1589	143	4.73	1373	153	3.93	1373	148	4.48
280	1600	144	4.76	1384	154	3.96	1403	151	4.57
308	1635	147	4.87	1392	155	3.98	1413	152	4.61
336	1656	149	4.93	1397	155	4.00	1429	154	4.66
364	1685	152	5.02	1413	157	4.05	1445	155	4.71

Table F.16: Results of total creep results (c)

Mix ID	M16W			M40S			M40W		
Applied stress	9.8 MPa			10.7 MPa			9.8 MPa		
Stress/strength ratio	30%			30%			30%		
Age (days)	Average cumulative strain ($\times 10^6$)	Specific creep ($\times 10^{-6}$ MPa)	Creep coefficient (Creep factor)	Average cumulative strain ($\times 10^6$)	Specific creep ($\times 10^{-6}$ MPa)	Creep coefficient (Creep factor)	Average cumulative strain ($\times 10^6$)	Specific creep ($\times 10^{-6}$ MPa)	Creep coefficient (Creep factor)
1	93	10	0.28	104	12	0.35	48	5	0.16
2	125	14	0.38	123	14	0.41	77	9	0.25
3	195	22	0.59	205	23	0.69	141	16	0.46
4	245	28	0.75	245	28	0.83	224	25	0.73
5	296	33	0.90	259	29	0.87	237	26	0.77
6	315	35	0.96	285	32	0.96	261	29	0.85
7	336	38	1.02	325	37	1.10	304	34	0.99
14	416	47	1.27	392	44	1.32	384	43	1.25
21	459	52	1.40	504	57	1.70	445	49	1.45
28	539	61	1.64	581	65	1.96	536	60	1.75
56	776	87	2.37	765	86	2.59	771	86	2.51
84	917	103	2.80	869	98	2.94	904	100	2.95
112	1024	115	3.12	987	111	3.33	971	108	3.17
140	1189	134	3.63	1133	127	3.83	1157	129	3.77
168	1264	142	3.85	1213	136	4.10	1235	137	4.03
196	1283	144	3.91	1283	144	4.33	1309	145	4.27
224	1384	156	4.22	1365	153	4.61	1435	159	4.68
252	1437	161	4.38	1411	159	4.77	1467	163	4.78
280	1467	165	4.47	1427	160	4.82	1469	163	4.79
308	1488	167	4.54	1445	162	4.88	1499	167	4.89
336	1509	170	4.60	1469	165	4.96	1512	168	4.93
364	1520	171	4.63	1493	168	5.05	1528	170	4.98

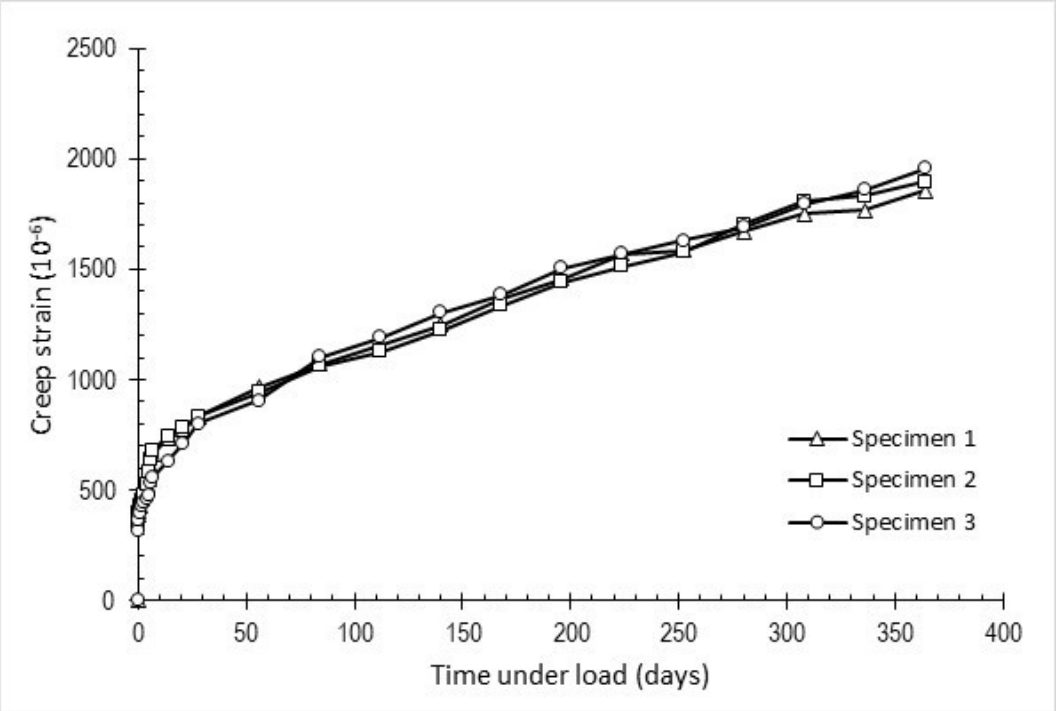

Figure F.1: Creep strains of sealed Reference specimens

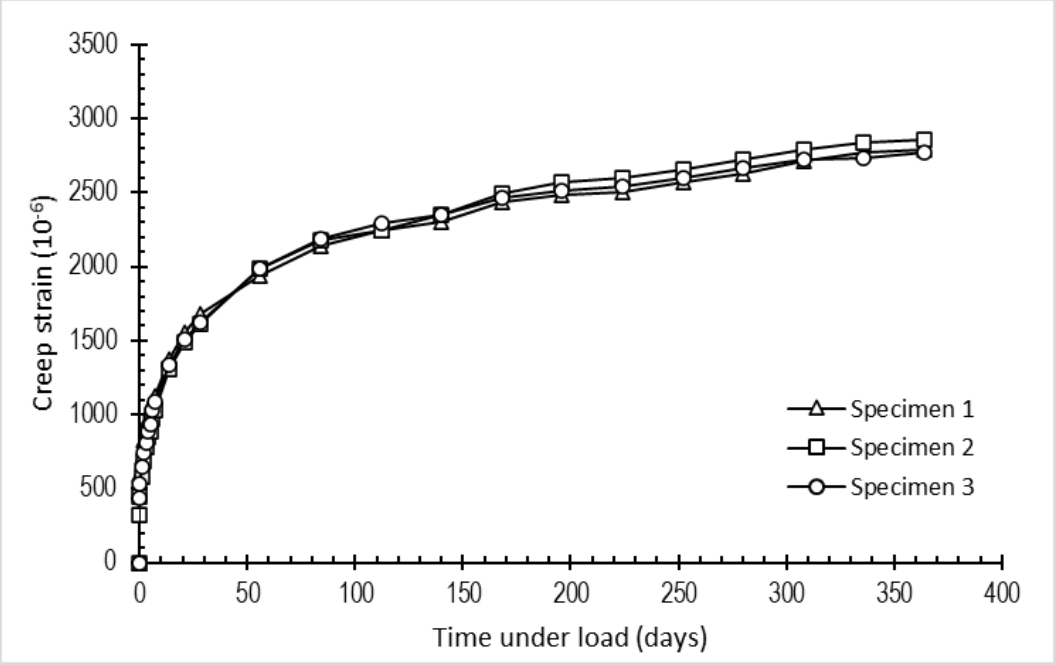

Figure F.2: Creep strains of unsealed Reference specimens

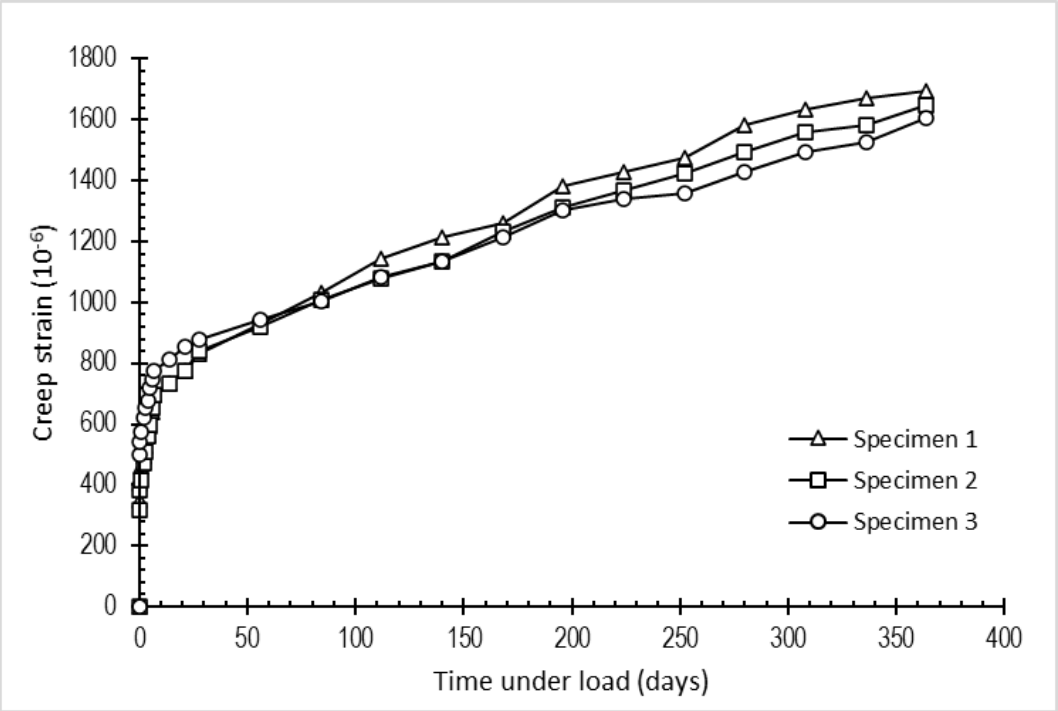

Figure F.3: Creep strains of sealed M8 specimens

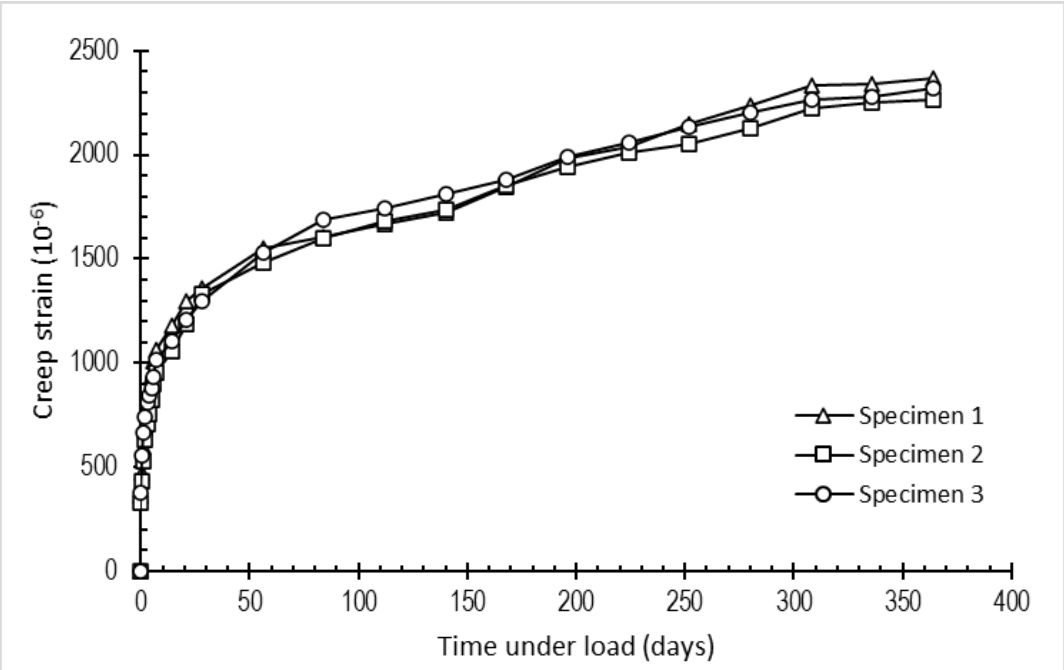

Figure F.4: Creep strains of unsealed M8 specimens

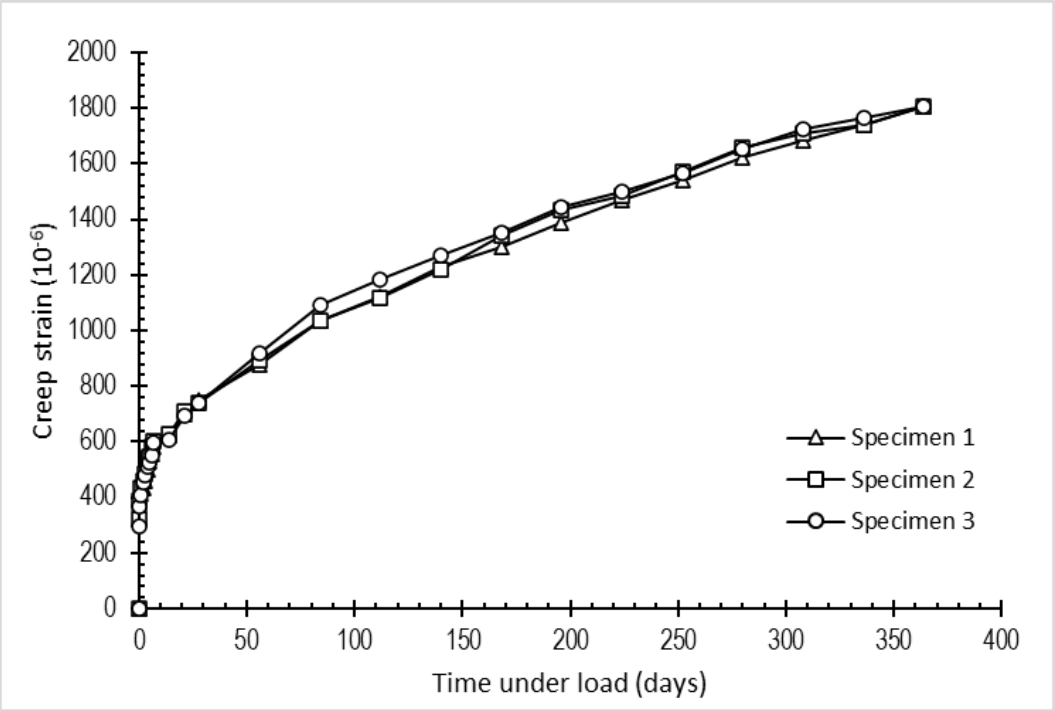

Figure F.5: Creep strains of sealed M16 specimens

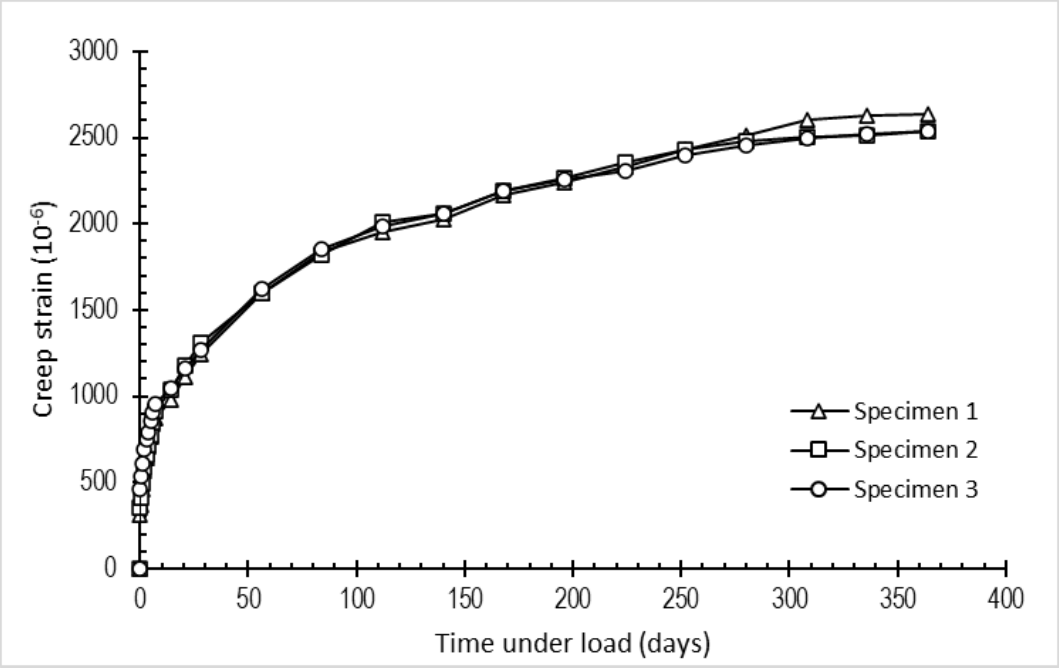

Figure F.6: Creep strains of unsealed M16 specimens

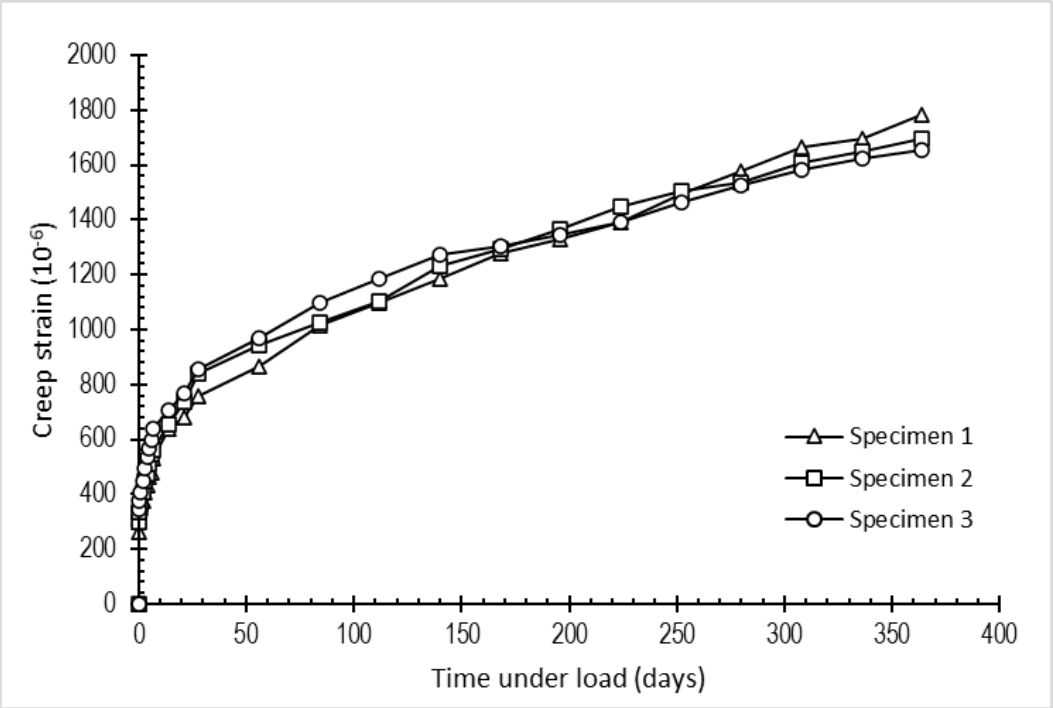

Figure F.7: Creep strains of sealed M40 specimens

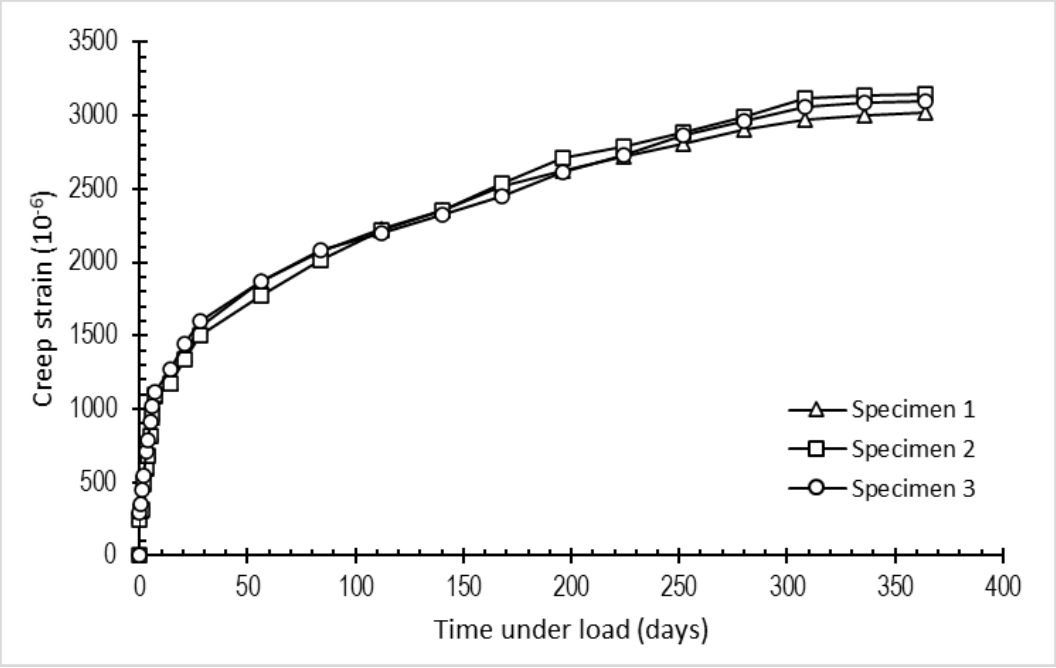

Figure F.8: Creep strains of unsealed M40 specimens

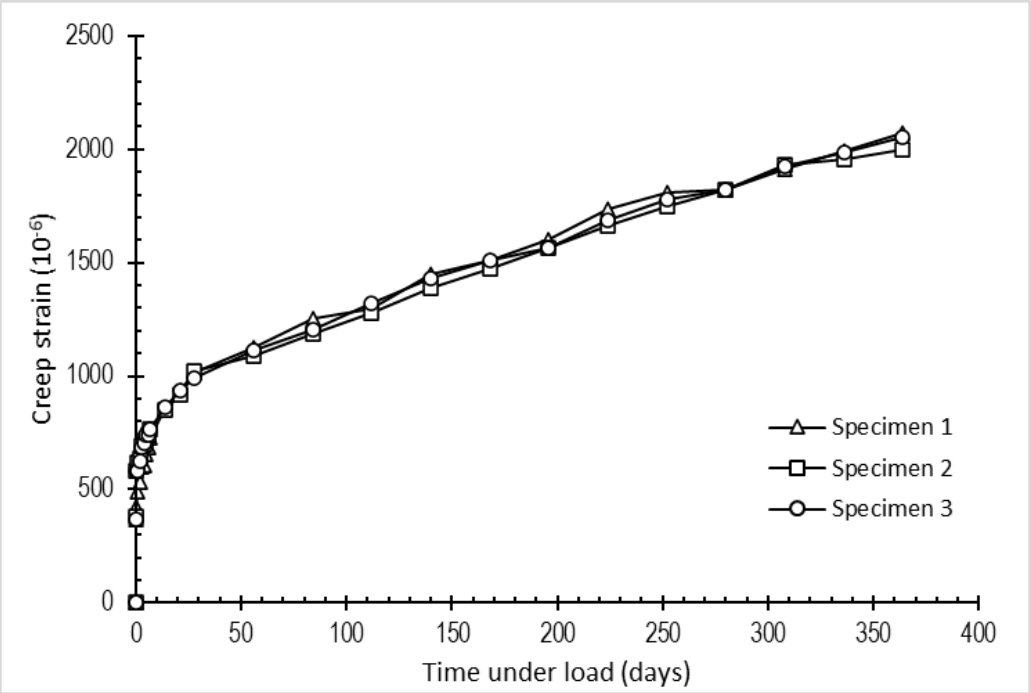

Figure F.9: Creep strains of sealed M8S specimens

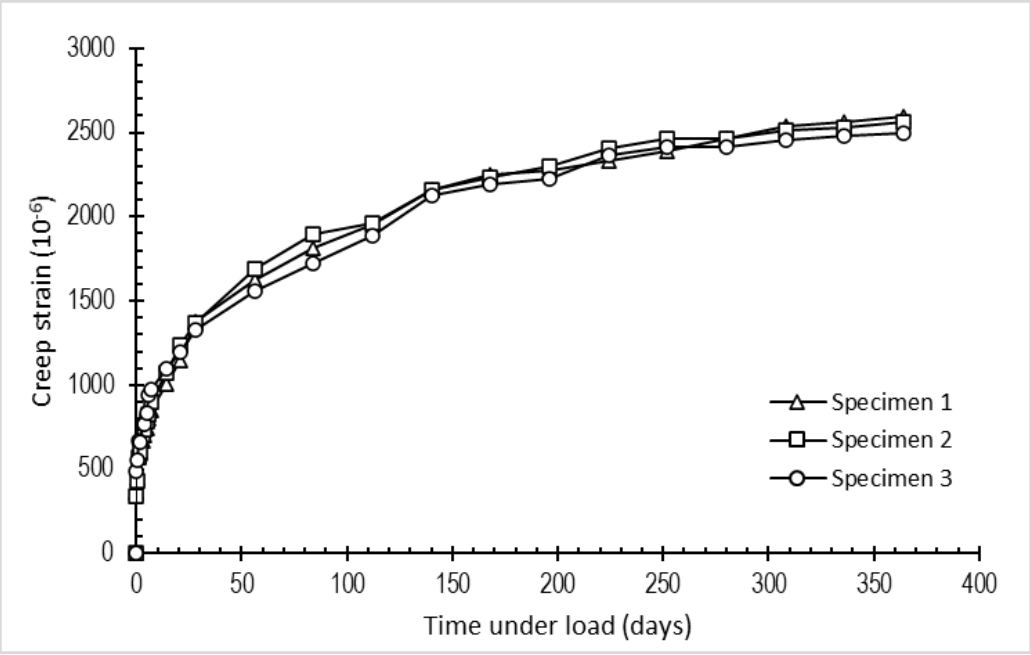

Figure F.10: Creep strains of unsealed M8S specimens

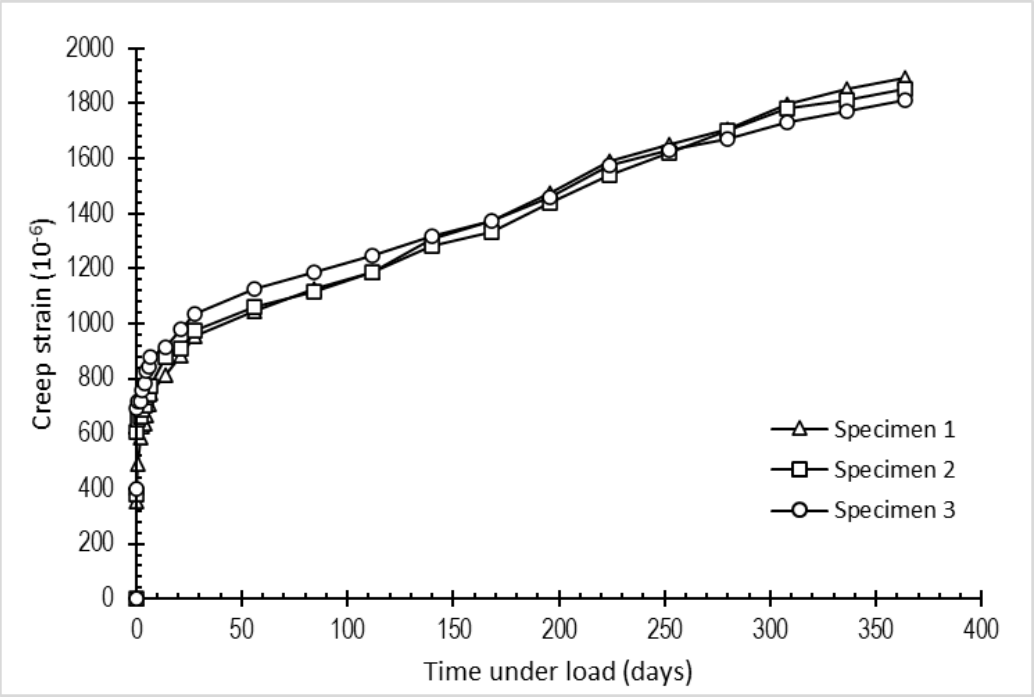

Figure F.11: Creep strains of sealed M8W specimens

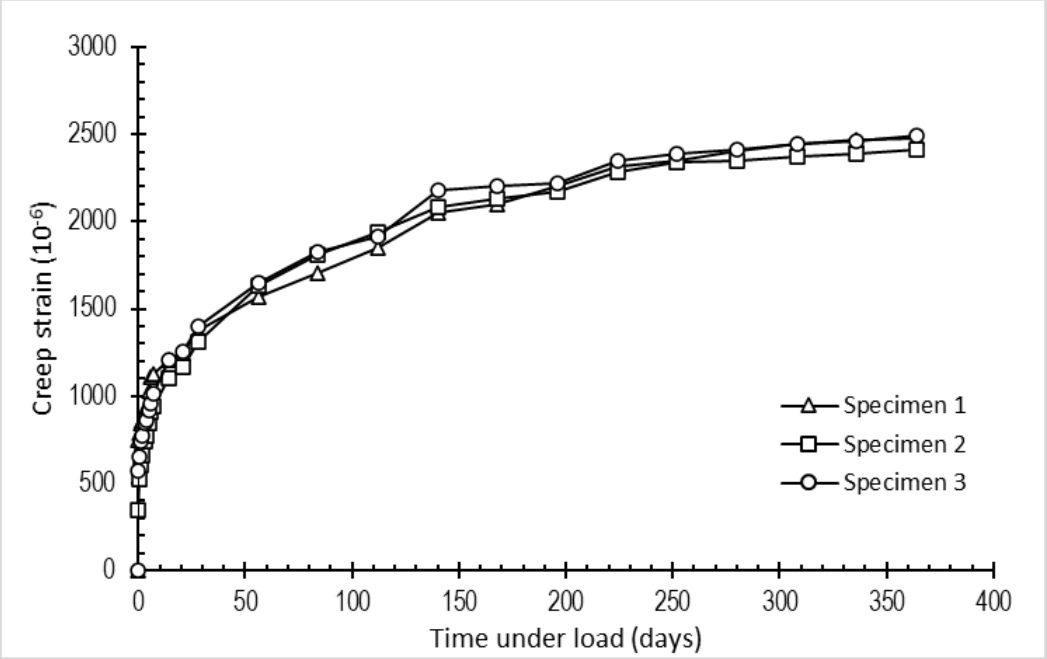

Figure F.12: Creep strains of unsealed M8W specimens

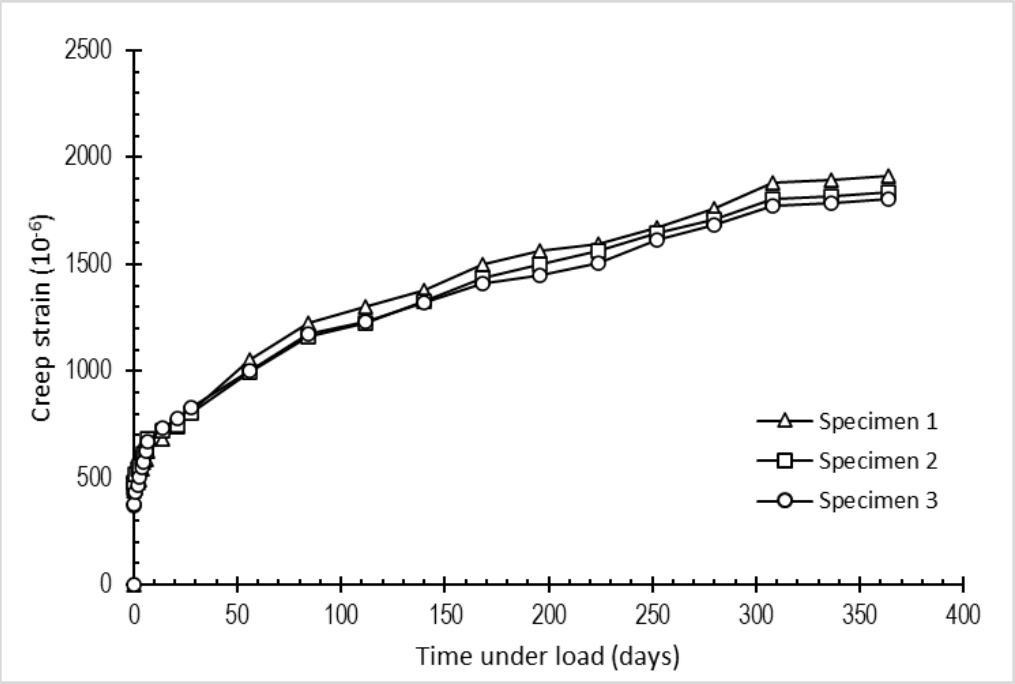

Figure F.13: Creep strains of sealed M16S specimens

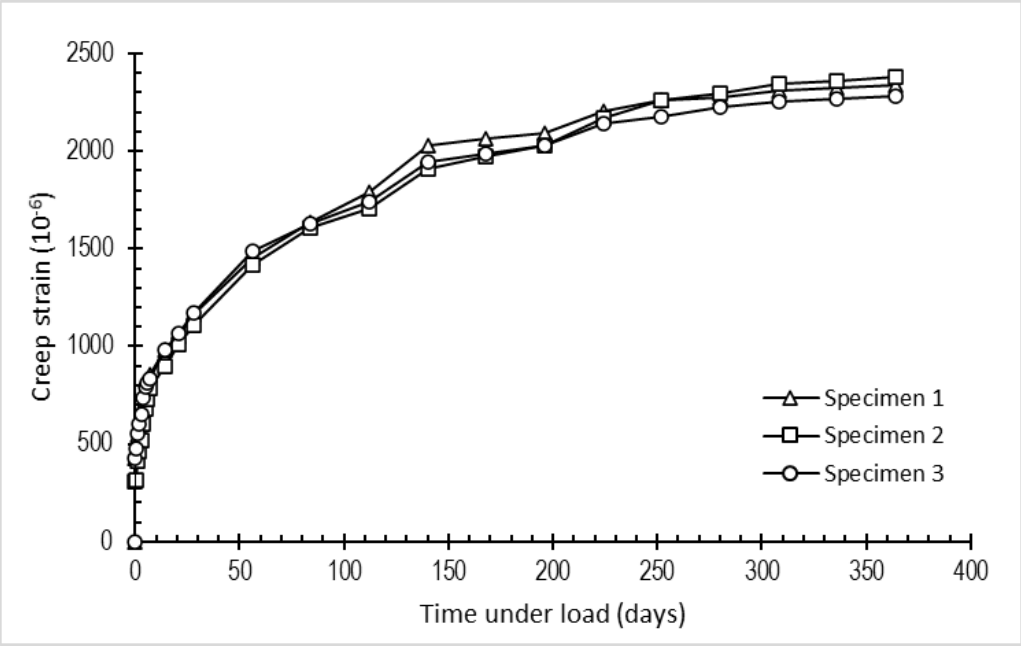

Figure F.14: Creep strains of unsealed M16S specimens

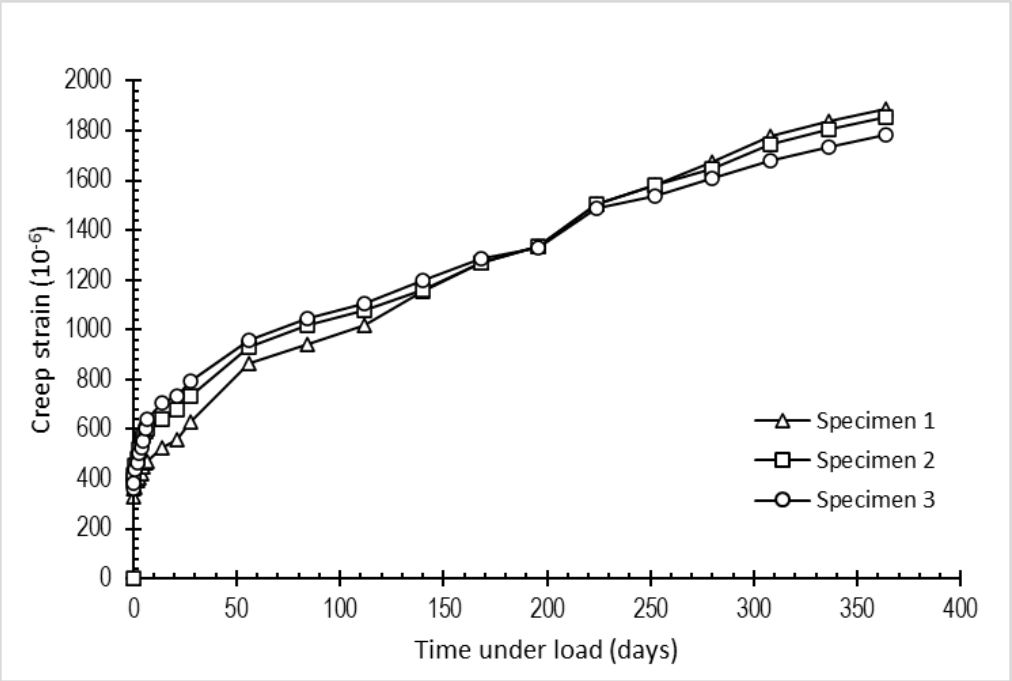

Figure F.15: Creep strains of sealed M16W specimens

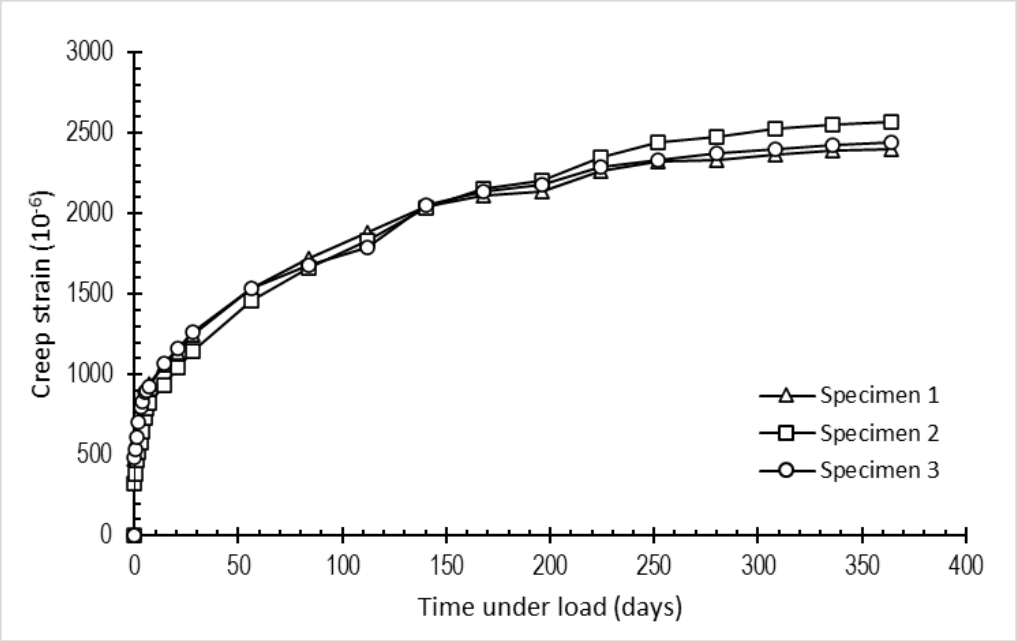

Figure F.16: Creep strains of unsealed M16W specimens

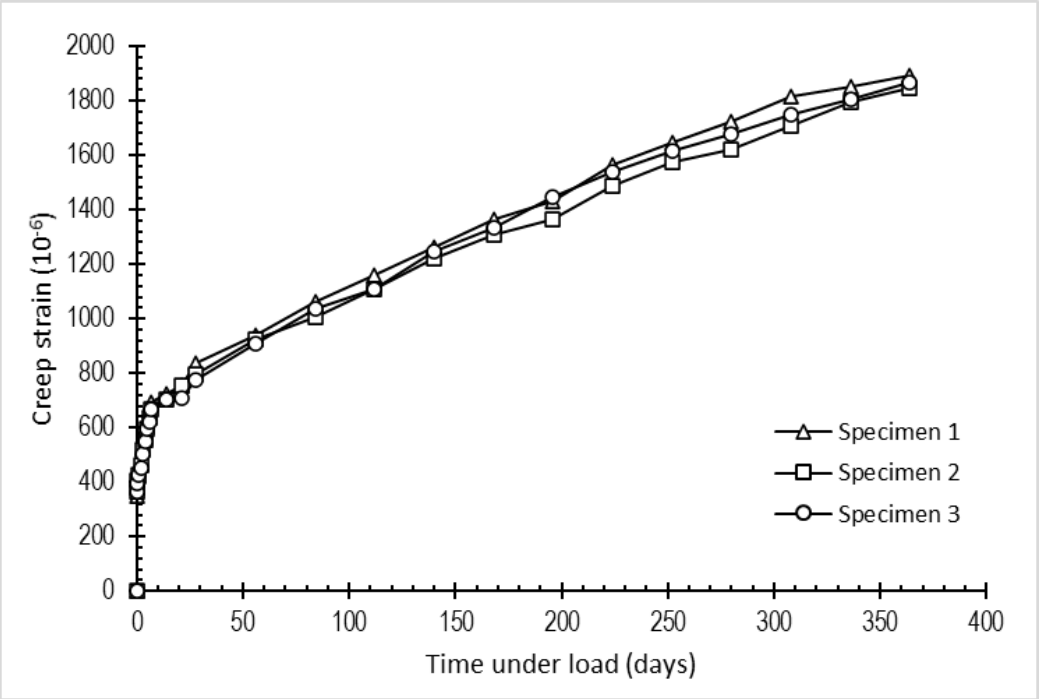

Figure F.17: Creep strains of sealed M40S specimens

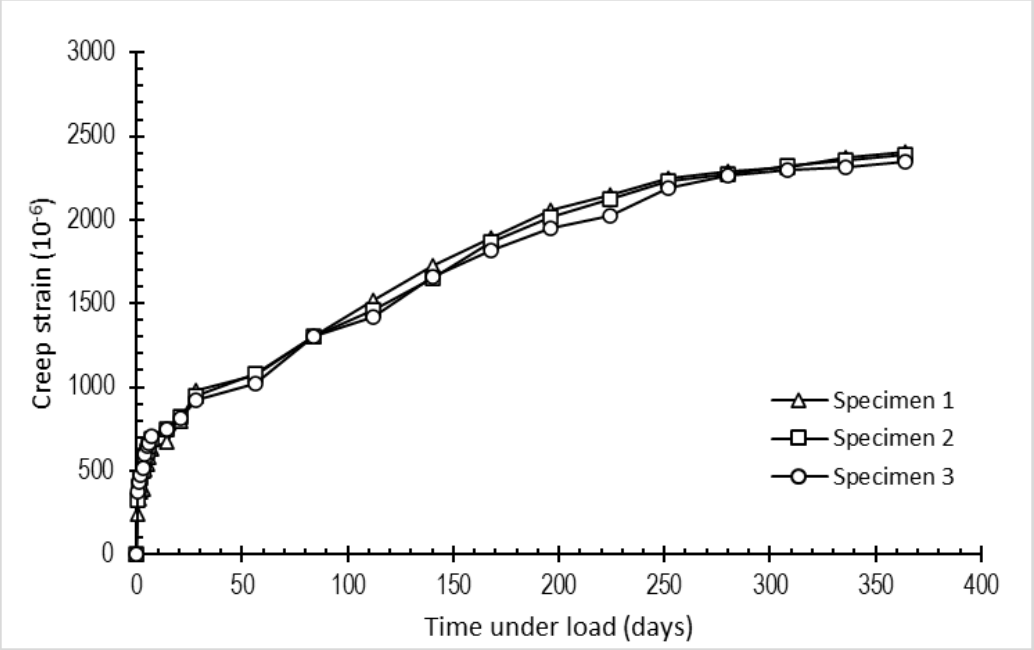

Figure F.18: Creep strains of unsealed M40S specimens

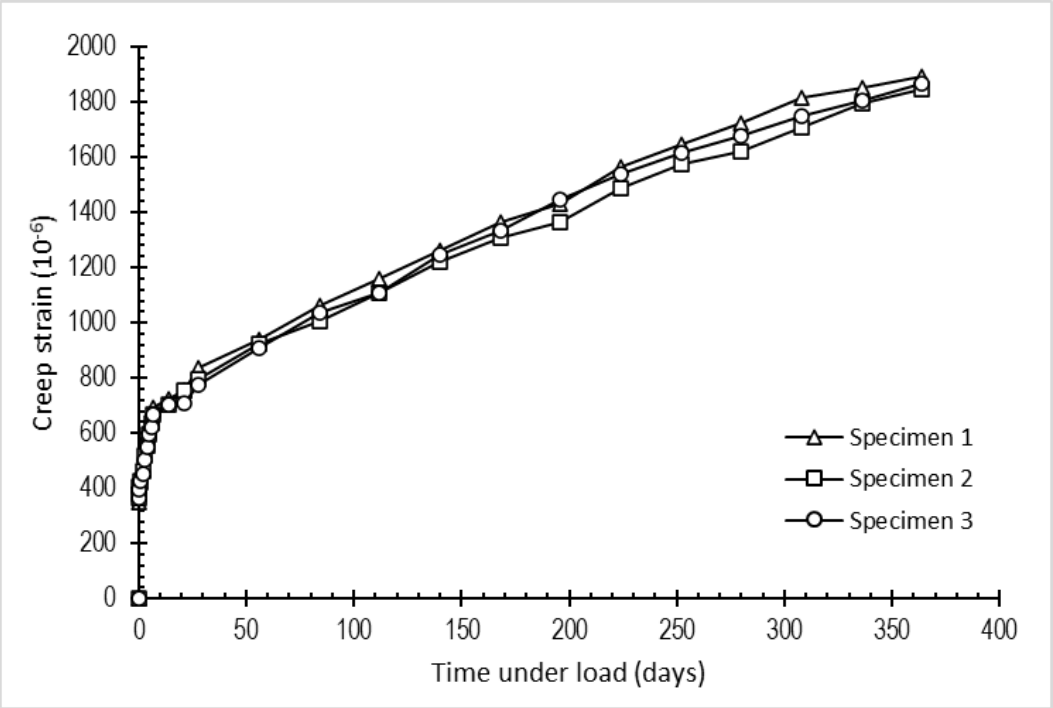

Figure F.19: Creep strains of sealed M40W specimens

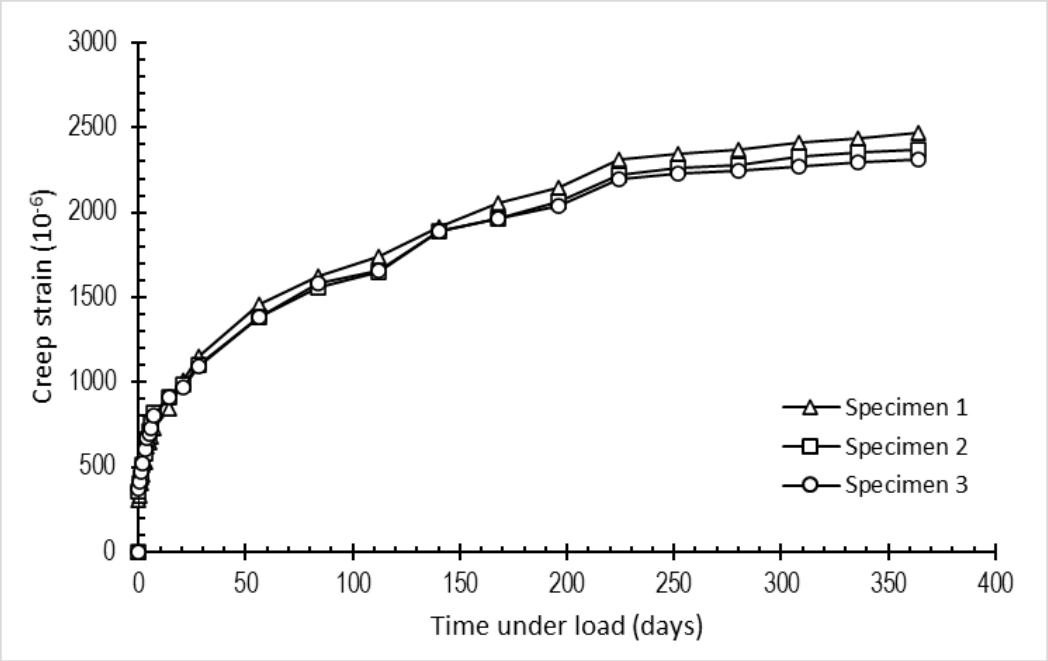

Figure F.20: Creep strains of unsealed M40W specimens